

T H E V I R T U A L L A B O R A T O R Y

# THE ALGORITHMIC BEAUTY OF PLANTS

PRZEMYSŁAW PRUSINKIEWICZ • ARISTID LINDENMAYER



S P R I N G E R - V E R L A G



Aristid Lindenmayer 1925–1989

Przemyslaw Prusinkiewicz  
Aristid Lindenmayer

# The Algorithmic Beauty of Plants

With  
James S. Hanan  
F. David Fracchia  
Deborah Fowler  
Martin J. M. de Boer  
Lynn Mercer

With 150 Illustrations, 48 in Color

This edition of *The Algorithmic Beauty of Plants* is the electronic version of the book that was published by Springer-Verlag, New York, in 1990 and reprinted in 1996. The electronic version has been produced using the original L<sup>A</sup>T<sub>E</sub>X files and digital illustrations.

©2004 Przemyslaw Prusinkiewicz  
All rights reserved.

Front cover design: The roses in the foreground (*Roses* by D. R. Fowler, J. Hanan and P. Prusinkiewicz [1990]) were modeled using L-systems. Distributed ray-tracing with one extended light source was used to simulate depth of field. The roses were placed on a background image (photography by G. Rossbach), which was scanned digitally and post-processed.

# Preface

The beauty of plants has attracted the attention of mathematicians for centuries. Conspicuous geometric features such as the bilateral symmetry of leaves, the rotational symmetry of flowers, and the helical arrangements of scales in pine cones have been studied most extensively. This focus is reflected in a quotation from Weyl [159, page 3], “Beauty is bound up with symmetry.”

*Mathematics  
and beauty*

This book explores two other factors that organize plant structures and therefore contribute to their beauty. The first is the elegance and relative simplicity of *developmental algorithms*, that is, the rules which describe plant development in time. The second is *self-similarity*, characterized by Mandelbrot [95, page 34] as follows:

When each piece of a shape is geometrically similar to the whole, both the shape and the cascade that generate it are called self-similar.

This corresponds with the biological phenomenon described by Herman, Lindenmayer and Rozenberg [61]:

In many growth processes of living organisms, especially of plants, regularly repeated appearances of certain multicellular structures are readily noticeable.... In the case of a compound leaf, for instance, some of the lobes (or leaflets), which are parts of a leaf at an advanced stage, have the same shape as the whole leaf has at an earlier stage.

Thus, self-similarity in plants is a result of developmental processes. By emphasizing the relationship between growth and form, this book follows a long tradition in biology. D’Arcy Thompson [143] traces its origins to the late seventeenth century, and comments:

*Growth and  
form*

Organic form itself is found, mathematically speaking, to be a function of time.... We might call the form of an organism an *event in space-time*, and not merely a *configuration in space*.

This concept is echoed by Hallé, Oldeman and Tomlinson [58]:

The idea of the form implicitly contains also the history of such a form.

*Modeling of  
plants*

The developmental processes are captured using the formalism of *L-systems*. They were introduced in 1968 by Lindenmayer [82] as a theoretical framework for studying the development of simple multicellular organisms, and subsequently applied to investigate higher plants and plant organs. After the incorporation of geometric features, plant models expressed using L-systems became detailed enough to allow the use of computer graphics for realistic visualization of plant structures and developmental processes.

The emphasis on graphics has several motivations. A visual comparison of models with real structures is an important component of model validation. The display of parameters and processes not observable directly in living organisms may assist in the analysis of their physiology, and thus present a valuable tool for educational purposes. From an aesthetic perspective, plants present a wealth of magnificent objects for image synthesis. The quest for photorealism challenges modeling and rendering algorithms, while a departure from realism may offer a fresh view of known structures.

The application of computer graphics to biological structures is only one of many factors that contribute to the interdisciplinary character of this book. For example, the notion of L-systems is a part of formal language theory, rooted in the theory of algorithms. The application of L-systems to plant description has been studied by biologists, and involves various methods of general mathematics. Self-similarity relates plant structures to the geometry of fractals. Computer-aided visualization of these structures, and the processes that create them, joins science with art.

*About the book*

The study of an area that combines so many disciplines is very stimulating. Some results may be of special interest to students of biology or computer graphics, but a much wider circle of readers, generally interested in science, may find mathematical plant models inspiring, and the open problems worth further thought. Consequently, all basic concepts are presented in a self-contained manner, assuming only general knowledge of mathematics at the junior college level.

This book focuses on original research results obtained by the authors in the scope of the cooperation between the Theoretical Biology Group, directed by Aristid Lindenmayer at the University of Utrecht, and the Computer Graphics Group, working under the supervision of Przemyslaw Prusinkiewicz at the University of Regina. Technically, the book evolved from the SIGGRAPH '88 and '89 course notes *Lindenmayer systems, fractals, and plants*, published by Springer-Verlag in the series *Lecture Notes in Biomathematics* [112]. The present volume has been extended with edited versions of recent journal and conference papers (see Sources), as well as previously unpublished results.

Aristid Lindenmayer is the author of the notion of L-systems which forms the main thread of the book. He also played an essential role in the reported research by suggesting topics for study, guiding the construction of specific plant models, monitoring their correctness and

participating in many discussions of biological and mathematical problems. Seriously ill, Professor Lindenmayer co-authored and edited several chapters, but was not able to participate in the completion of this work. If any inaccuracies or mistakes remain, he could not prevent them. Still, in spite of unavoidable shortcomings, we hope that this book will convey his and our excitement of applying mathematics to explore the beauty of plants.

## Acknowledgements

While preparing this book, we received extraordinary support and help from many people, and we are deeply thankful to all of them. First of all, we would like to thank those who were directly involved in the underlying research and software development. Craig Kolb wrote the ray tracer *rayshade* used to render many of the images included in the book. Allan Snider developed several software tools, including a previewer for *rayshade*, and provided valuable expertise in ray-tracing. Daryl Hepting developed software for rendering sets defined by iterated function systems and provided diagrams for Chapter 8. Norma Fuller modeled several man-made objects incorporated into the images.

We would like to thank Zdzisław Pawlak and Grzegorz Rozenberg who initiated the contact between the Theoretical Biology Group at the University of Utrecht and the Computer Graphics Group at the University of Regina. Benoit Mandelbrot and Heinz-Otto Peitgen made it possible to conduct parts of the reported research at Yale University and the University of Bremen.

We are also grateful to all those who shared their knowledge with us and made suggestions reflected in this book. Discussions and correspondence with Jules Bloomenthal, Mark de Does, Pauline Hogeweg, Jacqueline and Hermann Lück, Gavin Miller, Laurie Reuter, Dietmar Saupe and Alvy Ray Smith were particularly fruitful.

Research reported in this book was funded by grants from the Natural Sciences and Engineering Research Council of Canada, as well as an equipment donation and a research grant from Apple Computer, Inc. We are particularly grateful to Mark Cutter for making the support from Apple possible. The Graphics Laboratory at the University of Regina also enjoys continued support from the university. The influence of Lawrence Symes and R. Brien Maguire is deeply appreciated. In addition, the University of Regina and the University of Utrecht contributed towards travel expenses.

We would like to thank Springer-Verlag and in particular, Gerhard Rossbach and Nina LaVoy from the Springer West Coast Office, for the expedient publishing of this book.

Finally, we would like to thank our families and friends for their love, support and patience while we worked on this book.

*Przemyslaw Prusinkiewicz*  
*James Hanan*  
*F. David Fracchia*  
*Deborah R. Fowler*  
*Martin J. M. de Boer*  
*Lynn Mercer*  
Regina, Canada  
May 1990



## Sources

In the preparation of this book, edited parts of the following publications were used:

- P. Prusinkiewicz and J. Hanan. *Lindenmayer systems, fractals, and plants*, volume 79 of *Lecture Notes in Biomathematics*. Springer-Verlag, Berlin, 1989. [Chapters 1, 3, 5]
- P. Prusinkiewicz, A. Lindenmayer and J. Hanan. Developmental models of herbaceous plants for computer imagery purposes. Proceedings of SIGGRAPH '88 (Atlanta, Georgia, August 1-5, 1988), in *Computer Graphics*, 22(4):141–150, 1988. Used with the permission of the Association for Computing Machinery. [Chapters 1, 3, 5]
- P. Prusinkiewicz and J. Hanan. Visualization of botanical structures and processes using parametric L-systems. In D. Thalmann, editor, *Scientific visualization and graphics simulation*, pages 183–201. J. Wiley & Sons, 1990. [Chapters 1–5]
- D. Fowler, J. Hanan and P. Prusinkiewicz. Modelling spiral phyllotaxis. *computers & graphics*, 13(3):291–296, 1989. [Chapter 4]
- J. S. Hanan. PLANTWORKS: A software system for realistic plant modelling. Master's thesis, University of Regina, 1988. [Chapter 5]
- F. D. Fracchia, P. Prusinkiewicz and M. J. M. de Boer. Animation of the development of multicellular structures. In N. Magnenat-Thalmann and D. Thalmann, editors, *Computer Animation '90*, pages 3–18. Springer-Verlag, Tokyo, 1990. [Chapter 7]
- F. D. Fracchia, P. Prusinkiewicz, and M. J. M. de Boer. Visualization of the development of multicellular structures. In *Proceedings of Graphics Interface '90*, pages 267–277, 1990. [Chapter 7]
- L. Mercer, P. Prusinkiewicz, and J. Hanan. The concept and design of a virtual laboratory. In *Proceedings of Graphics Interface '90*, pages 149–155, 1990. [Appendix 8.2]



# Contents

<b>1</b>	<b>Graphical modeling using L-systems</b>	<b>1</b>
1.1	Rewriting systems . . . . .	1
1.2	DOL-systems . . . . .	3
1.3	Turtle interpretation of strings . . . . .	6
1.4	Synthesis of DOL-systems . . . . .	11
1.4.1	Edge rewriting . . . . .	11
1.4.2	Node rewriting . . . . .	13
1.4.3	Relationship between edge and node rewriting . . . . .	18
1.5	Modeling in three dimensions . . . . .	18
1.6	Branching structures . . . . .	21
1.6.1	Axial trees . . . . .	21
1.6.2	Tree OL-systems . . . . .	23
1.6.3	Bracketed OL-systems . . . . .	24
1.7	Stochastic L-systems . . . . .	28
1.8	Context-sensitive L-systems . . . . .	30
1.9	Growth functions . . . . .	36
1.10	Parametric L-systems . . . . .	40
1.10.1	Parametric OL-systems . . . . .	41
1.10.2	Parametric 2L-systems . . . . .	43
1.10.3	Turtle interpretation of parametric words . . . . .	46
<b>2</b>	<b>Modeling of trees</b>	<b>51</b>
<b>3</b>	<b>Developmental models of herbaceous plants</b>	<b>63</b>
3.1	Levels of model specification . . . . .	64
3.1.1	Partial L-systems . . . . .	64
3.1.2	Control mechanisms in plants . . . . .	65
3.1.3	Complete models . . . . .	68
3.2	Branching patterns . . . . .	70
3.3	Models of inflorescences . . . . .	71
3.3.1	Monopodial inflorescences . . . . .	71
3.3.2	Sympodial inflorescences . . . . .	82
3.3.3	Polypodial inflorescences . . . . .	86
3.3.4	Modified racemes . . . . .	93

<b>4</b>	<b>Phyllotaxis</b>	<b>99</b>
4.1	The planar model . . . . .	100
4.2	The cylindrical model . . . . .	109
<b>5</b>	<b>Models of plant organs</b>	<b>119</b>
5.1	Predefined surfaces . . . . .	119
5.2	Developmental surface models . . . . .	120
5.3	Models of compound leaves . . . . .	128
<b>6</b>	<b>Animation of plant development</b>	<b>133</b>
6.1	Timed DOL-systems . . . . .	135
6.2	Selection of growth functions . . . . .	139
6.2.1	Development of nonbranching filaments . . . . .	140
6.2.2	Development of branching structures . . . . .	142
<b>7</b>	<b>Modeling of cellular layers</b>	<b>145</b>
7.1	Map L-systems . . . . .	145
7.2	Graphical interpretation of maps . . . . .	150
7.3	Microsorium linguaeforme . . . . .	153
7.4	Dryopteris thelypteris . . . . .	162
7.5	Modeling spherical cell layers . . . . .	166
7.6	Modeling 3D cellular structures . . . . .	168
<b>8</b>	<b>Fractal properties of plants</b>	<b>175</b>
8.1	Symmetry and self-similarity . . . . .	177
8.2	Plant models and iterated function systems . . . . .	178
	<b>Epilogue</b>	<b>191</b>
	<b>Appendix A Software environment for plant modeling</b>	<b>193</b>
A.1	A virtual laboratory in botany . . . . .	193
A.2	List of laboratory programs . . . . .	198
	<b>Appendix B About the figures</b>	<b>201</b>
	<b>Appendix C Turtle interpretation of symbols</b>	<b>209</b>
	<b>Bibliography</b>	<b>211</b>
	<b>Index</b>	<b>225</b>

# Chapter 1

## Graphical modeling using L-systems

Lindenmayer systems — or L-systems for short — were conceived as a mathematical theory of plant development [82]. Originally, they did not include enough detail to allow for comprehensive modeling of higher plants. The emphasis was on plant topology, that is, the neighborhood relations between cells or larger plant modules. Their geometric aspects were beyond the scope of the theory. Subsequently, several geometric interpretations of L-systems were proposed with a view to turning them into a versatile tool for plant modeling. Throughout this book, an interpretation based on turtle geometry is used [109]. Basic notions related to L-system theory and their turtle interpretation are presented below.

### 1.1 Rewriting systems

The central concept of L-systems is that of rewriting. In general, rewriting is a technique for defining complex objects by successively replacing parts of a simple initial object using a set of *rewriting rules* or *productions*. The classic example of a graphical object defined in terms of rewriting rules is the *snowflake curve* (Figure 1.1), proposed in 1905 by von Koch [155]. Mandelbrot [95, page 39] restates this construction as follows:

*Koch  
construction*

One begins with *two shapes*, an *initiator* and a *generator*. The latter is an oriented broken line made up of  $N$  equal sides of length  $r$ . Thus each stage of the construction begins with a broken line and consists in replacing each straight interval with a copy of the generator, reduced and displaced so as to have the same end points as those of the interval being replaced.

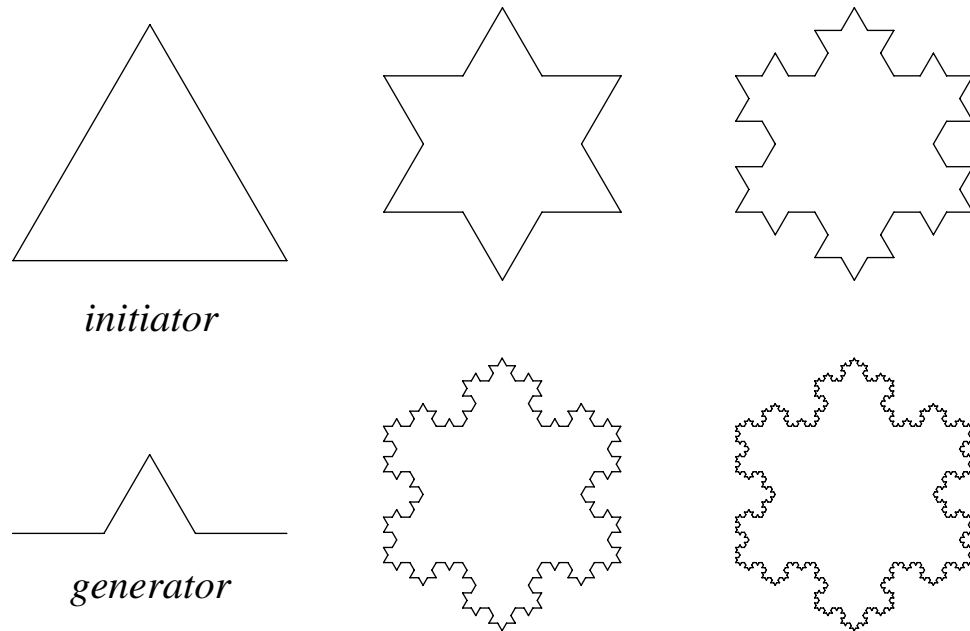


Figure 1.1: Construction of the snowflake curve

While the Koch construction recursively replaces open polygons, rewriting systems that operate on other objects have also been investigated. For example, Wolfram [160, 161] studied patterns generated by rewriting elements of rectangular arrays. A similar array-rewriting mechanism is the cornerstone of Conway's popular *game of life* [49, 50]. An important body of research has been devoted to various graph-rewriting systems [14, 33, 34].

### Grammars

The most extensively studied and the best understood rewriting systems operate on character strings. The first formal definition of such a system was given at the beginning of this century by Thue [128], but a wide interest in string rewriting was spawned in the late 1950s by Chomsky's work on formal grammars [13]. He applied the concept of rewriting to describe the syntactic features of natural languages. A few years later Backus and Naur introduced a rewriting-based notation in order to provide a formal definition of the programming language ALGOL-60 [5, 103]. The equivalence of the Backus-Naur form (BNF) and the context-free class of Chomsky grammars was soon recognized [52], and a period of fascination with syntax, grammars and their application to computer science began. At the center of attention were sets of strings — called formal languages — and the methods for generating, recognizing and transforming them.

### L-systems

In 1968 a biologist, Aristid Lindenmayer, introduced a new type of string-rewriting mechanism, subsequently termed L-systems [82]. The essential difference between Chomsky grammars and L-systems lies in

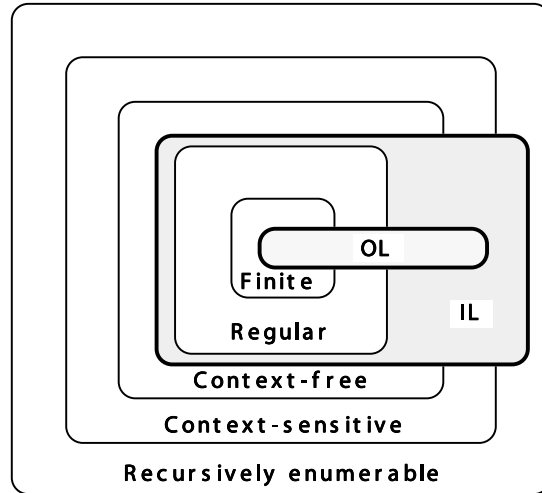


Figure 1.2: Relations between Chomsky classes of languages and language classes generated by L-systems. The symbols OL and IL denote language classes generated by context-free and context-sensitive L-systems, respectively.

the method of applying productions. In Chomsky grammars productions are applied sequentially, whereas in L-systems they are applied in parallel and simultaneously replace all letters in a given word. This difference reflects the biological motivation of L-systems. Productions are intended to capture cell divisions in multicellular organisms, where many divisions may occur at the same time. Parallel production application has an essential impact on the formal properties of rewriting systems. For example, there are languages which can be generated by context-free L-systems (called OL-systems) but not by context-free Chomsky grammars [62, 128] (Figure 1.2).

## 1.2 DOL-systems

This section presents the simplest class of L-systems, those which are deterministic and context-free, called DOL-systems. The discussion starts with an example that introduces the main idea in intuitive terms.

Consider strings (words) built of two letters  $a$  and  $b$ , which may occur many times in a string. Each letter is associated with a rewriting rule. The rule  $a \rightarrow ab$  means that the letter  $a$  is to be replaced by the string  $ab$ , and the rule  $b \rightarrow a$  means that the letter  $b$  is to be replaced by  $a$ . The rewriting process starts from a distinguished string called the axiom. Assume that it consists of a single letter  $b$ . In the first derivation step (the first step of rewriting) the axiom  $b$  is replaced

*Example*

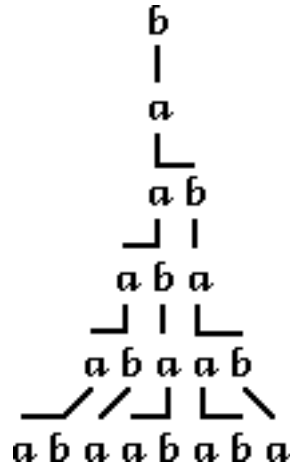


Figure 1.3: Example of a derivation in a DOL-system

by  $a$  using production  $b \rightarrow a$ . In the second step  $a$  is replaced by  $ab$  using production  $a \rightarrow ab$ . The word  $ab$  consists of two letters, both of which are *simultaneously* replaced in the next derivation step. Thus,  $a$  is replaced by  $ab$ ,  $b$  is replaced by  $a$ , and the string  $aba$  results. In a similar way, the string  $aba$  yields  $abaab$  which in turn yields  $abaababa$ , then  $abaababaabaab$ , and so on (Figure 1.3).

Formal definitions describing DOL-systems and their operation are given below. For more details see [62, 127].

#### *L-system*

Let  $V$  denote an alphabet,  $V^*$  the set of all words over  $V$ , and  $V^+$  the set of all nonempty words over  $V$ . A *string OL-system* is an ordered triplet  $G = \langle V, \omega, P \rangle$  where  $V$  is the *alphabet* of the system,  $\omega \in V^+$  is a nonempty word called the *axiom* and  $P \subset V \times V^*$  is a finite *set of productions*. A production  $(a, \chi) \in P$  is written as  $a \rightarrow \chi$ . The letter  $a$  and the word  $\chi$  are called the *predecessor* and the *successor* of this production, respectively. It is assumed that for any letter  $a \in V$ , there is at least one word  $\chi \in V^*$  such that  $a \rightarrow \chi$ . If no production is explicitly specified for a given predecessor  $a \in V$ , the *identity production*  $a \rightarrow a$  is assumed to belong to the set of productions  $P$ . An OL-system is *deterministic* (noted *DOL-system*) if and only if for each  $a \in V$  there is exactly one  $\chi \in V^*$  such that  $a \rightarrow \chi$ .

#### *Derivation*

Let  $\mu = a_1 \dots a_m$  be an arbitrary word over  $V$ . The word  $\nu = \chi_1 \dots \chi_m \in V^*$  is *directly derived* from (or *generated* by)  $\mu$ , noted  $\mu \Rightarrow \nu$ , if and only if  $a_i \rightarrow \chi_i$  for all  $i = 1, \dots, m$ . A word  $\nu$  is generated by  $G$  in a derivation of *length*  $n$  if there exists a *developmental sequence* of words  $\mu_0, \mu_1, \dots, \mu_n$  such that  $\mu_0 = \omega$ ,  $\mu_n = \nu$  and  $\mu_0 \Rightarrow \mu_1 \Rightarrow \dots \Rightarrow \mu_n$ .



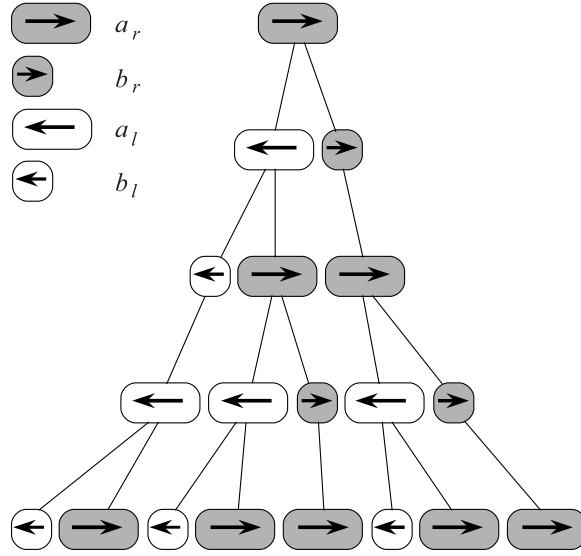


Figure 1.4: Development of a filament (*Anabaena catenula*) simulated using a DOL-system

The following example provides another illustration of the operation of DOL-systems. The formalism is used to simulate the development of a fragment of a multicellular filament such as that found in the blue-green bacteria *Anabaena catenula* and various algae [25, 84, 99]. The symbols  $a$  and  $b$  represent cytological states of the cells (their size and readiness to divide). The subscripts  $l$  and  $r$  indicate cell polarity, specifying the positions in which daughter cells of type  $a$  and  $b$  will be produced. The development is described by the following L-system:

*Anabaena*

$$\begin{aligned}
 \omega & : a_r \\
 p_1 & : a_r \rightarrow a_l b_r \\
 p_2 & : a_l \rightarrow b_l a_r \\
 p_3 & : b_r \rightarrow a_r \\
 p_4 & : b_l \rightarrow a_l
 \end{aligned}
 \tag{1.1}$$

Starting from a single cell  $a_r$  (the axiom), the following sequence of words is generated:

$$\begin{aligned}
 & a_r \\
 & a_l b_r \\
 & b_l a_r a_r \\
 & a_l a_l b_r a_l b_r \\
 & b_l a_r b_l a_r a_r b_l a_r a_r \\
 & \dots
 \end{aligned}$$

Under a microscope, the filaments appear as a sequence of cylinders of various lengths, with *a*-type cells longer than *b*-type cells. The corresponding schematic image of filament development is shown in Figure 1.4. Note that due to the discrete nature of L-systems, the continuous growth of cells between subdivisions is not captured by this model.

### 1.3 Turtle interpretation of strings

The geometric interpretation of strings applied to generate schematic images of *Anabaena catenula* is a very simple one. Letters of the L-system alphabet are represented graphically as shorter or longer rectangles with rounded corners. The generated structures are one-dimensional chains of rectangles, reflecting the sequence of symbols in the corresponding strings.

*Previous  
methods*

In order to model higher plants, a more sophisticated graphical interpretation of L-systems is needed. The first results in this direction were published in 1974 by Frijters and Lindenmayer [46], and Hogeweg and Hesper [64]. In both cases, L-systems were used primarily to determine the branching topology of the modeled plants. The geometric aspects, such as the lengths of line segments and the angle values, were added in a post-processing phase. The results of Hogeweg and Hesper were subsequently extended by Smith [136, 137], who demonstrated the potential of L-systems for realistic image synthesis.

Szillard and Quinton [141] proposed a different approach to L-system interpretation in 1979. They concentrated on image representations with rigorously defined geometry, such as chain coding [43], and showed that strikingly simple DOL-systems could generate the intriguing, convoluted curves known today as *fractals* [95]. These results were subsequently extended in several directions. Siromoney and Subramanian [135] specified L-systems which generate classic space-filling curves. Dekking investigated the limit properties of curves generated by L-systems [32] and concentrated on the problem of determining the fractal (Hausdorff) dimension of the limit set [31]. Prusinkiewicz focused on an interpretation based on a LOGO-style turtle [1] and presented more examples of fractals and plant-like structures modeled using L-systems [109, 111]. Further applications of L-systems with turtle interpretation include realistic modeling of herbaceous plants [117], description of *kolam* patterns (an art form from Southern India) [112, 115, 133, 134], synthesis of musical scores [110] and automatic generation of space-filling curves [116].

*Turtle*

The basic idea of turtle interpretation is given below. A *state* of the *turtle* is defined as a triplet  $(x, y, \alpha)$ , where the Cartesian coordinates  $(x, y)$  represent the turtle's *position*, and the angle  $\alpha$ , called the *heading*, is interpreted as the direction in which the turtle is facing. Given the *step size*  $d$  and the *angle increment*  $\delta$ , the turtle can respond to



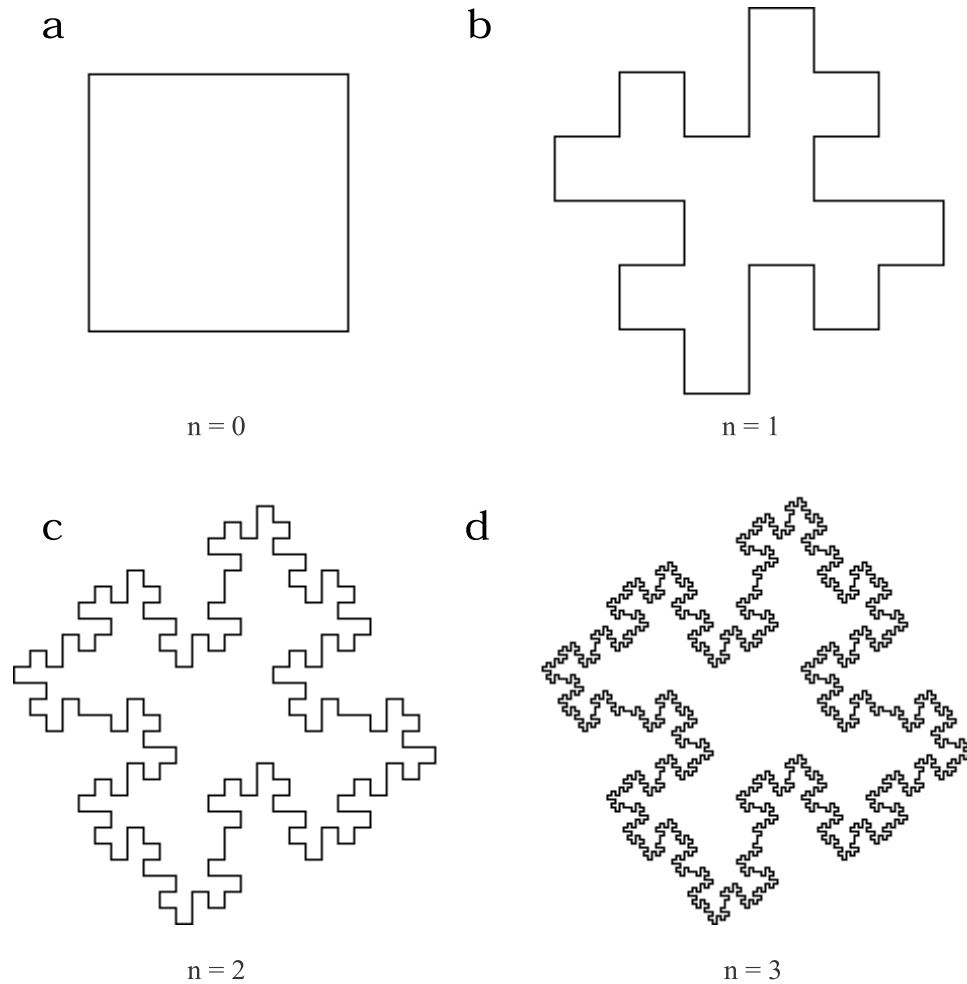


Figure 1.6: Generating a quadratic Koch island

between the endpoints of the successor polygon equal to the length of the predecessor segment.

The above example reveals a close relationship between Koch constructions and L-systems. The initiator corresponds to the axiom and the generator corresponds to the production successor. The predecessor  $F$  represents a single edge. L-systems specified in this way can be perceived as *codings* for Koch constructions. Figure 1.7 presents further examples of Koch curves generated using L-systems. A slight complication occurs if the curve is not connected; a second production (with the predecessor  $f$ ) is then required to keep components the proper distance from each other (Figure 1.8). The ease of modifying L-systems makes them suitable for developing new Koch curves. For example, one can start from a particular L-system and observe the results of inserting, deleting or replacing some symbols. A variety of curves obtained this way are shown in Figure 1.9.

*Koch  
constructions  
vs. L-systems*

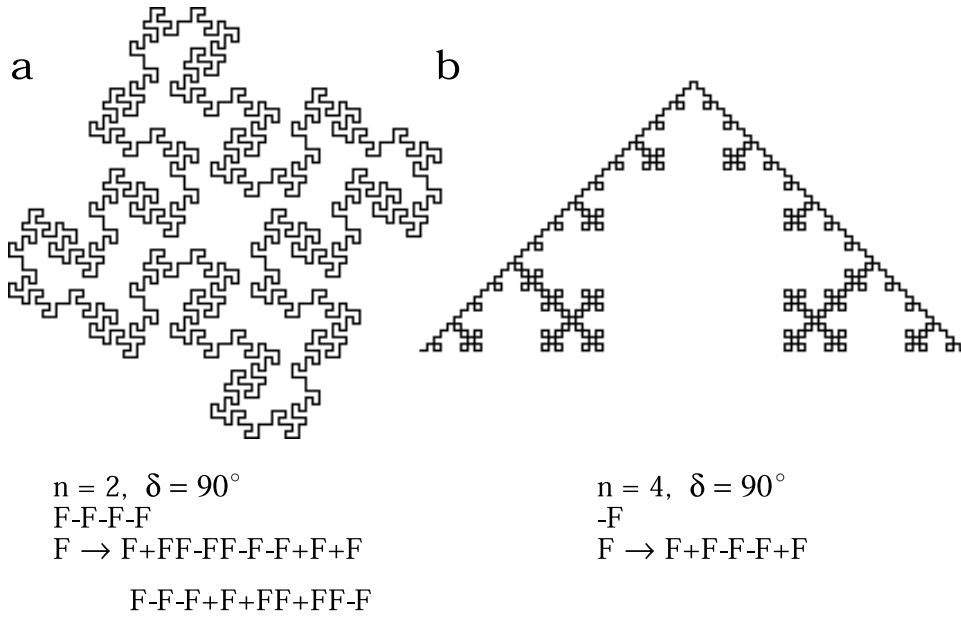
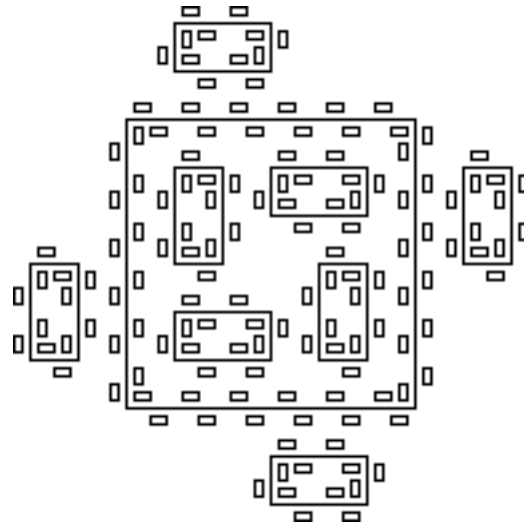


Figure 1.7: Examples of Koch curves generated using L-systems: (a) Quadratic Koch island [95, page 52], (b) A quadratic modification of the snowflake curve [95, page 139]



$n = 2, \delta = 90^\circ$   
 $F+F+F+F$   
 $F \rightarrow F+f-FF+F+FF+Ff+FF-f+FF-F-FF-Ff-FFF$   
 $f \rightarrow fffff$

Figure 1.8: Combination of islands and lakes [95, page 121]

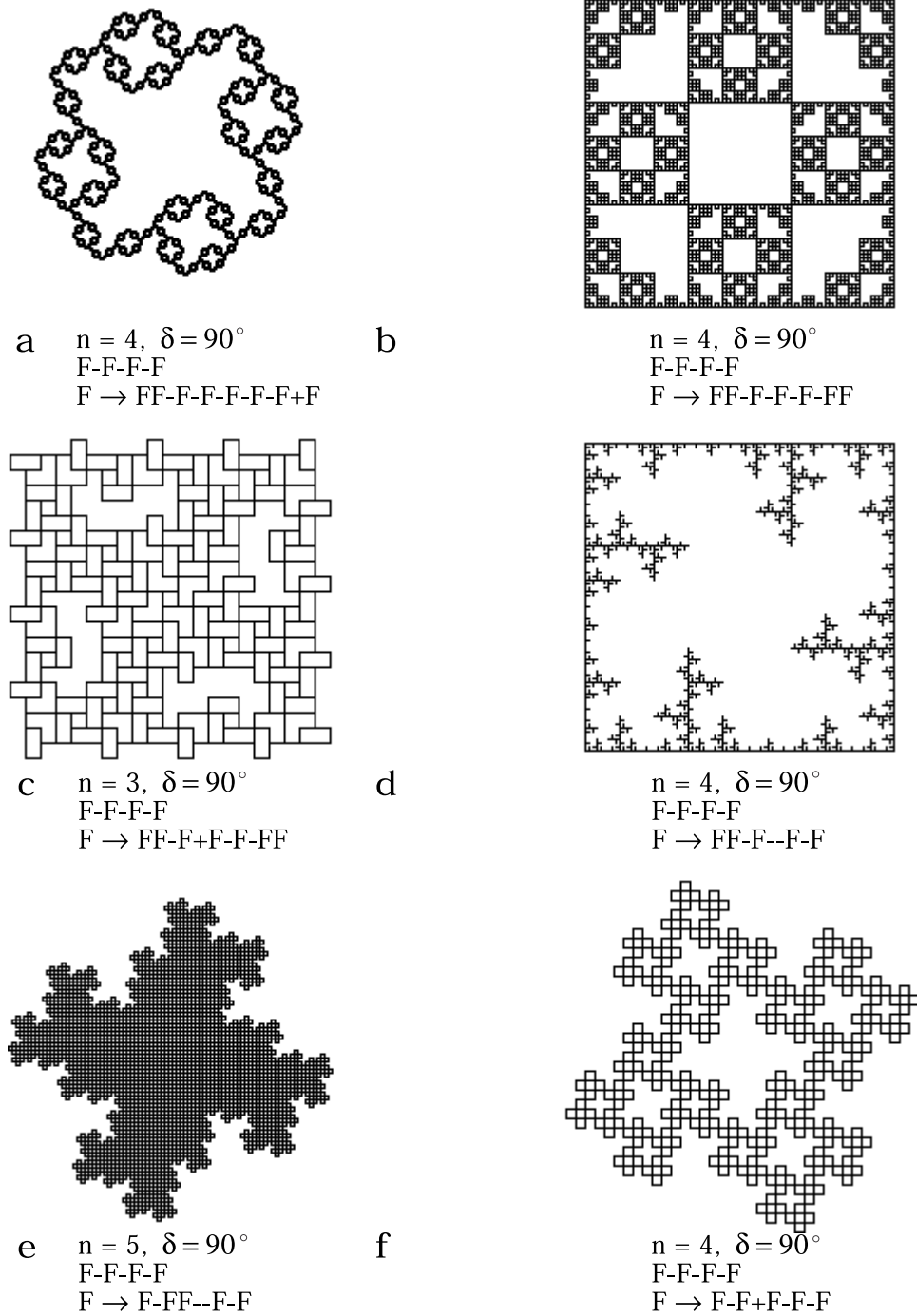


Figure 1.9: A sequence of Koch curves obtained by successive modification of the production successor

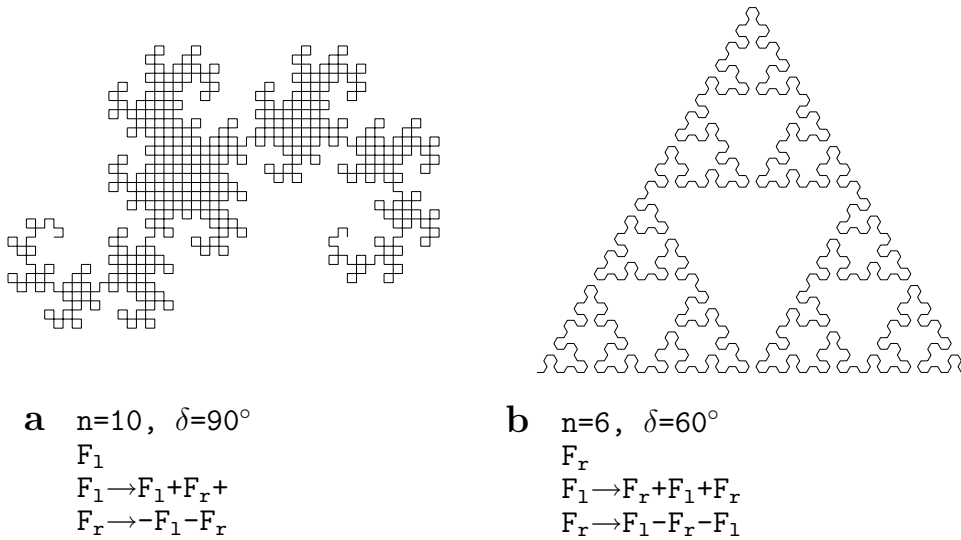


Figure 1.10: Examples of curves generated by edge-rewriting L-systems: (a) the dragon curve [48], (b) the Sierpiński gasket [132]

## 1.4 Synthesis of DOL-systems

Random modification of productions gives little insight into the relationship between L-systems and the figures they generate. However, we often wish to construct an L-system which captures a given structure or sequence of structures representing a developmental process. This is called the *inference problem* in the theory of L-systems. Although some algorithms for solving it were reported in the literature [79, 88, 89], they are still too limited to be of practical value in the modeling of higher plants. Consequently, the methods introduced below are more intuitive in nature. They exploit two modes of operation for L-systems with turtle interpretation, called *edge rewriting* and *node rewriting* using terminology borrowed from graph grammars [56, 57, 87]. In the case of edge rewriting, productions substitute figures for polygon edges, while in node rewriting, productions operate on polygon vertices. Both approaches rely on capturing the recursive structure of figures and relating it to a tiling of a plane. Although the concepts are illustrated using abstract curves, they apply to branching structures found in plants as well.

### 1.4.1 Edge rewriting

Edge rewriting can be viewed as an extension of Koch constructions. For example, Figure 1.10a shows the *dragon curve* [21, 48, 95] and the L-system that generated it. Both the  $F_l$  and  $F_r$  symbols represent edges created by the turtle executing the “move forward” command. The productions substitute  $F_l$  or  $F_r$  edges by pairs of lines forming

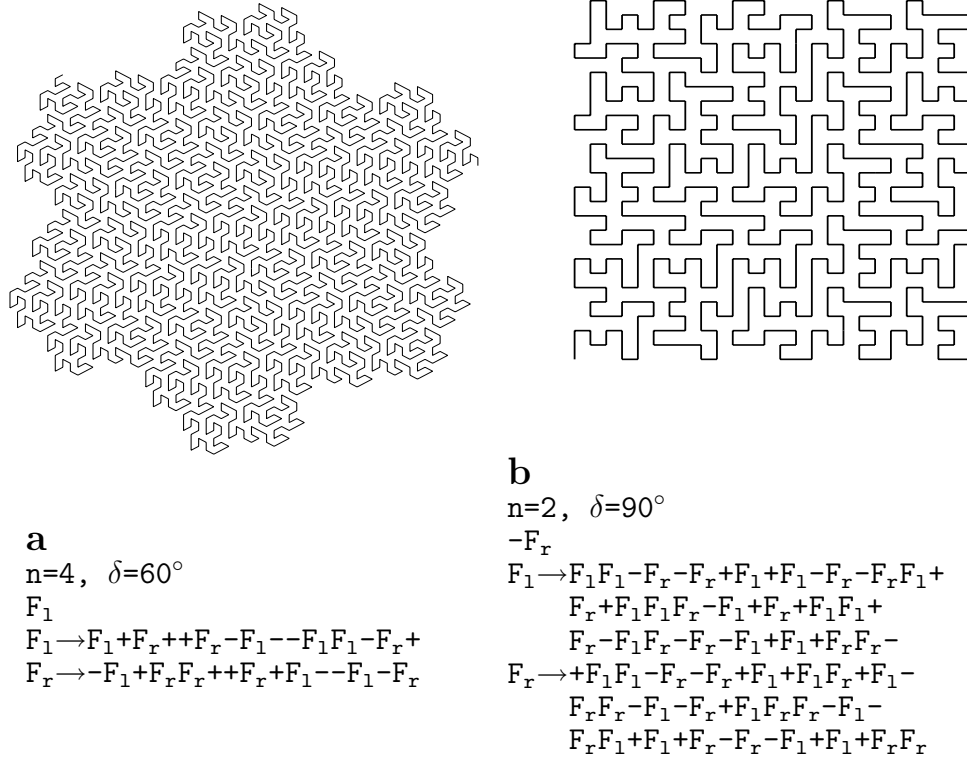


Figure 1.11: Examples of FASS curves generated by edge-rewriting L-systems: (a) hexagonal Gosper curve [51], (b) quadratic Gosper curve [32] or E-curve [96]

left or right turns. Many interesting curves can be obtained assuming two types of edges, “left” and “right.” Figures 1.10b and 1.11 present additional examples.

### *FASS curve construction*

The curves included in Figure 1.11 belong to the class of *FASS* curves (an acronym for space-filling, self-avoiding, simple and self-similar) [116], which can be thought of as finite, self-avoiding approximations of curves that pass through *all* points of a square (space-filling curves [106]). McKenna [96] presented an algorithm for constructing FASS curves using edge replacement. It exploits the relationship between such a curve and a recursive subdivision of a square into tiles. For example, Figure 1.12 shows the tiling that corresponds to the E-curve of Figure 1.11b. The polygon replacing an edge  $F_l$  (Figure 1.12a) approximately fills the square on the left side of  $F_l$  (b). Similarly, the polygon replacing an edge  $F_r$  (c) approximately fills the square on the right side of that edge (d). Consequently, in the next derivation step, each of the 25 tiles associated with the curves (b) or (d) will be covered by their reduced copies (Figure 1.11b). A recursive application of this argument indicates that the whole curve is approximately space-filling. It is also self-avoiding due to the following two properties:



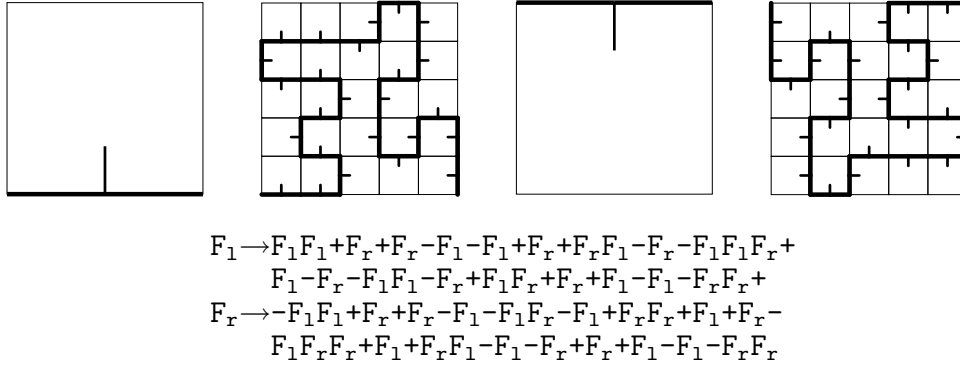


Figure 1.12: Construction of the E-curve on the square grid. Left and right edges are distinguished by the direction of ticks.

- the generating polygon is self-avoiding, and
- no matter what the relative orientation of the polygons lying on two adjacent tiles, their union is a self-avoiding curve.

The first property is obvious, while the second can be verified by considering all possible relative positions of a pair of adjacent tiles.

Using a computer program to search the space of generating polygons, McKenna found that the E-curve is the simplest FASS curve obtained by edge replacement in a square grid. Other curves require generators with more edges (Figure 1.13). The relationship between edge rewriting and tiling of the plane extends to branching structures, providing a method for constructing and analyzing L-systems which operate according to the edge-rewriting paradigm (see Section 1.10.3).

### 1.4.2 Node rewriting

The idea of node rewriting is to substitute new polygons for nodes of the predecessor curve. In order to make this possible, turtle interpretation is extended by symbols which represent arbitrary subfigures. As shown in Figure 1.14, each subfigure  $A$  from a set of subfigures  $\mathcal{A}$  is represented by:

*Subfigures*

- two *contact points*, called the *entry point*  $P_A$  and the *exit point*  $Q_A$ , and
- two *direction vectors*, called the *entry vector*  $\vec{p}_A$  and the *exit vector*  $\vec{q}_A$ .

During turtle interpretation of a string  $\nu$ , a symbol  $A \in \mathcal{A}$  incorporates the corresponding subfigure into a picture. To this end,  $A$  is translated

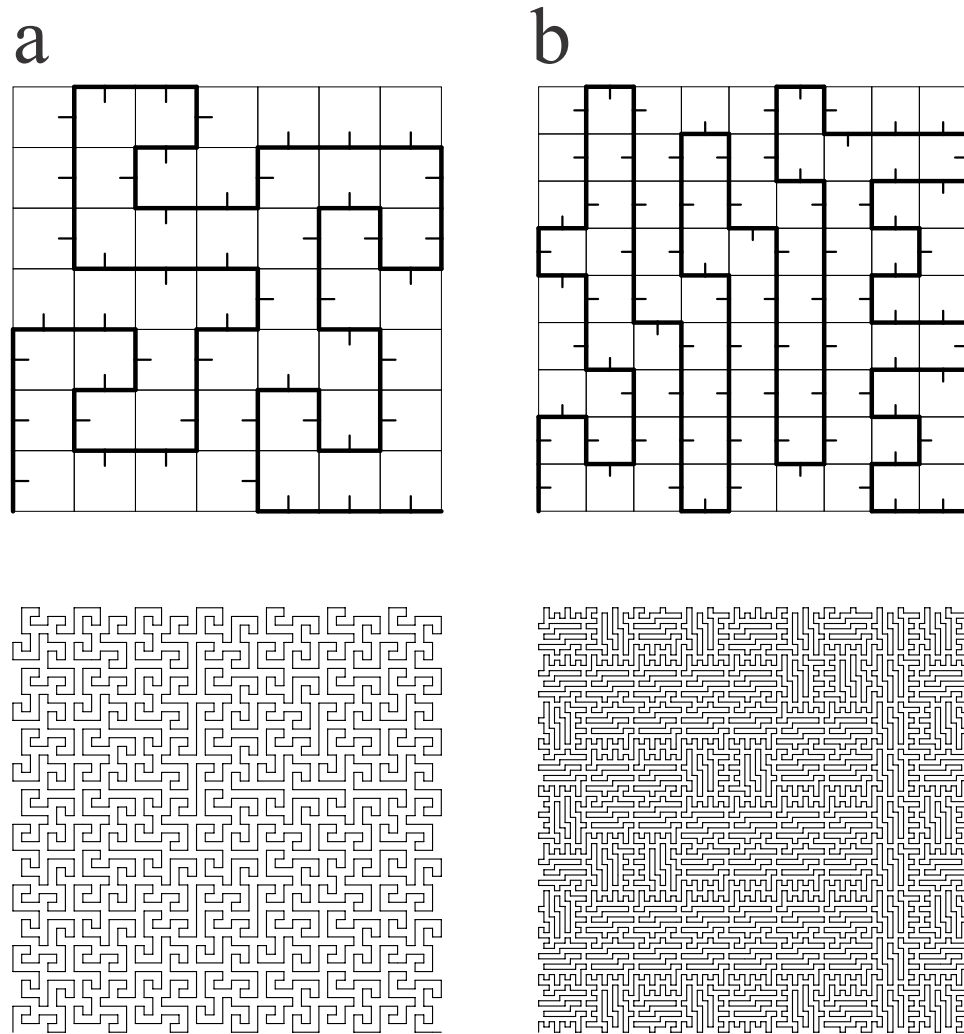


Figure 1.13: Examples of FASS curves generated on the square grid using edge replacement: (a) a SquaRecurve (grid size  $7 \times 7$ ), (b) an E-tour (grid size  $9 \times 9$ ). Both curves are from [96].

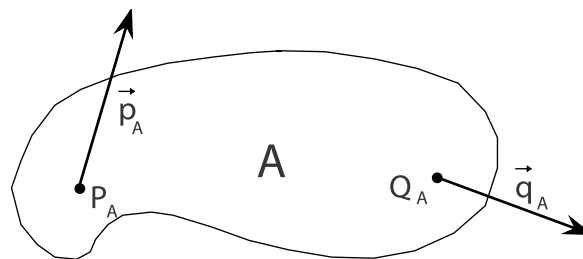


Figure 1.14: Description of a subfigure  $A$

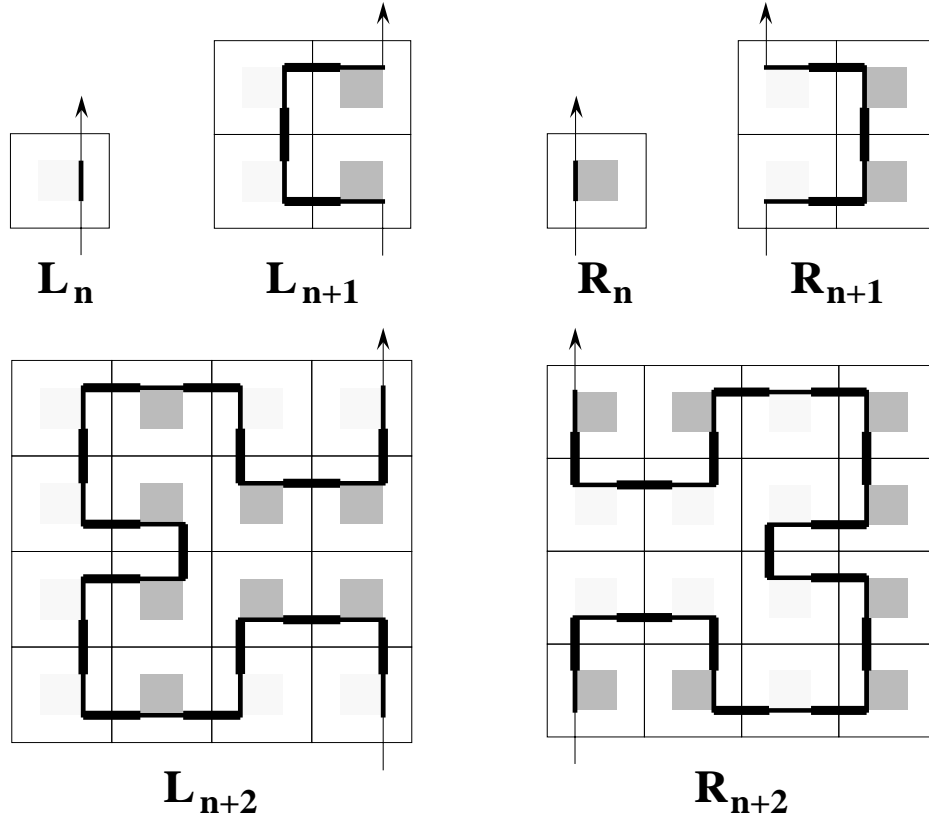


Figure 1.15: Recursive construction of the Hilbert curve [63] in terms of node replacement

and rotated in order to align its entry point  $P_A$  and direction  $\vec{p}_A$  with the current position and orientation of the turtle. Having placed  $A$ , the turtle is assigned the resulting exit position  $Q_A$  and direction  $\vec{q}_A$ .

For example, assuming that the contact points and directions of subfigures  $L_n$  and  $R_n$  are as in Figure 1.15, the figures  $L_{n+1}$  and  $R_{n+1}$  are captured by the following formulas:

*Recursive formulas*

$$\begin{aligned} L_{n+1} &= +R_n F - L_n F L_n - F R_n + \\ R_{n+1} &= -L_n F + R_n F R_n + F L_n - \end{aligned}$$

Suppose that curves  $L_0$  and  $R_0$  are given. One way of evaluating the string  $L_n$  (or  $R_n$ ) for  $n > 0$  is to generate successive strings recursively, in the order of decreasing value of index  $n$ . For example, the computation of  $L_2$  would proceed as follows:

$$\begin{aligned} L_2 &= +R_1 F - L_1 F L_1 - F R_1 + \\ &= +(-L_0 F + R_0 F R_0 + F L_0 -) F - (+R_0 F - L_0 F L_0 - F R_0 +) \\ &\quad F(+R_0 F - L_0 F L_0 - F R_0 +) - F(-L_0 F + R_0 F R_0 + F L_0 -) + \end{aligned}$$

Thus, the generation of string  $L_n$  can be considered as a string-rewriting mechanism, where the symbols on the left side of the recursive formulas are substituted by corresponding strings on the right side. The substitution proceeds in a parallel way with  $F$ ,  $+$  and  $-$  replacing themselves. Since all indices in any given string have the same value, they can be dropped, provided that a global count of derivation steps is kept. Consequently, string  $L_n$  can be obtained in a derivation of length  $n$  using the following L-system:

$$\begin{aligned}\omega &: L \\ p_1 &: L \rightarrow +RF - LFL - FR+ \\ p_2 &: R \rightarrow -LF + RFR + FL-\end{aligned}$$

*Pure curves*

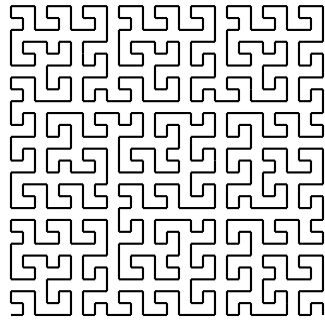
In order to complete the curve definition, it is necessary to specify the subfigures represented by symbols  $L$  and  $R$ . In the special case of *pure curves* [116], these subfigures are reduced to single points. Thus, one can assume that symbols  $L$  and  $R$  are erased (replaced by the empty string) at the end of the derivation. Alternatively, they can be left in the string and ignored by the turtle during string interpretation. This second approach is consistent with previous definitions of turtle interpretation [109, 112]. A general discussion of the relationship between recurrent formulas and L-systems is presented in [61, 62].

*FASS curve construction*

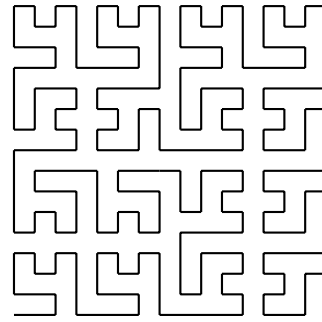
Construction of the L-system generating the Hilbert curve can be extended to other FASS curves [116]. Consider an array of  $m \times m$  square tiles, each including a smaller square, called a *frame*. The edges of the frame run at some distance from the tile's edges. Each frame bounds an open self-avoiding polygon. The endpoints of this polygon coincide with the two contact vertices of the frame. Suppose that a single-stroke line running through all tiles can be constructed by connecting the contact vertices of neighboring frames using short horizontal or vertical line segments. A FASS curve can be constructed by the recursive repetition of this connecting pattern. To this end, the array of  $m \times m$  connected tiles is considered a *macrotile* which contains an open polygon inscribed into a *macroframe*. An array of  $m \times m$  macrotiles is formed, and the polygons inscribed into the macroframes are connected together. This construction is carried out recursively, with  $m \times m$  macrotiles at level  $n$  yielding one macrotile at level  $n + 1$ .

Tile arrangements suitable for the generation of FASS curves can be found algorithmically, by searching the space of all possible arrangements on a grid of a given size. Examples of curves synthesized this way are given in Figures 1.16 and 1.17.

As in the case of edge rewriting, the relationship between node rewriting and tilings of the plane extends to branching structures. It offers a method for synthesizing L-systems that generate objects with a given recursive structure, and links methods for plant generation based on L-systems with those using iterated function systems [7] (see Chapter 8).

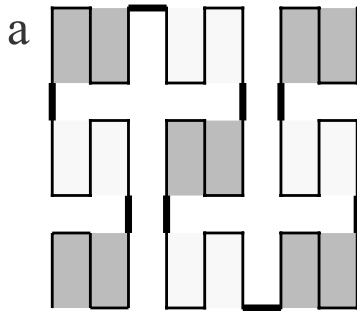


**a**  
 $n=3, \delta=90^\circ$   
 -L  
 $L \rightarrow LF+RFR+FL-F-LFLFL-FRFR+$   
 $R \rightarrow -LFLF+RFRFR+F+RF-LFL-FR$

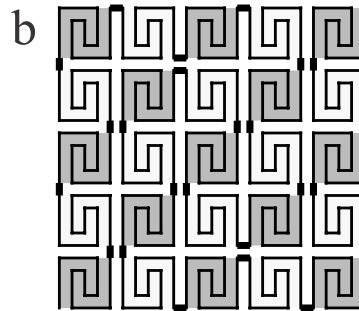


**b**  
 $n=2, \delta=90^\circ$   
 -L  
 $L \rightarrow LFLF+RFR+FLFL-FRF-LFL-$   
 $FR+F+RF-LFL-FRFRFR+$   
 $R \rightarrow -LFLFLF+RFR+FL-F-LF+RFR+$   
 $FLF+RFRF-LFL-FRFR$

Figure 1.16: Sample FASS curves constructed using tiles with contact points positioned along a tile edge: (a)  $3 \times 3$  tiles form a macrotile, (b)  $4 \times 4$  tiles form a macrotile



**a**  $n=2, \delta=90^\circ$   
 L  
 $L \rightarrow LFRFL-F-RFLFR+F+LFRFL$   
 $R \rightarrow RFLFR+F+LFRFL-F-RFLFR$



**b**  $n=2, \delta=45^\circ$   
 L  
 $L \rightarrow L+F+R-F-L+F+R-F-L-F-R+F+L-F-R-F-L+F+R-F-L-F-R-F-$   
 $L+F+R+F+L+F+R-F-L+F+R+F+L-R-F+F+L+F+R-F-L+F+R-F-L$   
 $R \rightarrow R-F-L+F+R-F-L+F+R+F+L-F-R+F+L+F+R-F-L+F+R+F+L+F+$   
 $R-F-L-F-R-F-L+F+R-F-L-F-R+F+L-F-R-F-L+F+R-F-L+F+R$

Figure 1.17: Sample FASS curves constructed using tiles with contact points positioned diagonally: (a)  $3 \times 3$  tiles form a macrotile (Peano curve [106]), (b)  $5 \times 5$  tiles form a macrotile

### 1.4.3 Relationship between edge and node rewriting

The classes of curves that can be generated using the edge-rewriting and node-rewriting techniques are not disjoint. For example, reconsider the L-system that generates the dragon curve using edge replacement:

$$\begin{aligned}\omega &: F_l \\ p_1 &: F_l \rightarrow F_l + F_r + \\ p_2 &: F_r \rightarrow -F_l - F_r\end{aligned}$$

Assume temporarily that a production predecessor can contain more than one letter; thus an entire subword can be replaced by the successor of a single production (a formalization of this concept is termed *pseudo-L-systems* [109]). The dragon-generating L-system can be rewritten as:

$$\begin{aligned}\omega &: Fl \\ p_1 &: Fl \rightarrow Fl + rF + \\ p_2 &: rF \rightarrow -Fl - rF\end{aligned}$$

where the symbols  $l$  and  $r$  are not interpreted by the turtle. Production  $p_1$  replaces the letter  $l$  by the string  $l + rF$ — while the leading letter  $F$  is left intact. In a similar way, production  $p_2$  replaces the letter  $r$  by the string  $-Fl - r$  and leaves the trailing  $F$  intact. Thus, the L-system can be transformed into node-rewriting form as follows:

$$\begin{aligned}\omega &: Fl \\ p_1 &: l \rightarrow l + rF + \\ p_2 &: r \rightarrow -Fl - r\end{aligned}$$

In practice, the choice between edge rewriting and node rewriting is often a matter of convenience. Neither approach offers an automatic, general method for constructing L-systems that capture given structures. However, the distinction between edge and node rewriting makes it easier to understand the intricacies of L-system operation, and in this sense assists in the modeling task. Specifically, the problem of filling a region by a self-avoiding curve is biologically relevant, since some plant structures, such as leaves, may tend to fill a plane without overlapping [38, 66, 67, 94].

## 1.5 Modeling in three dimensions

Turtle interpretation of L-systems can be extended to three dimensions following the ideas of Abelson and diSessa [1]. The key concept is to represent the current *orientation* of the turtle in space by three vectors  $\vec{H}, \vec{L}, \vec{U}$ , indicating the turtle's *heading*, the direction to the *left*, and the direction *up*. These vectors have unit length, are perpendicular to each

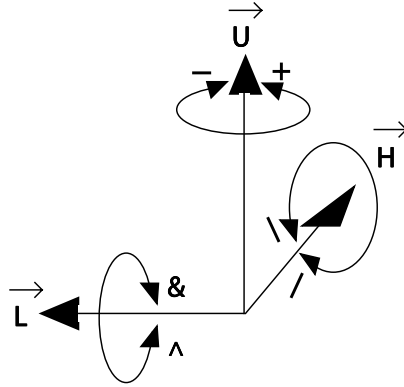


Figure 1.18: Controlling the turtle in three dimensions

other, and satisfy the equation  $\vec{H} \times \vec{L} = \vec{U}$ . Rotations of the turtle are then expressed by the equation

$$\begin{bmatrix} \vec{H}' & \vec{L}' & \vec{U}' \end{bmatrix} = \begin{bmatrix} \vec{H} & \vec{L} & \vec{U} \end{bmatrix} \mathbf{R},$$

where  $\mathbf{R}$  is a  $3 \times 3$  rotation matrix [40]. Specifically, rotations by angle  $\alpha$  about vectors  $\vec{U}, \vec{L}$  and  $\vec{H}$  are represented by the matrices:

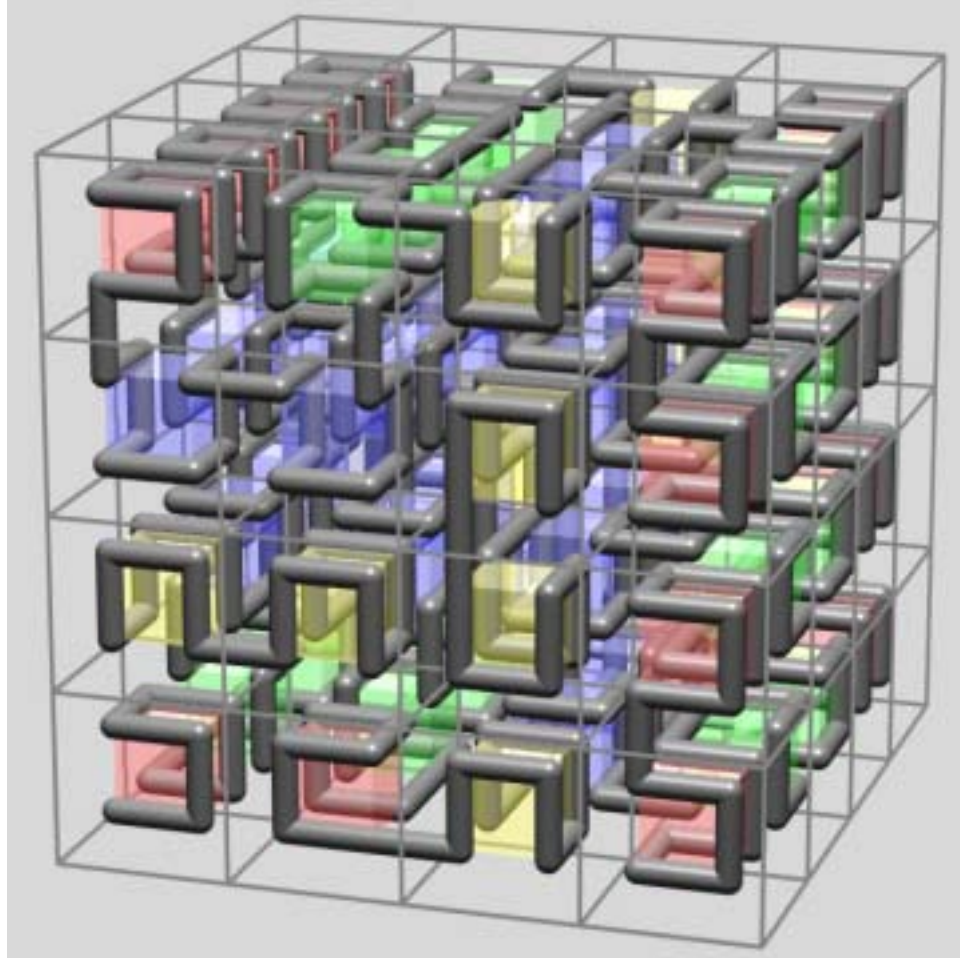
$$\mathbf{R}_{\mathbf{U}}(\alpha) = \begin{bmatrix} \cos \alpha & \sin \alpha & 0 \\ -\sin \alpha & \cos \alpha & 0 \\ 0 & 0 & 1 \end{bmatrix}$$

$$\mathbf{R}_{\mathbf{L}}(\alpha) = \begin{bmatrix} \cos \alpha & 0 & -\sin \alpha \\ 0 & 1 & 0 \\ \sin \alpha & 0 & \cos \alpha \end{bmatrix}$$

$$\mathbf{R}_{\mathbf{H}}(\alpha) = \begin{bmatrix} 1 & 0 & 0 \\ 0 & \cos \alpha & -\sin \alpha \\ 0 & \sin \alpha & \cos \alpha \end{bmatrix}$$

The following symbols control turtle orientation in space (Figure 1.18):

- + Turn left by angle  $\delta$ , using rotation matrix  $\mathbf{R}_{\mathbf{U}}(\delta)$ .
- Turn right by angle  $\delta$ , using rotation matrix  $\mathbf{R}_{\mathbf{U}}(-\delta)$ .
- & Pitch down by angle  $\delta$ , using rotation matrix  $\mathbf{R}_{\mathbf{L}}(\delta)$ .
- ^ Pitch up by angle  $\delta$ , using rotation matrix  $\mathbf{R}_{\mathbf{L}}(-\delta)$ .
- \ Roll left by angle  $\delta$ , using rotation matrix  $\mathbf{R}_{\mathbf{H}}(\delta)$ .
- / Roll right by angle  $\delta$ , using rotation matrix  $\mathbf{R}_{\mathbf{H}}(-\delta)$ .
- | Turn around, using rotation matrix  $\mathbf{R}_{\mathbf{U}}(180^\circ)$ .



$n=2, \delta=90^\circ$

A

$A \rightarrow B-F+CFC+F-D&F\wedge D-F+\&&CFC+F+B//$

$B \rightarrow A&F\wedge CFB\wedge F\wedge D\wedge\wedge-F-D\wedge|F\wedge B|FC\wedge F\wedge A//$

$C \rightarrow |D\wedge|F\wedge B-F+C\wedge F\wedge A&&FA&F\wedge C+F+B\wedge F\wedge D//$

$D \rightarrow |CFB-F+B|FA&F\wedge A&&FB-F+B|FC//$

Figure 1.19: A three-dimensional extension of the Hilbert curve [139]. Colors represent three-dimensional “frames” associated with symbols A (red), B (blue), C (green) and D (yellow).



As an example of a three-dimensional object created using an L-system, consider the extension of the Hilbert curve shown in Figure 1.19. The L-system was constructed with the node-replacement technique discussed in the previous section, using cubes and “macrocubes” instead of tiles and macrotiles.

## 1.6 Branching structures

According to the rules presented so far, the turtle interprets a character string as a sequence of line segments. Depending on the segment lengths and the angles between them, the resulting line is self-intersecting or not, can be more or less convoluted, and may have some segments drawn many times and others made invisible, but it always remains just a single line. However, the plant kingdom is dominated by branching structures; thus a mathematical description of tree-like shapes and methods for generating them are needed for modeling purposes. An axial tree [89, 117] complements the graph-theoretic notion of a rooted tree [108] with the botanically motivated notion of branch axis.

### 1.6.1 Axial trees

A *rooted tree* has edges that are labeled and directed. The edge sequences form paths from a distinguished node, called the *root* or *base*, to the *terminal nodes*. In the biological context, these edges are referred to as *branch segments*. A segment followed by at least one more segment in some path is called an *internode*. A terminal segment (with no succeeding edges) is called an *apex*.

An *axial tree* is a special type of rooted tree (Figure 1.20). At each of its nodes, at most one outgoing *straight* segment is distinguished. All remaining edges are called *lateral* or *side* segments. A sequence of segments is called an *axis* if:

- the first segment in the sequence originates at the root of the tree or as a lateral segment at some node,
- each subsequent segment is a straight segment, and
- the last segment is not followed by any straight segment in the tree.

Together with all its descendants, an axis constitutes a *branch*. A branch is itself an axial (sub)tree.

Axes and branches are ordered. The axis originating at the root of the entire plant has order zero. An axis originating as a lateral segment of an  $n$ -order parent axis has order  $n + 1$ . The order of a branch is equal to the order of its lowest-order or *main* axis.

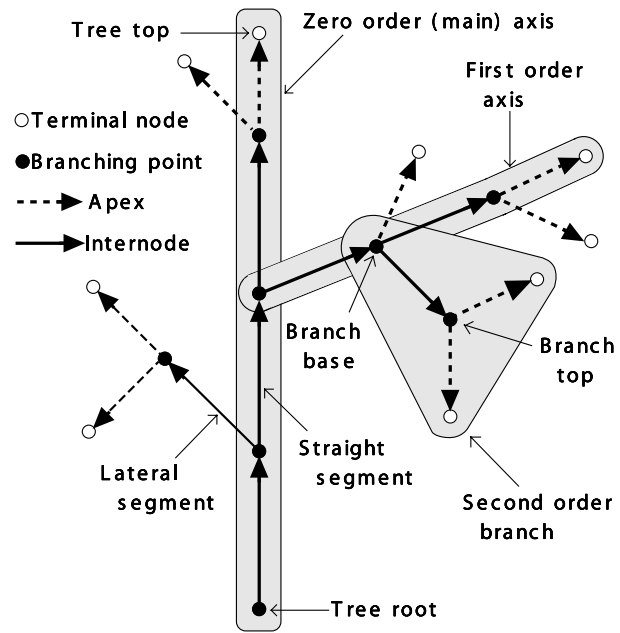


Figure 1.20: An axial tree

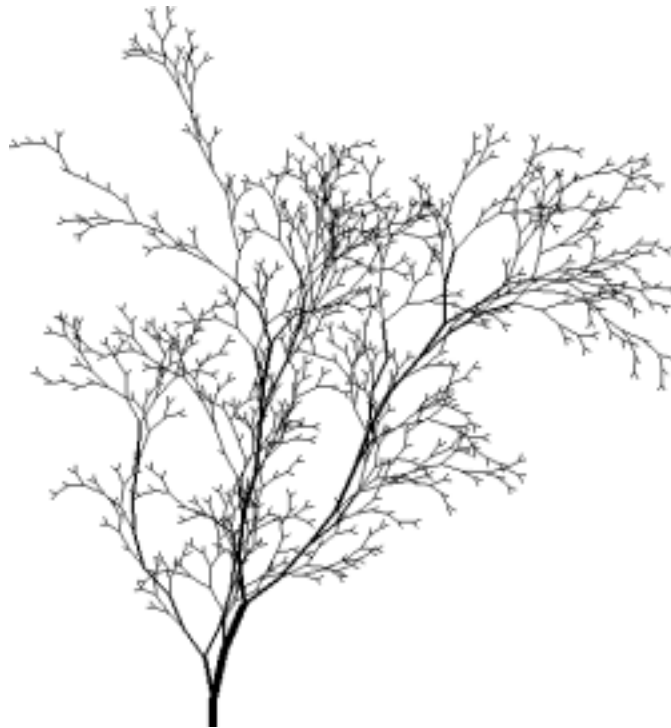


Figure 1.21: Sample tree generated using a method based on Horton–Strahler analysis of branching patterns

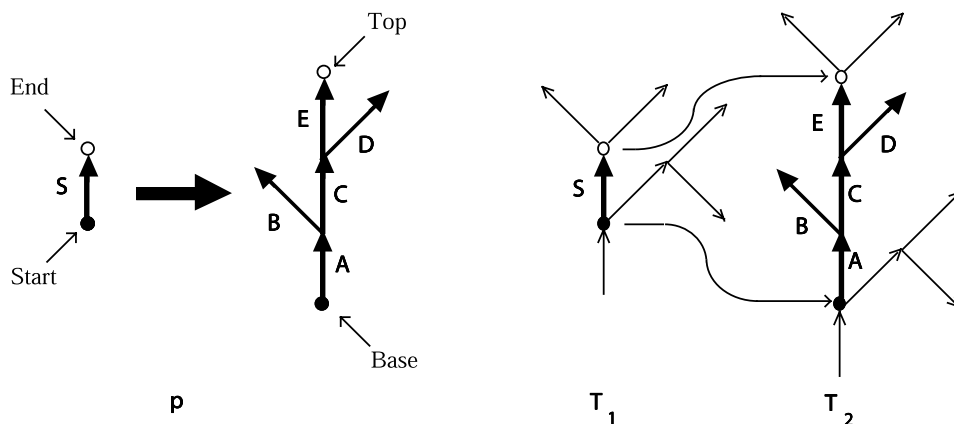


Figure 1.22: A tree production  $p$  and its application to the edge  $S$  in a tree  $T_1$

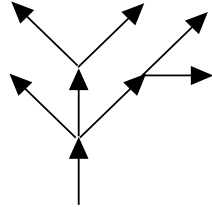
Axial trees are purely topological objects. The geometric connotation of such terms as straight segment, lateral segment and axis should be viewed at this point as an intuitive link between the graph-theoretic formalism and real plant structures.

The proposed scheme for ordering branches in axial trees was introduced originally by Gravelius [53]. MacDonald [94, pages 110–121] surveys this and other methods applicable to biological and geographical data such as stream networks. Of special interest are methods proposed by Horton [70, 71] and Strahler, which served as a basis for synthesizing botanical trees [37, 152] (Figure 1.21).

### 1.6.2 Tree OL-systems

In order to model development of branching structures, a rewriting mechanism can be used that operates directly on axial trees. A rewriting rule, or *tree production*, replaces a predecessor edge by a successor axial tree in such a way that the starting node of the predecessor is identified with the successor's base and the ending node is identified with the successor's top (Figure 1.22).

A *tree OL-system*  $G$  is specified by three components: a set of edge labels  $V$ , an initial tree  $\omega$  with labels from  $V$ , and a set of tree productions  $P$ . Given the L-system  $G$ , an axial tree  $T_2$  is directly derived from a tree  $T_1$ , noted  $T_1 \Rightarrow T_2$ , if  $T_2$  is obtained from  $T_1$  by simultaneously replacing each edge in  $T_1$  by its successor according to the production set  $P$ . A tree  $T$  is generated by  $G$  in a derivation of length  $n$  if there exists a sequence of trees  $T_0, T_1, \dots, T_n$  such that  $T_0 = \omega, T_n = T$  and  $T_0 \Rightarrow T_1 \Rightarrow \dots \Rightarrow T_n$ .



$F[+F][-F[-F]F]F[+F][-F]$

Figure 1.23: Bracketed string representation of an axial tree

### 1.6.3 Bracketed OL-systems

The definition of tree L-systems does not specify the data structure for representing axial trees. One possibility is to use a list representation with a tree topology. Alternatively, axial trees can be represented using *strings with brackets* [82]. A similar distinction can be observed in Koch constructions, which can be implemented either by rewriting edges and polygons or their string representations. An extension of turtle interpretation to strings with brackets and the operation of bracketed L-systems [109, 111] are described below.

Two new symbols are introduced to delimit a branch. They are interpreted by the turtle as follows:

*Stack operations*

- [ Push the current state of the turtle onto a pushdown stack. The information saved on the stack contains the turtle's position and orientation, and possibly other attributes such as the color and width of lines being drawn.
- ] Pop a state from the stack and make it the current state of the turtle. No line is drawn, although in general the position of the turtle changes.

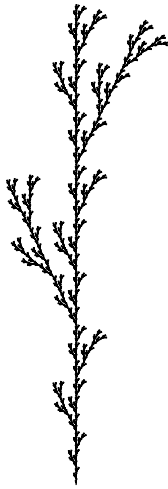
An example of an axial tree and its string representation are shown in Figure 1.23.

*2D structures*

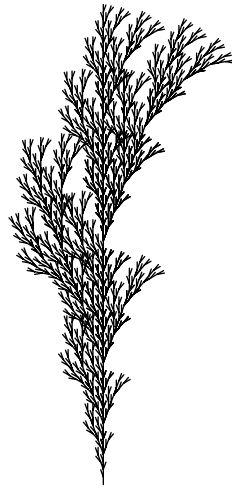
Derivations in bracketed OL-systems proceed as in OL-systems without brackets. The brackets replace themselves. Examples of two-dimensional branching structures generated by bracketed OL-systems are shown in Figure 1.24.

*Bush-like structure*

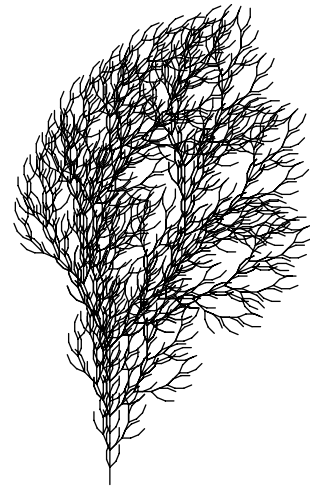
Figure 1.25 is an example of a three-dimensional bush-like structure generated by a bracketed L-system. Production  $p_1$  creates three new branches from an apex of the old branch. A branch consists of an edge  $F$  forming the initial internode, a leaf  $L$  and an apex  $A$  (which will subsequently create three new branches). Productions  $p_2$  and  $p_3$



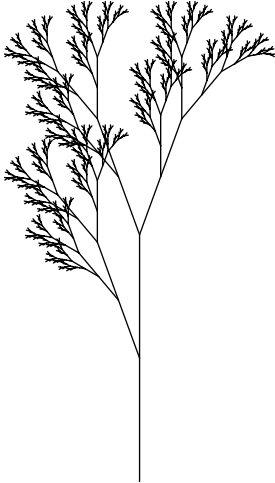
**a**  
 $n=5, \delta=25.7^\circ$   
 $F$   
 $F \rightarrow F [+F] F [-F] F$



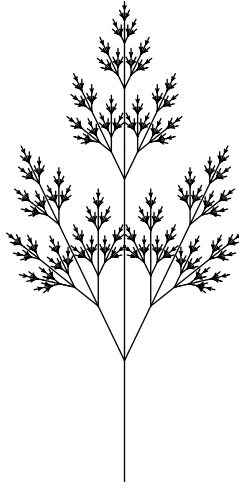
**b**  
 $n=5, \delta=20^\circ$   
 $F$   
 $F \rightarrow F [+F] F [-F] [F]$



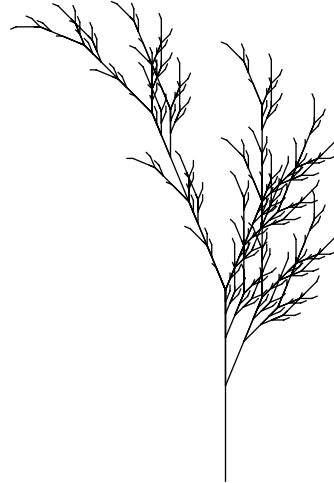
**c**  
 $n=4, \delta=22.5^\circ$   
 $F$   
 $F \rightarrow FF - [-F+F+F] +$   
 $[+F-F-F]$



**d**  
 $n=7, \delta=20^\circ$   
 $X$   
 $X \rightarrow F [+X] F [-X] + X$   
 $F \rightarrow FF$



**e**  
 $n=7, \delta=25.7^\circ$   
 $X$   
 $X \rightarrow F [+X] [-X] FX$   
 $F \rightarrow FF$



**f**  
 $n=5, \delta=22.5^\circ$   
 $X$   
 $X \rightarrow F - [[X] + X] + F [+FX] - X$   
 $F \rightarrow FF$

Figure 1.24: Examples of plant-like structures generated by bracketed OL-systems. L-systems (a), (b) and (c) are edge-rewriting, while (d), (e) and (f) are node-rewriting.



$n=7, \delta=22.5^\circ$

$\omega : A$   
 $p_1 : A \rightarrow [ \&FL!A ] // // // ' [ \&FL!A ] // // // // ' [ \&FL!A ]$   
 $p_2 : F \rightarrow S // // // F$   
 $p_3 : S \rightarrow F L$   
 $p_4 : L \rightarrow [ ' ' ' \wedge \wedge \{ -f+f+f- | -f+f+f \} ]$

Figure 1.25: A three-dimensional bush-like structure

specify internode growth. In subsequent derivation steps the internode gets longer and acquires new leaves. This violates a biological rule of *subapical growth* (discussed in detail in Chapter 3), but produces an acceptable visual effect in a still picture. Production  $p_4$  specifies the leaf as a filled polygon with six edges. Its boundary is formed from the edges  $f$  enclosed between the braces  $\{$  and  $\}$  (see Chapter 5 for further discussion). The symbols  $!$  and  $'$  are used to decrement the diameter of segments and increment the current index to the color table, respectively.

*Plant  
with flowers*

Another example of a three-dimensional plant is shown in Figure 1.26. The L-system can be described and analyzed in a way similar to the previous one.



## 1.7 Stochastic L-systems

All plants generated by the same deterministic L-system are identical. An attempt to combine them in the same picture would produce a striking, artificial regularity. In order to prevent this effect, it is necessary to introduce specimen-to-specimen variations that will preserve the general aspects of a plant but will modify its details.

Variation can be achieved by randomizing the turtle interpretation, the L-system, or both. Randomization of the interpretation alone has a limited effect. While the geometric aspects of a plant — such as the stem lengths and branching angles — are modified, the underlying topology remains unchanged. In contrast, stochastic application of productions may affect both the topology and the geometry of the plant. The following definition is similar to that of Yokomori [162] and Eichhorst and Savitch [35].

*L-system*

A *stochastic OL-system* is an ordered quadruplet  $G_\pi = \langle V, \omega, P, \pi \rangle$ . The alphabet  $V$ , the axiom  $\omega$  and the set of productions  $P$  are defined as in an OL-system (page 4). Function  $\pi : P \rightarrow (0, 1]$ , called the *probability distribution*, maps the set of productions into the set of *production probabilities*. It is assumed that for any letter  $a \in V$ , the sum of probabilities of all productions with the predecessor  $a$  is equal to 1.

*Derivation*

We will call the derivation  $\mu \Rightarrow \nu$  a *stochastic derivation* in  $G_\pi$  if for each *occurrence* of the letter  $a$  in the word  $\mu$  the probability of applying production  $p$  with the predecessor  $a$  is equal to  $\pi(p)$ . Thus, different productions with the same predecessor can be applied to various occurrences of the same letter in one derivation step.

*Example*

A simple example of a stochastic L-system is given below.

$$\begin{aligned} \omega &: F \\ p_1 &: F \xrightarrow{.33} F[+F]F[-F]F \\ p_2 &: F \xrightarrow{.33} F[+F]F \\ p_3 &: F \xrightarrow{.34} F[-F]F \end{aligned}$$

The production probabilities are listed above the derivation symbol  $\rightarrow$ . Each production can be selected with approximately the same probability of 1/3. Examples of branching structures generated by this L-system with derivations of length 5 are shown in Figure 1.27. Note that these structures look like different specimens of the same (albeit fictitious) plant species.

*Flower field*

A more complex example is shown in Figure 1.28. The field consists of four rows and four columns of plants. All plants are generated by a stochastic modification of the L-system used to generate Figure 1.26.



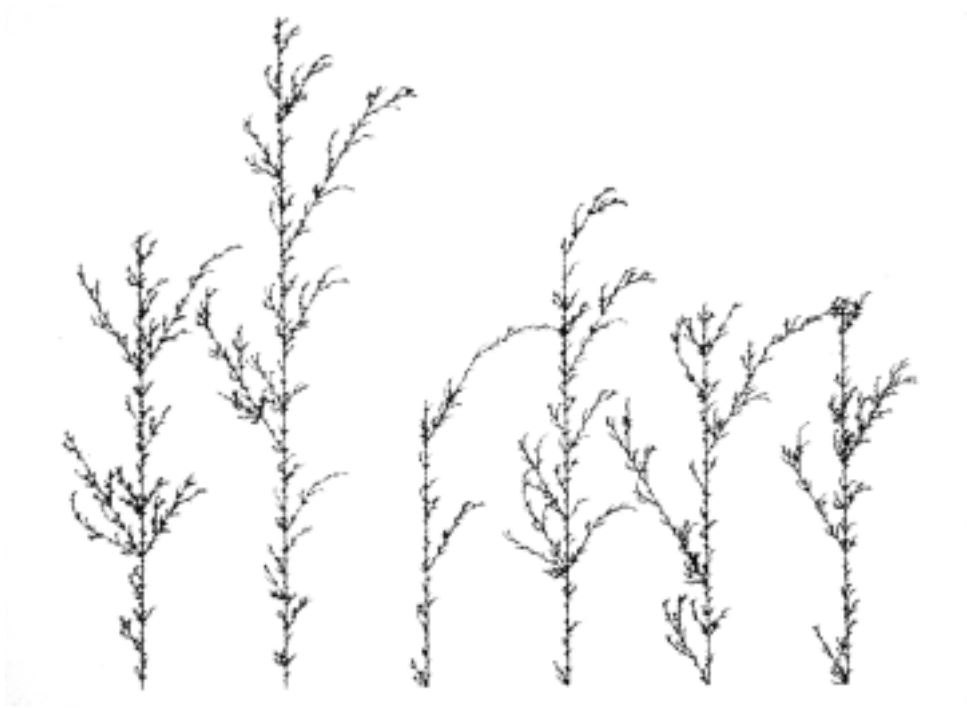


Figure 1.27: Stochastic branching structures



Figure 1.28: Flower field

The essence of this modification is to replace the original production  $p_3$  by the following three productions:

$$\begin{aligned} p'_3 &: \text{seg} \xrightarrow{.33} \text{seg} [ // \& \& \text{leaf} ] [ // \wedge \wedge \text{leaf} ] F \text{seg} \\ p''_3 &: \text{seg} \xrightarrow{.33} \text{seg} F \text{seg} \\ p'''_3 &: \text{seg} \xrightarrow{.34} \text{seg} \end{aligned}$$

Thus, in any step of the derivation, the stem segment **seg** may either grow and produce new leaves (production  $p'_3$ ), grow without producing new leaves (production  $p''_3$ ), or not grow at all (production  $p'''_3$ ). All three events occur with approximately the same probability. The resulting field appears to consist of various specimens of the same plant species. If the same L-system was used again (with different seed values for the random number generator), a variation of this image would be obtained.

## 1.8 Context-sensitive L-systems

*Context in  
string  
L-systems*

Productions in OL-systems are context-free; i.e. applicable regardless of the context in which the predecessor appears. However, production application may also depend on the predecessor's context. This effect is useful in simulating interactions between plant parts, due for example to the flow of nutrients or hormones. Various context-sensitive extensions of L-systems have been proposed and studied thoroughly in the past [62, 90, 128]. *2L-systems* use productions of the form  $a_l < a > a_r \rightarrow \chi$ , where the letter  $a$  (called the *strict predecessor*) can produce word  $\chi$  if and only if  $a$  is preceded by letter  $a_l$  and followed by  $a_r$ . Thus, letters  $a_l$  and  $a_r$  form the left and the right *context* of  $a$  in this production. Productions in *1L-systems* have one-sided context only; consequently, they are either of the form  $a_l < a \rightarrow \chi$  or  $a > a_r \rightarrow \chi$ . OL-systems, 1L-systems and 2L-systems belong to a wider class of *IL-systems*, also called *(k,l)-systems*. In a (k,l)-system, the left context is a word of length  $k$  and the right context is a word of length  $l$ .

In order to keep specifications of L-systems short, the usual notion of IL-systems has been modified here by allowing productions with different context lengths to coexist within a single system. Furthermore, context-sensitive productions are assumed to have precedence over context-free productions with the same strict predecessor. Consequently, if a context-free and a context-sensitive production both apply to a given letter, the context-sensitive one should be selected. If no production applies, this letter is replaced by itself as previously assumed for OL-systems.

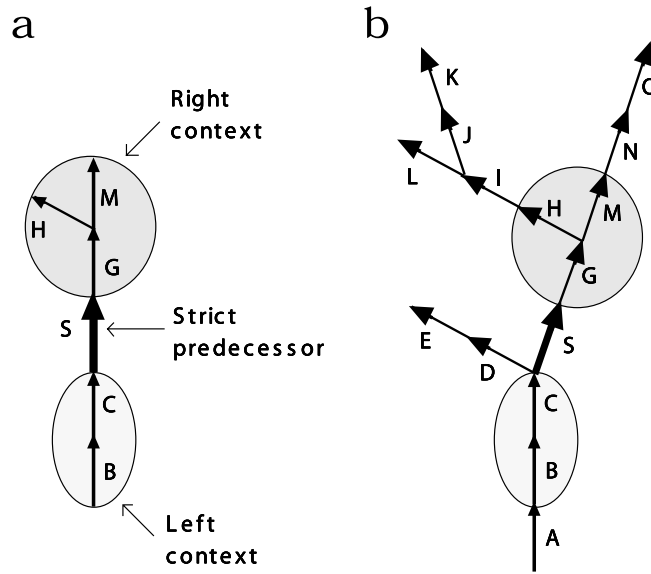


Figure 1.29: The predecessor of a context-sensitive tree production (a) matches edge  $S$  in a tree  $T$  (b)

The following sample 1L-system makes use of context to simulate signal propagation throughout a string of symbols:

*Signal propagation*

$$\begin{aligned} \omega &: baaaaaaaa \\ p_1 &: b < a \rightarrow b \\ p_2 &: \quad b \rightarrow a \end{aligned}$$

The first few words generated by this L-system are given below:

*baaaaaaaaa*  
*abaaaaaaaa*  
*aabaaaaaaaa*  
*aaabaaaaaaaa*  
*aaaabaaaaaa*  
 ...

The letter  $b$  moves from the left side to the right side of the string.

A context-sensitive extension of tree L-systems requires neighbor edges of the replaced edge to be tested for context matching. A predecessor of a context-sensitive production  $p$  consists of three components: a path  $l$  forming the left context, an edge  $S$  called the strict predecessor, and an axial tree  $r$  constituting the right context (Figure 1.29). The asymmetry between the left context and the right context reflects the fact that there is only one path from the root of a tree to a given edge, while there can be many paths from this edge to various terminal nodes. Production  $p$  matches a given occurrence of the edge  $S$  in a tree  $T$  if  $l$  is a path in  $T$  terminating at the starting node of  $S$ , and  $r$  is a subtree

*Context in tree L-systems*

of  $T$  originating at the ending node of  $S$ . The production can then be applied by replacing  $S$  with the axial tree specified as the production successor.

The introduction of context to bracketed L-systems is more difficult than in L-systems without brackets, because the bracketed string representation of axial trees does not preserve segment neighborhood. Consequently, the context matching procedure may need to skip over symbols representing branches or branch portions. For example, Figure 1.29 indicates that a production with the predecessor  $BC < S > G[H]M$  can be applied to symbol  $S$  in the string

$$ABC[DE][SG[HI[JK]L]MNO],$$

which involves skipping over symbols  $[DE]$  in the search for left context, and  $I[JK]L$  in the search for right context.

Within the formalism of bracketed L-systems, the left context can be used to simulate control signals that propagate *acropetally*, *i.e.*, from the root or basal leaves towards the apices of the modeled plant, while the right context represents signals that propagate *basipetally*, *i.e.*, from the apices towards the root. For example, the following 1L-system simulates propagation of an acropetal signal in a branching structure that does not grow:

$$\begin{aligned} \#ignore &: +- \\ \omega &: F_b[+F_a]F_a[-F_a]F_a[+F_a]F_a \\ p_1 &: F_b < F_a \rightarrow F_b \end{aligned}$$

Symbol  $F_b$  represents a segment already reached by the signal, while  $F_a$  represents a segment that has not yet been reached. The  $\#ignore$  statement indicates that the geometric symbols  $+$  and  $-$  should be considered as non-existent while context matching. Images representing consecutive stages of signal propagation (corresponding to consecutive words generated by the L-system under consideration) are shown in Figure 1.30a.

The propagation of a basipetal signal can be simulated in a similar way (Figure 1.30b):

$$\begin{aligned} \#ignore &: +- \\ \omega &: F_a[+F_a]F_a[-F_a]F_a[+F_a]F_b \\ p_1 &: F_a > F_b \rightarrow F_b \end{aligned}$$

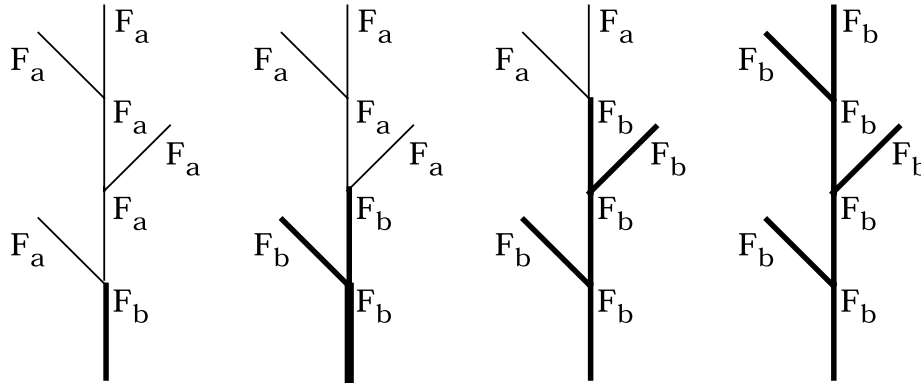
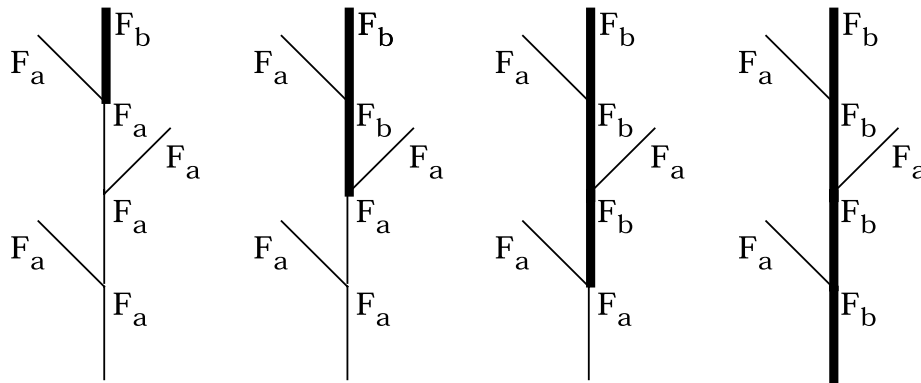
**a****b**

Figure 1.30: Signal propagation in a branching structure: (a) acropetal, (b) basipetal

The operation of context-sensitive L-systems is examined further using examples obtained by Hogeweg and Hesper [64]. In 1974, they published the results of an exhaustive study of 3,584 patterns generated by a class of bracketed 2L-systems defined over the alphabet  $\{0,1\}$ . Some of these patterns had plant-like shapes. Subsequently, Smith significantly improved the quality of the generated images using state-of-the-art computer imagery techniques [136, 137]. Sample structures generated by L-systems similar to those proposed by Hogeweg and Hesper are shown in Figure 1.31. The differences are related to the geometric interpretation of the resulting strings. According to the original interpretation, consecutive branches are issued alternately to the left and right, whereas turtle interpretation requires explicit specification of branching angles within the L-system.

*L-systems of  
Hogeweg,  
Hesper and  
Smith*

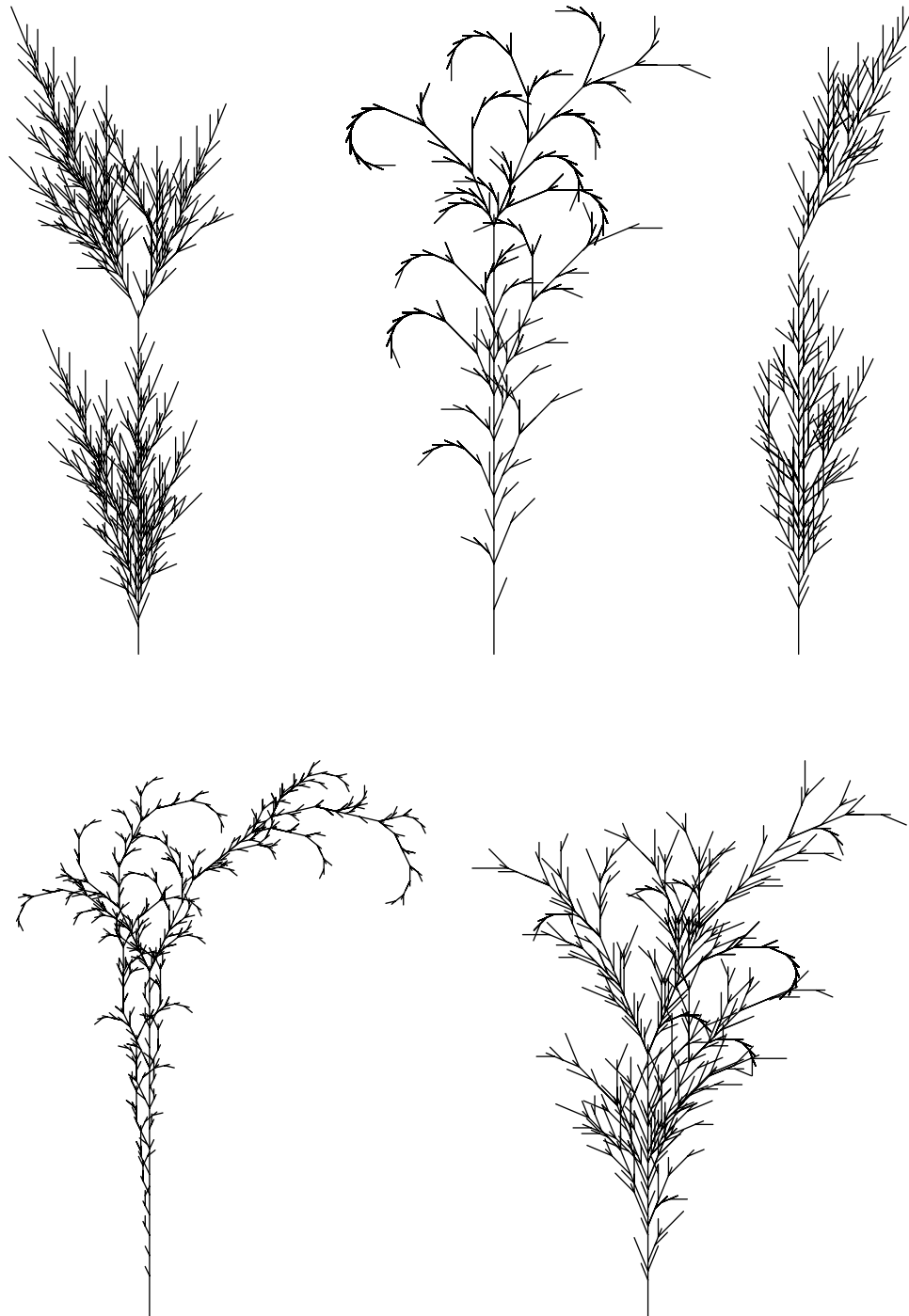


Figure 1.31: Examples of branching structures generated using L-systems based on the results of Hogeweg and Hesper [64]

- a**  $n=30, \delta=22.5^\circ$   
 #ignore: +-F  
 F1F1F1  
 $0 < 0 > 0 \rightarrow 0$   
 $0 < 0 > 1 \rightarrow 1[+F1F1]$   
 $0 < 1 > 0 \rightarrow 1$   
 $0 < 1 > 1 \rightarrow 1$   
 $1 < 0 > 0 \rightarrow 0$   
 $1 < 0 > 1 \rightarrow 1F1$   
 $1 < 1 > 0 \rightarrow 0$   
 $1 < 1 > 1 \rightarrow 0$   
 $* < + > * \rightarrow -$   
 $* < - > * \rightarrow +$
- b**  $n=30, \delta=22.5^\circ$   
 #ignore: +-F  
 F1F1F1  
 $0 < 0 > 0 \rightarrow 1$   
 $0 < 0 > 1 \rightarrow 1[-F1F1]$   
 $0 < 1 > 0 \rightarrow 1$   
 $0 < 1 > 1 \rightarrow 1$   
 $1 < 0 > 0 \rightarrow 0$   
 $1 < 0 > 1 \rightarrow 1F1$   
 $1 < 1 > 0 \rightarrow 1$   
 $1 < 1 > 1 \rightarrow 0$   
 $* < + > * \rightarrow -$   
 $* < - > * \rightarrow +$
- c**  $n=26, \delta=25.75^\circ$   
 #ignore: +-F  
 F1F1F1  
 $0 < 0 > 0 \rightarrow 0$   
 $0 < 0 > 1 \rightarrow 1$   
 $0 < 1 > 0 \rightarrow 0$   
 $0 < 1 > 1 \rightarrow 1[+F1F1]$   
 $1 < 0 > 0 \rightarrow 0$   
 $1 < 0 > 1 \rightarrow 1F1$   
 $1 < 1 > 0 \rightarrow 0$   
 $1 < 1 > 1 \rightarrow 0$   
 $* < - > * \rightarrow +$   
 $* < + > * \rightarrow -$
- d**  $n=24, \delta=25.75^\circ$   
 #ignore: +-F  
 F0F1F1  
 $0 < 0 > 0 \rightarrow 1$   
 $0 < 0 > 1 \rightarrow 0$   
 $0 < 1 > 0 \rightarrow 0$   
 $0 < 1 > 1 \rightarrow 1F1$   
 $1 < 0 > 0 \rightarrow 1$   
 $1 < 0 > 1 \rightarrow 1[+F1F1]$   
 $1 < 1 > 0 \rightarrow 1$   
 $1 < 1 > 1 \rightarrow 0$   
 $* < + > * \rightarrow -$   
 $* < - > * \rightarrow +$
- e**  $n=26, \delta=22.5^\circ$   
 #ignore: +-F  
 F1F1F1  
 $0 < 0 > 0 \rightarrow 0$   
 $0 < 0 > 1 \rightarrow 1[-F1F1]$   
 $0 < 1 > 0 \rightarrow 1$   
 $0 < 1 > 1 \rightarrow 1$   
 $1 < 0 > 0 \rightarrow 0$   
 $1 < 0 > 1 \rightarrow 1F1$   
 $1 < 1 > 0 \rightarrow 1$   
 $1 < 1 > 1 \rightarrow 0$   
 $* < + > * \rightarrow -$   
 $* < - > * \rightarrow +$

Figure 1.31 (continued): L-systems of Hogeweg and Hesper

## 1.9 Growth functions

*Exponential  
growth*

During the synthesis of a plant model it is often convenient to distinguish productions that specify the branching pattern from those that describe elongation of plant segments. This separation can be observed in some of the L-systems considered so far. For example, in L-systems (d), (e) and (f) from Figure 1.24 the first productions capture the branching patterns, while the remaining productions, equal in all cases to  $F \rightarrow FF$ , describe elongation of segments represented by sequences of symbols  $F$ . The number of letters  $F$  in a string  $\chi_n$  originating from a single letter  $F$  is doubled in each derivation step, thus the elongation is exponential, with  $\text{length}(\chi_n) = 2^n$ .

*Basic  
properties*

A function that describes the number of symbols in a word in terms of its derivation length is called a *growth function*. The theory of L-systems contains an extensive body of results on growth functions [62, 127]. The central observation is that the growth functions of DOL-systems are independent of the letter ordering in the productions and derived words. Consequently, the relation between the number of letter occurrences in a pair of words  $\mu$  and  $\nu$ , such that  $\mu \Rightarrow \nu$ , can be conveniently expressed using matrix notation.

Let  $G = \langle V, \omega, P \rangle$  be a DOL-system and assume that letters of the alphabet  $V$  have been ordered,  $V = \{a_1, a_2, \dots, a_m\}$ . Construct a square matrix  $Q_{m \times m}$ , where entry  $q_{ij}$  is equal to the number of occurrences of letter  $a_j$  in the successor of the production with predecessor  $a_i$ . Let  $\underline{a}_i^k$  denote the number of occurrences of letter  $a_i$  in the word  $x$  generated by  $G$  in a derivation of length  $k$ . The definition of direct derivation in a DOL-system implies that

$$\begin{bmatrix} \underline{a}_1^k & \underline{a}_2^k & \cdots & \underline{a}_m^k \end{bmatrix} \begin{bmatrix} q_{11} & q_{12} & \cdots & q_{1m} \\ q_{21} & q_{22} & \cdots & q_{2m} \\ \vdots & & & \\ q_{m1} & q_{m2} & \cdots & q_{mm} \end{bmatrix} = \begin{bmatrix} \underline{a}_1^{k+1} & \underline{a}_2^{k+1} & \cdots & \underline{a}_m^{k+1} \end{bmatrix}.$$

This matrix notation is useful in the analysis of growth functions. For example, consider the following L-system:

$$\begin{aligned} \omega &: a \\ p_1 &: a \rightarrow ab \\ p_2 &: b \rightarrow a \end{aligned} \tag{1.2}$$

The relationship between the number of occurrences of letters  $a$  and  $b$  in two consecutively derived words is

$$\begin{bmatrix} \underline{a}^k & \underline{b}^k \end{bmatrix} \begin{bmatrix} 1 & 1 \\ 1 & 0 \end{bmatrix} = \begin{bmatrix} \underline{a}^{k+1} & \underline{b}^{k+1} \end{bmatrix}$$



or

$$\underline{a}^{k+1} = \underline{a}^k + \underline{b}^k = \underline{a}^k + \underline{a}^{k-1}$$

for  $k = 1, 2, 3, \dots$ . From the axiom it follows that  $\underline{a}^0 = 1$  and  $\underline{a}^1 = \underline{b}^0 = 0$ . Thus, the number of letters  $a$  in the strings generated by the L-system specified in equation (1.2) grows according to the Fibonacci series:  $1, 1, 2, 3, 5, 8, \dots$ . This growth function was implemented by productions  $p_2$  and  $p_3$  in the L-system generating the bush in Figure 1.25 (page 26) to describe the elongation of its internodes.

Polynomial growth functions of arbitrary degree can be obtained using L-systems of the following form:

*Polynomial growth*

$$\begin{aligned} \omega &: a_0 \\ p_1 &: a_0 \rightarrow a_0a_1 \\ p_2 &: a_1 \rightarrow a_1a_2 \\ p_3 &: a_2 \rightarrow a_2a_3 \\ p_4 &: a_3 \rightarrow a_3a_4 \\ &\vdots \end{aligned}$$

The matrix  $Q$  is given below:

$$Q = \begin{bmatrix} 1 & 1 & 0 & 0 & \cdots \\ 0 & 1 & 1 & 0 & \cdots \\ 0 & 0 & 1 & 1 & \cdots \\ 0 & 0 & 0 & 1 & \cdots \\ & & & \vdots & \end{bmatrix}$$

Thus, for any  $i, k \geq 1$ , the number  $\underline{a}_i^k$  of occurrences of symbol  $a_i$  in the string generated in a derivation of length  $k$  satisfies the equality

$$\underline{a}_i^k + \underline{a}_{i+1}^k = \underline{a}_{i+1}^{k+1}.$$

Taking into consideration the axiom, the distribution of letters  $a_i$  as a function of the derivation length is captured by the following table (only non-zero terms are shown):

$k$	$\underline{a}_0^k$	$\underline{a}_1^k$	$\underline{a}_2^k$	$\underline{a}_3^k$	$\underline{a}_4^k$	$\underline{a}_5^k$	$\underline{a}_6^k$	$\underline{a}_7^k$
0	1							
1	1	1						
2	1	2	1					
3	1	3	3	1				
4	1	4	6	4	1			
5	1	5	10	10	5	1		
6	1	6	15	20	15	6	1	
7	1	7	21	35	35	21	7	1
				$\vdots$				

This table represents the Pascal triangle, thus for any  $k \geq i \geq 1$  its terms satisfy the following equality:

$$\underline{a}_i^k = \binom{k}{i} = \frac{k(k-1)\cdots(k-i+1)}{1 \cdot 2 \cdots i}$$

Consequently, the number of occurrences of letter  $a_i$  as a function of the derivation length  $k$  is expressed by a polynomial of degree  $i$ . By identifying letter  $a_i$  with the turtle symbol  $F$ , it is possible to model internode elongation expressed by polynomials of arbitrary degree  $i \geq 0$ . This observation was generalized by Szilard [140], who developed an algorithm for constructing a DOL-system with growth functions specified by any positive, nondecreasing polynomials with integer coefficients [62, page 276].

### Characterization

The examples of growth functions considered so far include exponential and polynomial functions. Rozenberg and Salomaa [127, pages 30–38] show that, in general, the growth function  $f_G(n)$  of any DOL-system  $G = \langle V, \omega, P \rangle$  is a combination of polynomial and exponential functions:

$$f_G(n) = \sum_{i=1}^s P_i(n) \rho_i^n \quad \text{for } n \geq n_0, \quad (1.3)$$

where  $P_i(n)$  denotes a polynomial with integer coefficients,  $\rho_i$  is a non-negative integer, and  $n_0$  is the total number of letters in the alphabet  $V$ . Unfortunately, many growth processes observed in nature cannot be described by equation (1.3). Two approaches are then possible within the framework of the theory of L-systems.

### Sigmoidal growth

The first is to extend the size  $n_0$  of the alphabet  $V$ , so that the growth process of interest will be captured by the initial derivation steps,  $\omega = \mu_0 \Rightarrow \mu_1 \Rightarrow \cdots \Rightarrow \mu_{n_0}$ , before equation (1.3) starts to apply. For example, the L-system

$$\begin{aligned} \omega &: a_0 \\ p_i &: a_i \rightarrow a_{i+1} b_0 \quad \text{for } i < k \\ p_{k+j} &: b_j \rightarrow b_{j+1} F \quad \text{for } j < l \end{aligned} \quad (1.4)$$

over the alphabet  $V = \{a_0, a_1, \dots, a_k\} \cup \{b_0, b_1, \dots, b_l\} \cup \{F\}$  can be used to approximate a sigmoidal elongation of a segment represented by a sequence of symbols  $F$  (Figure 1.32). The term *sigmoidal* refers to a function with a plot in the shape of the letter S. Such functions are commonly found in biological processes [143], with the initial part of the curve representing the growth of a young organism, and the latter part corresponding to the organism close to its final size.

### Square-root growth

The second approach to the synthesis of growth functions outside the class captured by equation (1.3) is to use context-sensitive L-systems. For example, the following 2L-system has a growth function given by  $f_G(n) = \lfloor \sqrt{n} \rfloor + 4$ , where  $\lfloor x \rfloor$  is the floor function.

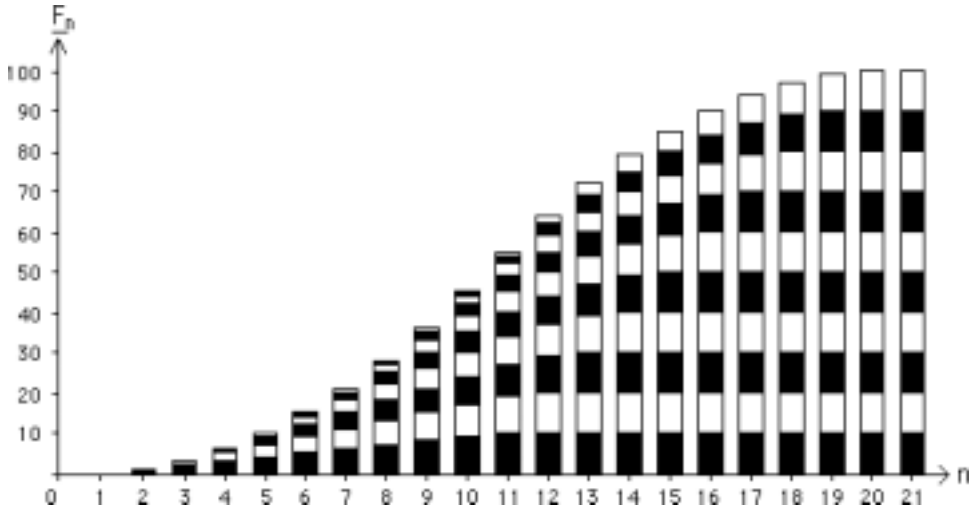


Figure 1.32: A sigmoidal growth function implemented using the L-system in equation (1.4), for  $k = l = 20$

$$\begin{aligned}
 \omega &: XF_uF_aX \\
 p_1 &: F_u < F_a > F_a \rightarrow F_u \\
 p_2 &: F_u < F_a > X \rightarrow F_dF_a \\
 p_3 &: F_a < F_a > F_d \rightarrow F_d \\
 p_4 &: X < F_a > F_d \rightarrow F_u \\
 p_5 &: F_u \rightarrow F_a \\
 p_6 &: F_d \rightarrow F_a
 \end{aligned}
 \tag{1.5}$$

The operation of this L-system is illustrated in Figure 1.33. Productions  $p_1$  and  $p_3$ , together with  $p_5$  and  $p_6$ , propagate symbols  $F_u$  and  $F_d$  up and down the string of symbols  $\mu$ . Productions  $p_2$  and  $p_4$  change the propagation direction, after symbol  $X$  marking a string end has been reached by  $F_u$  or  $F_d$ , respectively. In addition,  $p_2$  extends the string with a symbol  $F_a$ . Thus, the number of derivation steps increases by two between consecutive applications of production  $p_2$ . As a result, string extension occurs at derivation steps  $n$  expressed by the square of the string length, which yields the growth function  $\lfloor \sqrt{n} \rfloor + 4$ .

In practice it is often difficult, if not impossible, to find L-systems with the required growth functions. Vitányi [153] illustrates this by referring to sigmoidal curves:

*Limitations*

If we want to obtain sigmoidal growth curves with the original L-systems then not even the introduction of cell interaction can help us out. In the first place, we end up constructing quite unlikely flows of messages through the organism, which are more suitable to electronic computers, and in fact give the organism universal computing power. Secondly, and this is more fundamental, we can not obtain

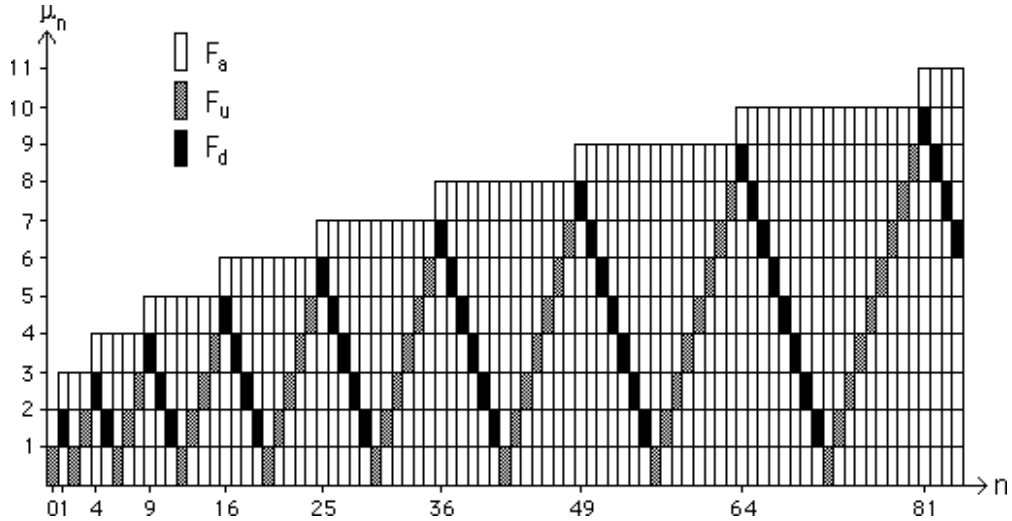


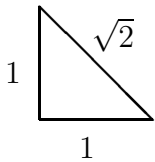
Figure 1.33: Square-root growth implemented using the L-system specified in equation (1.5)

growth which, always increasing the size of the organism, tends towards stability in the limit. The slowest increasing growth we can obtain by allowing cell interaction is logarithmic and thus can not at all account for the asymptotic behavior of sigmoidal growth functions.

In the next section we present an extension of L-systems that makes it possible to avoid this problem by allowing for explicit inclusion of growth functions into L-system specifications.

### 1.10 Parametric L-systems

*Motivation*



Although L-systems with turtle interpretation make it possible to generate a variety of interesting objects, from abstract fractals to plant-like branching structures, their modeling power is quite limited. A major problem can be traced to the reduction of all lines to integer multiples of the unit segment. As a result, even such a simple figure as an isosceles right-angled triangle cannot be traced exactly, since the ratio of its hypotenuse length to the length of a side is expressed by the irrational number  $\sqrt{2}$ . Rational approximation of line length provides only a limited solution, because the unit step must be the smallest common denominator of all line lengths in the modeled structure. Consequently, the representation of a simple plant module, such as an internode, may require a large number of symbols. The same argument applies to angles. Problems become even more pronounced while simulating changes to the modeled structure over time, since some growth functions cannot be expressed conveniently using L-systems. Generally, it is difficult

to capture continuous phenomena, since the obvious technique of discretizing continuous values may require a large number of quantization levels, yielding L-systems with hundreds of symbols and productions. Consequently, model specification becomes difficult, and the mathematical beauty of L-systems is lost.

In order to solve similar problems, Lindenmayer proposed that numerical parameters be associated with L-system symbols [83]. He illustrated this idea by referring to the continuous development of branching structures and diffusion of chemical compounds in a nonbranching filament of *Anabaena catenula*. Both problems were revisited in later papers [25, 77]. A definition of parametric L-systems was formulated by Prusinkiewicz and Hanan [113] and is presented below.

### 1.10.1 Parametric OL-systems

Parametric L-systems operate on *parametric words*, which are strings of *modules* consisting of *letters* with associated *parameters*. The letters belong to an *alphabet*  $V$ , and the parameters belong to the set of *real numbers*  $\mathfrak{R}$ . A module with letter  $A \in V$  and parameters  $a_1, a_2, \dots, a_n \in \mathfrak{R}$  is denoted by  $A(a_1, a_2, \dots, a_n)$ . Every module belongs to the set  $M = V \times \mathfrak{R}^*$ , where  $\mathfrak{R}^*$  is the set of all finite sequences of parameters. The set of all strings of modules and the set of all nonempty strings are denoted by  $M^* = (V \times \mathfrak{R}^*)^*$  and  $M^+ = (V \times \mathfrak{R}^*)^+$ , respectively.

The real-valued *actual* parameters appearing in the words correspond with *formal* parameters used in the specification of L-system productions. If  $\Sigma$  is a set of formal parameters, then  $C(\Sigma)$  denotes a *logical expression* with parameters from  $\Sigma$ , and  $E(\Sigma)$  is an *arithmetic expression* with parameters from the same set. Both types of expressions consist of formal parameters and numeric constants, combined using the arithmetic operators  $+$ ,  $-$ ,  $*$ ,  $/$ ; the exponentiation operator  $\wedge$ , the relational operators  $<$ ,  $>$ ,  $=$ ; the logical operators  $!$ ,  $\&$ ,  $|$  (not, and, or); and parentheses  $()$ . Standard rules for constructing syntactically correct expressions and for operator precedence are observed. Relational and logical expressions evaluate to zero for false and one for true. A logical statement specified as the empty string is assumed to have value one. The sets of all correctly constructed logical and arithmetic expressions with parameters from  $\Sigma$  are noted  $\mathcal{C}(\Sigma)$  and  $\mathcal{E}(\Sigma)$ .

A *parametric OL-system* is defined as an ordered quadruplet  $G = \langle V, \Sigma, \omega, P \rangle$ , where

- $V$  is the *alphabet* of the system,
- $\Sigma$  is the *set of formal parameters*,
- $\omega \in (V \times \mathfrak{R}^*)^+$  is a nonempty parametric word called the *axiom*,
- $P \subset (V \times \Sigma^*) \times \mathcal{C}(\Sigma) \times (V \times \mathcal{E}(\Sigma))^*$  is a finite *set of productions*.

*Parametric words*

*Expressions*

*Parametric OL-system*

The symbols  $:$  and  $\rightarrow$  are used to separate the three components of a production: the *predecessor*, the *condition* and the *successor*. For example, a production with predecessor  $A(t)$ , condition  $t > 5$  and successor  $B(t + 1)CD(t \wedge 0.5, t - 2)$  is written as

$$A(t) : t > 5 \rightarrow B(t + 1)CD(t \wedge 0.5, t - 2). \quad (1.6)$$

### Derivation

A production *matches* a module in a parametric word if the following conditions are met:

- the letter in the module and the letter in the production predecessor are the same,
- the number of actual parameters in the module is equal to the number of formal parameters in the production predecessor, and
- the condition evaluates to *true* if the actual parameter values are substituted for the formal parameters in the production.

A matching production can be *applied* to the module, creating a string of modules specified by the production successor. The actual parameter values are substituted for the formal parameters according to their position. For example, production (1.6) above matches a module  $A(9)$ , since the letter  $A$  in the module is the same as in the production predecessor, there is one actual parameter in the module  $A(9)$  and one formal parameter in the predecessor  $A(t)$ , and the logical expression  $t > 5$  is true for  $t = 9$ . The result of the application of this production is a parametric word  $B(10)CD(3, 7)$ .

If a module  $a$  produces a parametric word  $\chi$  as the result of a production application in an L-system  $G$ , we write  $a \mapsto \chi$ . Given a parametric word  $\mu = a_1a_2\dots a_m$ , we say that the word  $\nu = \chi_1\chi_2\dots\chi_m$  is *directly derived* from (or *generated* by)  $\mu$  and write  $\mu \Longrightarrow \nu$  if and only if  $a_i \mapsto \chi_i$  for all  $i = 1, 2, \dots, m$ . A parametric word  $\nu$  is generated by  $G$  in a *derivation of length  $n$*  if there exists a sequence of words  $\mu_0, \mu_1, \dots, \mu_n$  such that  $\mu_0 = \omega$ ,  $\mu_n = \nu$  and  $\mu_0 \Longrightarrow \mu_1 \Longrightarrow \dots \Longrightarrow \mu_n$ .

### Example

An example of a parametric L-system is given below.

$$\begin{aligned} \omega &: B(2)A(4, 4) \\ p_1 &: A(x, y) : y \leq 3 \rightarrow A(x * 2, x + y) \\ p_2 &: A(x, y) : y > 3 \rightarrow B(x)A(x/y, 0) \\ p_3 &: B(x) : x < 1 \rightarrow C \\ p_4 &: B(x) : x \geq 1 \rightarrow B(x - 1) \end{aligned} \quad (1.7)$$

As in the case of non-parametric L-systems, it is assumed that a module replaces itself if no matching production is found in the set  $P$ . The words obtained in the first few derivation steps are shown in Figure 1.34.

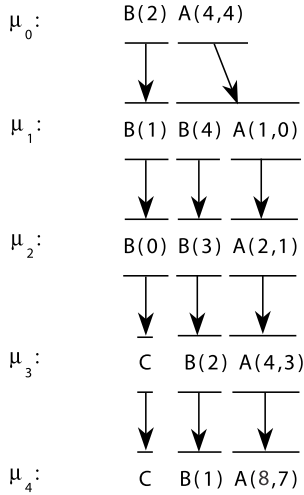


Figure 1.34: The initial sequence of strings generated by the parametric L-system specified in equation (1.7)

### 1.10.2 Parametric 2L-systems

Productions in parametric OL-systems are context-free, *i.e.*, applicable regardless of the context in which the predecessor appears. A context-sensitive extension is necessary to model information exchange between neighboring modules. In the parametric case, each component of the production predecessor (the left context, the strict predecessor and the right context) is a parametric word with letters from the alphabet  $V$  and formal parameters from the set  $\Sigma$ . Any formal parameters may appear in the condition and the production successor.

A sample context-sensitive production is given below:

$$A(x) < B(y) > C(z) : x + y + z > 10 \rightarrow E((x + y)/2)F((y + z)/2)$$

It can be applied to the module  $B(5)$  that appears in a parametric word

$$\dots A(4)B(5)C(6)\dots \tag{1.8}$$

since the sequence of letters  $A, B, C$  in the production and in parametric word (1.8) are the same, the numbers of formal parameters and actual parameters coincide, and the condition  $4 + 5 + 6 > 10$  is true. As a result of the production application, the module  $B(5)$  will be replaced by a pair of modules  $E(4.5)F(5.5)$ . Naturally, the modules  $A(4)$  and  $C(6)$  will be replaced by other productions in the same derivation step.

Parametric 2L-systems provide a convenient tool for expressing developmental models that involve diffusion of substances throughout an organism. A good example is provided by an extended model of the pattern of cells observed in *Anabaena catenula* and other blue-green bacteria [99]. This model was proposed by de Koster and Lindenmayer [25].

*Example*

*Anabaena with heterocysts*

```

#define CH 900 /* high concentration */
#define CT 0.4 /* concentration threshold */
#define ST 3.9 /* segment size threshold */
#include H /* heterocyst shape specification */
#ignore f ~ H

 $\omega$  : -(90)F(0,0,CH)F(4,1,CH)F(0,0,CH)
 $p_1$  : F(s,t,c) : t=1 & s>=6 →
      F(s/3*2,2,c)f(1)F(s/3,1,c)
 $p_2$  : F(s,t,c) : t=2 & s>=6 →
      F(s/3,2,c)f(1)F(s/3*2,1,c)
 $p_3$  : F(h,i,k) < F(s,t,c) > F(o,p,r) : s>ST|c>CT →
      F(s+.1,t,c+0.25*(k+r-3*c))
 $p_4$  : F(h,i,k) < F(s,t,c) > F(o,p,r) : !(s>ST|c>CT) →
      F(0,0,CH) ~ H(1)
 $p_5$  : H(s) : s<3 → H(s*1.1)

```

L-system 1.1: *Anabaena catenula*

Generally, the bacteria under consideration form a nonbranching filament consisting of two classes of cells: *vegetative cells* and *heterocysts*. Usually, the vegetative cells divide and produce two daughter vegetative cells. This mechanism is captured by the L-system specified in equation (1.1) and Figure 1.4 (page 5). However, in some cases the vegetative cells differentiate into heterocysts. Their distribution forms a well-defined pattern, characterized by a relatively constant number of vegetative cells separating consecutive heterocysts. How does the organism maintain constant spacing of heterocysts while growing? The model explains this phenomenon using a biologically well-motivated hypothesis that heterocyst distribution is regulated by nitrogen compounds produced by the heterocysts, transported from cell to cell across the filament, and decayed in the vegetative cells. If the compound's concentration in a young vegetative cell falls below a specific level, this cell differentiates into a heterocyst (L-system 1.1).

The `#define` statements assign values to numerical constants used in the L-system. The `#include` statement specifies the shape of a heterocyst (a disk) by referring to a library of predefined shapes (see Section 5.1). Cells are represented by modules  $F(s, t, c)$ , where  $s$  stands for cell length,  $t$  is cell type (0 - heterocyst, 1 and 2 - vegetative types<sup>1</sup>),

<sup>1</sup>The model of *Anabaena* introduced in Section 1.2 distinguished between four types of cells:  $a_r$ ,  $b_r$ ,  $a_l$  and  $b_l$ . Cells  $b$  do not divide and can be considered as young forms of the corresponding cells  $a$ . Thus, the vegetative type 1 considered here embraces cells  $a_r$  and  $b_r$ , while type 2 embraces  $a_l$  and  $b_l$ . The formal relationship between the four-cell and two-cell models is further discussed in Chapter 6.



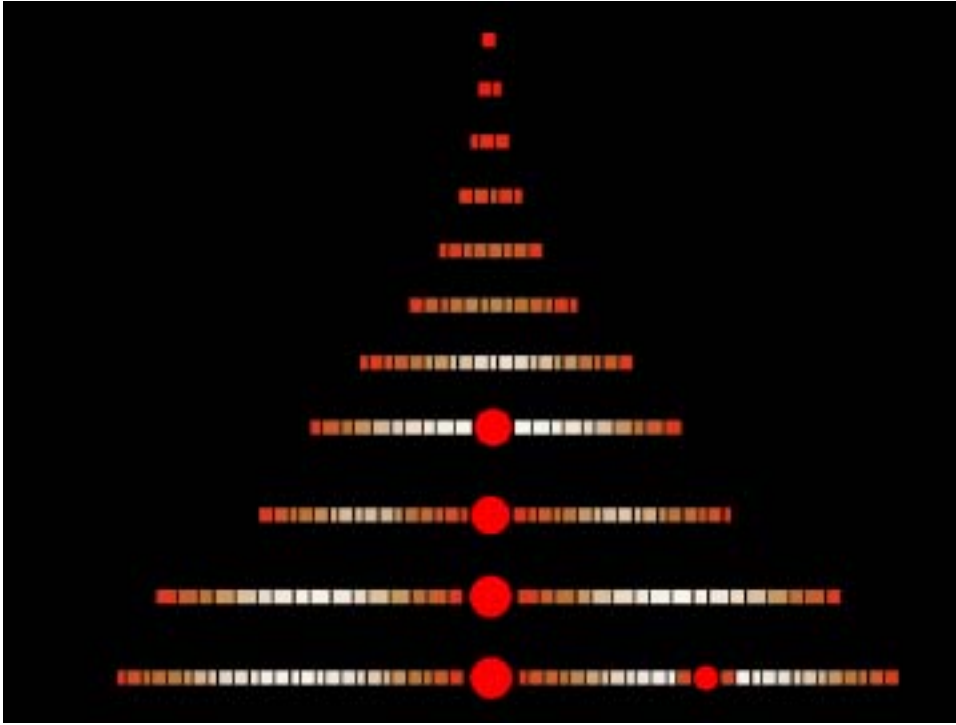


Figure 1.35: Development of *Anabaena catenula* with heterocysts, simulated using parametric L-system 1.1

and  $c$  represents the concentration of nitrogen compounds. Productions  $p_1$  and  $p_2$  describe division of the vegetative cells. They each create two daughter cells of unequal length. The difference between cells of type 1 and 2 lies in the ordering of the long and short daughter cells. Production  $p_3$  captures the processes of transportation and decay of the nitrogen compounds. Their concentration  $c$  is related to the concentration in the neighboring cells  $k$  and  $r$ , and changes in each derivation step according to the formula

$$c' = c + 0.25(k + r - 3 * c).$$

Production  $p_4$  describes differentiation of a vegetative cell into a heterocyst. The condition specifies that this process occurs when the cell length does not exceed the threshold value  $ST = 3.9$  (which means that the cell is young enough), and the concentration of the nitrogen compounds falls below the threshold value  $CT = 0.4$ . Production  $p_5$  describes the subsequent growth of the heterocyst.

Snapshots of the developmental sequence of *Anabaena* are given in Figure 1.35. The vegetative cells are shown as rectangles, colored according to the concentration of the nitrogen compounds (white means low concentration). The heterocysts are represented as red disks. The values of parameters  $CH$ ,  $CT$  and  $ST$  were selected to provide the

correct distribution of the heterocysts, and correspond closely to the values reported in [25]. The mathematical model made it possible to estimate these parameters, although they are not directly observable.

### 1.10.3 Turtle interpretation of parametric words

If one or more parameters are associated with a symbol interpreted by the turtle, the value of the first parameter controls the turtle's state. If the symbol is not followed by any parameter, default values specified outside the L-system are used as in the non-parametric case. The basic set of symbols affected by the introduction of parameters is listed below.

- $F(a)$  Move forward a step of length  $a > 0$ . The position of the turtle changes to  $(x', y', z')$ , where  $x' = x + a\vec{H}_x$ ,  $y' = y + a\vec{H}_y$  and  $z' = z + a\vec{H}_z$ . A line segment is drawn between points  $(x, y, z)$  and  $(x', y', z')$ .
- $f(a)$  Move forward a step of length  $a$  without drawing a line.
- $+(a)$  Rotate around  $\vec{v}$  by an angle of  $a$  degrees. If  $a$  is positive, the turtle is turned to the left and if  $a$  is negative, the turn is to the right.
- $\&(a)$  Rotate around  $\vec{l}$  by an angle of  $a$  degrees. If  $a$  is positive, the turtle is pitched down and if  $a$  is negative, the turtle is pitched up.
- $/(a)$  Rotate around  $\vec{h}$  by an angle of  $a$  degrees. If  $a$  is positive, the turtle is rolled to the right and if  $a$  is negative, it is rolled to the left.

It should be noted that symbols  $+$ ,  $\&$ ,  $\wedge$ , and  $/$  are used both as letters of the alphabet  $V$  and as operators in logical and arithmetic expressions. Their meaning depends on the context.

*Row of trees*

The following examples illustrate the operation of parametric L-systems with turtle interpretation. The first L-system is a coding of a Koch construction generating a variant of the snowflake curve (Figure 1.1 on page 2). The initiator (production predecessor) is the hypotenuse  $AB$  of a right triangle  $ABC$  (Figure 1.36). The first and the fourth edge of the generator subdivide  $AB$  into segments  $AD$  and  $DB$ , while the remaining two edges traverse the altitude  $CD$  in opposite directions. From elementary geometry it follows that the lengths of these segments satisfy the equations

$$q = c - p \quad \text{and} \quad h = \sqrt{pq}.$$

The edges of the generator can be associated with four triangles that are similar to  $ABC$  and tile it without gaps. According to the relationship between curve construction by edge rewriting and planar tilings

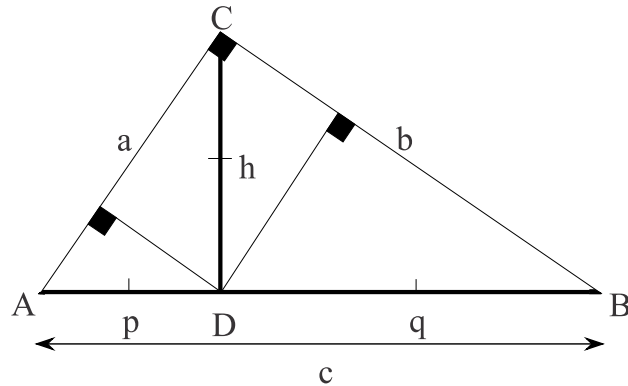


Figure 1.36: Construction of the generator for a “row of trees.” The edges are associated with triangles indicated by ticks.

(Section 1.4.1), the generated curve will approximately fill the triangle  $ABC$ . The corresponding L-system is given below:

```
#define c 1
#define p 0.3
#define q c - p
#define h (p * q) ^ 0.5
```

```
 $\omega : F(1)$ 
 $p_1 : F(x) \rightarrow F(x * p) + F(x * h) - -F(x * h) + F(x * q)$ 
```

The resulting curve is shown in Figure 1.37a. In order to better visualize its structure, the angle increment has been set to  $86^\circ$  instead of  $90^\circ$ . The curve fills different areas with unequal density. This results from the fact that all edges, whether long or short, are replaced by the generator in every derivation step. A modified curve that fills the underlying triangle in a more uniform way is shown in Figure 1.37b. It was obtained by delaying the rewriting of shorter segments with respect to the longer ones, as specified by the following L-system.

```
 $\omega : F(1, 0)$ 
 $p_1 : F(x, t) : t = 0 \rightarrow F(x * p, 2) + F(x * h, 1) -$ 
 $-F(x * h, 1) + F(x * q, 0)$ 
 $p_2 : F(x, t) : t > 0 \rightarrow F(x, t - 1)$ 
```

The next example makes use of node rewriting (Section 1.4.2). The construction recursively subdivides a rectangular tile  $ABCD$  into two tiles,  $AEFD$  and  $BCFE$ , similar to  $ABCD$  (Figure 1.38). The lengths of the edges form the proportion

$$\frac{a}{b} = \frac{b}{\frac{1}{2}a},$$

*Branching  
structure*

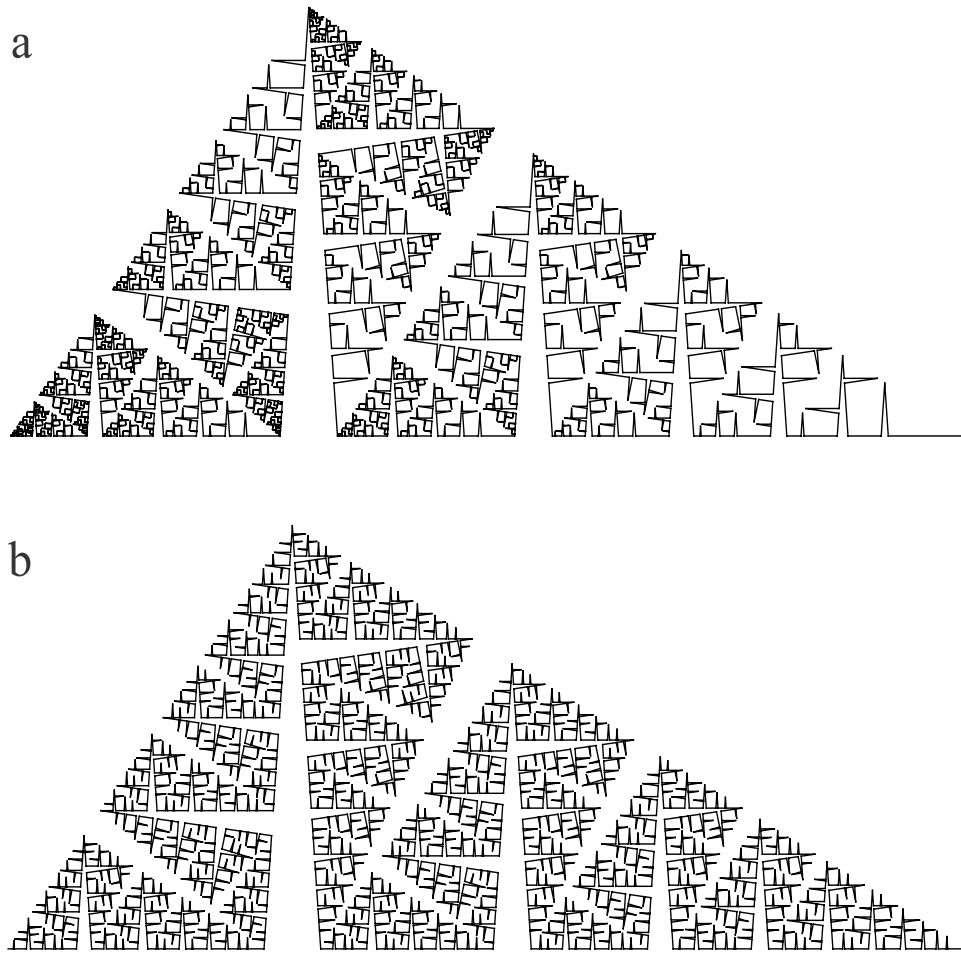


Figure 1.37: Two curves suggesting a “row of trees.” Curve (b) is from [95, page 57].

which implies that  $b = a/\sqrt{2}$ . Each tile is associated with a single-point frame lying in the tile center. The tiles are connected by a branching line specified by the following L-system:

$$\begin{aligned}
 \#define \quad R \quad 1.456 \\
 \omega : \quad A(1) \\
 p_1 : \quad A(s) \rightarrow F(s)[+A(s/R)][-A(s/R)]
 \end{aligned}
 \tag{1.9}$$

The ratio of branch sizes  $R$  slightly exceeds the theoretical value of  $\sqrt{2}$ . As a result, the branching structure shown in Figure 1.39 is self-avoiding. The angle increment was set arbitrarily to  $\delta = 85^\circ$ .

The L-system in equation (1.9) operates by appending segments of decreasing length to the structures obtained in previous derivation steps. Once a segment has been incorporated, its length does not change. A structure with identical proportions can be obtained by

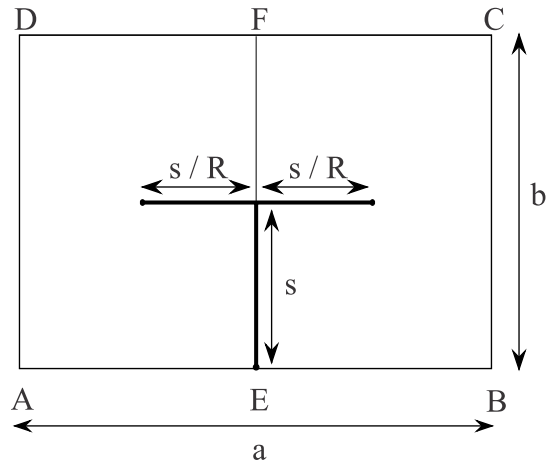


Figure 1.38: Tiling associated with a space-filling branching pattern

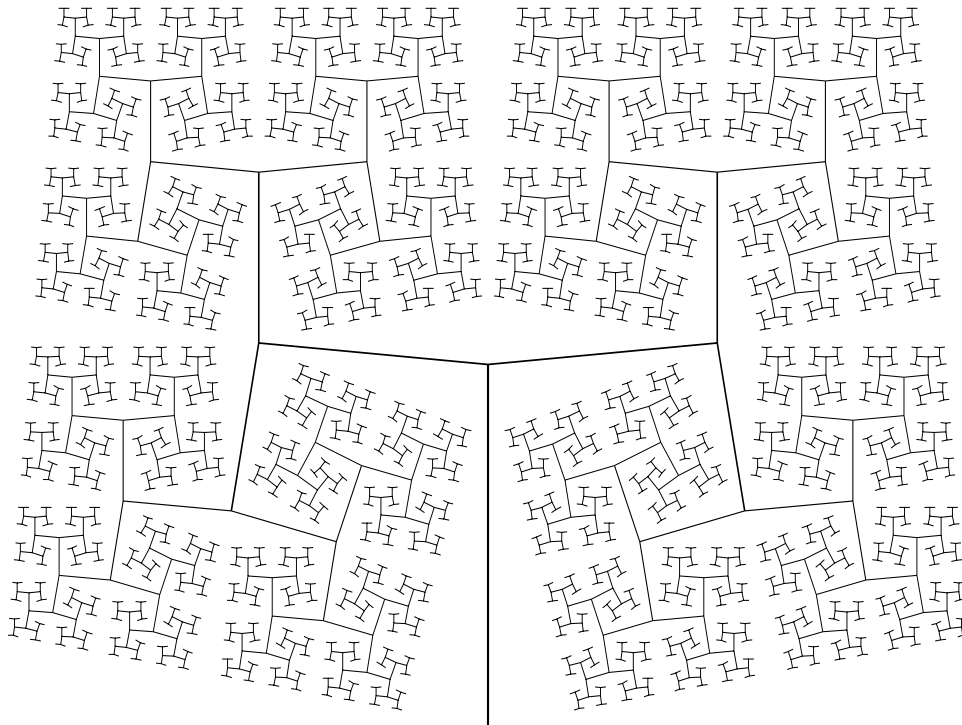


Figure 1.39: A branching pattern generated by the L-system specified in equation (1.9)

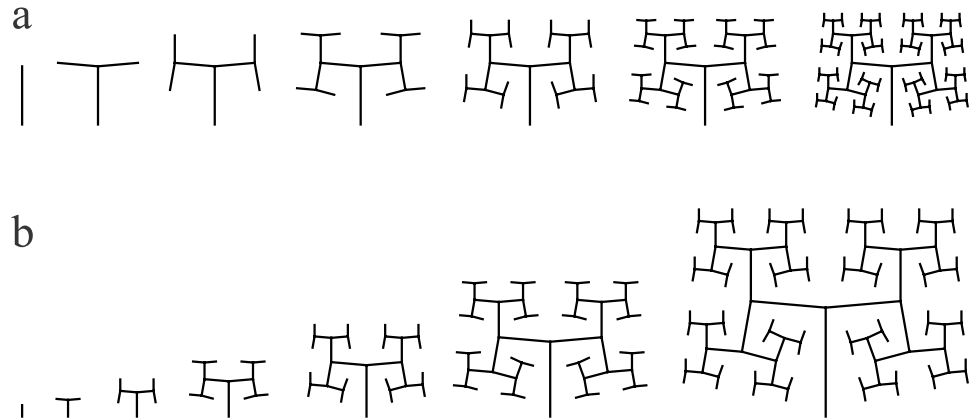


Figure 1.40: Initial sequences of figures generated by the L-systems specified in equations (1.9) and (1.10)

appending segments of constant length and increasing the lengths of previously created segments by constant  $R$  in each derivation step. The corresponding L-system is given below.

$$\begin{aligned}
 \omega &: A \\
 p_1 &: A \quad \rightarrow F(1)[+A][-A] \\
 p_2 &: F(s) \quad \rightarrow F(s * R)
 \end{aligned}
 \tag{1.10}$$

The initial sequence of structures obtained by both L-systems are compared in Figure 1.40. Sequence (a) emphasizes the fractal character of the resulting structure. Sequence (b) suggests the growth of a tree. The next two chapters show that this is not a mere coincidence, and the L-system specified in equation (1.10) is a simple, but in principle correct, developmental model of a *sympodial* branching pattern found in many herbaceous plants and trees.

# Chapter 2

## Modeling of trees

Computer simulation of branching patterns has a relatively long history. The first model was proposed by Ulam [149], (see also [138, pages 127–131]), and employed the concept of *cellular automata* that had been developed earlier by von Neumann and Ulam [156]. The branching pattern is created iteratively, starting with a single colored cell in a triangular grid, then coloring cells that touch one and only one vertex of a cell colored in the previous iteration step.

*Cellular-space models*

This basic idea gave rise to several extensions. Meinhardt [97, Chapter 15] substituted the triangular grid with a square one, and used the resulting cellular space to examine biological hypotheses related to the formation of net-like structures. In addition to pure branching patterns, his models capture the effect of branch reconnection or *anastomosis* that may take place between the veins of a leaf. Greene [54] extended cellular automata to three dimensions, and applied the resulting *voxel space automata* to simulate growth processes that react to the environment. For instance, Figure 2.1 presents the growth of a vine over a house. Cohen [15] simulated the development of a branching pattern using expansion rules that operate in a continuous “density field” rather than a discrete cellular or voxel space.

The common feature of these approaches is the emphasis on interactions between various elements of a growing structure, as well as the structure and the environment. Although interactions clearly influence the development of real plants, they also add to the complexity of the models. This may explain why simpler models, ignoring even such fundamental factors as collisions between branches, have been prevalent to date. The first model in that category was proposed by Honda [65] who studied the form of trees using the following assumptions (Figure 2.2).

*Honda’s model*

- Tree segments are straight and their girth is not considered.
- A mother segment produces two daughter segments through one branching process.



Figure 2.1: *Organic architecture* by Greene [54]

- The lengths of the two daughter segments are shortened by constant ratios,  $r_1$  and  $r_2$ , with respect to the mother segment.
- The mother segment and its two daughter segments are contained in the same *branch plane*. The daughter segments form constant *branching angles*,  $a_1$  and  $a_2$ , with respect to the mother branch.
- The branch plane is fixed with respect to the direction of gravity so as to be closest to a horizontal plane.<sup>1</sup> An exception is made for branches attached to the main trunk. In this case, a constant *divergence angle*  $\alpha$  between consecutively issued lateral segments is maintained (cf. Chapter 4).

By changing numerical parameters, Honda obtained a wide variety of tree-like shapes. With some improvements [38], his model was applied to investigate branching patterns of real trees [39, 66, 67, 68]. Subsequently, different rules for branching angles were proposed to capture the structure of trees in which planes of successive bifurcations are perpendicular to each other [69]. The results of Honda served as a basis for the tree models proposed by Aono and Kunii [2]. They suggested

---

<sup>1</sup>More formally, the line perpendicular to the mother segment and lying in the branch plane is horizontal.



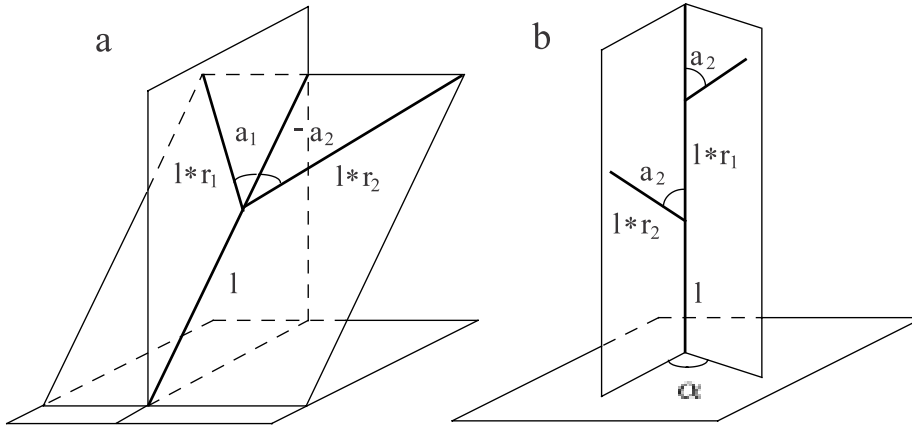


Figure 2.2: Specification of tree geometry according to Honda [65]

several extensions to his model, the most important of which was the biasing of branch positions in a particular direction, applied to produce the effects of wind, phototropism and gravity. A similar concept was introduced previously by Cohen [15], while more accurate physically-based methods for branch bending were developed by de Reffye [28] and Armstrong [4].

The models of Honda and Aono and Kunii were rendered using straight lines of constant or varying width to represent “tree skeletons.” A substantial improvement in the realism of synthetic images was achieved by Bloomenthal [11] and Oppenheimer [105], who introduced curved branches, carefully modeled surfaces around branching points, and textured bark and leaves (Figure 2.3).

The approaches stemming from the work of Honda defined branching structures using deterministic algorithms. In contrast, stochastic mechanisms are essential to the group of tree models proposed by Reeves and Blau [119], de Reffye *et al.* [30], and Remphrey, Neal and Steeves [120]. Although these models were described using different terminologies, they share the basic paradigm of specifying tree structures in terms of probabilities with which branches are formed. The work of Reeves and Blau aimed at producing tree-like shapes without delving into biological details of the modeled structures (Figure 2.4). In contrast, de Reffye *et al.* [29] used a stochastic approach to simulate the development of real plants by modeling the activity of buds at discrete time intervals. Given a clock signal, a bud can either:

- do nothing,
- become a flower,
- become an internode terminated by a new straight apex and one or more lateral apices subtended by leaves, or
- die and disappear.

*Realism*

*Stochastic models*

*Approach of de Reffye*



Figure 2.3: *Acer graphics* by Bloomenthal [11]



Figure 2.4: A forest scene by Reeves [119] ©1984 Pixar



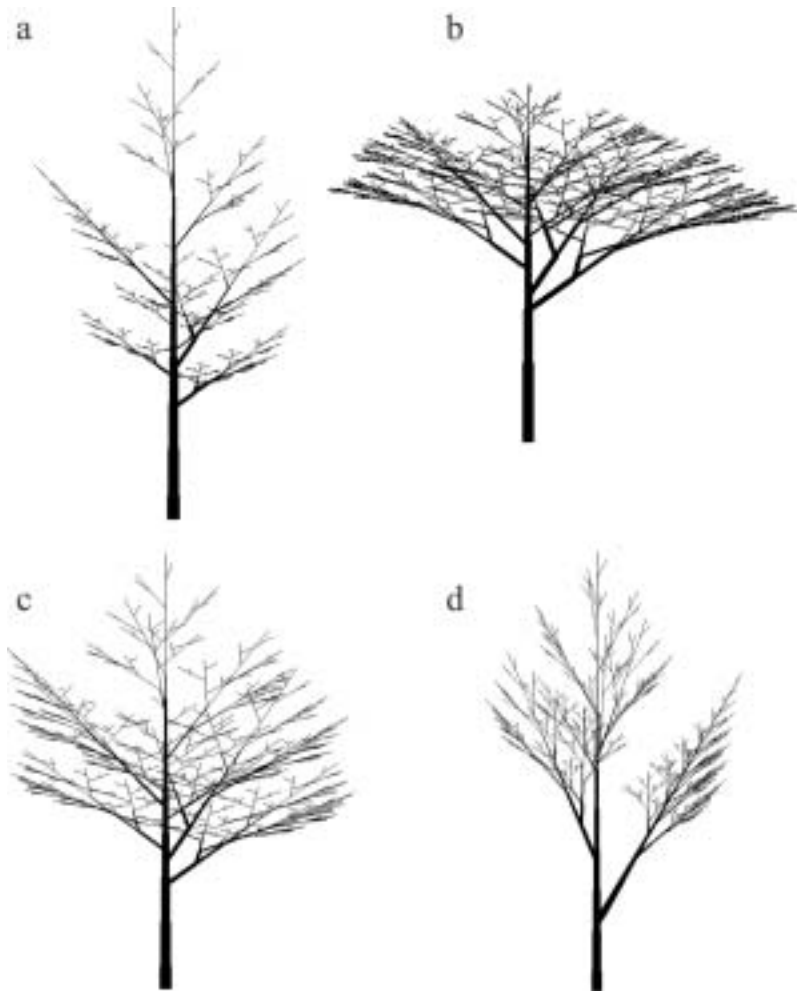
Figure 2.5: Oil palm tree canopy from CIRAD Modelisation Laboratory

These events occur according to stochastic laws characteristic for each variety and each species. The geometric parameters, such as the length and diameter of an internode, as well as branching angles, are also calculated according to stochastic laws.

The basic types of developmental rules incorporated into this method correspond to the 23 different types of tree architectures identified by Hallé, Oldeman and Tomlinson [58]. Detailed models of selected plant species were developed and are described in the literature [16, 20, 26, 27, 76]. A sample tree model is shown in Figure 2.5. The approach of Remphrey [120, 121, 122] is similar to that of de Reffye, except that larger time steps are used (one year in the model of bearberry described in [120]). Consequently, the stochastic rules must describe the entire configuration of lateral shoots that can be formed over a one-year period.

The application of L-systems to the generation of botanical trees was first considered by Aono and Kunii [2]. They referred to the original definition of L-systems [82] and found them unsuitable to model the complex branching patterns of higher plants. However, their arguments do not extend to parametric L-systems with turtle interpretation. For example, the L-system in Figure 2.6 implements those tree models of Honda [65] in which one of the branching angles is equal to 0, yielding a *monopodial* structure with clearly delineated main and lateral axes (see Section 3.2 for a formal characterization).

*Application of  
L-systems*



```

n = 10
#define r1 0.9    /* contraction ratio for the trunk */
#define r2 0.6    /* contraction ratio for branches */
#define a0 45     /* branching angle from the trunk */
#define a2 45     /* branching angle for lateral axes */
#define d 137.5  /* divergence angle */
#define w_r 0.707 /* width decrease rate */

ω : A(1,10)
p1 : A(1,w) : * → !(w)F(1) [&(a0)B(1*r2,w*w_r)]/(d)A(1*r1,w*w_r)
p2 : B(1,w) : * → !(w)F(1) [-(a2)$C(1*r2,w*w_r)]C(1*r1,w*w_r)
p3 : C(1,w) : * → !(w)F(1) [(a2)$B(1*r2,w*w_r)]B(1*r1,w*w_r)

```

Figure 2.6: Examples of the monopodial tree-like structures of Honda [65], generated using L-systems

According to production  $p_1$ , the apex of the main axis  $A$  produces an internode  $F$  and a lateral apex  $B$  in each derivation step. Constants  $r_1$  and  $r_2$  specify contraction ratios for the straight and lateral segments,  $a_0$  and  $a_2$  are branching angles and  $d$  is the divergence angle. Module  $!(w)$  sets the line width to  $w$ , thus production  $p_1$  decreases the width of the daughter segments with respect to the mother segment by the factor  $w_r = 0.707$ . This constant satisfies a postulate by Leonardo da Vinci [95, page 156], according to which “all the branches of a tree at every stage of its height when put together are equal in thickness to the trunk below them.” In the case where a mother branch of diameter  $w_1$  gives rise to two daughter branches of equal diameter  $w_2$ , this postulate yields the equation  $w_1^2 = 2w_2^2$ , which gives a value for  $w_r$  equal to  $w_2/w_1 = 1/\sqrt{2} \approx 0.707$ . A general discussion of the relationships between the diameters of the mother and daughter branches is included in the book by Macdonald [94, pages 131–135].

Productions  $p_2$  and  $p_3$  describe subsequent development of the lateral branches. In each derivation step, the straight apex (either  $B$  or  $C$ ) issues a lateral apex of the next order at angle  $a_2$  or  $-a_2$  with respect to the mother axis. Two productions are employed to create lateral apices alternately to the left and right. The symbol  $\$$  rolls the turtle around its own axis so that vector  $\vec{L}$  pointing to the left of the turtle (Section 1.5) is brought to a horizontal position. Consequently, the branch plane is “closest to a horizontal plane,” as required by Honda’s model. From a technical point of view,  $\$$  modifies the turtle orientation in space according to the formulae

$$\vec{L} = \frac{\vec{V} \times \vec{H}}{|\vec{V} \times \vec{H}|} \quad \text{and} \quad \vec{U} = \vec{H} \times \vec{L},$$

where vectors  $\vec{H}$ ,  $\vec{L}$  and  $\vec{U}$  are the heading, left and up vectors associated with the turtle,  $\vec{v}$  is the direction opposite to gravity, and  $|\vec{A}|$  denotes the length of vector  $\vec{A}$ . The tree-like structures shown in Figure 2.6 were generated using the values of constants listed in Table 2.1, and coincide with the structures presented by Honda.

Figure	$r_1$	$r_2$	$a_0$	$a_2$
a	0.9	0.6	45	45
b	0.9	0.9	45	45
c	0.9	0.8	45	45
d	0.9	0.7	30	-30

Table 2.1: Constants for the monopodial tree structures in Figure 2.6

*Monopodial branching*

*Branch width*

*Keeping turtle’s orientation*

*Sympodial  
branching*

A slightly different L-system, specified in Figure 2.7, captures *sympodial* structures, where both daughter segments form non-zero angles with the mother segment. In this case the activity of the main apex is reduced to the formation of the trunk  $F$  and a pair of lateral apices  $B$  (production  $p_1$ ). The subsequent branching pattern is captured by production  $p_2$ . The sample structures in Figure 2.7 were obtained using the constants listed in Table 2.2, and correspond to the models presented by Aono and Kunii.

The L-systems considered so far have been designed in a manner that emphasizes their relation to the models described in the literature. Specifically, all segments are assigned their final length at the time of creation, and no further elongation occurs. As pointed out in Section 1.10.3, similar structures can be obtained by creating new segments of constant length and increasing the lengths of previously created segments by a constant factor in each derivation step. A sample L-system constructed according to this paradigm is given in Figure 2.8.

*Ternary  
branching*

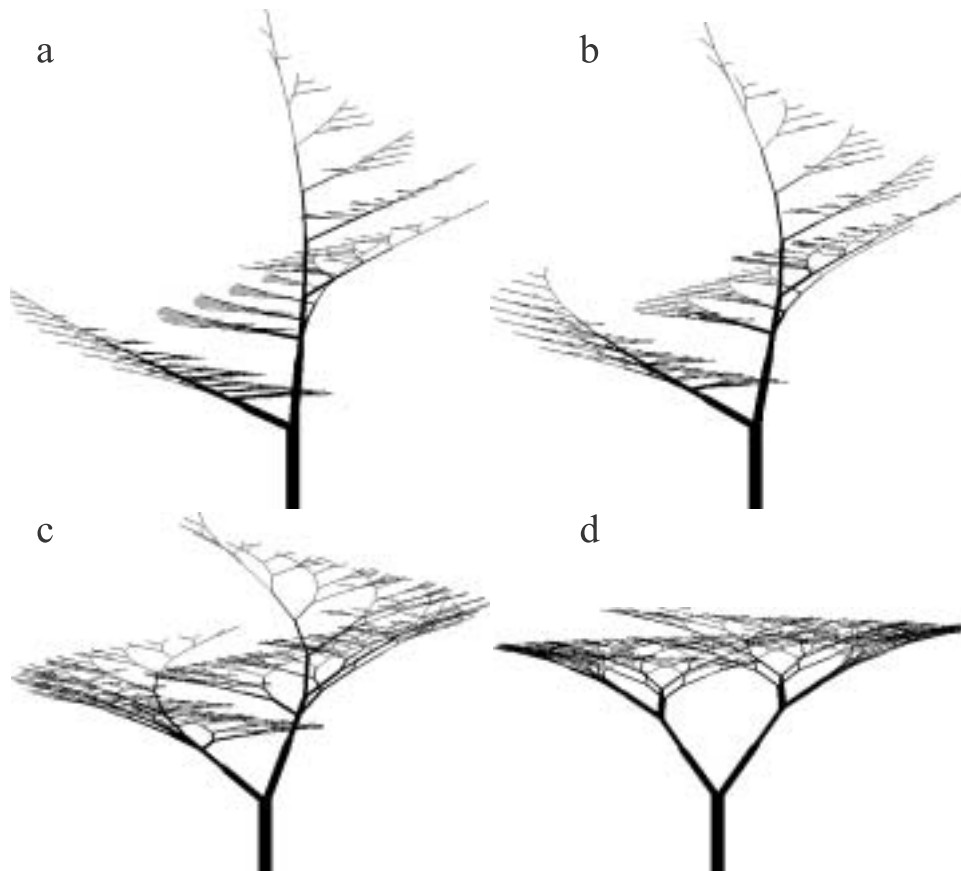
The overall structure of the tree is defined by production  $p_1$ . In each derivation step, apex  $A$  produces three new branches terminated by their own apices. Parameter  $w$  and constant  $v_r$  relate the width of the mother branch  $w_1$  to that of the daughter branches  $w_2$ . According to da Vinci's postulate  $w_1^2 = 3w_2^2$ , thus  $v_r = w_1/w_2 = \sqrt{3} \approx 1.732$ . Productions  $p_2$  and  $p_3$  capture the gradual elongation of branches and the increase in their diameter over time.

*Tropism*

The bending of branches is simulated by slightly rotating the turtle in the direction of a predefined *tropism vector*  $\vec{T}$  after drawing each segment (Figure 2.9). The orientation adjustment  $\alpha$  is calculated using the formula  $\alpha = e |\vec{H} \times \vec{T}|$ , where  $e$  is a parameter capturing axis susceptibility to bending. This heuristic formula has a physical motivation; if  $\vec{T}$  is interpreted as a force applied to the endpoint of vector  $\vec{H}$ , and  $\vec{H}$  can rotate around its starting point, the torque is equal to  $\vec{H} \times \vec{T}$ . The parameters relevant to the generation of the tree-like structures in Figure 2.8 are listed in Table 2.3. A more realistic rendering of the tree in Figure 2.8d is presented in Figure 2.10.

Figure	$r_1$	$r_2$	$a_1$	$a_2$
a	0.9	0.7	5	65
b	0.9	0.7	10	60
c	0.9	0.8	20	50
d	0.9	0.8	35	35

Table 2.2: Constants for the sympodial tree structures in Figure 2.7



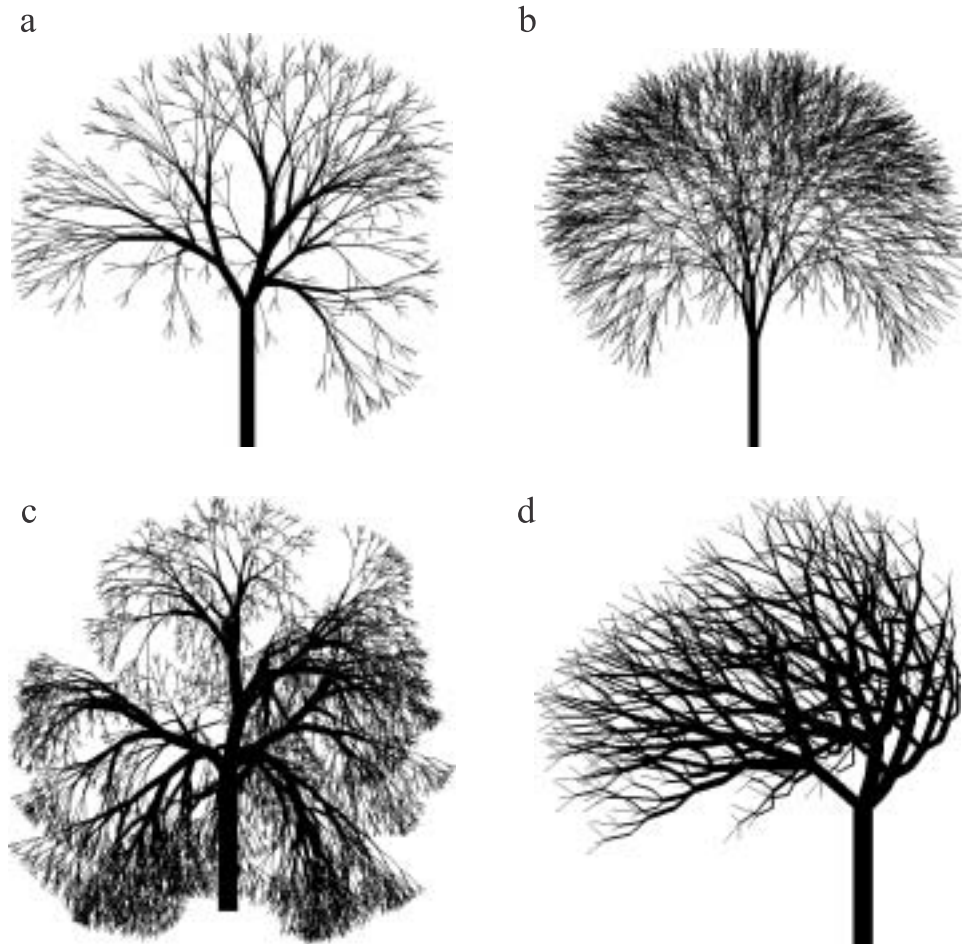
```

n = 10
#define r1 0.9 /* contraction ratio 1 */
#define r2 0.7 /* contraction ratio 2 */
#define a1 10 /* branching angle 1 */
#define a2 60 /* branching angle 2 */
#define wr 0.707 /* width decrease rate */

ω : A(1,10)
p1 : A(l,w) : * → !(w)F(l) [&(a1)B(l*r1,w*wr)]
      / (180) [&(a2)B(l*r2,w*wr)]
p2 : B(l,w) : * → !(w)F(l) [+ (a1)$B(l*r1,w*wr)]
      [- (a2)$B(l*r2,w*wr)]

```

Figure 2.7: Examples of the symphydial tree-like structures of Aono and Kunii [2], generated using L-systems



```

#define d1 94.74      /* divergence angle 1 */
#define d2 132.63   /* divergence angle 2 */
#define a 18.95       /* branching angle */
#define lr 1.109    /* elongation rate */
#define vr 1.732    /* width increase rate */

ω : !(1)F(200)/(45)A
p1 : A : * → !(vr)F(50) [&(a)F(50)A]/(d1)
      [&(a)F(50)A]/(d2) [&(a)F(50)A]
p2 : F(1) : * → F(1*lr)
p3 : !(w) : * → !(w*vr)

```

Figure 2.8: Examples of tree-like structures with ternary branching



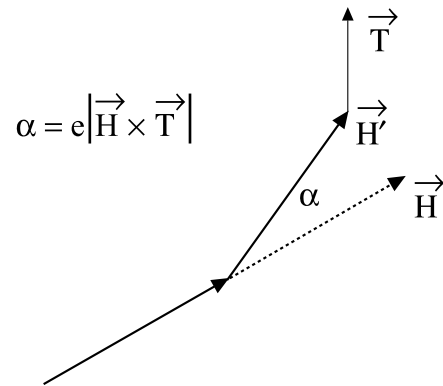


Figure 2.9: Correction  $\alpha$  of segment orientation  $\vec{H}$  due to tropism  $\vec{T}$

Figure	$d_1$	$d_2$	$a$	$l_r$	$\vec{T}$	$e$	$n$
a	94.74	132.63	18.95	1.109	0.00,-1.00,0.00	0.22	6
b	137.50	137.50	18.95	1.109	0.00,-1.00,0.00	0.14	8
c	112.50	157.50	22.50	1.790	-0.02,-1.00,0.00	0.27	8
d	180.00	252.00	36.00	1.070	-0.61,0.77,-0.19	0.40	6

Table 2.3: Constants for the tree structures in Figure 2.8



Figure 2.10: *Medicine Lake* by Musgrave *et al.* [101]

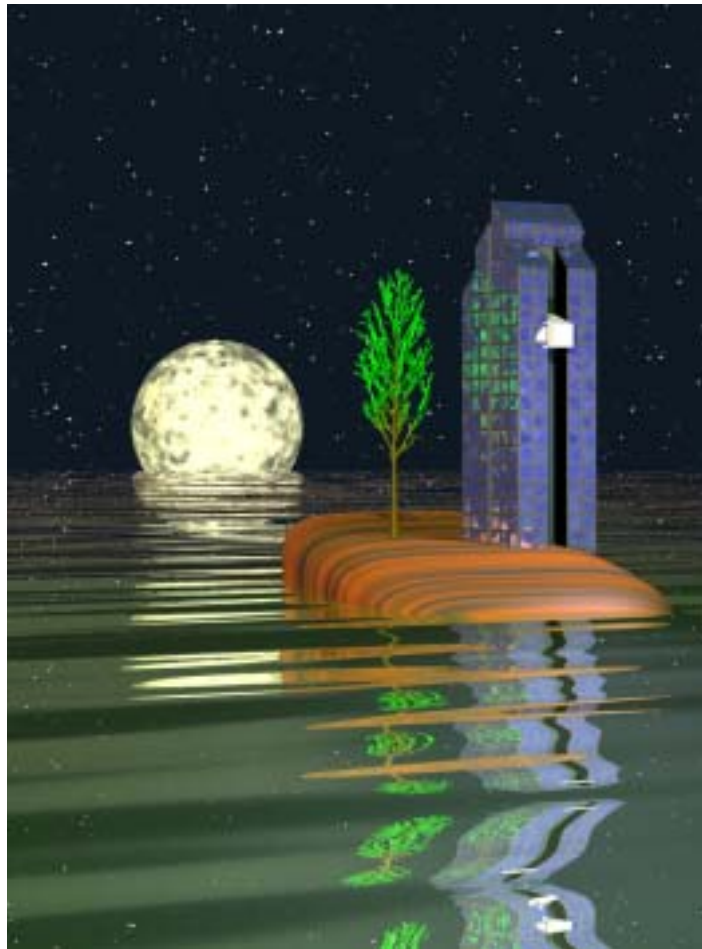


Figure 2.11: A surrealistic elevator

### *Conclusions*

The examples given above demonstrate that the tree models of Honda, as well as their derivatives studied by Aono and Kunii, can be expressed using the formalism of L-systems. In a separate study, Shebell [130] also showed that L-systems can be applied to generate the architectural tree models of Hallé, Oldeman and Tomlinson [58]. These results indicate that L-systems may play an important role as a tool for biologically-correct simulation of tree development and synthesis of realistic tree images. However, the tree-like shapes created so far are rather generic (Figure 2.11), and models of particular tree species, directly based on biological data, are yet to be developed. L-systems have found more applications in the domain of realistic modeling of herbaceous plants, discussed in the next chapter.

# Chapter 3

## Developmental models of herbaceous plants

The examples of trees presented in the previous chapter introduce L-systems as a plant modeling tool. They also illustrate one of the most striking features of the generative approach to modeling, called *data base amplification* [136]. This term refers to the generation of complex-looking objects from very concise descriptions – in our case, L-systems comprised of small numbers of productions. Yet in spite of the small size, the specification of L-systems is not a trivial task.

In the case of highly self-similar structures, the synthesis methods based on edge rewriting and node rewriting are of assistance, as illustrated by the examples considered in Section 1.10.3. However, a more general approach is needed to model the large variety of developmental patterns and structures found in nature.

The methodology presented in this chapter is based on the simulation of the development of real plants. Thus, a particular form is modeled by capturing the essence of the *developmental process* that leads to this form. This approach has two distinctive features.

*Developmental models*

- **Emphasis on the space-time relation between plant parts.** In many plants, organs in various stages of development can be observed at the same time. For example, some flowers may still be in the bud stage, others may be fully developed, and still others may have been transformed into fruits. If development is simulated down to the level of individual organs, such *phase effects* are reproduced in a natural way.
- **Inherent capability of growth simulation.** The mathematical model can be used to generate biologically correct images of plants at different ages and to create sequences of images illustrating plant development in time.

*Herbaceous  
plants*

The models are constructed under the assumption that organisms control the important aspects of their own development. According to Apter [3, page 44], this simplification must be accepted as a necessary evil, as long as the scope of the mathematical model is limited to an isolated plant. Consequently, this chapter focuses on the modeling and generation of growth sequences of *herbaceous* or non-woody plants, since internal control mechanisms play a predominant role in their development. In contrast, the form of woody plants is determined to a large extent by the environment, competition among branches and trees, and accidents [164].

### 3.1 Levels of model specification

*Partial  
L-systems*

*L-system  
schemata*

*Complete  
L-systems*

L-systems can be constructed with a variety of objectives in mind, ranging from a general classification of branching structures to detailed models suitable for image synthesis purposes. Accordingly, the L-systems presented in this chapter are specified at three levels of detail. The most abstract level, called *partial L-systems*, employs the notation of nondeterministic OL-systems to define the realm of possibilities within which structures of a given type may develop. Partial L-systems capture the main traits characterizing structural types, and provide a formal basis for their classification. Control mechanisms that resolve nondeterminism are introduced in the next level, termed *L-system schemata*.<sup>1</sup> The topology of individual plants and temporal aspects of their development are described at this level. Schemata are of particular interest from a biological point of view, as they provide an insight into the mechanisms that control plant development in nature. The geometric aspects are added in *complete L-systems* that include information concerning growth rates of internodes, the values of branching angles, and the appearance of organs. The difference between all three levels is illustrated using models of a single-flower shoot as a running example.

#### 3.1.1 Partial L-systems

*Single-flower  
shoot*

Consider the development of a shoot which, after a period of vegetative growth, produces a single flower. The partial L-system is given below.

$$\begin{aligned}
 \omega &: a \\
 p_1 &: a \rightarrow I[L]a \\
 p_2 &: a \rightarrow I[L]A \\
 p_3 &: A \rightarrow K
 \end{aligned}
 \tag{3.1}$$

The lower-case symbol  $a$  represents the *vegetative apex*, while the upper-case  $A$  is the *flowering apex*, capable of forming reproductive organs.

<sup>1</sup>In the literature, the term “scheme” is also used to denote the class of L-systems with the same alphabet and productions, but with different axioms [62, page 54].



Figure 3.1: Single-flower shoot

A derivation step corresponds to a *plastochron*, defined as the time interval between the production of successive internodes by the apex. At each step apex  $a$  has a choice of forming either leaf  $L$ , internode  $I$  and new apex  $a$  (production  $p_1$ ), or forming the same structures and transforming itself into a flowering apex  $A$  ( $p_2$ ), which subsequently creates flower  $K$  ( $p_3$ ). Once this transformation or *developmental switch* has taken place it cannot be reversed, since there is no rule allowing the transformation of  $A$  to  $a$ . Examples of strings generated by the L-system specified in equation (3.1) are given below.

$$\begin{array}{lll}
 a & a & a \\
 I[L]A & I[L]a & I[L]a \\
 I[L]K & I[L]I[L]A & I[L]I[L]a \\
 I[L]K & I[L]I[L]K & I[L]I[L]I[L]A \\
 & I[L]I[L]K & I[L]I[L]I[L]K \\
 & & I[L]I[L]I[L]K
 \end{array}$$

A diagrammatic representation of a single-flower inflorescence is shown in Figure 3.1.

### 3.1.2 Control mechanisms in plants

A partial L-system does not specify the moments in which developmental switches occur. The timing of these switches is specified at the level of L-system schemata, which incorporate mechanisms that control plant development. In biology, these mechanisms are divided into two classes depending on the way information is transferred between modules. The term *lineage* (or *cellular descent*) refers to the transfer of information from an ancestor cell or module to its descendants. In contrast, *interaction* is the mechanism of information exchange between neighboring cells (for example, in the form of nutrients or hormones). Within the formalism of L-systems, lineage mechanisms are represented

*L-system  
schemata*

*Lineage vs.  
interaction*

by context-free productions found in OL-systems, while the simulation of interaction requires the use of context-sensitive 1L-systems and 2L-systems.<sup>2</sup> Several specific mechanisms are listed below. Although they are described from the modeling perspective, a relation to physiological processes observed in nature can often be found.

### Stochastic mechanism

The simplest method for implementing a developmental switch is to use a stochastic L-system. In this case the vegetative apex  $a$  has a probability  $\pi_1$  of staying in the vegetative state, and  $\pi_2$  of transforming itself into a flowering apex  $A$ .

$$\begin{aligned}\omega &: a \\ p_1 &: a \xrightarrow{\pi_1} I[L]a \\ p_2 &: a \xrightarrow{\pi_2} I[L]A \\ p_3 &: A \xrightarrow{1} K\end{aligned}$$

The probability distribution  $(\pi_1, \pi_2)$  is found experimentally, with  $\pi_1 + \pi_2 = 1$ .

### The effect of environment

Many plants change from a vegetative to a flowering state in response to environmental factors such as temperature or the number of daylight hours. Such effects can be modeled using one set of productions (called a *table*) for some number of derivation steps, then replacing it by another set:

*Table  
L-systems*

Table 1	Table 2
$\omega : a$	$p_1 : a \rightarrow I[L]A$
$p_1 : a \rightarrow I[L]a$	$p_2 : A \rightarrow K$

The concept of table L-systems (*TOL-systems*) was introduced and formalized by Rozenberg [62, 127]. Note that the use of tables provides only a partial solution to the problem of specifying the switching time, since a control mechanism external to the L-system is needed to select the appropriate table.

### Delay mechanism

The delay mechanism operates under the assumption that the apex undergoes a series of state changes that postpone the switch until a particular state is reached.

---

<sup>2</sup>The clarity of this dichotomy is somewhat obscured by parametric OL-systems, which can simulate the operation of context-sensitive L-systems using an infinite set of parameter values.

This is captured by the following L-system in the case of a single-flower shoot.

$$\begin{aligned}
 \omega & : a_0 \\
 p_i & : a_i \rightarrow I[L]a_{i+1} \quad 0 \leq i \leq n-1 \\
 p_n & : a_n \rightarrow I[L]A \\
 p_{n+1} & : A \rightarrow K
 \end{aligned}$$

According to this model, the apex *counts* the leaves it produces. While it may seem strange that a plant would count, it is known that some plant species produce a fixed number of leaves before they start flowering.

### Accumulation of components

A developmental mechanism based on the accumulation of components is similar to that of delay, but emphasizes the physiological nature of the counting process. According to this approach, counting is achieved by a monotonic increase or decrease in the concentration of certain cell components. This process can be captured by the following parametric L-system:

$$\begin{aligned}
 \omega & : a(0) \\
 p_1 & : a(c) : c < C \rightarrow I[L]a(c + \Delta c) \\
 p_2 & : a(c) : c \geq C \rightarrow I[L]A \\
 p_3 & : A : * \rightarrow K
 \end{aligned} \tag{3.2}$$

The parameter  $c$  indicates current concentration of the controlling components in the apex  $a$ . In each derivation step, this concentration is increased by a constant  $\Delta c$ . The developmental switch occurs when the concentration reaches the threshold value  $C$ .

### Development controlled by a signal

In many plants, the switch from a vegetative to a flowering state is caused by a flower-inducing signal transported from the basal leaves towards the apex. The time of signal initiation is determined using one of the previously described methods, for example by counting. A sample L-system is given below.

$$\begin{aligned}
 \omega & : D(1)a(1) \\
 p_1 & : a(i) : i < m \rightarrow a(i+1) \\
 p_2 & : a(i) : i = m \rightarrow I[L]a(1) \\
 p_3 & : D(i) : i < d \rightarrow D(i+1) \\
 p_4 & : D(i) : i = d \rightarrow S(1) \\
 p_5 & : S(i) : i < u \rightarrow S(i+1) \\
 p_6 & : S(i) : i = u \rightarrow \varepsilon \\
 p_7 & : S(i) < I : i = u \rightarrow IS(1) \\
 p_8 & : S(i) < a(j) : * \rightarrow I[L]A \\
 p_9 & : A : * \rightarrow K
 \end{aligned}$$

The apex  $a$  produces internodes  $I$  and leaves  $L$  on the main axis ( $p_2$ ). The time between the production of two consecutive segments, or the plastochron of the main axis, is equal to  $m$  derivation steps ( $p_1$ ). After a delay of  $d$  steps ( $p_3$ ), a signal  $S$  is sent from the plant base towards the apices ( $p_4$ ). This signal is transported along the main axis with a delay of  $u$  steps per internode  $I$  ( $p_5, p_7$ ). Production  $p_6$  removes the signal from a node after it has been transported along the structure ( $\varepsilon$  stands for the empty string). When the signal reaches the apex,  $a$  is transformed into flowering state  $A$  ( $p_8$ ) which yields flower  $K$  ( $p_9$ ). Note that the signal has to propagate faster than one node per plastochron ( $u < m$ ), otherwise it would not be able to catch up with the apex. The above processes are illustrated by the following developmental sequence, for  $d = 4$ ,  $m = 2$  and  $u = 1$ .

$$\begin{array}{l}
 D(1)a(1) \\
 D(2)a(2) \\
 D(3)I[L]a(1) \\
 D(4)I[L]a(2) \\
 S(1)I[L]I[L]a(1) \\
 IS(1)[L]I[L]a(2) \\
 I[L]IS(1)[L]I[L]a(1) \\
 I[L]I[L]IS(1)[L]a(2) \\
 I[L]I[L]I[L]A \\
 I[L]I[L]I[L]K
 \end{array}$$

Although the above model may appear unnecessarily complicated, signals are indispensable in the simulation of complex flowering sequences discussed later.

### 3.1.3 Complete models

The L-systems considered so far are not directly suitable for image synthesis purposes. To this end, they must be completed with geometric information. The relation between an L-system scheme and a corresponding complete L-system is discussed using the model of crocuses shown in Figure 3.2 as an example.

*Crocus*

The development is controlled using a delay expressed as an accumulation mechanism (equation (3.2)). In contrast to L-system schemes in which symbols represent module types, the L-system in Figure 3.2 is specified in terms of turtle symbols. Production  $p_1$  describes the creation of successive internodes  $F$  and leaves  $L$  by the vegetative apex  $a$ . The leaves branch from the stem at an angle of  $30^\circ$  and spiral around the main axis with a divergence angle equal to  $137.5^\circ$  (see Chapter 4). Productions  $p_2$  and  $p_3$  describe the developmental switch and the creation of flower  $K$  taking place respectively in steps  $T_a$  and  $T_{a+1}$ . Productions  $p_4$  and  $p_5$  capture the development of leaves and flowers until they reach their final shapes  $T_L$  and  $T_K$  steps after creation. For each





```

#define Ta 7          /* developmental switch time */
#define TL 9          /* leaf growth limit */
#define TK 5          /* flower growth limit */
#include L(0),L(1),...,L(TL) /* leaf shapes */
#include K(0),K(1),...,K(TK) /* flower shapes */

ω : a(1)
p1 : a(t) : t < Ta → F(1) [∑i=030 ∼L(i)] / (137.5) a(t+1)
p2 : a(t) : t = Ta → F(20)A
p3 : A : * → ∼K(0)
p4 : L(t) : t < TL → L(t+1)
p5 : K(t) : t < TK → K(t+1)
p6 : F(1) : 1 < 2 → F(1+0.2)

```

Figure 3.2: Crocuses

branch			
main apex terminates		main apex continues	
all lateral apices terminate	some lateral apices continue	all lateral apices terminate	some lateral apices continue
terminal	sympodial	monopodial	polypodial

Table 3.1: Basic growth patterns of branching structures

value of parameter  $t$ , the corresponding organ shapes  $L(t)$  and  $K(t)$  are modeled using bicubic patches incorporated into the plant structure as described in Section 5.1. Production  $p_6$  specifies the gradual elongation of internodes.

## 3.2 Branching patterns

*Subapical growth*

The partial L-system in equation (3.1) and the related schemata employ *subapical growth* mechanisms in which new branches are created exclusively by apices. All herbaceous plants develop this way. The architecture of a branching structure is to a large extent determined by the relationships between *terminal* and *continuing* apices. While a continuing apex produces branches again and again, a terminal one either gives rise to an appendage such as a flower or dies. The possible combinations are listed in Table 3.1. Of the four terms assigned to these possibilities, two are commonly used in biology, namely, *sympodial* and *monopodial*, while the other two terms are introduced here to denote the remaining cases, usually not characterized in the literature.

*Expression using L-systems*

The above branching patterns can be represented conveniently using partial bracketed L-systems. Let  $A, B, C$  denote continuing apices,  $X$  a terminal apex, and  $I$  an internode. The terminal and sympodial patterns are characterized by rules of the form

$$A \rightarrow I[B]^n[X]^m X,$$

with  $n = 0, m > 0$  in the case of terminal patterns and  $n > 0, m \geq 0$  in the case of sympodial patterns. The important property is that the main apex terminates its development in all these cases.

Monopodial and polypodial patterns have rules of the form

$$A \rightarrow I[B]^n[X]^m C,$$

with  $n = 0, m > 0$  in the case of monopodial patterns and  $n > 0, m \geq 0$  in the case of polypodial ones. In these cases, it is important that the apex remains active.

The terms defined here apply to branching structures in general, whether they only produce vegetative organs (branches and leaves) or reproductive organs as well. In the latter case, the terminal organs develop from flower buds to flowers to fruits but do not give rise to vegetative structures (there are exceptions to this statement but they can be neglected here).

### 3.3 Models of inflorescences

The following discussion focuses on the modeling of compound flowering structures or *inflorescences*. In some cases an entire shoot system can be considered an inflorescence, in others only some of the branches bear flowers and are inflorescences. Inflorescence architecture is an elaboration of branching structures in general.

In the domain of botanical applications of L-systems, the study of inflorescences has played a particularly visible role [44, 45, 46, 47, 77, 86]. Unfortunately, the terms used for the various inflorescence types are not uniform in the literature. Besides a purely morphological terminology, attempts have been made to construct a “typological” terminology, expressing the “essential” features of flowering structures [144, 145, 157, 158]. However, these terms are not generally accepted [12]. A compromise has been proposed by D. and U. Müller-Doblies [100], which serves as a basis for the classification that guides this presentation.

*Classification*

#### 3.3.1 Monopodial inflorescences

##### Simple racemes (open)

Racemes are characteristically monopodial inflorescences; a shoot has lateral apices with terminal structures and a main apex that continues to development. A raceme is *open* if the main apex does not form a flower. The partial L-system for this widely occurring type of inflorescence is:

$$\begin{aligned} \omega &: a \\ p_1 &: a \rightarrow I[L]a \\ p_2 &: a \rightarrow I[L]A \\ p_3 &: A \rightarrow I[K]A \end{aligned} \tag{3.3}$$

This system differs from that modeling a shoot with a single flower (equation (3.1)) only in production  $p_3$ . Here it is designed to repeatedly produce lateral flowers (Figure 3.3), while in the previous system  $A$  produces a single flower.

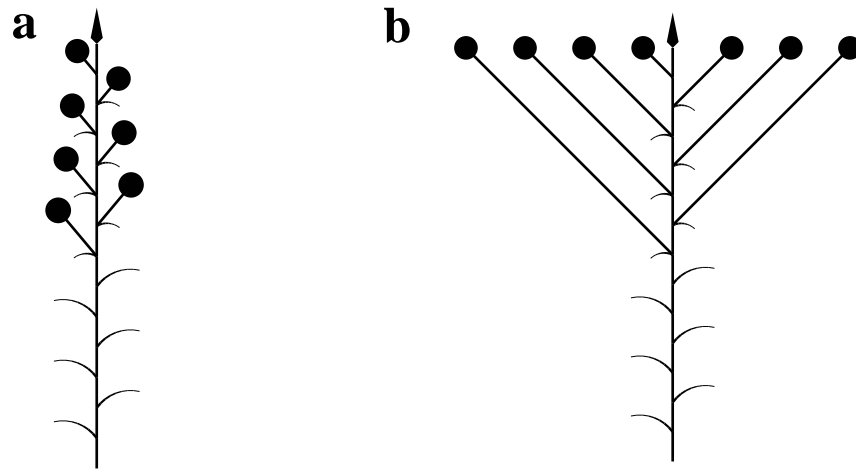


Figure 3.3: Open racemes: (a) elongated form, (b) planar form



Figure 3.4: Lily-of-the-valley

The flowering sequence in open racemes is always *acropetal* (from base to top). This can be observed after substituting production  $p_3$  in the L-system in equation (3.3) with productions  $p'_3$  and  $p_4$ , which use indexed symbols  $K_i$  to denote subsequent stages of flower development.

*Acropetal  
sequence*

$$\begin{aligned} p'_3 &: A \rightarrow I[IK_0]A \\ p_4 &: K_i \rightarrow K_{i+1}, \quad i \geq 0 \end{aligned}$$

The indexed notation  $K_i \rightarrow K_{i+1}$  stands for a (potentially infinite) set of productions  $K_0 \rightarrow K_1, K_1 \rightarrow K_2, K_2 \rightarrow K_3, \dots$ . The developmental sequence begins as follows:

$$\begin{aligned} &A \\ &I[IK_0]A \\ &I[IK_1]I[IK_0]A \\ &I[IK_2]I[IK_1]I[IK_0]A \\ &I[IK_3]I[IK_2]I[IK_1]I[IK_0]A \\ &\dots \end{aligned}$$

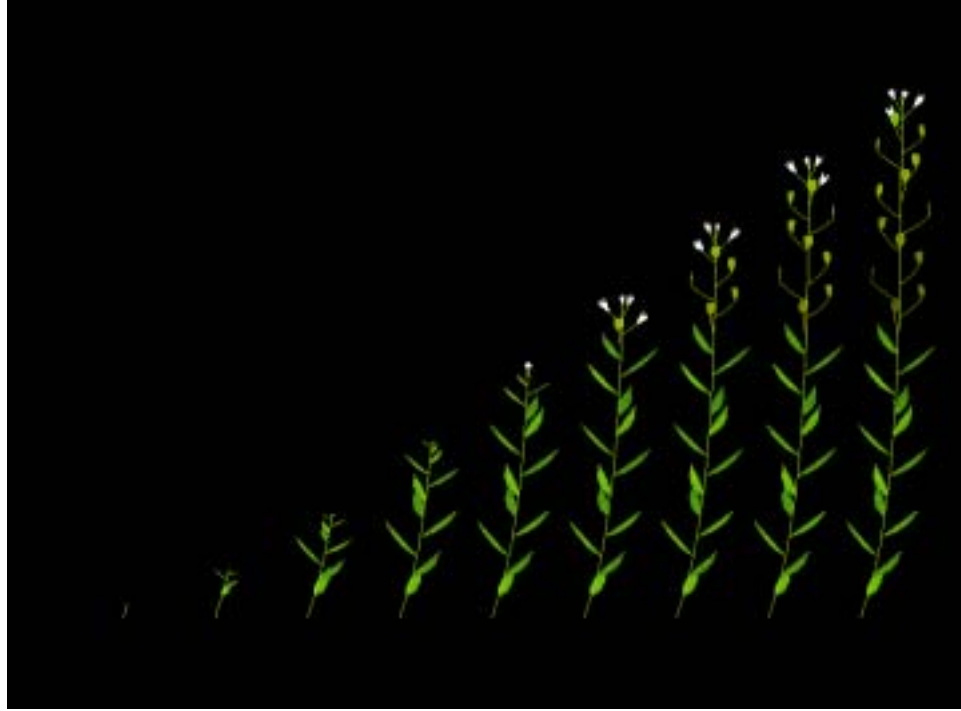
At each developmental stage the inflorescence contains a sequence of flowers of different ages. The flowers newly created by the apex are delayed in their development with respect to the older ones situated at the stem base. Graphically, this effect is illustrated by the model of a lily-of-the-valley shown in Figure 3.4. The following quotation from d’Arcy Thompson [143] applies:

*Lily-of-the-  
valley*

A flowering spray of lily-of-the-valley exemplifies a growth-gradient, after a simple fashion of its own. Along the stalk the growth-rate falls away; the florets are of descending age, from flower to bud; their graded differences of age lead to an exquisite gradation of size and form; the time-interval between one and another, or the “space-time relation” between them all, gives a peculiar quality – we may call it phase-beauty – to the whole.

Another example of “phase beauty” can be seen in the shoot of shepherd’s purse (*Capsella bursa-pastoris*) shown in Figure 3.5. Productions  $p_1$ ,  $p_2$  and  $p_3$  describe the activities of the apex in the vegetative and flowering states, in accordance with the L-system in equation (3.3). The developmental switch is implemented using a delay mechanism. Productions  $p_4$  and  $p_5$  capture the linear elongation of internodes in time, while  $p_6$  and  $p_7$  describe the gradual increase of the angle at which the flower stalks branch from the main stem. Productions  $p_8$ ,  $p_9$  and  $p_{11}$  specify the shapes of leaves  $L$ , flower petals  $K$  and fruits  $X$  using developmental surface models discussed in Section 5.2. Production  $p_{10}$  controls the flowering time. Symbol % in the successor of production  $p_{11}$  simulates the fall of petals by cutting them off the structure at the time of fruit formation. The default value of the angle increment corresponding to the symbol + with no parameter is  $18^\circ$ .

*Capsella*



```

ω  : I(9)a(13)
p1  : a(t) : t>0 → [&(70)L]/(137.5)I(10)a(t-1)
p2  : a(t) : t=0 → [&(70)L]/(137.5)I(10)A
p3  : A    : *   → [&(18)u(4)FFI(10)I(5)X(5)KKKK]
                    / (137.5)I(8)A
p4  : I(t) : t>0 → FI(t-1)
p5  : I(t) : t=0 → F
p6  : u(t) : t>0 → &(9)u(t-1)
p7  : u(t) : t=0 → &(9)
p8  : L    : *   → [ { .-FI(7)+FI(7)+FI(7)} ]
                    [ { .+FI(7)-FI(7)-FI(7)} ]
p9  : K    : *   → [ & { .+FI(2)--FI(2)} ]
                    [ & { .-FI(2)++FI(2)} ] / (90)
p10 : X(t) : t>0 → X(t-1)
p11 : X(t) : t=0 → ^ (50) [ [-GGGG++ [GGG[++G{.}.].].
                    ++GGGG.--GGG.--G.} ] %

```

Figure 3.5: Development of *Capsella bursa-pastoris*. Every fourth derivation step is shown.



Figure 3.6: Apple twig

### Simple raceme (closed)

The inflorescence of an apple tree (Figure 3.6) provides an example of a closed raceme. In this case, the main apex eventually terminates its development and produces a terminal flower (Figure 3.7). The corresponding partial L-system is given below.

$$\begin{aligned}
 \omega &: a \\
 p_1 &: a \rightarrow I[L]a \\
 p_2 &: a \rightarrow I[L]A \\
 p_3 &: A \rightarrow I[K]A \\
 p_4 &: A \rightarrow K
 \end{aligned}$$

Developmental switches are associated with two symbols,  $a$  and  $A$ . Thus, in order to obtain an L-system scheme it is necessary to specify how both of these switches will be controlled.

The flowering sequence is usually acropetal but could also be basipetal, *i.e.*, progressing downward after the formation of the terminal flower on the main axis. In the latter case a basipetal signal, as discussed in Section 1.8, can be applied to induce the transformation of dormant flower buds into flowers.

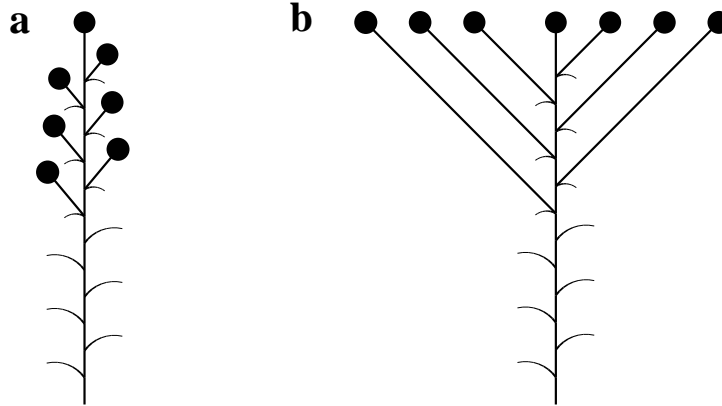


Figure 3.7: Closed racemes: (a) elongated form, (b) planar form

### Compound raceme (open dibotryoid)

Racemes can also occur on complex branching structures. The simplest of these inflorescences is one with open racemes on the first order branches as well as on the main axis (Figure 3.8a). This two-level compound structure (thus *dibotryoid*) is described by the following partial L-system.

$$\begin{aligned}
 \omega &: a \\
 p_1 &: a \rightarrow I[L]a \\
 p_2 &: a \rightarrow I[L]A \\
 p_3 &: A \rightarrow I[L][b]A \\
 p_4 &: A \rightarrow I[L][b]B \\
 p_5 &: b \rightarrow I[L]b \\
 p_6 &: b \rightarrow I[L]B \\
 p_7 &: B \rightarrow I[K]B
 \end{aligned} \tag{3.4}$$

Three developmental transformations are necessary: the first for the change from leaf to branch creation along the main axis (production  $p_2$ ), the second for the switch from branching to lateral flower creation on the main axis ( $p_4$ ), and the third for the transition from leaf to lateral flower formation along the first-order branches ( $p_6$ ). Each branch is subtended by a leaf, which is why productions  $p_3$  and  $p_4$  specify two appendages  $L$  and  $b$ . Branches with flowers  $K$  need not have subtending leaves, which is reflected in production  $p_7$ .

*Single-signal  
model*

Within each component raceme, the flowering sequence is always acropetal, but the timing of switches has a crucial impact on the overall flowering sequence and appearance of the plant. For example, let us assume that the switch from leaf to branch production is controlled by a delay, while the remaining two switches are caused by an acropetal flower-inducing signal (representing the hormone *florigen*). Such a development is captured by L-system 3.1 (see below). Initially, the veg-



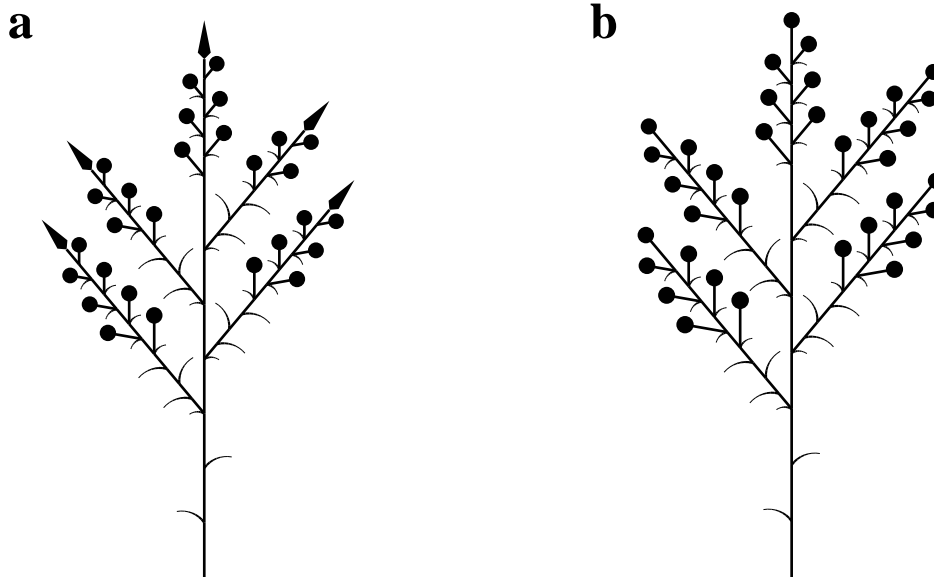


Figure 3.8: Dibotryoids: (a) open, (b) closed

```

#define d 13          /* delay for sending florigen */
#define e 3          /* delay for creating branches */
#define m 2          /* plastochron - main axis */
#define n 3          /* plastochron - lateral axis */
#define u 1          /* signal delay - main axis */
#define v 1          /* signal delay - lateral axis */

ω : S(0)a(1,0)
p1 :      a(t,c) : t<m          → a(t+1,c)
p2 :      a(t,c) : (t=m)&(c<e) → I(0,u) [L] a(1,c+1)
p3 :      a(t,c) : (t=m)&(c=e) → I(0,u) [L] [b(1)]a(1,c)
p4 :      b(t)   : t<n          → b(t+1)
p5 :      b(t)   : t=n          → I(0,v) [L] b(1)
p6 :      S(t)   : *            → S(t+1)
p7 :  S(t) < I(i,j) : t=d       → I(1,j)
p8 :      I(i,j) : (0<i)&(i<j) → I(i+1,j)
p9 :  I(i,j) < I(k,l) : (i=j)&(k=0) → I(1,l)
p10 : I(i,j) < a(k,l) : i>0      → I[L] [b(1)]B
p11 : I(i,j) < b(k)   : i>0      → I[L]B
p12 :      B      : *            → I[K]B

```

L-system 3.1: A model of dibotryoids

etative apex  $a$  creates internodes  $I$  and leaves  $L$  with plastochron  $m$  (productions  $p_1$  and  $p_2$ ). After the creation of  $e$  leaves a developmental switch occurs, and apex  $a$  starts creating branches with the same plastochron ( $p_3$ ). The change of state is indicated by the value of the second parameter in the module  $a(t, c)$ , which is now equal to  $e$ . The lateral apices  $b$  create internodes and leaves with plastochron  $n$  ( $p_4$  and  $p_5$ ). After a delay of  $d$  steps from the beginning of the simulation ( $p_6$ ), the flowering signal is introduced to the basal internode ( $p_7$ ), as indicated by a non-zero value of the first parameter in the module  $I(i, j)$ . The signal is passed along an axis at the rate of  $j$  steps per internode ( $p_8$  and  $p_9$ ), where  $j = u$  for the main axis and  $j = v$  for the lateral axes. These rates are assigned to internodes by productions  $p_2$ ,  $p_3$  and  $p_5$ . When the signal reaches an apex (either  $a$  or  $b$ ), the apex is transformed into flowering state  $B$  ( $p_{10}$  and  $p_{11}$ ). From then on, new flowers  $K$  are produced in each derivation step ( $p_{12}$ ).

### Model analysis

In order to analyze the plant structure and flowering sequence resulting from the above development, let  $T_k$  denote the time at which apex  $b$  of the  $k$ -th lateral axis is transformed into the flowering state, and  $l_k$  denote the length of this axis (expressed as the number of internodes) at the transformation time. It is assumed here that the first  $e$  leaves count as lateral axes, thus  $k > e$ . Since it takes  $km$  time units to produce  $k$  internodes along the main axis and  $l_k n$  time units to produce  $l_k$  internodes on the lateral axis, we obtain:

$$T_k = km + l_k n$$

On the other hand, the transformation occurs when the signal reaches the apex. The signal is sent  $d$  time units after the development starts. It uses  $ku$  time units to travel through  $k$  zero-order internodes and  $l_k v$  time units to travel through  $l_k$  first-order internodes:

$$T_k = d + ku + l_k v$$

Solving the above system of equations for  $l_k$  and  $T_k$  (and ignoring for simplicity some inaccuracy due to the fact that this system does not guarantee integer solutions), we obtain:

$$T_k = k \frac{un - vm}{n - v} + d \frac{n}{n - v}$$

$$l_k = -k \frac{m - u}{n - v} + \frac{d}{n - v}$$

In order to analyze the above solutions, let us first notice that the signal transportation delay  $v$  must be less than the plastochron of the lateral axes  $n$ , otherwise the signal would never reach the lateral apices. Under this assumption, the sign of the expression  $\Delta = un - vm$  determines the overall flowering sequence, which is acropetal for  $\Delta > 0$  (Figure 3.9) and basipetal for  $\Delta < 0$  (Figure 3.10). If  $\Delta = 0$ , all flowering switches

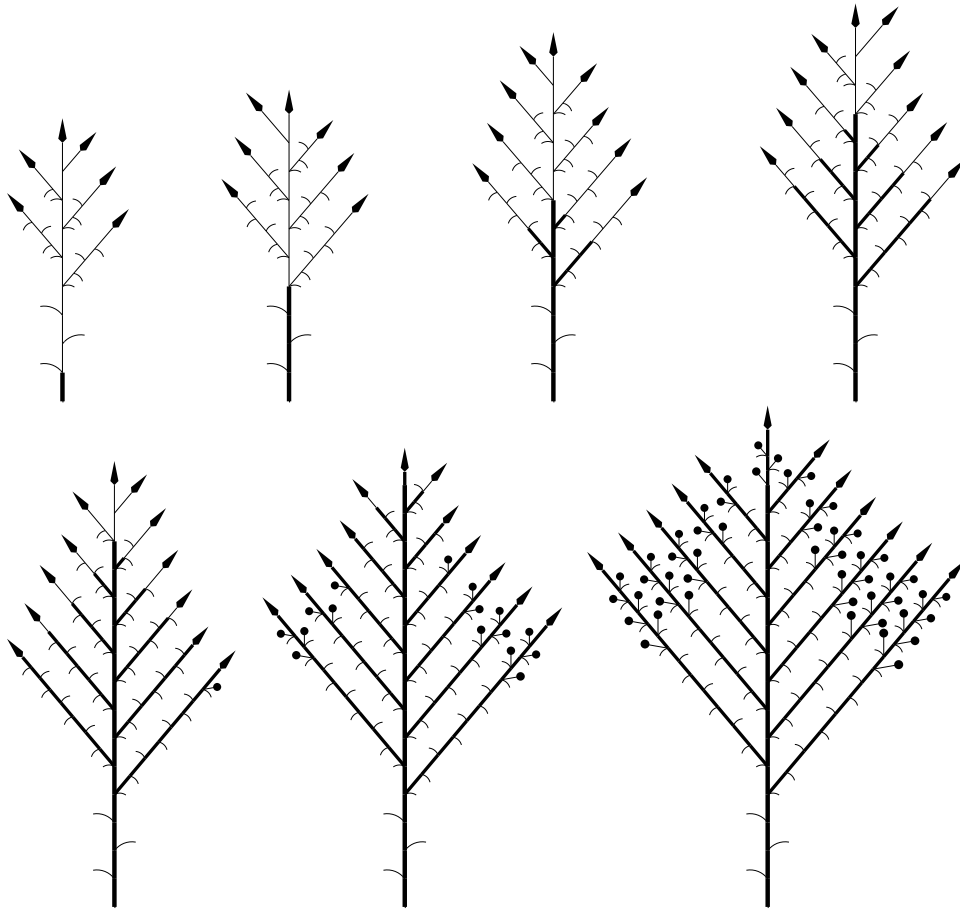


Figure 3.9: An acropetal flowering sequence in an open dibotryoid:  $m = 2$ ,  $n = 3$ ,  $u = v = 1$ ,  $\Delta = 0.5$ ; derivation lengths: 15 – 18 – 21 – 24 – 27 – 30 – 33

occur simultaneously. The sign of the expression  $m - u$  determines whether the vegetative part of the shoot is more developed at the base ( $m - u < 0$ ) or near the top of the structure ( $m - u > 0$ ). Figure 3.11 shows a model of a member of the mint family that exhibits a basipetal flowering sequence.

### Compound racemes (closed dibotryoids)

This inflorescence type differs from the previous one only in that each branch, including the main axis, bears a terminal flower (Figure 3.8b). A partial L-system can be obtained from that of equation (3.4) by adding one more production:

$$p_8 : B \rightarrow K$$

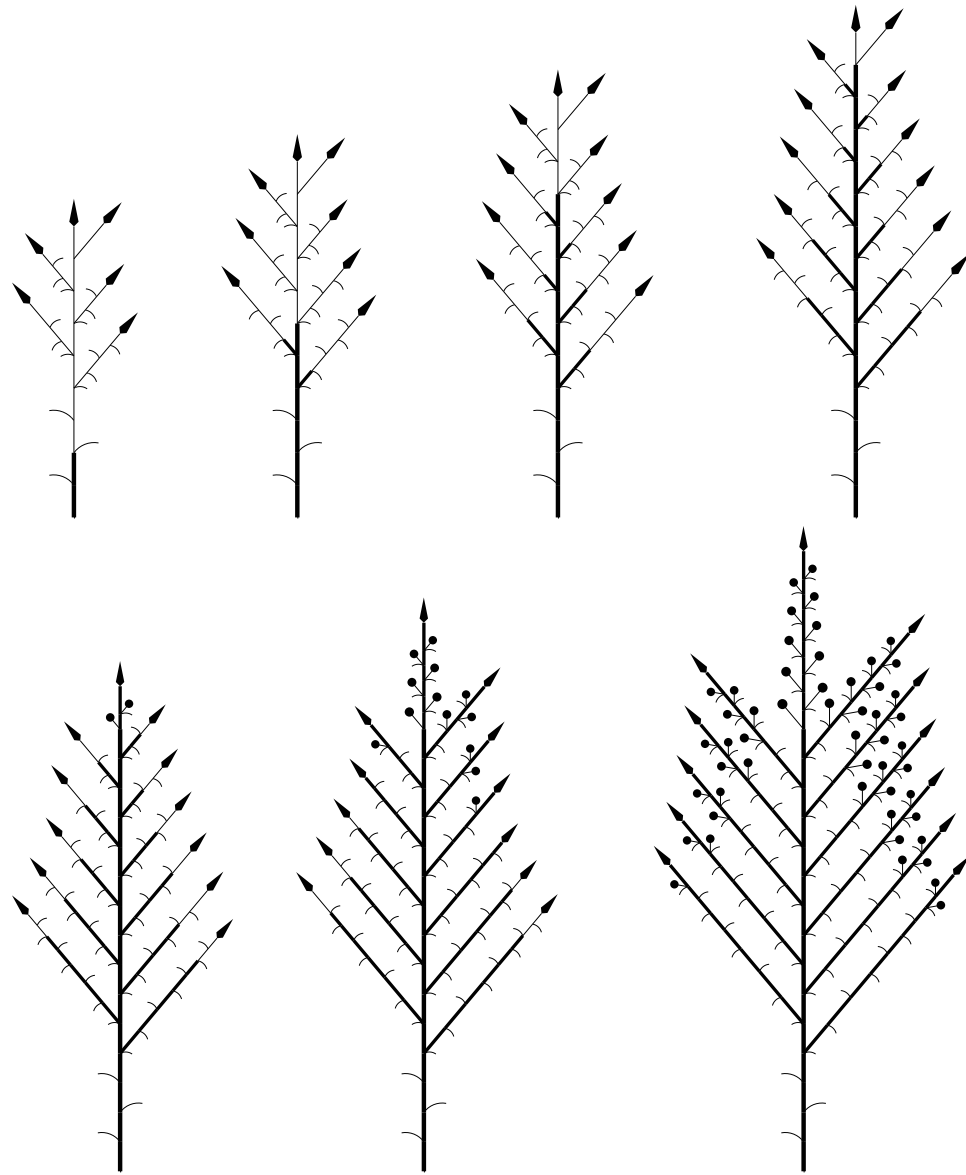


Figure 3.10: A basipetal flowering sequence in an open dibotryoid:  $m = 2$ ,  $n = 5$ ,  $u = 1$ ,  $v = 3$ ,  $\Delta = -0.5$ ; derivation lengths: 16 – 20 – 24 – 28 – 32 – 36 – 40

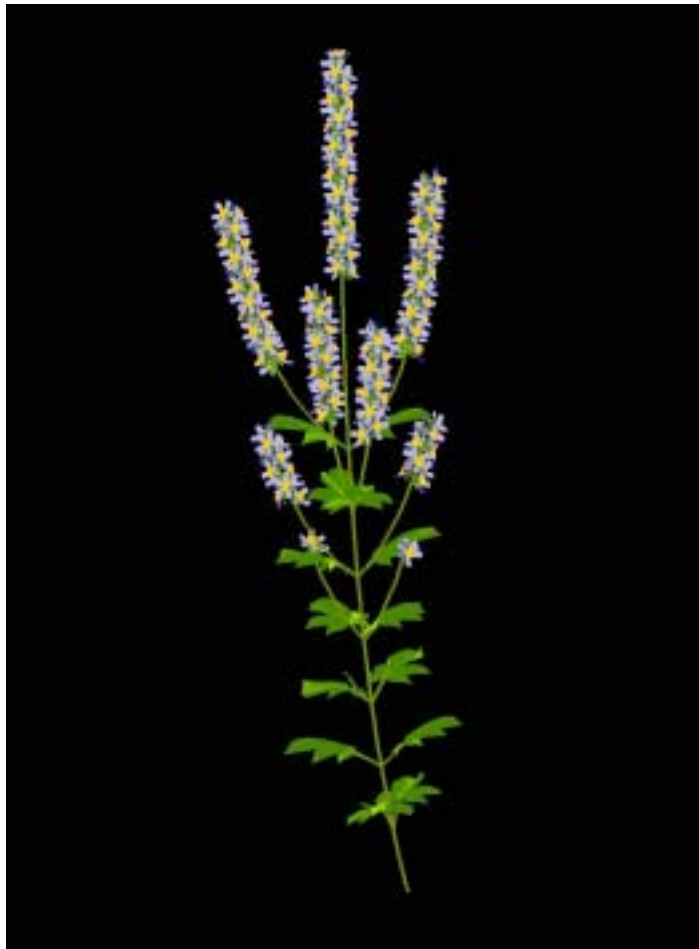


Figure 3.11: A mint

### Compound raceme (closed tribotryoid)

Racemic inflorescences can be compounded to a higher number of levels. The following is a partial L-system for a closed tribotryoid inflorescence, where closed racemes occur on second-order branches as well as on the terminal portions of first-order branches and of the main axis (Figure 3.12). The developmental process involves six developmental transformations.

$$\begin{array}{ll}
 \omega : a & p_7 : B \rightarrow I[L][c]B \\
 p_1 : a \rightarrow I[L]a & p_8 : B \rightarrow I[L][c]C \\
 p_2 : a \rightarrow I[L]A & p_9 : c \rightarrow I[L]c \\
 p_3 : A \rightarrow I[L][b]A & p_{10} : c \rightarrow I[L]C \\
 p_4 : A \rightarrow I[L][b]B & p_{11} : C \rightarrow I[K]C \\
 p_5 : b \rightarrow I[L]b & p_{12} : C \rightarrow K \\
 p_6 : b \rightarrow I[L]B &
 \end{array}$$

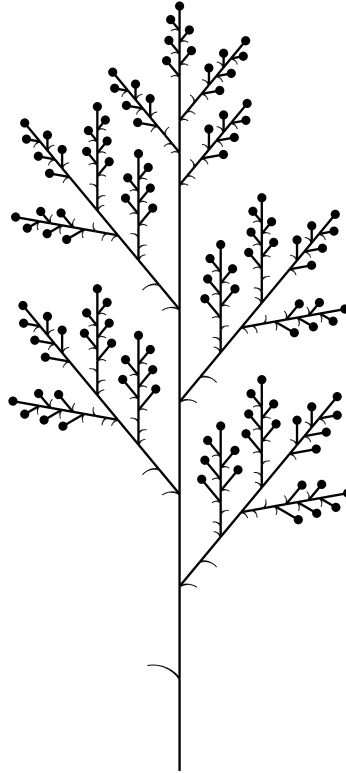


Figure 3.12: Closed tribotryoid

### 3.3.2 Sympodial inflorescences

#### Simple cymes (open)

In racemes, the apex of the main axis produces lateral branches and continues to grow. In contrast, the apex of the main axis in *cymes* turns into a flower shortly after a few lateral branches have been initiated. Their apices turn into flowers as well, and second-order branches take over. In time, branches of higher and higher order are produced. Thus, the basic structure of a cymose inflorescence is captured by the partial L-system:

$$\begin{aligned}
 \omega &: a \\
 p_1 &: a \rightarrow I[L]a \\
 p_2 &: a \rightarrow I[L]A \\
 p_3 &: A \rightarrow I[A]K
 \end{aligned}
 \tag{3.5}$$

As in the open raceme, there is a single symbol with alternative rules which specify that the vegetative apex  $a$  may change into a flower-producing apex  $A$ . Any one of the previously discussed mechanisms is available for timing this decision. Figure 3.13a shows an open cyme with branches curving in a spiral fashion, while Figure 3.13b shows one

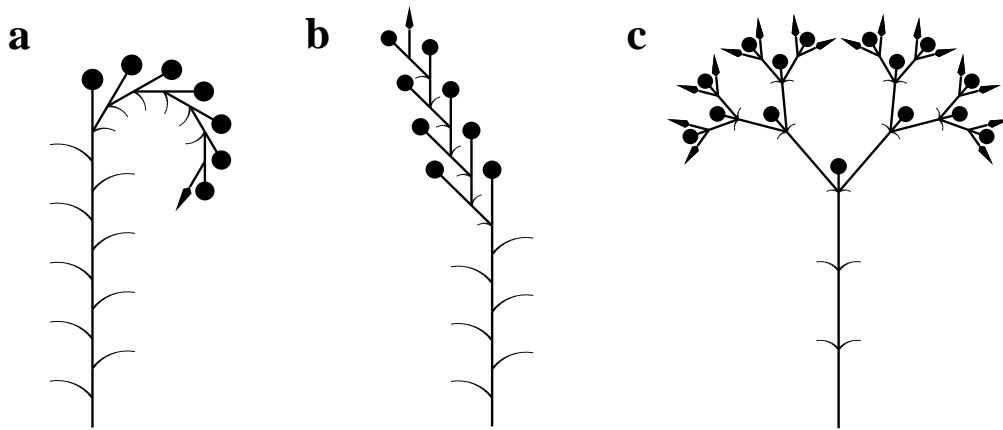


Figure 3.13: Open cymes: (a) spiral form, (b) zig-zag form, (c) double

with a zig-zag branching form.

### Double cymes (open)

Frequently, not one but two lateral apices are produced under each terminal apex as in Figure 3.13c. In this case the partial L-system is:

$$\begin{aligned}
 \omega &: a \\
 p_1 &: a \rightarrow I[L]a \\
 p_2 &: a \rightarrow I[L]A \\
 p_3 &: A \rightarrow I[A][A]K
 \end{aligned} \tag{3.6}$$

The two continuing lateral apices may develop at approximately equal rates (with the same plastochron) or with different rates, giving rise to asymmetric inflorescences. For example, the following L-system scheme describes the development of rose campion (*Lychnis coronaria*) as analyzed by Robinson [126]:

*Lychnis*

$$\begin{aligned}
 \omega &: A_7 \\
 p_1 &: A_7 \rightarrow I[A_0][A_4]IK_0 \\
 p_2 &: A_i \rightarrow A_{i+1}, & 0 \leq i < 7 \\
 p_3 &: K_i \rightarrow K_{i+1}, & i \geq 0
 \end{aligned}$$

Production  $p_1$  shows that at their creation time, the lateral apices have different states  $A_0$  and  $A_4$ . Consequently, the first apex requires eight derivation steps to produce a flower and new branches, while the second requires only four steps. Each flower undergoes a sequence of changes, progressing from the bud stage to an open flower to a fruit. This developmental sequence is illustrated in Figure 3.14. According to production  $p_1$ , the lateral apices branch at an angle of  $45^\circ$  and lie in a plane perpendicular to that defined by the mother axis and its sibling. Production  $p_3$  describes the linear elongation of internodes, while  $p_4$



```

#include L(0),L(1),... /* leaf shapes */
#include K(0),K(1),... /* flower shapes */

 $\omega$  : A(7)
 $p_1$  : A(t) : t=7  $\rightarrow$  FI(20) [&(60)~L(0)]/(90) [&(45)A(0)]/(90)
      [&(60)~L(0)]/(90) [&(45)A(4)]FI(10)~K(0)
 $p_2$  : A(t) : t<7  $\rightarrow$  A(t+1)
 $p_3$  : I(t) : t>0  $\rightarrow$  FFI(t-1)
 $p_4$  : L(t) : *  $\rightarrow$  L(t+1)
 $p_5$  : K(t) : *  $\rightarrow$  K(t+1)

```

Figure 3.14: Development of *Lychnis coronaria*



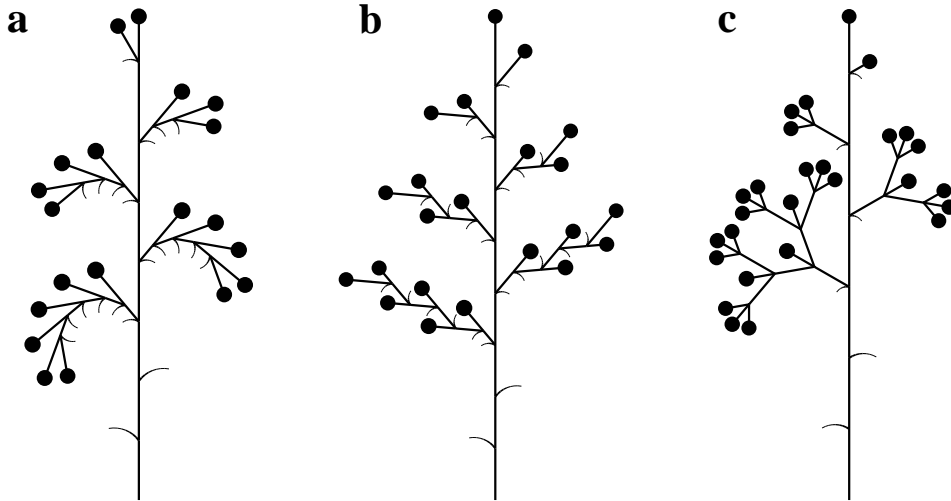


Figure 3.15: Thyrus: (a) spiral form, (b) zig-zag form, (c) double

and  $p_5$  capture the development of leaves and flowers over time. It is interesting to note that at different developmental stages there are some open flowers that have a relatively uniform distribution over the entire plant structure. This is advantageous to the plant since it increases the time span over which seeds will be produced.

### Cymes (closed)

Sympodial inflorescences that produce a terminal flower at some point during their development are called *closed cymes*. They result from the addition of production

$$p_4 : A \rightarrow K$$

to the L-systems specified in (3.5) and (3.6), which define open single and open double cymes.

### Thyrus (closed)

A *thyrus* is an inflorescence with branches of cymes borne on a monopodially branching axis. Thus, it represents a mixed sympodial and monopodial organization. Depending on the orientation of the flowers, a distinction between a thyrus with cymes in a spiral form and in a zig-zag form can be made (Figure 3.15, a and b). Both of these types are described by the following partial L-system:

$$\begin{aligned}
\omega &: a \\
p_1 &: a \rightarrow I[L]a \\
p_2 &: a \rightarrow I[L]A \\
p_3 &: A \rightarrow I[L][B]A \\
p_4 &: A \rightarrow K \\
p_5 &: B \rightarrow I[B]K \\
p_6 &: B \rightarrow K
\end{aligned}$$

In addition, a thyrus may have double cymes (Figure 3.15c). In the closed structure there are three developmental transformations. The first represents the change from vegetative to flowering development on the main axis (production  $p_2$ ). The second is necessary for the closure of the main axis with a terminal flower ( $p_4$ ). Both switches are related to the monopodial development of the main axis. The third transformation is responsible for the formation of the flowers that terminate the development of the sympodial structures ( $p_6$ ).

### 3.3.3 Polypodial inflorescences

#### Panicle

The term *polypodial* is not used in the botanical literature but is coined here to draw attention to the type of branching that represents continuing development of the main axis as well as of the lateral apices of a branch. The corresponding inflorescence type is usually called a *panicle*. The presence of two continuing apices at each new node is expressed by the following production:

$$A \rightarrow I[L][A]A$$

Since there can be nodes near the base of the plant that do not bear branches, the usual initial rules are included to model the transition from a purely vegetative to a flowering state. The resulting partial L-system is:

$$\begin{aligned}
\omega &: a \\
p_1 &: a \rightarrow I[L]a \\
p_2 &: a \rightarrow I[L]A \\
p_3 &: A \rightarrow I[L][A]A \\
p_4 &: A \rightarrow K
\end{aligned}$$

An example of a paniculate structure is shown in Figure 3.16. Note the presence of higher order branching and the lack of terminal racemes. Due to the repetitive application of production  $p_3$  at various levels of branching, the resulting structure is highly self-similar. The model includes only two types of developmental transformations: the switch

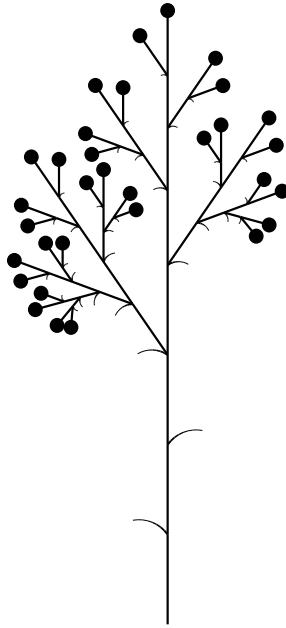


Figure 3.16: Panicle (elongated form)

from purely vegetative growth to the formation of the branching structure (production  $p_2$ ), and the creation of terminal flowers ( $p_4$ ). The timing of the last production determines the flowering sequence of the plant. Two possible control mechanisms will be examined in detail, using developmental models of the branching part of wall lettuce (*Mycelis muralis*) as examples.

The development of *Mycelis* is difficult to model for two reasons. First, the plant exhibits a basipetal flowering sequence, which means that flowering starts at the top of the plant and proceeds downwards. Secondly, at some developmental stages the plant has an *acrotonic* structure, where the upper branches are more developed than the lower ones. Both phenomena are in a sense counter-intuitive, since it would seem that the older branches situated near the plant base should start growing and producing flowers before the younger ones at the plant top. To explain these effects, several models were proposed and formally analyzed by Janssen and Lindenmayer [77]. Their *model II* is restated here as parametric L-system 3.2.

The axiom consists of three components. Modules  $F$  and  $A(0)$  represent the initial segment and the apex of the main axis. Module  $I(20)$  is the source of a signal representing florigen. In nature, florigen is sent towards the apex by leaves located at the plant base, which is not included in this model.

The developmental process consists of two phases that take place along the main axis and are repeated recursively in branches of higher orders. First, the main axis is formed in a process of subapical growth

*Mycelis**Model II*

```

#include 0                /* flower shape specification */
#ignore / + ~ 0

 $\omega$  : I(20)FA(0)
 $p_1$  : S < A(t)          : *  $\rightarrow$  T(0)~0
 $p_2$  : A(t)              : t>0  $\rightarrow$  A(t-1)
 $p_3$  : A(t)              : t=0  $\rightarrow$  [(+30)G]F/(180)A(2)
 $p_4$  : S < F            : *  $\rightarrow$  FS
 $p_5$  : F > T(c)         : *  $\rightarrow$  T(c+1)FU(c-1)
 $p_6$  : U(c) < G         : *  $\rightarrow$  I(c)FA(2)
 $p_7$  : I(c)             : c>0  $\rightarrow$  I(c-1)
 $p_8$  : I(c)             : c=0  $\rightarrow$  S
 $p_9$  : S                : *  $\rightarrow$   $\epsilon$ 
 $p_{10}$  : T(c)           : *  $\rightarrow$   $\epsilon$ 

```

L-system 3.2: *Mycelis muralis* – Model II

specified by production  $p_3$ . The apex produces consecutive segments  $F$  at the rate of one segment every three derivation steps (the delay is controlled by production  $p_2$ ), and initiates branches  $G$  positioned at an angle of  $30^\circ$  with respect to the main axis. The symbol  $G$  is interpreted here in the same way as  $F$ . At this stage, the branches do not develop further, which simulates the effect of *apical dominance* or the inhibition of branch development during the active production of new branches by the apex.

After a delay of 20 derivation steps, counted using production  $p_7$ , an acropetal flower-inducing signal  $S$  is sent by production  $p_8$ . Production  $p_4$  transports  $S$  across the segments at the rate of one internode per step. Since new internodes are produced by the apex at a three times slower rate, the signal eventually reaches the apex. At this point, the second developmental phase begins. Production  $p_1$  transforms apex  $A(t)$  into a bud  $O$ . Further branch production is stopped and a signal  $T(c)$  is sent towards the base in order to enable the development of lateral branches. Parameter  $c$  is incremented by production  $p_5$  each time signal  $T(c)$  traverses an internode. Subsequently, production  $p_6$  introduces the value of parameter  $c$  into the corresponding branches, using module  $U(c)$  as a carrier. The successor of production  $p_6$  has the same format as the axiom, thus module  $I(c)$  determines the delay between the initiation of branch development and time signal  $S$ , sent to terminate further internode creation. This delay  $c$  is smallest for the top branches and increases towards the plant base. Consequently, parameter  $c$  can be interpreted as the *growth potential* of the branches, allowing lower branches to grow longer than the higher ones. On the other hand, the development of the upper branches starts sooner, thus in some stages they will be more developed than the lower ones, and the flowering sequence will progress downwards, corresponding to ob-

```

#include K          /* flower shape specification */
#consider M S T V

 $\omega$  : I(20)FA(0)
p1 : S < A(t) : * → TV K
p2 : V < A(t) : * → TV K
p3 : A(t) : t>0 → A(t-1)
p4 : A(t) : t=0 → M[+(30)G]F/(180)A(2)
p5 : S < M : * → S
p6 : S > T : * → T
p7 : T < G : * → FA(2)
p8 : V < M : * → S
p9 : T > V : * → W
p10 : W : * → V
p11 : I(t) : t>0 → I(t-1)
p12 : I(t) : t=0 → S

```

L-system 3.3: *Mycelis muralis* – Model III

servations of the real plant [77].

A diagrammatic developmental sequence of *Mycelis muralis* simulated using L-system 3.2 is shown in Figure 3.17. Initially, the segments are shown as bright green. The passage of florigen  $S$  turns them purple, and the lifting of apical dominance changes their color to dark green. Figure 3.18 represents a three-dimensional rendering of the same model. The three-dimensional structure differs from the two-dimensional diagram only in details. The angle value associated with the module “/” in production  $p_3$  has been changed to  $137.5^\circ$ , resulting in a spiral arrangement of lateral branches around the mother axis. The leaves subtending branches have been included in the model, and flowers have been assumed to undergo a series of changes from bud to open flower to fruit.

Another developmental model of *Mycelis*, referred to here as *model III*, is given by L-system 3.3. The initial phases of development are the same as in model II. First, apex  $A$  creates the main axis and initiates lateral branches (productions  $p_3$  and  $p_4$ ). Symbol  $M$  in the successor of production  $p_4$  marks consecutive branching points. After a delay of 20 steps ( $\omega$ ) counted by production  $p_{11}$ , flowering signal  $S$  is generated at the inflorescence base ( $p_{12}$ ) and sent up along the main axis ( $p_5$ ). Upon reaching the apex,  $S$  induces its transformation into a terminal flower  $K$ , and initiates two basipetal signals  $T$  and  $V$  ( $p_1$ ). The basipetal signals also can be initiated by production  $p_2$ , which is needed for the proper timing of signals in the topmost lateral branch. Signal  $T$  propagates basipetally at the rate of one internode per derivation step ( $p_6$ ) and lifts apical dominance, thus allowing the lateral branches to grow ( $p_7$ ). The presence of the second basipetal signal  $V$  is the distinctive

*Model III*

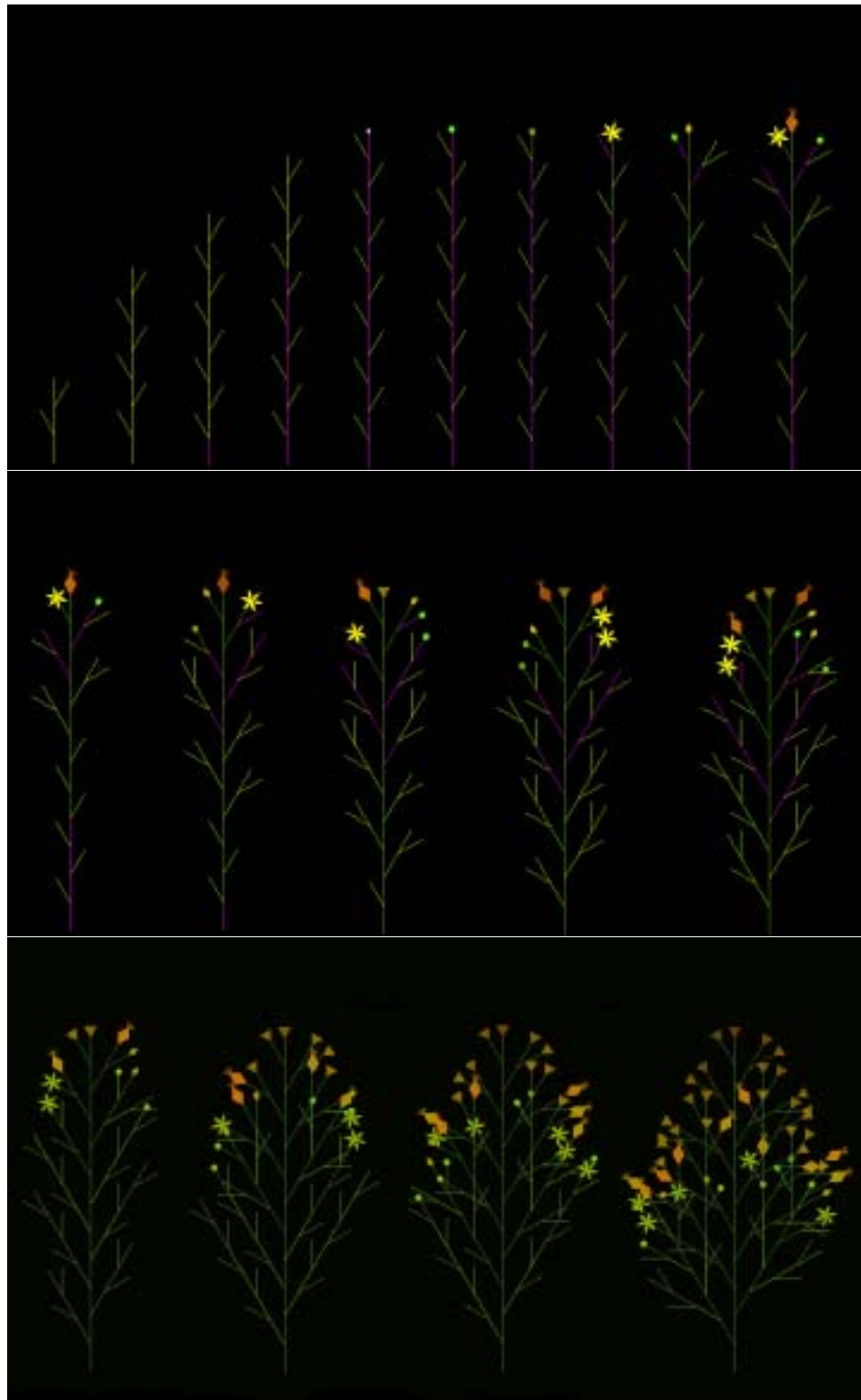


Figure 3.17: Development of *Mycelis muralis*

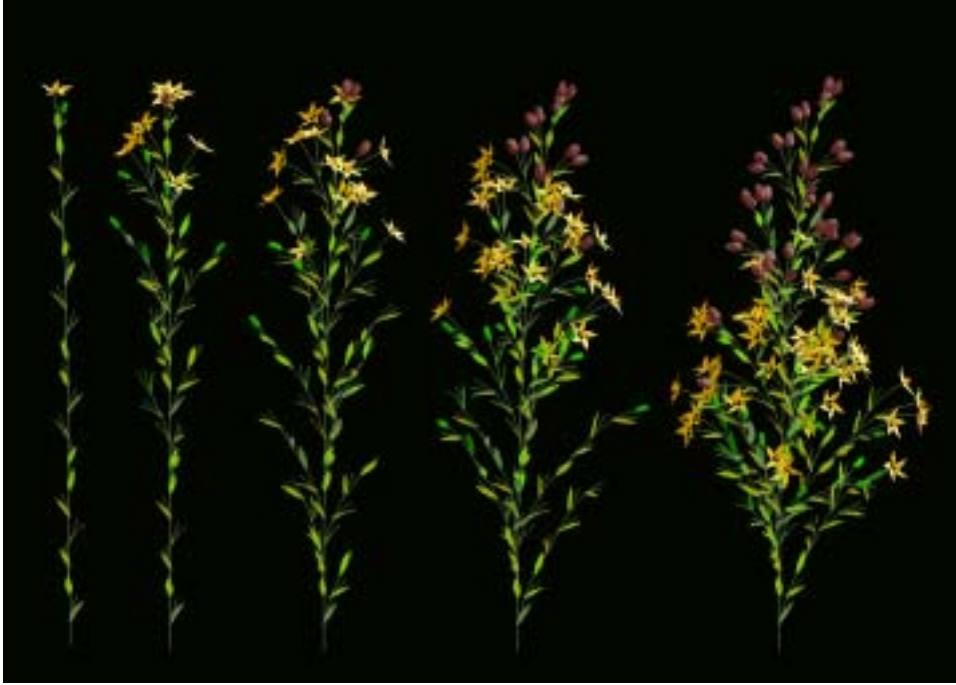


Figure 3.18: A three-dimensional rendering of the *Mycelis* model

feature of model III. Its role is to enable the formation of flowers on the lateral branches by generating the flowering signal  $S$  at their bases ( $p_8$ ). Since signal  $V$  propagates down the main axis at the rate of one internode per two derivation steps ( $p_9, p_{10}$ ), the interval between the lifting of apical dominance by signal  $T$  and induction of flowering signal  $S$  by signal  $V$  increases linearly towards the inflorescence base. This allows the lower branches to grow longer than the upper ones, resulting in a structure that is more developed near the base than near the apex in later developmental stages.

This entire control process repeats recursively for each axis: its apex is transformed into a flower by signal  $S$ , the growth of lateral axes is successively enabled by signal  $T$ , and the second basipetal signal  $V$  is sent to induce the flowering signal  $S$  in the next-order axes. Consequently, a basipetal flowering sequence is observed along all axes of the panicle.

Model II controls the flowering on lateral branches using growth potential  $c$  accumulated by signal  $T$  on its way down, while model III employs the time interval between signals  $T$  and  $V$  for the same purpose. Since both models produce identical developmental sequences, it is not possible to decide which one is more faithful to nature without gathering additional data related to plant physiology. Nevertheless, the models clearly indicate that the flowering sequence of *Mycelis* cannot be explained simply in terms of two commonly recognized mechanisms,

*Biological  
relevance*



$n=10, \delta = 60^\circ$

```
#include K /* flower shape specification */
```

```
 $\omega$  : A~K
 $p_1$  : A      : *      → [-/~K] [+/~K] I(0)/(90)A
 $p_2$  : I(t)  : !(t=2) → FI(t+1)
 $p_3$  : I(t)  : t=2    → I(t+1) [-FFA] [+FFA]
```

Figure 3.19: Lilac inflorescences



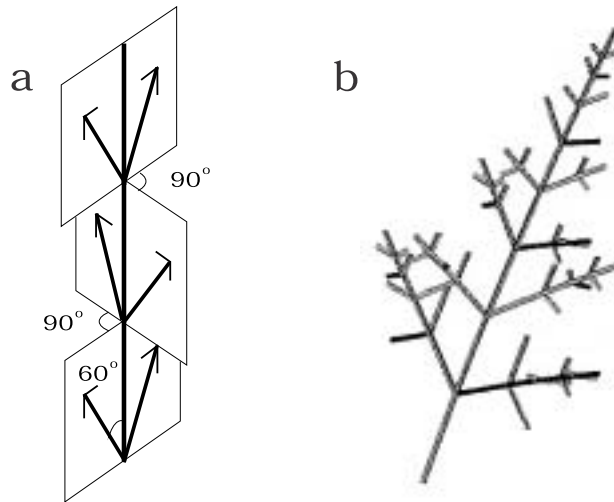


Figure 3.20: Geometry of a lilac inflorescence: (a) the decussate branching pattern, (b) the inflorescence skeleton without flowers

the flowering signal and the lifting of apical dominance. Another factor, whether it is an accumulated delay or a third signal, is needed. The mathematical models bring forward evidence and assist in formulating plausible hypotheses related to the control mechanisms that may be employed by nature. The final answer will require further study of the real plant.

The models of *Mycelis* employ relatively complicated control processes to explain the developmental sequence of a plant. On the other hand, if only a static image of a panicle in a particular developmental stage is needed, much simpler L-systems can be used. The L-system that generates the lilac inflorescences shown in Figure 3.19 is an example. Production  $p_1$  describes the subapical development of an axis. Production  $p_2$  models linear elongation of internodes in time and introduces a delay before  $p_3$  creates the lateral axes. The rotation of the apex by  $90^\circ$  ( $p_1$ ) results in a *decussate* branching pattern with consecutive pairs of  $(n + 1)$ -order axes lying in the planes that pass through the  $n$ -order axis and are perpendicular to each other (Figure 3.20). A scene including lilac inflorescences is shown in Figure 3.21.

*Lilac*

### 3.3.4 Modified racemes

There are four frequently encountered types of inflorescences that are morphological modifications of racemes. Their mature forms are of a special kind and need to be specified separately.



Figure 3.21: The garden of L

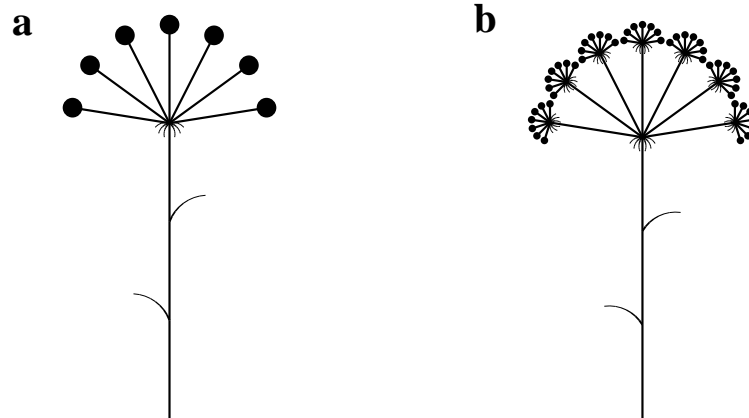


Figure 3.22: Umbels: (a) simple, (b) compound

### Umbel

An *umbel* is characterized by more than two internodes attached to a single node, resulting in a typical umbrella-like shape. In a simple umbel there are flowers at the ends of the lateral internodes (Figure 3.22a), while in compound umbels the branching pattern is repeated recursively a certain number of times (Figure 3.22b). The partial L-system for a simple umbel is

$$\begin{aligned}\omega &: A \\ p_1 &: A \rightarrow I[IK]^n\end{aligned}$$

and for a compound umbel of recursion depth two is

$$\begin{aligned}\omega &: A \\ p_1 &: A \rightarrow I[IB]^k B \\ p_2 &: B \rightarrow I[IC]^l C \\ p_3 &: C \rightarrow I[IK]^m\end{aligned}$$

This type of inflorescence is commonly found in the family Umbelliferae. For example, Figure 3.23 presents a model of a wild carrot. Note that the size of leaves decreases towards the top of the plant, producing a phase effect similar to that observed in simple racemes. In contrast, the most developed inflorescence is placed at the top of the plant, indicating developmental control by a hormone similar to that observed in mints (Figure 3.11).

*Wild carrot*

### Spike

An elongated raceme with closely packed flowers is called a *spike*. Many grasses and sedges have this kind of inflorescence (Figure 3.24a). See Figure 4.17 (page 117) for a realistic model.



Figure 3.23: Wild carrot

### Spadix

A fleshy elongated raceme is called a *spadix*, and is frequently found in the family Araceae (Figure 3.24b).

### Capitulum

A fleshy spherical or disk-shaped raceme is called a *capitulum* or “head.” The sunflower head is an inflorescence of this kind, the oldest flowers being at the margin and the youngest at the center (Figure 3.24c). Members of the family Compositae commonly have this type of structure. One characteristic feature is the spatial arrangement of components, such as flowers or seeds, which form early discernible spiral patterns. A detailed description of these patterns is presented in the next chapter.

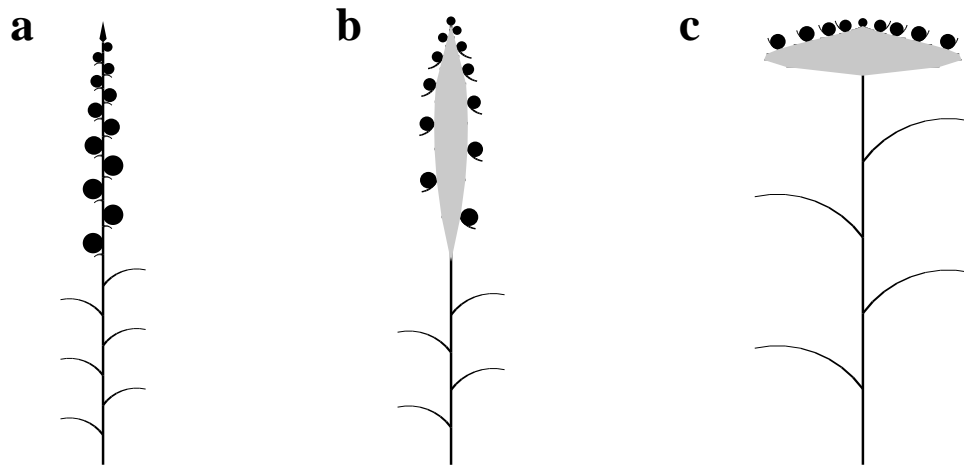


Figure 3.24: Modified racemes: (a) spike, (b) spadix, (c) capitulum



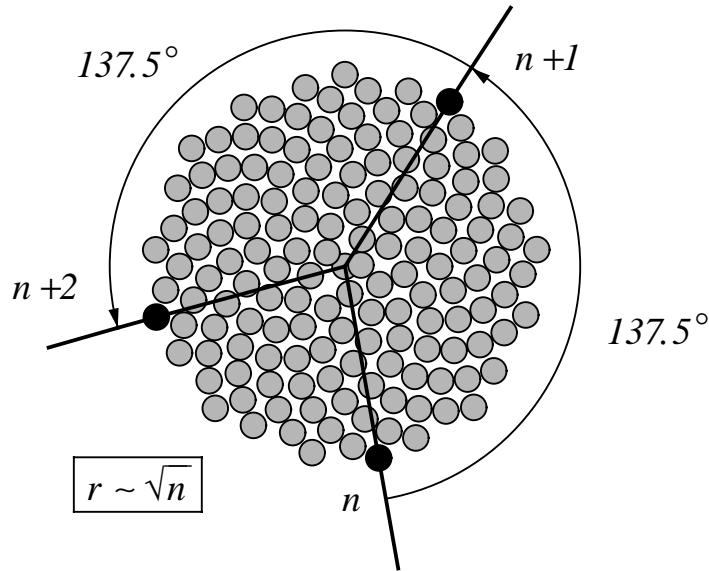
# Chapter 4

## Phyllotaxis

The regular arrangement of lateral organs (leaves on a stem, scales on a cone axis, florets in a composite flower head) is an important aspect of plant form, known as *phyllotaxis*. The extensive literature generated by biologists' and mathematicians' interest in phyllotaxis is reviewed by Erickson [36] and Jean [78]. The proposed models range widely from purely geometric descriptions (for example, Coxeter [17]) to complex physiological hypotheses tested by computer simulations (Hellendoorn and Lindenmayer [59], Veen and Lindenmayer [151], Young [163]). This chapter presents two models suitable for the synthesis of realistic images of flowers and fruits that exhibit spiral phyllotactic patterns.

Both models relate phyllotaxis to packing problems. The first operates in a plane and was originally proposed by Vogel [154] to describe the structure of a sunflower head. A further detailed analysis was given by Ridley [124, 125]. The second model reduces phyllotaxis to the problem of packing circles on the surface of a cylinder. Its analysis was presented by van Iterson [75] and reviewed extensively by Erickson [36].

The area of phyllotaxis is dominated by intriguing mathematical relationships. One of them is the "remarkable fact that the numbers of spirals which can be traced through a phyllotactic pattern are predominantly integers of the Fibonacci sequence" [36, p. 54]. For example, Coxeter [17] notes that the pineapple displays eight rows of scales sloping to the left and thirteen rows sloping to the right. Furthermore, it is known that the ratios of consecutive Fibonacci numbers  $F_{k+1}/F_k$  converge towards the golden mean  $\tau = (\sqrt{5} + 1)/2$ . The *Fibonacci angle*  $360^\circ\tau^{-2}$ , approximately equal to  $137.5^\circ$ , is the key to the first model discussed in this chapter.



```

#define a 137.5 /* divergence angle */
#include D      /* disk shape specification */

omega : A(0)
p1 : A(n) : * -> +(a) [f(n^0.5)~D]A(n+1)

```

Figure 4.1: Pattern of florets in a sunflower head, according to Vogel's formula

## 4.1 The planar model

### *Vogel's formula*

In order to describe the pattern of florets (or seeds) in a sunflower head, Vogel [154] proposed the formula

$$\phi = n * 137.5^\circ, \quad r = c\sqrt{n}, \quad (4.1)$$

where:

- $n$  is the ordering number of a floret, counting outward from the center. This is the reverse of floret age in a real plant.
- $\phi$  is the angle between a reference direction and the position vector of the  $n^{\text{th}}$  floret in a polar coordinate system originating at the center of the capitulum. It follows that the *divergence angle* between the position vectors of any two successive florets is constant,  $\alpha = 137.5^\circ$ .
- $r$  is the distance between the center of the capitulum and the center of the  $n^{\text{th}}$  floret, given a constant scaling parameter  $c$ .



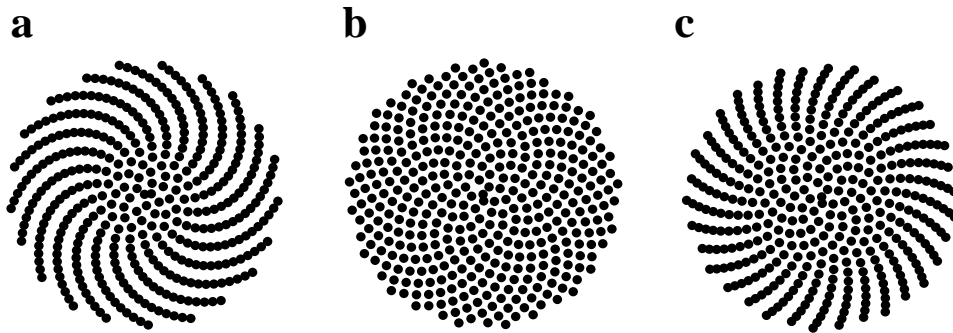


Figure 4.2: Generating phyllotactic patterns on a disk. These three patterns differ only by the value of the divergence angle  $\alpha$ , equal to (a)  $137.3^\circ$ , (b)  $137.5^\circ$  (the correct value), and (c)  $137.6^\circ$ .

The distribution of florets described by formula (4.1) is shown in Figure 4.1. The square-root relationship between the distance  $r$  and the floret ordering number  $n$  has a simple geometric explanation. Assuming that all florets have the same size and are densely packed, the total number of florets that fit inside a disc of radius  $r$  is proportional to the disk area. Thus, the ordering number  $n$  of the most outwardly positioned floret in the capitulum is proportional to  $r^2$ , or  $r \sim \sqrt{n}$ .

The divergence angle of  $137.5^\circ$  is much more difficult to explain. Vogel [154] derives it using two assumptions.

- Each new floret is issued at a fixed angle  $\alpha$  with respect to the preceding floret.
- The position vector of each new floret fits into the largest existing gap between the position vectors of the older florets.

Ridley [125] does not object to these basic assumptions, but indicates that they are insufficient to explain the origin of the Fibonacci angle, and points to several arbitrary steps present in Vogel's derivation. He describes the main weakness as follows:

While it is reasonable to assume that the plant could contain genetic information determining the divergence angle to some extent, it is completely impossible for this alone to fix the divergence angle to the incredible accuracy occurring in nature, since natural variation in biological phenomena is normally rather wide. For example, for the 55- and 89-parastichies to be conspicuous, as occurs in most sunflower heads,  $d$  must lie between  $\frac{21}{55}$  and  $\frac{34}{89}$ , a relative accuracy of one part in 1869.

The critical role of the divergence angle  $\alpha$  is illustrated in Figure 4.2.

*Model  
justification*



Figure 4.3: Close-up of a daisy capitulum

*Parastichies*

Although a comprehensive justification of Vogel's formula may require further research, the model correctly describes the arrangement of florets visible in actual capitula. The most prominent feature is two sets of spirals or *parastichies*, one turning clockwise, the other counterclockwise, which are composed of nearest neighboring florets. The number of spirals in each set is always a member of the Fibonacci sequence; 21 and 34 for a small capitulum, up to 89 and 144 or even 144 and 233 for large ones. For example, the capitulum of a daisy (Figure 4.3) exhibits 34 clockwise spirals and 21 counterclockwise spirals, with directions determined by following the spirals outwards from the capitulum center. In the image of a domestic sunflower capitulum (Figure 4.4), one can discern 34 spirals running clockwise and 55 spirals running counterclockwise. The number of perceived spirals depends on the capitulum size expressed in terms of the number of component florets. If the field of attention is limited to a circle approximately  $2/3$  the size of the entire sunflower capitulum in Figure 4.4, the number of discernible spirals becomes 34 and 21.

Figure 4.4: Domestic sunflower head





```

#define S          /* seed shape */
#define R          /* ray floret shape */
#include M N O P  /* petal shapes */

 $\omega$  : A(0)
p1 : A(n) : *  $\rightarrow$  +(137.5)[f(n0.5)C(n)]A(n+1)
p2 : C(n) : n  $\leq$  440  $\rightarrow$  ~S
p3 : C(n) : 440 < n & n  $\leq$  565  $\rightarrow$  ~R
p4 : C(n) : 565 < n & n  $\leq$  580  $\rightarrow$  ~M
p5 : C(n) : 580 < n & n  $\leq$  595  $\rightarrow$  ~N
p6 : C(n) : 595 < n & n  $\leq$  610  $\rightarrow$  ~O
p7 : C(n) : 610 < n  $\rightarrow$  ~P

```

The dependence of the number of parastichies on the size of the field of attention is yet another intriguing aspect of spiral phyllotaxis, as pointed out in the following excerpt from a letter by Alan Turing<sup>1</sup> quoted in [18]:

According to the theory I am working on now there is a continuous advance from one pair of parastichy numbers to another, during the growth of a single plant. . . . You will be inclined to ask how one can move continuously from one integer to another. The reason is this — on any specimen there are different ways in which the parastichy numbers can be reckoned; some are more natural than others. During the growth of a plant the various parastichy numbers come into prominence at different stages. One can also observe the phenomenon in space (instead of in time) on a sunflower. It is natural to count the outermost florets as say  $21 + 34$ , but the inner ones might be counted as  $8 + 13$ . . . . I don't know any really satisfactory account, though I hope to get one myself in about a year's time.

A complete model of a flower head, suitable for realistic image synthesis, should contain several organs of various shapes. This is easily achieved by associating different surfaces with specific ranges of the index  $n$ . For example, consider the L-system that generates the sunflower head (Figure 4.4). The layout of components is specified by production  $p_1$ , similar to that of the L-system in Figure 4.1. Productions  $p_2$  to  $p_7$  determine colors and shapes of components as a function of the derivation step number. The entire structure shown in Figure 4.4 was generated in 630 steps. Alternatively, random selection of similar surfaces could have been employed to prevent the excessive regularity of the resulting image.

*Sunflower head*

Other extensions to the basic model consist of varying organ orientation in space and changing their altitude from the plane of the head as a function of  $n$ . For example, the sunflower plants included in Figure 4.5 have flowers in four developmental stages: buds, young flowers starting to open, open flowers and older flowers where the petals begin to droop. All flowers are generated using approximately the same number of florets. The central florets are represented by the same surface at each stage. The shape and orientation of surfaces representing petals vary from one stage to another. The plants have been modeled as dibotryoids, with a single signal inducing a basipetal flowering sequence, as described in the previous chapter.

---

<sup>1</sup>To computer scientists, Alan Turing is best known as the inventor of the *Turing machine* [146], which plays an essential role in defining the notion of an algorithm. However, biologists associate Turing's name primarily with his 1952 paper, "The chemical basis of morphogenesis" [147], which pioneered the use of mathematical models in the study of pattern formation and advocated the application of computers to simulate biological phenomena.



Figure 4.5: Sunflower field



Figure 4.6: Zinnias

*Other examples*

The zinnias (Figures 4.6 and 4.7) illustrate the effect of changing a petal's altitude, size and orientation as a function of  $n$ . The height at which a petal is placed decreases by a small amount as  $n$  increases. The size of each successive petal is incremented linearly. The orientation is also adjusted linearly by a small angle increment. Thus, petals with small values of index  $n$  are placed more vertically, while petals with larger indices  $n$  are more horizontal. Although the family Compositae offers the most examples of phyllotactic patterns, the same model can be applied to synthesize images of other flowers, such as water-lilies (Figures 4.8 and 4.9) and roses (Figure 4.10).

Figure 4.7: Close-up of zinnias







Figure 4.8: Water-lily



Figure 4.9: Lily pond





Figure 4.10: Roses

## 4.2 The cylindrical model

The spiral patterns evident in elongated organs such as pine cones, fir cones and pineapples, can be described by models that position components, in this case scales, on the surface of a cylinder. Van Iterson [75] divides phyllotactic patterns on cylinders into *simple* and *conjugate* ones. In the case of a simple arrangement, all components lie on a single *generative helix*. In contrast, conjugate patterns consist of two or more interleaved helices. This paper discusses simple phyllotactic patterns only. They are generally characterized by the formula

*Basic model*

$$\phi = n * \alpha, \quad r = \text{const}, \quad H = h * n, \quad (4.2)$$

where:

- $n$  is the ordering number of a scale, counting from the bottom of the cylinder;
- $\phi$ ,  $r$  and  $H$  are the cylindrical coordinates of the  $n^{\text{th}}$  scale;
- $\alpha$  is the divergence angle between two consecutive scales (as in the planar case, it is assumed to be constant); and
- $h$  is the vertical distance between two consecutive scales (measured along the main axis of the cylinder).

*Implementation  
using  
L-systems*

A parametric L-system that generates the pattern described by formula (4.2) is given in Figure 4.11. The operation of this L-system simulates the natural process of subapical development characterized by sequential production of consecutive modules by the top part of the growing plant or organ. The apex  $A$  produces internodes  $f(h)$  along the main axis of the modeled structure. Associated with each internode is a disk  $\sim D$  placed at a distance  $r$  from the axis. This offset is achieved by moving the disk away from the axis using the module  $f(r)$ , positioned at a right angle with respect to the axis by  $\&(90)$ . The spiral disk distribution is due to the module  $/(a)$ , which rotates the apex around its own axis by the divergence angle in each derivation step.

*Analysis of  
model geometry*

In the planar model, the constant divergence angle  $\alpha = 137.5^\circ$  is found across a large variety of flower heads. The number of perceived parastichies is determined by the capitulum size, and it changes as the distance from the capitulum center increases. In contrast, a phyllotactic pattern on the surface of a cylinder is uniform along the entire cylinder length. The number of evident parastichies depends on the values of parameters  $\alpha$  and  $h$ . The key problem, both from the viewpoint of understanding the geometry of the pattern and applying it to generate synthetic images, is to express the divergence angle  $\alpha$  and the vertical displacement  $h$  as a function of the numbers of evident parastichies encircling the cylinder in the clockwise and counterclockwise directions. A solution to this problem was proposed by van Iterson [75] and reviewed by Erickson [36]. Our presentation closely follows that of Erickson.

The phyllotactic pattern can be explained in terms of circles packed on the surface of the cylinder. An evident parastichy consists of a sequence of tangent circles, the ordering numbers of which form an arithmetic sequence with difference  $m$ . The number  $m$  is referred to as the *parastichy order*. Thus, the circles on the cylinder surface may be arranged in two congruent 2-parastichies, five congruent 5-parastichies, and so on. The angular displacement between two consecutive circles in an  $m$ -parastichy is denoted by  $\delta_m$ . By definition,  $\delta_m$  belongs to the range  $(-\pi, \pi]$  radians. The relation between the angular displacement  $\delta_m$  and the divergence angle  $\alpha$  is expressed by the equation

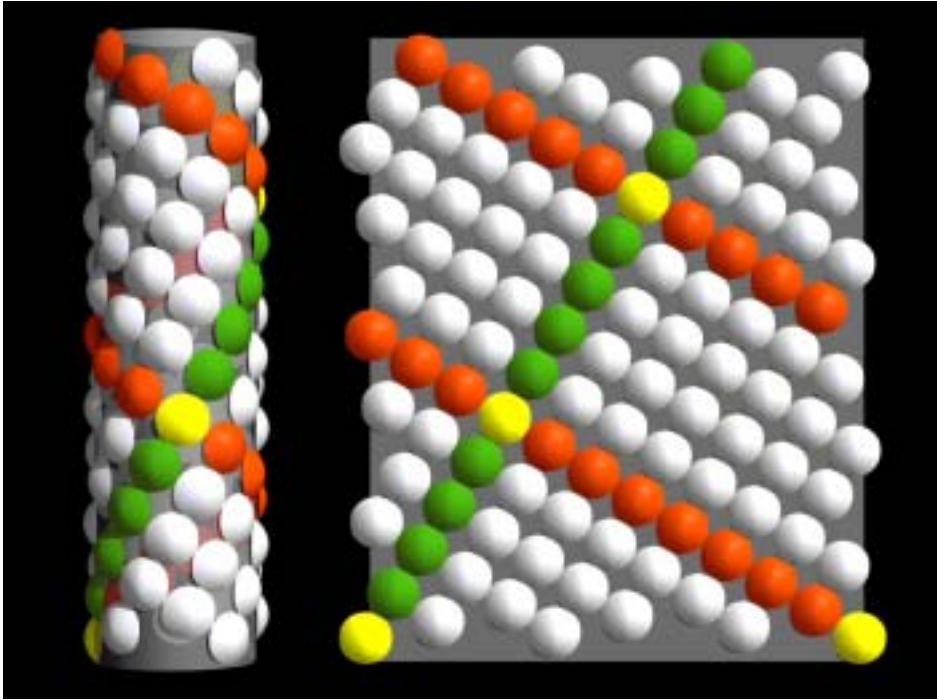
$$\delta_m = m\alpha - \Delta_m 2\pi, \quad (4.3)$$

where  $\Delta_m$  is an integer called the *encyclic number*. It is the number of turns around the cylinder, rounded to the nearest integer, which the generative helix describes between two consecutive points of the  $m$ -parastichy.

Usually, one can perceive two series of parastichies running in opposite directions (Figure 4.11). The second parastichy satisfies an equation analogous to (4.3):

$$\delta_n = n\alpha - \Delta_n 2\pi \quad (4.4)$$

Consider the  $m$ - and  $n$ -parastichies starting at circle 0. In their paths across the cylinder, they will intersect again at circle  $mn$ . Assume



```

#define a 137.5281 /* divergence angle */
#define h 35.3 /* vertical displacement */
#define r 500 /* component offset from main axis */
#include D /* disk shape specification */

 $\omega$  : A
 $p_1$  : A : *  $\rightarrow$  [ $\&(90)f(r)\sim D$ ]f(h)/(a)A

```

Figure 4.11: Parastichies on the surface of a cylinder and on the unrolled cylinder. The L-system generates the cylindrical pattern.

that  $m$  and  $n$  are relatively prime; otherwise the phyllotactic pattern would have to contain several circles lying at the same height  $H$  and, contrary to the initial assumption, would not be simple. The circle  $mn$  is the first point of intersection between the  $m$ -parastichy and the  $n$ -parastichy above circle 0. Consequently, the path from circle 0 to  $mn$  along the  $m$ -parastichy, and back to 0 along the  $n$ -parastichy, encircles the cylinder exactly once. The section of  $m$ -parastichy between circles 0 and  $mn$  consists of  $n+1$  circles (including the endpoints), so the angular distance between the circles 0 and  $mn$  is equal to  $n\delta_m$ . Similarly, the distance between circles 0 and  $mn$ , measured along the  $n$ -parastichy, can be expressed as  $m\delta_n$ . As a result,

$$n\delta_m - m\delta_n = \pm 2\pi. \quad (4.5)$$

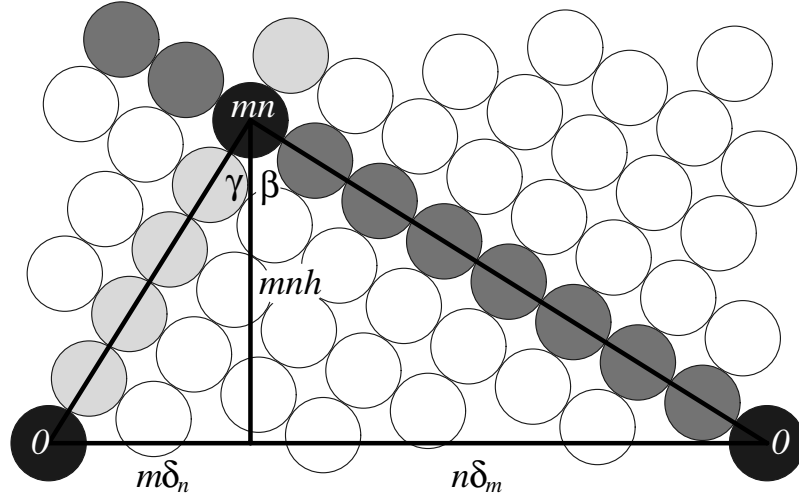


Figure 4.12: An opposite parastichy triangle (as in Erickson [36, Fig. 3.8]). The base is formed by the circumference of the cylinder. The sides are formed by the parastichies.

The signs in equation (4.5) correspond to the assumption that the spirals encircle the cylinder in opposite directions; thus one of the values  $\delta$  is positive and the other one is negative. Substituting the right sides of equations (4.3) and (4.4) for  $\delta_m$  and  $\delta_n$  yields

$$n\Delta_m - m\Delta_n = \pm 1. \quad (4.6)$$

To further analyze the pertinent geometric relationships, the cylinder is cut along the vertical line passing through the center of circle 0 and “unrolled” (Figure 4.11). The two parastichies and the circumference of the cylinder passing through point 0 form a triangle as shown in Figure 4.12. The perpendicular to the base from point  $mn$  divides this triangle into two right triangles. If  $d$  denotes the diameter of the circles, then

$$(n\delta_m)^2 + (mnh)^2 = (nd)^2$$

and

$$(m\delta_n)^2 + (mnh)^2 = (md)^2.$$

The above system of equations can be solved with respect to  $h$  and  $d$ :

$$h = \sqrt{(\delta_m^2 - \delta_n^2)/(n^2 - m^2)} \quad (4.7)$$

$$d = \sqrt{(n^2\delta_m^2 - m^2\delta_n^2)/(n^2 - m^2)} \quad (4.8)$$

or, taking into consideration equation (4.5),

$$d = \sqrt{2\pi(n\delta_m + m\delta_n)/(n^2 - m^2)}. \quad (4.9)$$

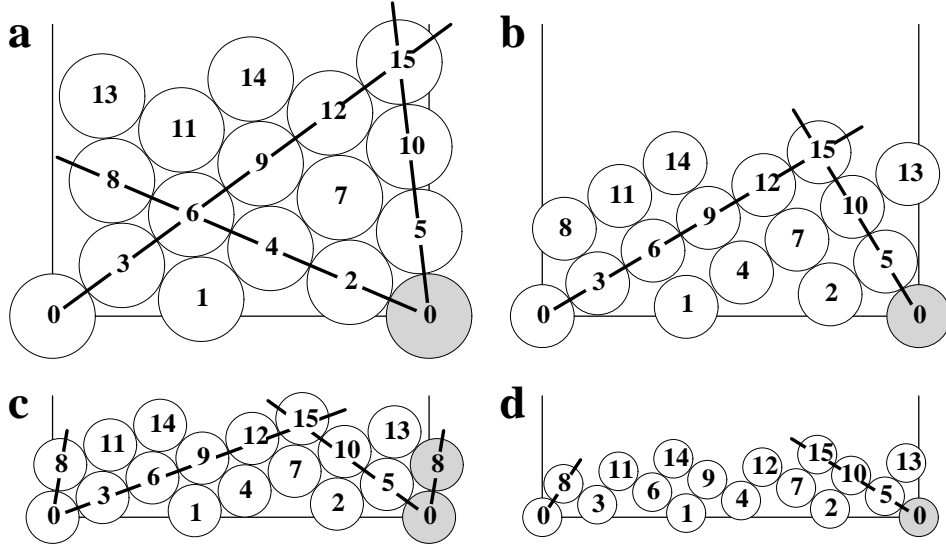


Figure 4.13: Patterns of tangent circles drawn on the surface of a cylinder as a function of circle diameter

The problem is to determine values of  $\delta_m$  and  $\delta_n$ . They are not simply functions of parameters  $m$  and  $n$ . Figure 4.13 shows that, for a given  $m$  and  $n$ , the values of  $\delta_m$  and  $\delta_n$  can be chosen from a certain range, yielding parastichies of different steepness. In order to determine this range, observe that at its limits the phyllotactic pattern changes; one previously evident parastichy disappears and another is formed. Thus, at the range limit, *three* evident parastichies coexist. It follows from Figure 4.13 that at one end of the range the third parastichy has order  $|m-n|$ , and at the other end it has order  $(m+n)$ . Three coexisting parastichies imply that each circle is tangent to six other circles. In other words, all circles lie in the vertices of a regular hexagonal grid, as seen in Figure 4.13a and c. Consequently, the angle  $\beta + \gamma$  at vertex  $mn$  (Figure 4.12) is equal to  $2\pi/3$ . Expressing the base of the triangle in terms of its two sides and their included angle results in

$$(2\pi)^2 = (nd)^2 + (md)^2 - 2(nd)(md) \cos(2\pi/3)$$

or, after simplification,

$$d = 2\pi/\sqrt{m^2 + mn + n^2}. \quad (4.10)$$

Equations (4.9) and (4.10) yield

$$n\delta_m + m\delta_n = 2\pi(n^2 - m^2)/(m^2 + mn + n^2). \quad (4.11)$$

Solving the system of equations (4.5) and (4.11) with respect to  $\delta_m$  and  $\delta_n$  produces

$$\delta_m = \pi(m + 2n)/(m^2 + mn + n^2) \quad (4.12)$$

and

$$\delta_n = \pi(2m + n)/(m^2 + mn + n^2). \quad (4.13)$$

Given the values of  $\delta_m$  and  $\delta_n$ , the divergence angle  $\alpha$  can be found from either equation (4.3) or (4.4), assuming that the encyclic numbers  $\Delta_m$  or  $\Delta_n$  are known. It follows from the definition that these numbers are the *smallest* positive integers satisfying equation (4.6). A systematic method for solving this equation, based on the theory of continuous fractions, is presented by van Iterson [75]. Erickson [36] points out that in practice the solution can often be found by guessing. Another possibility is to look for the smallest pair of numbers  $(\Delta_m, \Delta_n)$  satisfying (4.6) using a simple computer program.

*Pattern  
construction*

In conclusion, a phyllotactic pattern characterized by a pair of numbers  $(m, n)$  can be constructed as follows:

1. Find  $\Delta_m$  and  $\Delta_n$  from equation (4.6).
2. Find the range of admissible values of the angular displacements  $\delta_m$  and  $\delta_n$ . The limits can be obtained from equations (4.12) and (4.13) using the values of  $m$  and  $n$  for one limit, and the pair  $(\min\{m, n\}, |m - n|)$  for the other.
3. For a chosen pair of admissible displacement values  $\delta_m$  and  $\delta_n$ , calculate the divergence angle  $\alpha$  from equation (4.3) or (4.4) and the vertical displacement  $h$  from equation (4.8).
4. Find the diameter  $d$  of the circles from equation (4.8).

The diameter  $d$  does not enter directly in any formula used for image synthesis, but serves as an estimate of the size of surfaces to be incorporated in the model. This algorithm was applied to produce Table 4.1 showing parameter values for which three parastichies coexist. Given a pattern with two parastichies, this table provides the limits of the divergence angle  $\alpha$ . For example, a (5,8) pattern can be formed for values of  $\alpha$  ranging from  $135.918365^\circ$  to  $138.139542^\circ$ , which correspond to the patterns (3,5,8) and (5,8,13), respectively.

*Triple-contact  
patterns*

Further information relating the divergence angle  $\alpha$  to the vertical displacement  $h$  for various phyllotactic patterns is shown in Figure 4.14. The arcs represent parameters of patterns with two parastichies  $(m, n)$ . The branching points represent parameters of patterns with three parastichies  $(m, n, m + n)$ .

$m,n,m+n$	$\alpha$ (degrees)	$h$	$d$
(1, 1, 2)	180.000000	1.81380	-
(1, 2, 3)	128.571426	0.777343	2.374821
(1, 3, 4)	96.923073	0.418569	1.742642
(2, 3, 5)	142.105270	0.286389	1.441462
(1, 4, 5)	77.142860	0.259114	1.371104
(3, 4, 7)	102.162163	0.147065	1.032949
(3, 5, 8)	135.918365	0.111049	0.897598
(2, 5, 7)	152.307693	0.139523	1.006115
(1, 5, 6)	63.870968	0.175529	1.128493
(4, 5, 9)	79.672134	0.089203	0.804479
(4, 7, 11)	98.709671	0.058510	0.651536
(3, 7, 10)	107.088600	0.068878	0.706914
(3, 8, 11)	131.752579	0.056097	0.637961
(5, 8, 13)	138.139542	0.042181	0.553204
(5, 7, 12)	150.275223	0.049921	0.601820
(2, 7, 9)	158.507462	0.081215	0.767613

Table 4.1: Cylinder formula values for triple-contact patterns

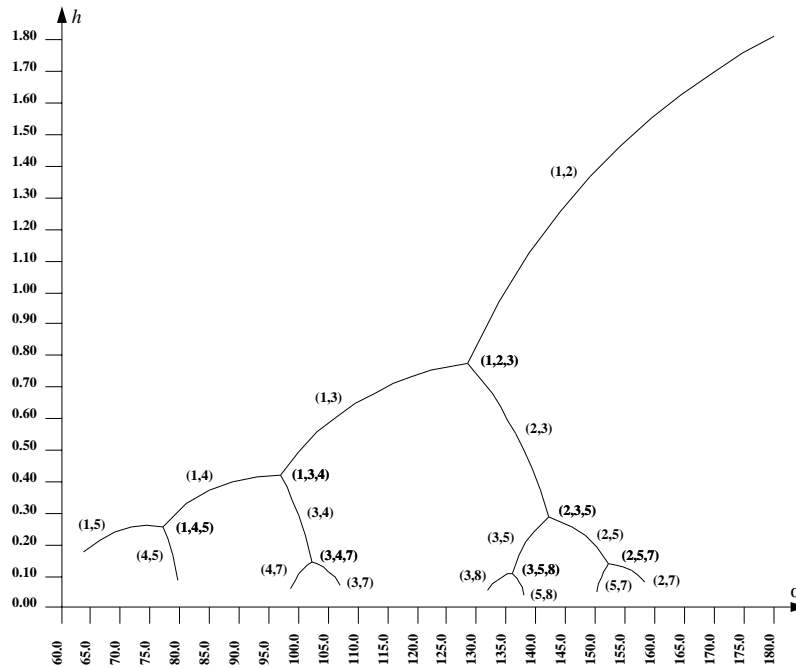


Figure 4.14: The vertical displacement  $h$  as a function of the divergence angle  $\alpha$  for various phyllotactic patterns

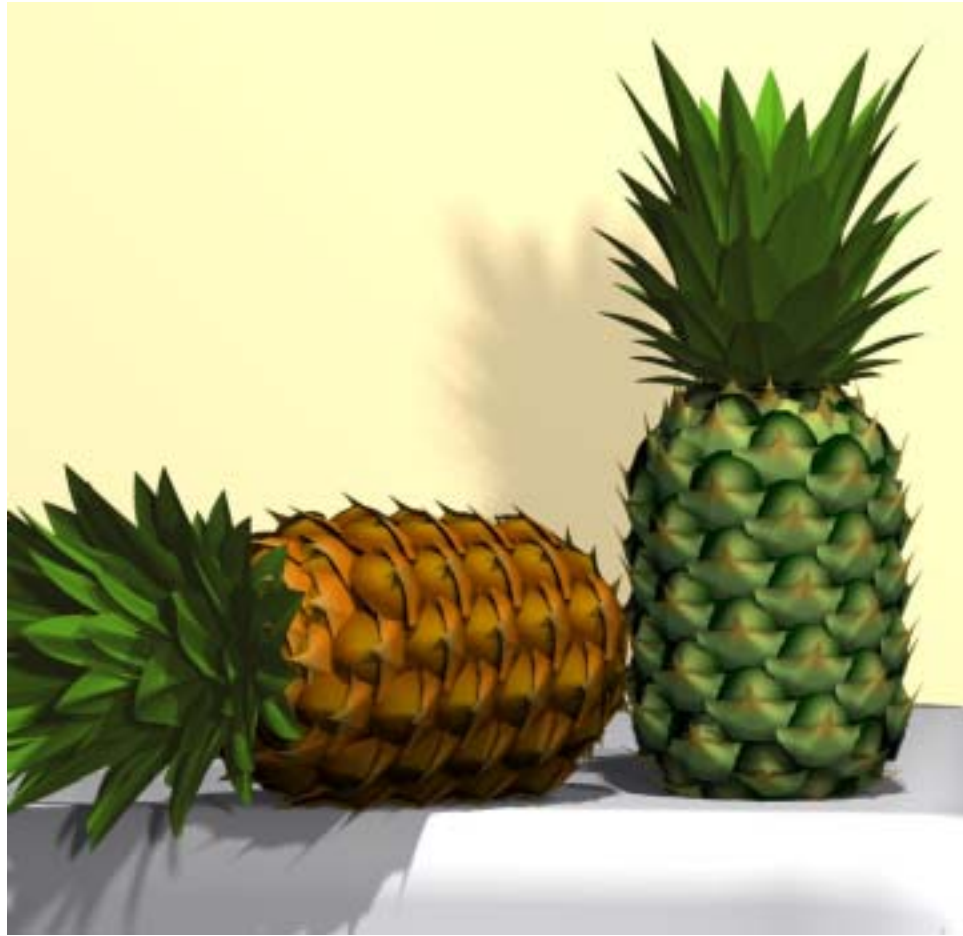


Figure 4.15: Pineapples

*Pineapple**Spruce cones**Sedge*

Models of fruits synthesized using the cylindrical model are shown in Figures 4.15 and 4.16. The pineapple (Figure 4.15) is an example of a pattern where a given scale has six neighbors, which belong to 5-, 8- and 13-parastichies. The corresponding divergence angle  $\alpha$  is equal to  $138.139542^\circ$ . The spruce cones (Figure 4.16) were generated using the values  $m = 5$ ,  $n = 8$  and  $\alpha = 137.5^\circ$  (the divergence angle  $\alpha$  for a (5, 8)-parastichy pattern belongs to the interval  $135.918365^\circ$  to  $138.139542^\circ$ ). From these values,  $h$  and  $d$  were calculated as a function of the radius of the cylinder. The effect of closing the bottom and top of the pineapple and spruce cones was achieved by decreasing the diameter of the cylinder and the size of the scales.

A variant of the model of phyllotaxis on a cylinder can be used to model organs that are conical rather than cylindrical in shape. For example, Figure 4.17 shows a model of the sedge *Carex laevigata*. L-system 4.1 generates the male spike. Production  $p_1$  specifies the basic





Figure 4.16: Spruce cones



Figure 4.17: *Carex laevigata*: the male spike, the entire shoot, the female spike

```

#define IRATE 1.025 /* internode growth rate */
#define SRATE 1.02 /* spikelet growth rate */
#include M          /* spikelet shape specification */

 $\omega$  : A
 $p_1$  : A : * → [&(5)f(1)~M(1)]F(0.2)/(137.5)A
 $p_2$  : M(s) : s<3 → M(s*SRATE)
 $p_3$  : f(s) : s<3 → f(s*SRATE)
 $p_4$  : &(s) : s<15 → &(s*SRATE)
 $p_5$  : F(i) : i<1 → F(i*IRATE)

```

L-system 4.1: The male spike of *Carex laevigata*

layout of the spikelets, similar to that given by the L-system in Figure 4.11. The top portion of the spike has a conical shape due to the growth of spikelets for some time after their creation by the apex. According to production  $p_2$ , a spikelet grows by factor  $SRATE$  in each derivation step, until it reaches the threshold size of 3. In an analogous way, productions  $p_3$ ,  $p_4$  and  $p_5$  capture the distance increase between spikelets and the spike axis, the increase of the branching angle, and the elongation of internodes.

The models of phyllotaxis deal with the arrangement of organs in space. For the purpose of mathematical analysis their shape is reduced to a simple geometric figure, usually a circle. However, in realistic images the exact shape of the organs must be captured as well. Several techniques suitable for this purpose are outlined in the next chapter.

# Chapter 5

## Models of plant organs

Many concepts presented in the previous chapters were illustrated using realistic images, but the modeling techniques for leaves and petals have not been described yet. Three approaches are discussed below.

### 5.1 Predefined surfaces

The standard computer graphics method for defining arbitrary surfaces makes use of *bicubic patches* [9, 10, 40]. A patch is defined by three polynomials of third degree with respect to parameters  $s$  and  $t$ . The following equation defines the  $x$  coordinate of a point on the patch:

*Bicubic patches*

$$\begin{aligned} x(s, t) = & a_{11}s^3t^3 + a_{12}s^3t^2 + a_{13}s^3t + a_{14}s^3 \\ & + a_{21}s^2t^3 + a_{22}s^2t^2 + a_{23}s^2t + a_{24}s^2 \\ & + a_{31}st^3 + a_{32}st^2 + a_{33}st + a_{34}s \\ & + a_{41}t^3 + a_{42}t^2 + a_{43}t + a_{44} \end{aligned}$$

Analogous equations define  $y(s, t)$  and  $z(s, t)$ . All coefficients are determined by interactively designing the desired shape on the screen of a graphics workstation. Complex surfaces are composed of several patches.

The surfaces are incorporated into a plant model in a manner similar to subfigures (Section 1.4.2). The L-system alphabet is extended to include symbols representing different surfaces. When the turtle encounters such a symbol preceded by a tilde ( $\sim$ ), the corresponding surface is drawn.

*Turtle interpretation*

The exact position and orientation of surface  $S$  representing an appendage is determined using a *contact point*  $P_S$ , the *heading vector*  $\vec{H}_S$  and the *up vector*  $\vec{v}_S$  as a reference (Figure 5.1). The surface is translated in such a way that its contact point matches the current position

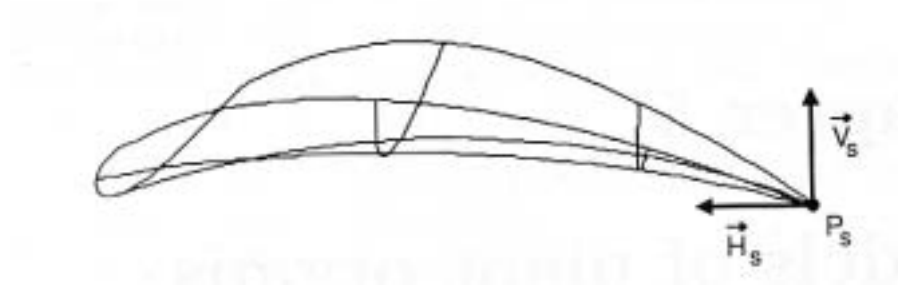


Figure 5.1: Specification of an appendage

of the turtle, and is rotated to align its heading and up vectors with the corresponding vectors of the turtle. If a surface represents an internal part of the structure such as an internode, a distinction between the entry and exit contact points is made.

### Examples

The majority of organs presented in this book have been modeled this way. The petals of sunflowers, zinnias, water-lilies and roses shown in Chapter 4 provide good examples. Figure 5.2 illustrates an additional improvement in the appearance of organs, made possible by the application of textures to the surfaces of leaves, flowers and vine branches.

## 5.2 Developmental surface models

Predefined surfaces do not “grow.” String symbols can be applied to control such features as the overall color and size of a surface, but the underlying shape remains the same. In order to simulate plant development fully, it is necessary to provide a mechanism for changing the shape as well as the size of surfaces in time. One approach is to trace surface boundaries using the turtle and fill the resulting polygons. A sample L-system is given below:

### Contour tracing

$$\begin{aligned} \omega &: L \\ p_1 &: L \rightarrow \{-FX + X - FX - | -FX + X + FX\} \\ p_2 &: X \rightarrow FX \end{aligned}$$

Production  $p_1$  defines leaf  $L$  as a closed planar polygon. The braces  $\{$  and  $\}$  indicate that this polygon should be filled. Production  $p_2$  increases the lengths of its edges linearly. The model of a fern shown in Figure 5.3 incorporates leaves generated using this method, with the angle increment equal to  $20^\circ$ . Note the phase effect due to the “growth” of polygons in time. A similar approach was taken to generate the leaves, flowers and fruits of *Capsella bursa-pastoris* (Figure 3.5 on page 74).

### Fern

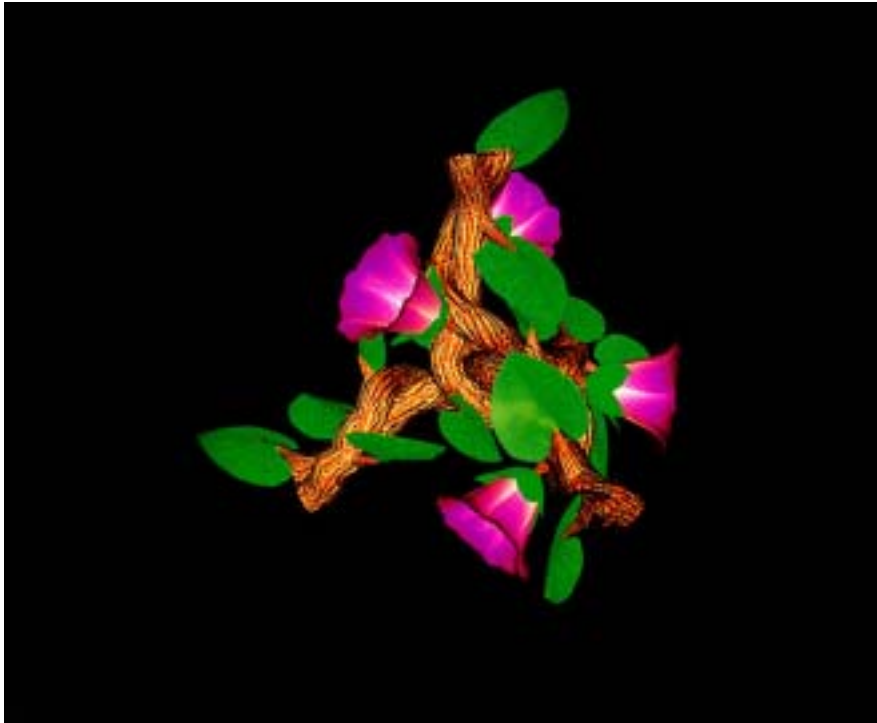


Figure 5.2: *Maraldi figure* by Greene [54]



Figure 5.3: The fern

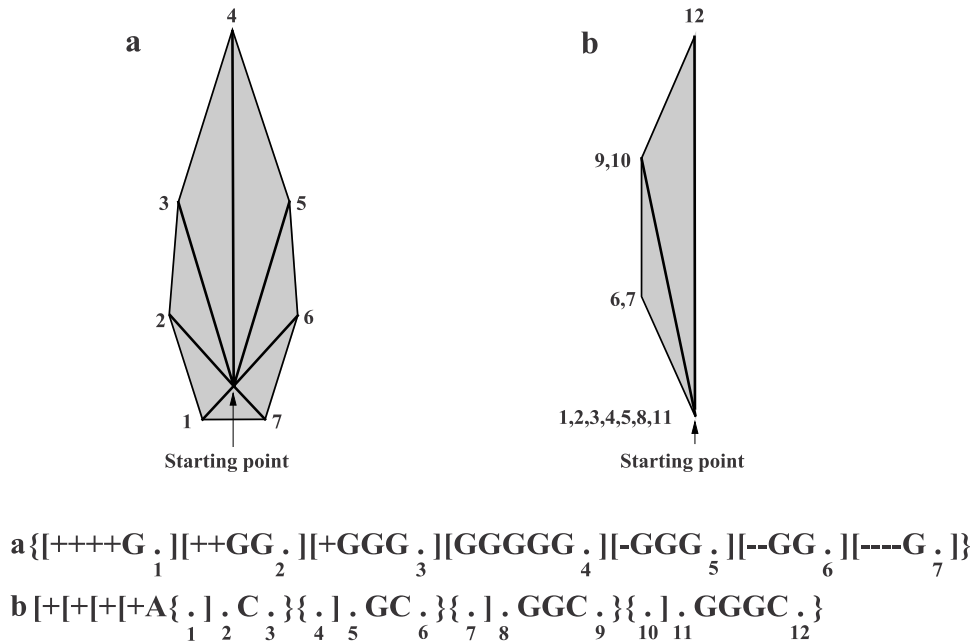


Figure 5.4: Surface specification using a tree structure as a framework

*Framework approach*

In practice, the tracing of polygon boundaries produces acceptable effects only in the case of small, flat surfaces. In other cases it is more convenient to use a tree structure as a *framework*. Polygon vertices are specified by a sequence of turtle positions marked by the dot symbol ( $\cdot$ ). An example is given in Figure 5.4a. The letter  $G$  has been used instead of  $F$  to indicate that the segments enclosed between the braces should not be interpreted as the edges of the constructed polygon. The numbers correspond to the order of vertex specification by the turtle.

*Cordate leaf*

Figure 5.5 shows the development of a *cordate leaf* modeled using this approach. The axiom contains symbols  $A$  and  $B$ , which initiate the left-hand and right-hand sides of the blade. Each of the productions  $p_1$  and  $p_2$  creates a sequence of axes starting at the leaf base and gradually diverging from the midrib. Production  $p_3$  increases the lengths of the axes. The axes close to the midrib are the longest since they were created first. Thus, the shape of this leaf is yet another manifestation of the phase effect. The leaf blade is defined as a union of triangles rather than a single polygon. Such triangulation is advantageous if the blade bends, for example due to tropism (Chapter 2). Figure 5.4b provides an additional illustration of the model by magnifying the left side of the leaf after four derivation steps.

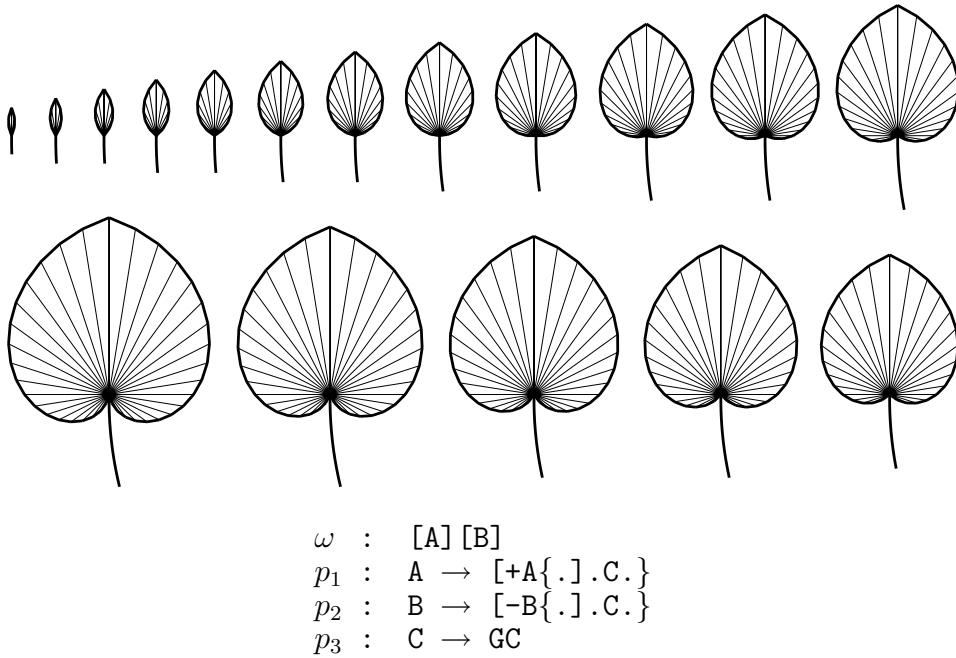


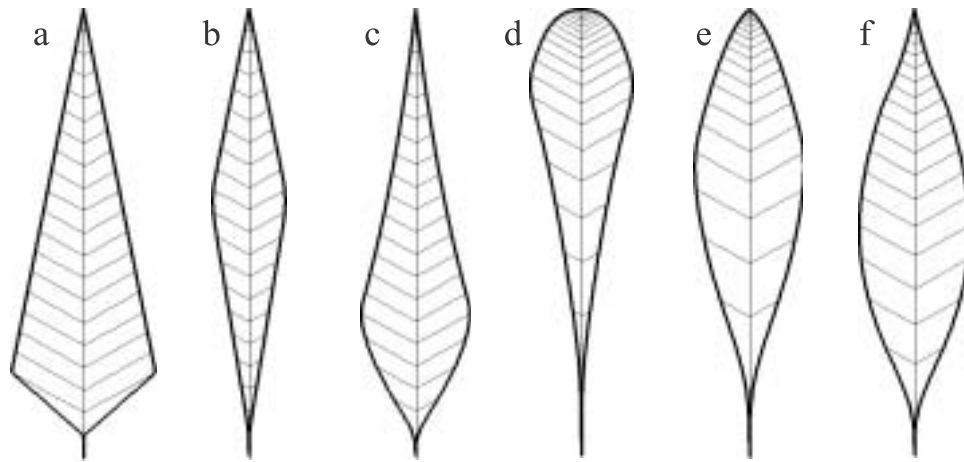
Figure 5.5: Developmental sequence of a cordate leaf generated using an L-system

The described method makes it possible to define a variety of leaves. Their shapes depend strongly on the growth rates of segments. For example, a family of simple leaves and the corresponding parametric L-system are shown in Figure 5.6.

*Simple leaves*

According to production  $p_1$ , in each derivation step apex  $A(t)$  extends the main leaf axis by segment  $G(LA, RA)$  and creates a pair of lateral apices  $B(t)$ . New lateral segments are added by production  $p_2$ . Parameter  $t$ , assigned to apices  $B$  by production  $p_1$ , plays the role of “growth potential” of the branches. It is decremented in each derivation step by a constant  $PD$ , and stops production of new lateral segments upon reaching 0. Segment elongation is captured by production  $p_3$ .

For the purpose of analysis, it is convenient to divide a leaf blade into two areas. In the basal area, the number of lateral segments is determined by the initial value of growth potential  $t$  and constant  $PD$ . Since the initial value of  $t$  assigned to apices  $B$  increases towards the leaf apex, the consecutive branches contain more and more segments. On the other hand, branches in the apical area exist for too short a time to reach their limit length. Thus, while traversing the leaf from the base towards the apex, the actual number of segments in a branch first increases, then decreases. As a result of these opposite tendencies, the leaf reaches its maximum width near the central part of the blade.



$n=20, \delta=60^\circ$

```
#define LA 5      /* initial length - main segment */
#define RA 1      /* growth rate - main segment */
#define LB 1      /* initial length - lateral segment */
#define RB 1      /* growth rate - lateral segment */
#define PD 1      /* growth potential decrement */
```

```
 $\omega$  : { .A(0) }
p1 : A(t) : * → G(LA,RA) [-B(t).] [A(t+1)] [+B(t).]
p2 : B(t) : t>0 → G(LB,RB)B(t-PD)
p3 : G(s,r) : * → G(s*r,r)
```

Figure 5.6: A family of simple leaves generated using a parametric L-system

Figure	LA	RA	LB	RB	PD
a	5	1.0	1.0	1.00	0.00
b	5	1.0	1.0	1.00	1.00
c	5	1.0	0.6	1.06	0.25
d	5	1.2	10.0	1.00	0.50
e	5	1.2	4.0	1.10	0.25
f	5	1.1	1.0	1.20	1.00

Table 5.1: Values of constants used to generate simple leaves

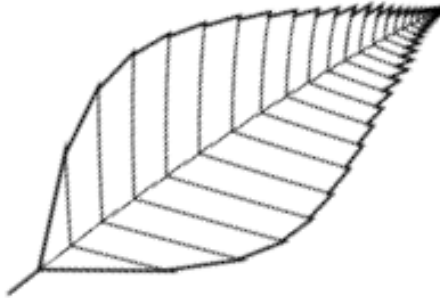




Figure 5.7: A rose in a vase

Table 5.1 lists the values of constants corresponding to particular shapes. For a given derivation length, the exact position of the branch with the largest number of segments is determined by  $PD$ . If  $PD$  is equal to 0, all lateral branches have an unlimited growth potential, and the basal part of the leaf does not exist (Figure 5.6a). If  $PD$  equals 1, the basal and apical parts contain equal numbers of lateral branches (Figures 5.6 b and f). Finer details of the leaf shape are determined by the growth rates. If the main axis segments and the lateral segments have the same growth rates ( $RA = RB$ ), the edges of the apical part of the leaf are straight (Figures 5.6 a and b). If  $RA$  is less than  $RB$ , the segments along the main axis elongate at a slower rate than the lateral segments, resulting in a concave shape of the apical part (Figures 5.6 c and f). In the opposite case, with  $RA$  greater than  $RB$ , the apical part is convex (Figures 5.6 d and e). The curvature of the basal edges can be analyzed in a similar way.

*Shape control*



$n=25, \delta=60^\circ$

```

#define LA 5      /* initial length - main segment */
#define RA 1.15  /* growth rate - main segment */
#define LB 1.3   /* initial length - lateral segment */
#define RB 1.25  /* growth rate - lateral segment */
#define LC 3     /* initial length - marginal notch */
#define RC 1.19  /* growth rate - marginal notch */

 $\omega$  :  [A(0,0).] [A(0,1).]
p1 :  A(t,d)   :  d=0  →  .G(LA,RA). [+B(t)G(LC,RC,t).]
                               [+B(t){.}A(t+1,d)
p2 :  A(t,d)   :  d=1  →  .G(LA,RA). [-B(t)G(LC,RC,t).]
                               [-B(t){.}A(t+1,d)
p3 :  B(t)     :  t>0  →  G(LB,RB)B(t-1)
p4 :  G(s,r)   :  *    →  G(s*r,r)
p5 :  G(s,r,t) :  t>1  →  G(s*r,r,t-1)

```

Figure 5.8: A rose leaf

### Rose leaf

Figure 5.7 shows a long-stemmed rose with the leaves modeled according to Figure 5.8. The L-system combines the concepts explored in Figures 5.5 and 5.6. The axiom contains modules  $A(0,0)$  and  $A(0,1)$ , which initiate the left-hand and right-hand side of the leaf. The development of the left side will be examined in detail. According to production  $p_1$ , in each derivation step apex  $A(t,0)$  extends the midrib by internodes  $G(LA, RA)$  and creates two colinear apices  $B(t)$  pointing to the left. Further extension of the lateral axes is specified by production  $p_3$ . The leaf blade is constructed as a sequence of trapezoids, with two vertices lying on the midrib and the other two vertices placed at the endpoints of a pair of lateral axes formed in consecutive derivation steps. The module  $G(LC, RC, t)$  introduces an offset responsible for the formation of notches at the leaf margin. Production  $p_4$  describes the elongation of internodes responsible for overall leaf shape, while production  $p_5$  controls the size of the notches. The development of the right side of the blade proceeds in a similar manner, with production  $p_2$

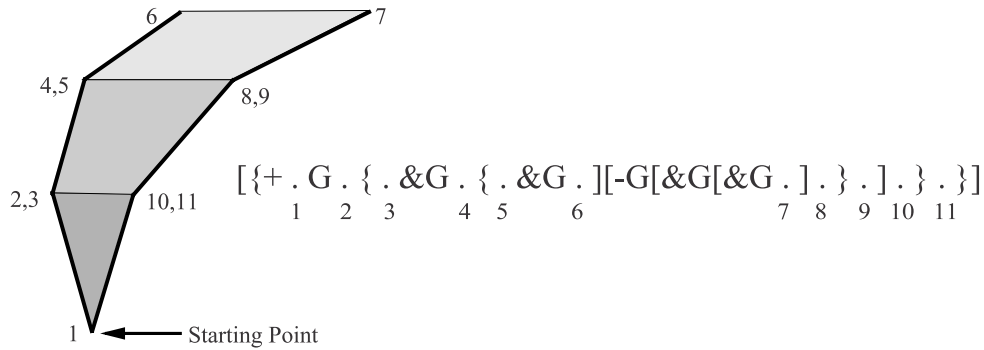


Figure 5.9: Surface specification using stacked polygons

recreating the midrib and creating lateral apices pointing to the right. The bending of the midrib to the right is a result of tropism.

In the examples discussed so far, the turtle specifies the vertices of one polygon, then moves on to the next. Further flexibility in surface definition can be achieved by interleaving vertex specifications for different polygons. The turtle interpretation of the braces is redefined in the following way. A string containing nested braces is evaluated using two data structures, an *array* of vertices representing the current polygon and a *polygon stack*. At the beginning of string interpretation, both structures are empty. The symbols {, } and . are then interpreted as follows:

*Nested polygons*

- { Start a new polygon by pushing the current polygon on the polygon stack and creating an empty current polygon.
- . Append the new vertex to the current polygon.
- } Draw the current polygon using the specified vertices, then pop a polygon from the stack and make it the current polygon.

An example of string interpretation involving nested braces is given in Figure 5.9.

The above technique was applied to construct the flowers of the lily-of-the-valley shown in Figure 3.4 (page 72), and magnified in Figure 5.10. A flower is represented by a polygon mesh consisting of five sequences of trapezoids spread between pairs of curved lines that emanate radially from the flower base. A single sequence is generated by the following L-system:

*Lily-of-the-valley*

$$\begin{aligned}
 \omega &: [X(36)A]/(72)[X(36)B] \\
 p_1 &: A \quad : * \rightarrow [ \&GA\{.\} \\
 p_2 &: B \quad : * \rightarrow B\&.G.\} \\
 p_3 &: X(a) : * \rightarrow X(a + 4.5)
 \end{aligned}$$

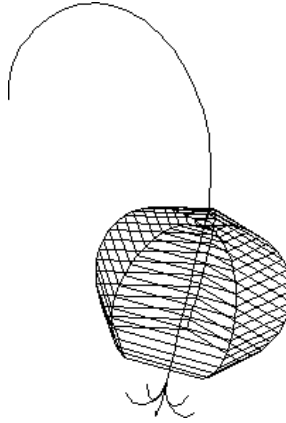


Figure 5.10: Structure of a lily-of-the-valley flower

Productions  $p_1$  and  $p_2$  create two adjacent framework lines and mark polygon vertices consistently with Figure 5.9. Production  $p_3$  controls the angle at which the framework lines leave the stalk at the flower base.

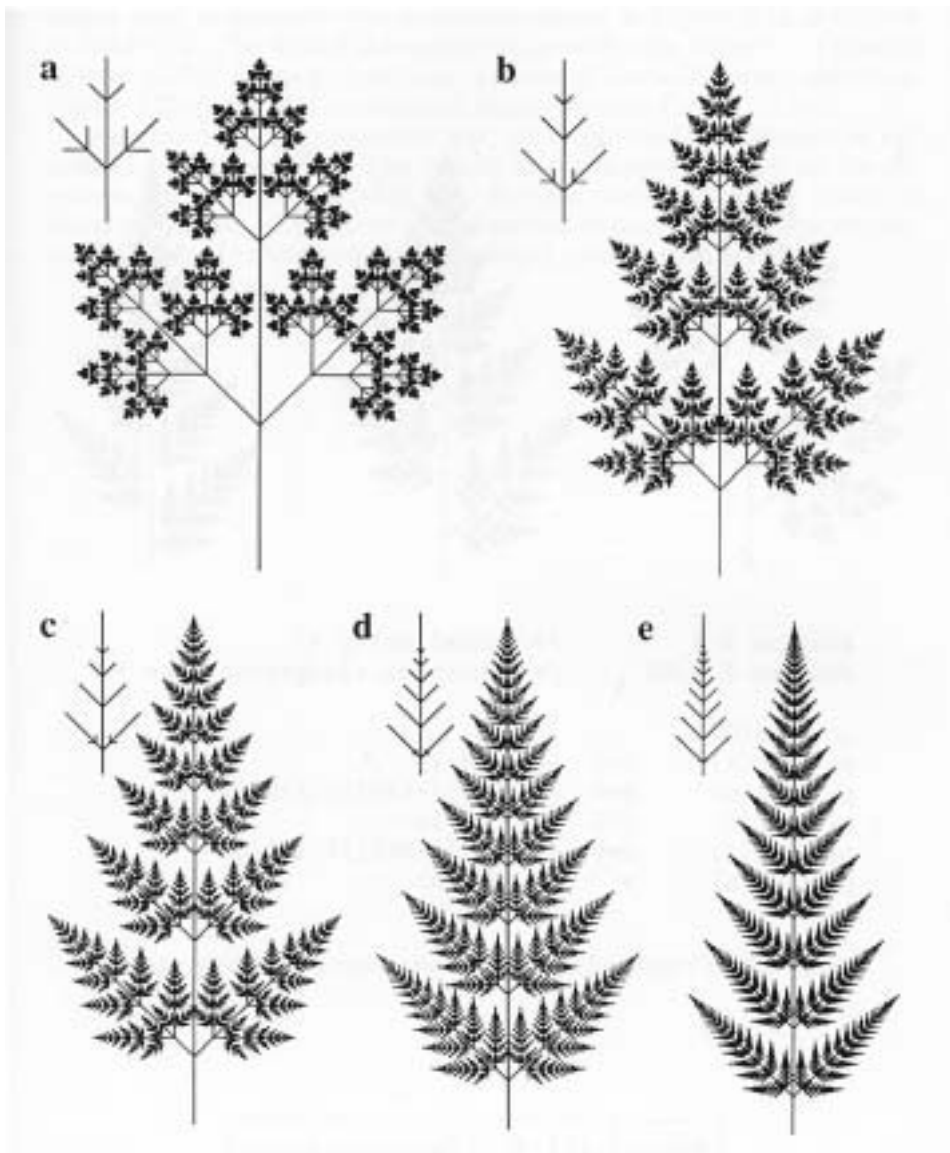
### 5.3 Models of compound leaves

So far, the discussion of organ models has focused on the definition of surfaces. However, in the case of highly self-similar structures, the individual surfaces become inconspicuous, and the expression of the geometric relationships between younger and older parts of the structure becomes the key issue. For example, Figure 5.11 shows compound leaves often found in the family Umbelliferae. According to production  $p_2$ , the apex  $A(0)$  creates two segments  $F(1)$  and a pair of lateral apices  $A(D)$  in each derivation step. Production  $p_1$  delays the development of the daughter branches by  $D$  steps with respect to the mother branch. This pattern is repeated recursively in branches of higher order. Production  $p_3$  gradually elongates the internodes, and in this way establishes proportions between parts of a leaf. The values of the con-

*Symmetric  
branching*

Figure	D	R	Derivation length
a	0	2.00	10
b	1	1.50	16
c	2	1.36	21
d	4	1.23	30
e	7	1.17	45

Table 5.2: Values of constants used to generate compound leaves



```

#define D 1          /* apical delay */
#define R 1.5        /* internode elongation rate */

 $\omega$  : A(0)
p1 : A(d) : d > 0 → A(d-1)
p2 : A(d) : d = 0 → F(1) [+A(D)] [-A(D)] F(1) A(0)
p3 : F(a) : * → F(a*R)

```

Figure 5.11: Compound leaves

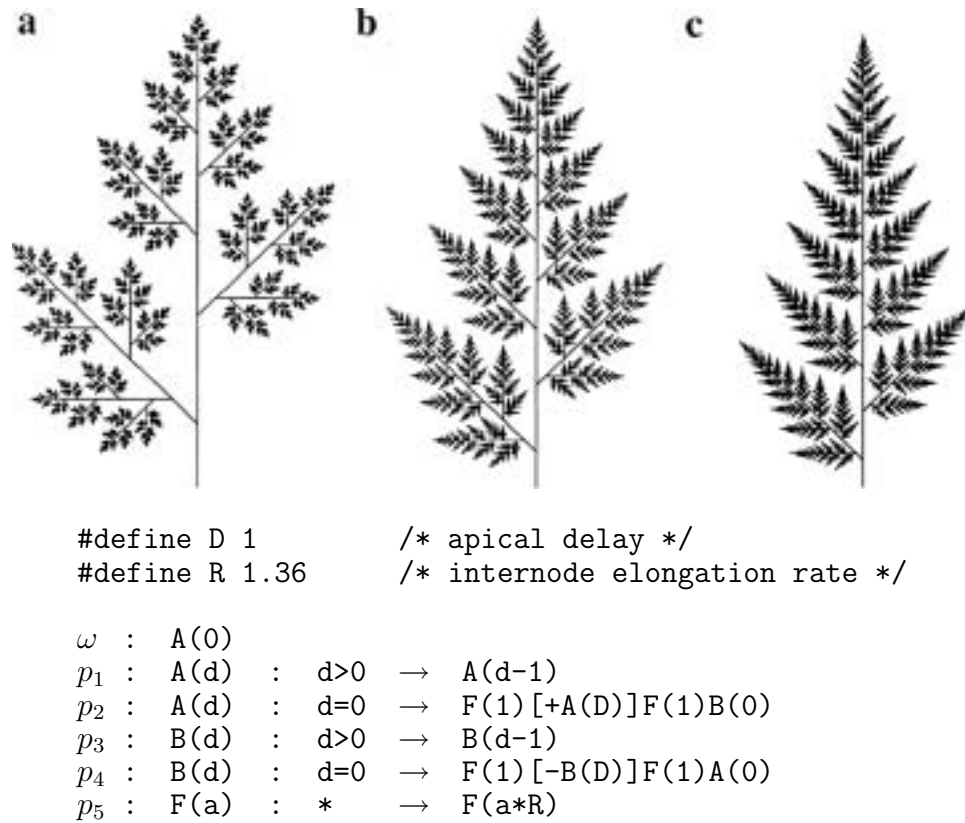


Figure 5.12: Compound leaves with alternating branching patterns

Figure	D	R	Derivation length
a	1	1.36	20
b	4	1.18	34
c	7	1.13	46

Table 5.3: Values of the constants used to generate compound leaves with alternating branches

starts used to generate the structures shown in Figure 5.11 are listed in Table 5.2. The model is sensitive to growth rate values — a change of 0.01 visibly alters proportions. Leaves of the wild carrot, shown in Figure 3.23 (page 96), correspond closely to case Figure 5.11b.

Another type of compound leaf, with alternating branches, is examined in Figure 5.12. The values of the constants used in the L-system are specified in Table 5.3. Further examples can be found in the next chapter, devoted to the animation of developmental processes, and Chapter 8, which ties developmental models with fractals.

*Alternating  
branching*





# Chapter 6

## Animation of plant development

The sequences of images used in Chapters 3 and 5 to illustrate the development of inflorescences and compound leaves suggest the possibility of using computer animation to visualize plant development. From a practical perspective, computer animation offers several advantages over traditional time-lapse photography.

*Motivation*

- Photography is sensitive to imperfections in the underlying experiment. A disease or even a temporary wilting of a plant may spoil months of filming.
- In nature, developmental processes are often masked by other phenomena. For example, the growth of leaves can be difficult to capture because of large changes in leaf positions during the day. Similarly, positions of tree branches may be affected by wind. Computer animation makes it possible to abstract from these distracting effects.
- Animation can be used when time-lapse photography is impractical because of the long development time of plants (e.g. years in the case of trees).
- In time-lapse photography, the initial position of the camera and the light conditions must be established a priori, without knowing the final shape of the plant. In computer animation all developmental stages of the modeled plant are known in advance, allowing for optimal selection of the model view.
- Animation can be applied to visualize developmental mechanisms that cannot be observed directly in real plants, such as the propagation of hormones and nutrients.

*Discrete  
character of  
L-systems*

- Animation offers an unprecedented means for visualizing the development of extinct plants on the basis of paleobotanical data.

The original formalism of L-systems provides a model of development that is discrete both in time and space. Discretization in time implies that the model states are known only at specific time intervals. Discretization in space means that the range of model states is limited to a finite number. Parametric L-systems remove the latter effect by assigning continuous attributes to model components. However, the model states are still known only in discrete time intervals. This presents a problem in animation, where a smooth progression of the developing forms is desirable.

This last statement requires further clarification. The very nature of animation is to produce the impression of continuous motion by displaying a sequence of still frames, captured at fixed time intervals. Why is a continuous model of plant development needed if it will be used to generate a fixed sequence of images in the final account? Wouldn't it be enough to retain the standard definition of L-systems and assume time slices fine enough to produce the desired progression of forms? This approach, while feasible and useful, has three major drawbacks.

- A model can be constructed assuming longer or shorter time intervals, but once the choice has been made, the time step is a part of the model and cannot be changed easily. From the viewpoint of computer animation it is preferable to control the time step by a single parameter, decoupled from the underlying L-system.
- The continuity criteria responsible for the smooth progression of shapes during animation can be specified more easily in the continuous time domain.
- It would be conceptually elegant to separate model development, defined in continuous time, from model observation, taking place in discrete intervals.

A developmental process is viewed as consisting of periods of continuous module expansion delimited by instantaneous module divisions. Special conditions are imposed to preserve the shape and growth rates of the organism during these qualitative changes. An analogy can be drawn to the theory of morphogenesis advanced by Thom [142], who viewed shape formation as a piecewise continuous process with singularities called *catastrophes*.

Formally, development taking place in continuous time is captured using the formalism of *timed DOL-systems*. The key difference between these L-systems and the types of L-systems considered so far lies in the definition of the derivation function. In “ordinary” L-systems, the derivation length is expressed as the number of derivation steps. In timed DOL-systems, the derivation length is associated with the total elapsed time since the beginning of the observation.

## 6.1 Timed DOL-systems

Let  $V$  be an alphabet and  $R$  the set of positive real numbers (including 0). The pair  $(a, \tau) \in V \times R$  is referred to as the *timed letter*  $a$ , and the number  $\tau$  is called the *age* of  $a$ . A sequence of timed letters,  $x = (a_1, \tau_1) \dots (a_n, \tau_n) \in (V \times R)^*$ , is called a *timed word* over alphabet  $V$ .

A *timed DOL-system* (*tDOL-system*) is a triplet  $G = \langle V, \omega, P \rangle$ , where

*Definition*

- $V$  is the alphabet of the L-system,
- $\omega \in (V \times R)^+$  is a nonempty timed word over  $V$ , called the initial word, and
- $P \subset (V \times R) \times (V \times R)^*$  is a finite set of productions.

Instead of writing  $((a, \beta), (b_1, \alpha_1) \dots (b_n, \alpha_n)) \in P$ , the notation  $(a, \beta) \rightarrow (b_1, \alpha_1) \dots (b_n, \alpha_n)$  is used. The parameter  $\beta$  is referred to as the *terminal age* of the letter  $a$ , and each parameter  $\alpha_i$  is the *initial age* assigned to the letter  $b_i$  by production  $P$ . The following assumptions are made:

- C1. For each letter  $a \in V$  there exists exactly one value  $\beta \in R$  such that  $(a, \beta)$  is the predecessor of a production in  $P$ .
- C2. If  $(a, \beta)$  is a production predecessor and  $(a, \alpha)$  is a timed letter that occurs in the successor of some production in  $P$ , then  $\beta > \alpha$ .

According to these conditions, each letter has a uniquely defined terminal age. Furthermore, an initial age assigned to a letter by a production must be smaller than its terminal age, *i.e.*, its *lifetime* ( $\beta - \alpha$ ) must be positive.

Let  $(a, \beta) \rightarrow (b_1, \alpha_1) \dots (b_n, \alpha_n)$  be a production in  $P$ . A function  $\mathcal{D} : ((V \times R)^+ \times R) \rightarrow (V \times R)^*$  is called a *derivation function* if it has the following properties:

*Derivation*

- A1.**  $\mathcal{D}((a_1, \tau_1) \dots (a_n, \tau_n), t) = \mathcal{D}((a_1, \tau_1), t) \dots \mathcal{D}((a_n, \tau_n), t)$
- A2.**  $\mathcal{D}((a, \tau), t) = (a, \tau + t)$ , if  $\tau + t \leq \beta$
- A3.**  $\mathcal{D}((a, \tau), t) = \mathcal{D}((b_1, \alpha_1) \dots (b_n, \alpha_n), t - (\beta - \tau))$ , if  $\tau + t > \beta$

A derivation in a timed DOL-system is defined in terms of two types of time variables. Global time  $t$  is common to the entire word under consideration, while local age values  $\tau_i$  are specific to each letter  $a_i$ .

Axiom **A1** identifies  $t$  as the variable that synchronizes the entire development, and specifies that the lineages of all letters can be considered independently from each other (thus, no interaction between letters is assumed). With the progress of time  $t$ , each letter “grows older” until its terminal age is reached (axiom **A2**). At this moment subdivision occurs and new letters are produced with initial age values specified by the corresponding production (axiom **A3**). Condition **C1** guarantees that the subdivision time is defined unambiguously, hence the development proceeds in a deterministic fashion. Condition **C2** guarantees that, for any value of time  $t$ , the recursive references specified by axiom **A3** will eventually end.

*Anabaena*

The above concepts are examined by formulating a timed DOL-system that simulates the development of a vegetative part of the *Anabaena catenula* filament. Given the discrete model expressed by equation (1.1) on page 5, the corresponding tDOL-system is as follows:

$$\begin{aligned}
 \omega &: (a_r, 0) \\
 p_1 &: (a_r, 1) \rightarrow (a_l, 0)(b_r, 0) \\
 p_2 &: (a_l, 1) \rightarrow (b_l, 0)(a_r, 0) \\
 p_3 &: (b_r, 1) \rightarrow (a_r, 0) \\
 p_4 &: (b_l, 1) \rightarrow (a_l, 0)
 \end{aligned} \tag{6.1}$$

In accordance with the discrete model, it is assumed that all cells have the same lifetime, equal to one time unit. The derivation tree is shown in Figure 6.1. The nodes of the tree indicate production applications specified by axiom **A3**, and the triangular “arcs” represent the continuous aging processes described by axiom **A2**. The vertical scale indicates global time. For example, at time  $t = 2.75$  the filament consists of three cells,  $b_l$ ,  $a_r$  and  $a_r$ , whose current age is equal to 0.75.

According to the definition of time intervals corresponding to axioms **A2** and **A3**, a production is applied *after* the age  $\tau + t$  exceeds the terminal age. Consequently, at division time the “old” cells still exist. For example, at time  $t = 2.0$  the filament consists of two cells,  $a_l$  and  $b_r$ , both of age  $\tau = 1$ .

The above L-system can be simplified by considering cells of type  $b$  as young forms of the cells of type  $a$ . This is suggested by Figure 6.1 where cells  $b$  simply precede cells  $a$  in time. The simplified L-system has two productions:

$$\begin{aligned}
 p_1 &: (a_r, 2) \rightarrow (a_l, 1)(a_r, 0) \\
 p_2 &: (a_l, 2) \rightarrow (a_l, 0)(a_r, 1)
 \end{aligned} \tag{6.2}$$

The corresponding derivation tree starting from cell  $(a_r, 1)$  is shown in Figure 6.2. Note the similarity to the tree from the previous example.

*Model  
observation*

Whether a natural developmental process or its mathematical model is considered, the choice of observation times and the act of observation should not affect the process itself. In other terms, each derived word should depend only on the *total elapsed time*  $t$ , and not on the partition

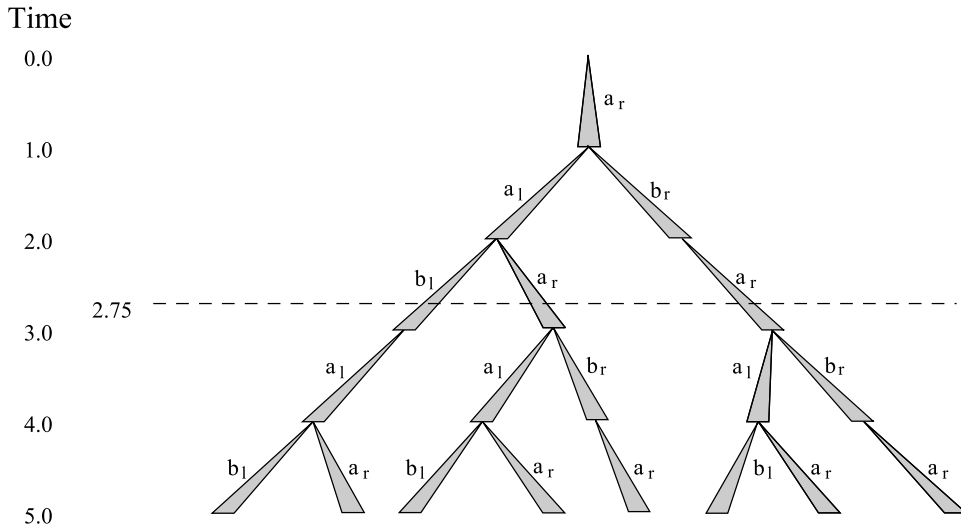


Figure 6.1: Derivation tree representing the continuous development of *Anabaena catenula* described by the L-system in equation (6.1). Sections of the triangles represent cell ages.

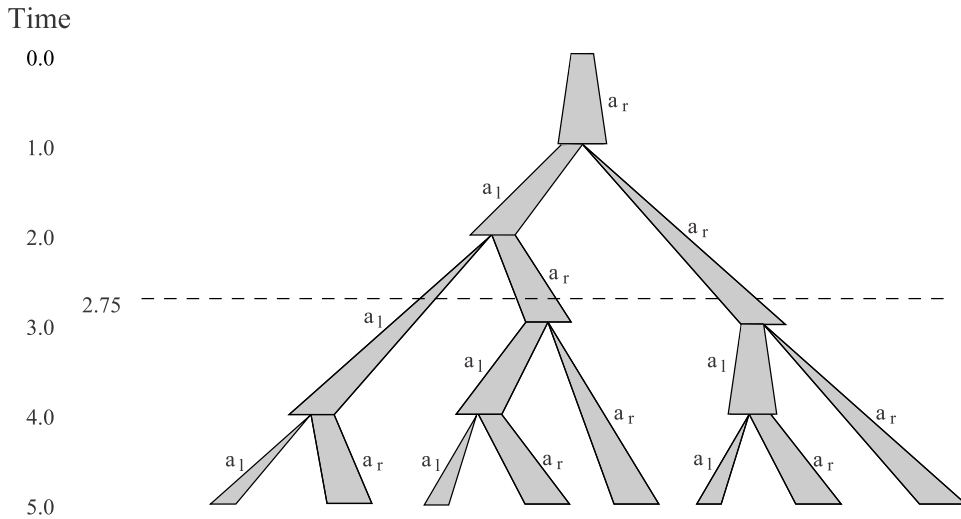


Figure 6.2: Derivation tree representing the continuous development of *Anabaena catenula* corresponding to the rules specified in equation (6.2)

of  $t$  into intervals. The following theorem shows that timed DOL-systems satisfy this postulate.

**Theorem.** Let  $G = \langle V, \omega, P \rangle$  be a tDOL-system, and  $x \in (V \times R)^+$  be a timed word over  $V$ . For any values of  $t_a, t_b \geq 0$ , the following holds:

$$\mathcal{D}(\mathcal{D}(x, t_a), t_b) = \mathcal{D}(x, t_a + t_b)$$

**Proof.** Let us first consider the special case where the word  $x$  consists of a single timed letter,  $(a_0, \tau_0)$ , and all productions in the set  $P$  take single letters into single letters. According to condition **C1**, there exists a unique sequence of productions from  $P$  such that:

$$(a_i, \beta_i) \rightarrow (a_{i+1}, \alpha_{i+1}), \quad i = 0, 1, 2, \dots$$

Let  $(a_k, \tau_k)$  be the result of the derivation of duration  $t_a$  that starts from  $(a_0, \tau_0)$ . According to axioms **A2** and **A3**, and assuming that  $t_a > \beta_0 - \tau_0$ , this derivation can be represented in the form

$$\begin{aligned} & \mathcal{D}((a_0, \tau_0), t_a) \\ &= \mathcal{D}((a_1, \alpha_1), t_a - (\beta_0 - \tau_0)) \\ &= \mathcal{D}((a_2, \alpha_2), t_a - (\beta_0 - \tau_0) - (\beta_1 - \alpha_1)) \\ &= \dots \\ &= \mathcal{D}((a_k, \alpha_k), t_a - (\beta_0 - \tau_0) - (\beta_1 - \alpha_1) - \dots - (\beta_{k-1} - \alpha_{k-1})) \\ &= (a_k, \tau_k), \end{aligned}$$

where

$$\tau_k = \alpha_k + [t_a - (\beta_0 - \tau_0) - \sum_{i=1}^{k-1} (\beta_i - \alpha_i)].$$

Since the sequence of recursive calls can be terminated only by an application of axiom **A2**, the index  $k$  and the age  $\tau_k$  satisfy the inequality

$$\alpha_k < \tau_k \leq \beta_k.$$

Due to condition **C2**, such an index  $k$  always exists and is unique.

Let us now consider a derivation of duration  $t_b > \beta_k - \tau_k$  that starts from  $(a_k, \tau_k)$ . Following the same reasoning, the result can be represented as  $(a_m, \tau_m)$ , where

$$\tau_m = \alpha_m + [t_b - (\beta_k - \tau_k) - \sum_{i=k+1}^{m-1} (\beta_i - \alpha_i)]$$

and

$$\alpha_m < \tau_m \leq \beta_m.$$

By substituting the value of  $\tau_k$  into the formula for  $\tau_m$ , we obtain after simple transformations

$$\tau_m = \alpha_m + [(t_a + t_b) - (\beta_0 - \tau_0) - \sum_{i=1}^{m-1} (\beta_i - \alpha_i)].$$

Thus, the timed letter  $(a_m, \tau_m)$  also results from the derivation of duration  $t_a + t_b$  starting with  $(a_0, \tau_0)$ :

$$(a_m, \tau_m) = \mathcal{D}(\mathcal{D}((a_0, \tau_0), t_a), t_b) = \mathcal{D}((a_0, \tau_0)x, t_a + t_b).$$

So far, we have considered only the case

$$t_a > \beta_0 - \tau_0, \quad t_b > \beta_k - \tau_k.$$

Two other cases, namely,

$$0 \leq t_a \leq \beta_0 - \tau_0, \quad t_b > \beta_k - \tau_k$$

and

$$t_a > \beta_0 - \tau_0, \quad 0 \leq t_b \leq \beta_k - \tau_k$$

can be considered in a similar way. The remaining case,

$$0 \leq t_a \leq \beta_0 - \tau_0, \quad 0 \leq t_b \leq \beta_k - \tau_k,$$

is a straightforward consequence of condition **C2**. This completes the proof of the special case. In general, a derivation that starts from a word  $(a_1, \tau_1) \dots (a_n, \tau_n)$  can be considered as  $n$  separate derivations, each starting from a single letter. This observation applies not only to the initial word specified at time  $t = 0$ , but also to any intermediate word generated during the derivation. Consequently, any *path* in the derivation tree can be considered as a sequence of mappings that takes single letters into single letters. Application of the previous reasoning separately to every path concludes the proof.  $\square$

## 6.2 Selection of growth functions

Timed L-systems capture qualitative changes in model topology corresponding to cell (or, in general, module) divisions, and return the age of each module as a function of the global time  $t$ . In order to complete model definition, it is also necessary to specify the shape of each module as a function of its age. Potentially, such growth functions can be estimated experimentally by observing real organisms [72, 73]. However, if detailed data is not available, growth functions can be selected from an appropriate class by choosing parameters so that the animation is smooth. This approach can be viewed as more than an *ad hoc* technique for constructing acceptable animated sequences. In fact, Thom presents it as a general methodology for studying morphogenesis [142, page 4]:

The essence of the method to be described here consists in supposing a priori the existence of a differential model underlying the process to be studied and, without knowing explicitly what the model is, deducing from the single assumption of its existence conclusions relating to the nature of the singularities of the process.

A technique for computing parameters of growth functions in the case of nonbranching filaments and simple branching structures is given below.

### 6.2.1 Development of nonbranching filaments

In a simple case of geometric interpretation of timed L-systems, symbols represent cells that elongate during their lifetime and divide upon reaching terminal age. Model geometry does not change suddenly, which means that

- the length of each cell is a continuous function of time, and
- the length of a cell before subdivision is equal to the sum of the lengths of the daughter cells.

*Continuity requirements*

The above *continuity requirements* are formalized in the context of a tDOL-system  $G = \langle V, \omega, P \rangle$  as follows:

- R1. Let  $[\alpha_{min}, \beta]$  describe the life span of a timed letter  $a \in V$ . The age  $\alpha_{min}$  is the minimum of the initial age values assigned to  $a$  by the axiom  $\omega$  or by some production in  $P$ . The terminal age  $\beta$  is determined by the predecessor of the production acting on symbol  $a$ . The *growth function*  $g(a, \tau)$ , which specifies the length of cell  $a$  as a function of age  $\tau$ , must be a continuous function of parameter  $\tau$  in the domain  $[\alpha_{min}, \beta]$ .
- R2. For each production  $(a, \beta) \rightarrow (b_1, \alpha_1) \dots (b_n, \alpha_n)$  in  $P$  the following equality holds:

$$g(a, \beta) = \sum_{i=1}^n g(b_i, \alpha_i) \quad (6.3)$$

In practice, requirement **R1** is used to select the class of growth functions under consideration, and the equations resulting from requirement **R2** are used to determine the parameters in function definitions.

*Linear growth*

For example, in the case of the timed L-system specified in equation (6.2), requirement **R2** takes the form

$$\begin{aligned} g(a_r, 2) &= g(a_l, 1) + g(a_r, 0) \\ g(a_l, 2) &= g(a_l, 0) + g(a_r, 1). \end{aligned} \quad (6.4)$$

Let us assume that the growth functions are linear functions of time:

$$\begin{aligned} g(a_l, \tau) &= A_l \tau + B_l \\ g(a_r, \tau) &= A_r \tau + B_r \end{aligned} \quad (6.5)$$



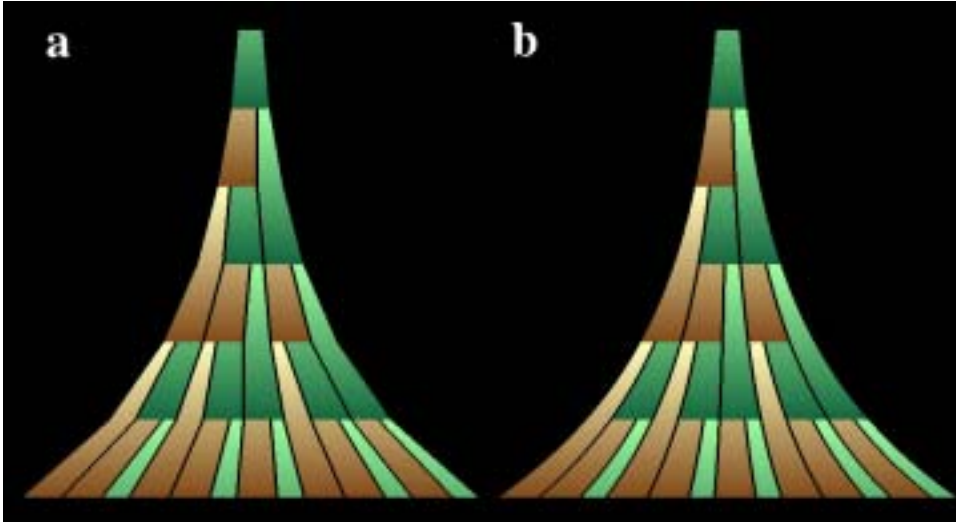


Figure 6.3: Diagrammatic representation of the development of *Anabaena catenula*, with (a) linear and (b) exponential growth of cells

By substituting equations (6.5) into (6.4), we obtain

$$\begin{aligned} 2A_r + B_r &= (1A_l + B_l) + (0A_r + B_r) & \text{or} & \quad 2A_r = A_l + B_l \\ 2A_l + B_l &= (0A_l + B_l) + (1A_r + B_r) & \text{or} & \quad 2A_l = A_r + B_r. \end{aligned}$$

The desired continuity of development is provided by all solutions of this system. They can be expressed in terms of coefficient  $c$ , which relates the growth rate of cells  $a_l$  to that of cells  $a_r$ :

$$\begin{aligned} A_l &= cA_r \\ B_l &= A_r(2 - c) \\ B_r &= A_r(2c - 1) \end{aligned}$$

Figure 6.3a illustrates the developmental process considered for  $c = 1$ . The diagram is obtained by plotting the cells in the filament as horizontal line segments on the screen. Colors indicate cell type and age. The observation time  $t$  ranges from 1 (at the top) to 7 (at the bottom), with increment  $\Delta t = 0.009$ .

The slopes of the side edges of the diagram represent growth rates of the entire structure. Notice that they remain constant in the periods between cell divisions, then change. This effect is disconcerting in animation, since the rate of organism growth suddenly increases with each cell division. In order to prevent this, it is necessary to extend requirements **R1** and **R2** to a higher order of continuity  $N$ . Specifically, equation (6.3) takes the form

$$g^{(k)}(a, \beta) = \sum_{i=1}^n g^{(k)}(b_i, \alpha_i) \quad \text{for } k = 0, 1, \dots, N, \quad (6.6)$$

where  $g^{(k)}(a, \tau)$  is the  $k^{\text{th}}$  derivative of the growth function  $g(a, \tau)$  with respect to age  $\tau$ .

*Exponential  
growth*

In the case of *Anabaena*, an attempt to achieve first-order continuity assuming linear growth functions yields an uninteresting solution,  $g(a_l, \tau) = g(a_r, \tau) \equiv 0$ . Thus, more complex growth functions must be considered, such as an exponential function that can be used to approximate the initial phase of sigmoidal growth. Assume that the growth function has the form

$$g(a_l, \tau) = g(a_r, \tau) = Ae^{B\tau}. \quad (6.7)$$

The objective is to find values of parameters  $A$  and  $B$  that satisfy equation (6.6) for  $k = 0, 1$ . By substituting equation (6.7) into (6.6), we obtain

$$AB^k e^{2B} = AB^k e^B + AB^k, \quad (6.8)$$

which implies that zero-order continuity yields continuity of infinite order in this case. Solution of equation (6.8) for any value of  $k$  yields

$$B = \ln \frac{1 + \sqrt{5}}{2} \approx 0.4812. \quad (6.9)$$

Parameter  $A$  is a scaling factor and can be chosen arbitrarily. The corresponding diagrammatic representation of development is shown in Figure 6.3b. The side edges of the diagram, representing the growth rates of the whole structure, are smooth exponential curves.

## 6.2.2 Development of branching structures

The notions of tDOL-system and growth function extend in a straightforward way to L-systems with brackets. For example, the following tDOL-system describes the recursive structure of the compound leaves analyzed in Section 5.3.

$$\begin{aligned} \omega &: (a, 0) \\ p_1 &: (a, 1) \rightarrow (s, 0)[(b, 0)][(b, 0)](a, 0) \\ p_2 &: (b, \beta) \rightarrow (a, 0) \end{aligned}$$

According to production  $p_1$ , apex  $a$  produces an internode  $s$ , two lateral apices  $b$  and a younger apex  $a$ . Production  $p_2$  transforms the lateral apices  $b$  into  $a$  after a delay  $\beta$ . The daughter branches recursively repeat the development of the mother branch.

Let us assume that the leaf development is first-order continuous, yielding the following equations for  $k = 0, 1$ :

$$g^{(k)}(a, 1) = g^{(k)}(s, 0) + g^{(k)}(a, 0) \quad (6.10)$$

$$g^{(k)}(b, 0) = 0 \quad (6.11)$$

$$g^{(k)}(b, \beta) = g^{(k)}(a, 0) \quad (6.12)$$

Equation (6.10) provides continuity along an existing axis upon the formation of a new internode  $s$ . Equation (6.11) specifies that a newly formed lateral apex  $b$  has zero length and zero growth rate. Equation (6.12) guarantees smooth transformation of apices  $b$  into apices  $a$ .

Let us further assume that apices  $a$  and internodes  $s$  expand exponentially,

$$g(a, \tau) = A_a e^{B_a \tau} \quad (6.13)$$

$$g(s, \tau) = A_s e^{B_s \tau}, \quad (6.14)$$

for  $\tau \in [0, 1]$ . The expansion of the lateral apices cannot be described by an exponential function, since it would not satisfy equations (6.11). Consequently, a polynomial growth function  $g(b, \tau)$  is chosen. Equations (6.11) and (6.12) fix the function's endpoints and the tangents at the endpoints. Thus, in general,  $g(b, \tau)$  must be a polynomial of degree three or more, such as

$$g(b, \tau) = A_b \tau^3 + B_b \tau^2 + C_b \tau + D_b. \quad (6.15)$$

The system of equations (6.10) through (6.12) is solved using the initial size  $A_a$  and the growth rate coefficient  $B_a$  as independent variables. By substituting (6.13) and (6.14) into equations (6.10) for  $k = 0, 1$ , we obtain

$$\begin{aligned} A_s &= A_a (e^{B_a} - 1) \\ B_s &= B_a. \end{aligned}$$

Equations (6.11) and (6.15) yield

$$C_b = D_b = 0.$$

Finally, substitution of (6.13) and (6.15) into (6.12) results in

$$\begin{aligned} A_b &= \frac{A_a}{\beta^3} (\beta B_a - 2) \\ B_b &= \frac{A_a}{\beta^2} (3 - \beta B_a). \end{aligned}$$

Figure 6.4 shows a sequence of images produced by this model using values  $\beta = A_a = 1$  and  $B_a = 0.48$ . The branching angles are equal to  $45^\circ$ . The observation time  $t$  ranges from 6.9 to 7.7, with an increment of 0.2. Note the gradual formation of lateral segments.

In the examples considered above, modules are represented as straight lines, with growth functions controlling line lengths. Other parameters, such as the branching angle, the diameter of segments and the size of predefined surfaces, can be controlled in an analogous way. Generally, any developmental model captured by an OL-system with turtle interpretation can be converted into a tDOL-system and animated.

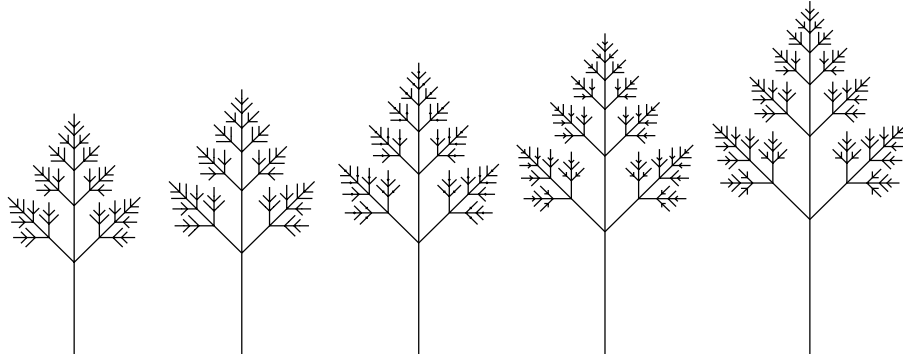


Figure 6.4: Developmental sequence of a branching structure modeled using a tDOL-system

# Chapter 7

## Modeling of cellular layers

String L-systems, the first formalism considered in this book, are suitable for the modeling of nonbranching filaments such as *Anabaena catenula*. The introduction of brackets extends the class of modeled structures to axial trees. However, many structures found in botany have a more complex topology, which can only be described by graphs with cycles. The developmental surface models presented in Section 5.2 make it possible to specify a limited class of these graphs. This chapter describes a more general approach and applies it to simulate the development of single-layered cellular structures such as those found in fern gametophytes, animal embryos and plant epidermis. All structures considered are of microscopic dimensions and relatively undifferentiated, yet the presented methods may bring us closer to the modeling of more complex patterns, such as the venation of leaves.

The modeling method consists of two stages. First, the *topology* of the cell division patterns are expressed using the formalism of *map L-systems*, which allows for the formation of cycles in a structure. At this stage the neighborhood relations between cells are established, but the cell shapes remain unspecified. Next, cell *geometry* is modeled using a dynamic method that takes into account the osmotic pressure inside the cells and the tension of cell walls. The development can be animated by considering periods of continuous cell expansion, delimited by instantaneous cell divisions.

### 7.1 Map L-systems

From a mathematical perspective, cellular layers can be represented using a class of planar graphs with cycles, called *maps* [148]. Nakamura *et al.* [102] characterize them as follows:

*Maps as models of cell layers*

- A map is a finite set of *regions*. Each region is surrounded by a boundary consisting of a finite, circular sequence of *edges* that meet at *vertices*.

- Each edge has one or two vertices associated with it. The one-vertex case occurs when an edge forms a loop. The edges cannot cross without forming a vertex and there are no vertices without an associated edge.
- Every edge is a part of the boundary of a region.
- The set of edges is connected. Specifically, there are no islands within regions.

A map corresponds to a microscopic view of a cellular layer. Regions represent cells, and edges represent cell walls perpendicular to the plane of view. The internal components of a cell are not considered.

*Map rewriting*

The process of cell division can be described by map rewriting. This notion is an extension of string rewriting as discussed in Section 1.2. In general, map-rewriting systems are categorized as *sequential* or *parallel*, and can be *region-controlled* or *edge-controlled* [87]. Since several cells may divide concurrently, a parallel rewriting system is needed. The second categorization has to do with the form of rewriting rules, which may express cell subdivisions in terms of region labels or edge labels. Both approaches are suitable for biological modeling purposes [22]. This chapter focuses on the edge-controlled formalism of *Binary Propagating Map OL-system with markers*, or mBPMOL-systems. It was proposed by Nakamura, Lindenmayer and Aizawa [102] as a refinement of the basic concept of map L-systems introduced by Lindenmayer and Rozenberg [91]. The name is derived as follows. A *map OL-system* is a parallel rewriting system that operates on maps and does not allow for interaction between regions. In other words, regions are modified irrespective of what happens to neighboring regions (a *context-free* mechanism). The system is *binary* because a region can split into at most two daughter regions. It is *propagating* in the sense that the edges cannot be erased, thus regions (cells) cannot fuse or die. The *markers* specify the positions of inserted edges that split the regions.

*mBPMOL-systems*

The choice of mBPMOL-systems as a modeling tool has two justifications. First, they are more powerful than other interactionless map-rewriting systems described in the literature [19, 22, 23]. In addition, markers have a biological counterpart in preprophase bands of microtubules, which coincide with the attachment sites for division walls formed during mitosis [55]. It should be noted, however, that *double wall* systems, introduced by J. and H. B. Lück [93], may be relatively easier to specify [23].

*Definition*

An mBPMOL-system  $\mathcal{G}$  consists of a finite alphabet of *edge labels*  $\Sigma$ , a *starting map*  $\omega$  with labels from  $\Sigma$ , and a finite set of *edge productions*  $P$ . In general, the edges are *directed*, which is indicated by a left or right arrow placed above the edge symbol. In some cases, the edge direction has no effect on the system operation. Such an edge is called *neutral* and no arrow is placed above the symbol denoting it. Each production is of the form  $A \rightarrow \alpha$ , where the directed or neutral

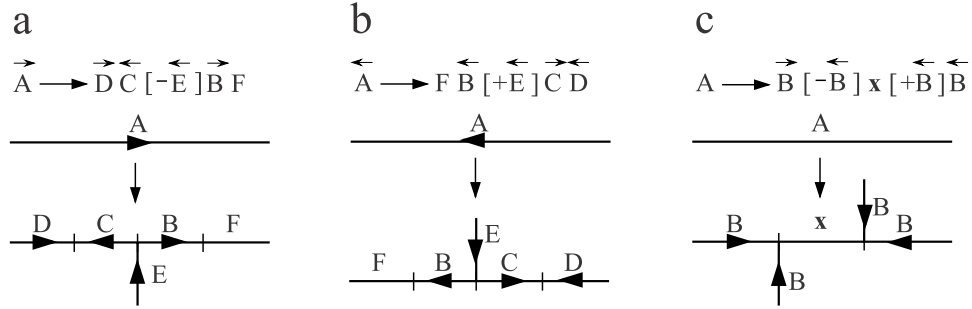


Figure 7.1: Examples of edge productions

edge  $A \in \Sigma$  is called the *predecessor*, and the string  $\alpha$ , composed of symbols from  $\Sigma$  and special symbols  $[, ], +$ , and  $-$ , is called the *successor*. The symbols outside square brackets specify the edge subdivision pattern. Arrows can be placed above edge symbols to indicate whether the successor edges have directions consistent with, or opposite to, the predecessor edge. Pairs of matching brackets  $[$  and  $]$  delimit *markers*, which specify possible attachment sites for region-dividing walls. The markers are viewed as short branches that can be connected to form a complete wall. The strings inside brackets consist of two symbols. The first symbol is either  $+$  or  $-$ , indicating whether the marker is placed to the left or to the right of the predecessor edge. The second symbol is the marker label, with or without an arrow. The left arrow indicates that the marker is directed towards the predecessor edge, and the right arrow indicates that the marker is directed away from that edge. If no arrow is present, the marker is neutral.

For example, in the production  $\vec{A} \rightarrow \vec{D}\vec{C}[-\vec{E}]\vec{B}\vec{F}$ , the directed predecessor  $A$  splits into four edges  $D$ ,  $C$ ,  $B$  and  $F$ , and produces a marker  $E$  (Figure 7.1a). Successor edges  $D$  and  $B$  have the same direction as  $A$ , edge  $C$  has the opposite direction, and  $F$  is neutral. Marker  $E$  is placed to the right of  $A$  and is directed towards  $A$ . Note that this same production could be written as  $\vec{A} \rightarrow \vec{F}\vec{B}[+\vec{E}]\vec{C}\vec{D}$  (Figure 7.1b). As an example of a production with a neutral predecessor, consider  $A \rightarrow \vec{B}[-\vec{B}]x[+\vec{B}]\vec{B}$ . In this case the result of production application does not depend on the assumed direction of the predecessor edge (Figure 7.1c).

*Production syntax*

A *derivation step* in an mBPMOL-system consists of two phases.

*Derivation*

- Each edge in the map is replaced by successor edges and markers using the corresponding edge production in  $P$ .
- Each region is scanned for *matching markers*.

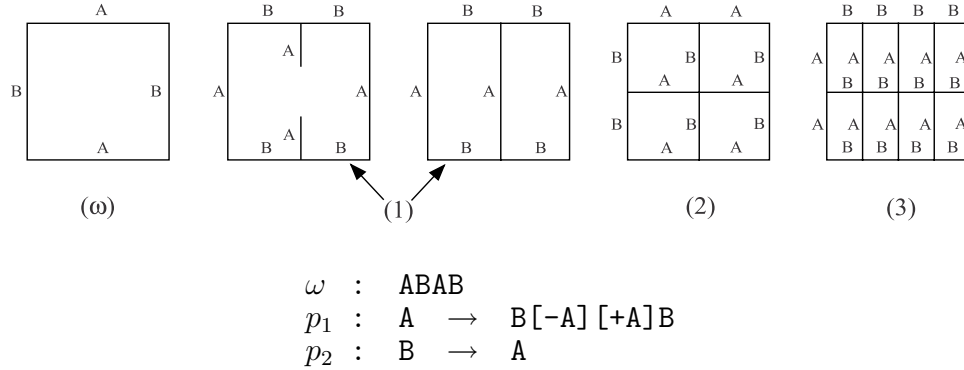


Figure 7.2: Example of a map L-system. In the first step, a distinction is made between the edge-rewriting phase and the connection of matching markers.

Two markers are considered matching if:

- they appear in the same region,
- they have the same label, and
- one marker is directed away from its incident edge while the other is directed towards the edge, or both markers are neutral.

If a match is found, the markers are joined to create a new edge that will split the region. The search for matching markers ends with the first match found, even though other markers entering the same region may also form a match. From the user’s perspective, the system behaves nondeterministically since it chooses the pair of markers to be connected. The unused markers are discarded.

*Examples*

The operation of mBPMOL-systems is illustrated in the following examples. The L-system shown in Figure 7.2 has two productions. Production  $p_1$  creates markers responsible for region division, while production  $p_2$  introduces a delay needed to subdivide the regions alternately by horizontal and vertical edges.

The L-system shown in Figure 7.3 is a modified version of the previous one. The only difference is the addition of an edge  $x$ , which separates the markers in the successor of production  $p_1$ . This edge creates a Z-shaped offset between the inserted edges  $A$ . Z-offsets and symmetric S-offsets (Figure 7.4) can be observed in many biological structures [22, 92].

Figure 7.5 illustrates the operation of an mBPMOL-system with directed edges. Productions  $p_1$  and  $p_3$  create markers. Production  $p_4$



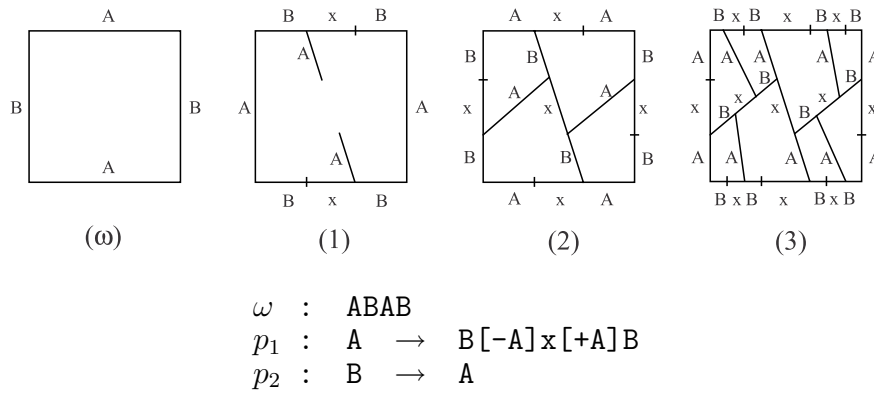


Figure 7.3: Example of a map L-system



Figure 7.4: Offsets between four regions that result from the division of two circles sharing a common edge: (a) Z-offset, (b) S-offset

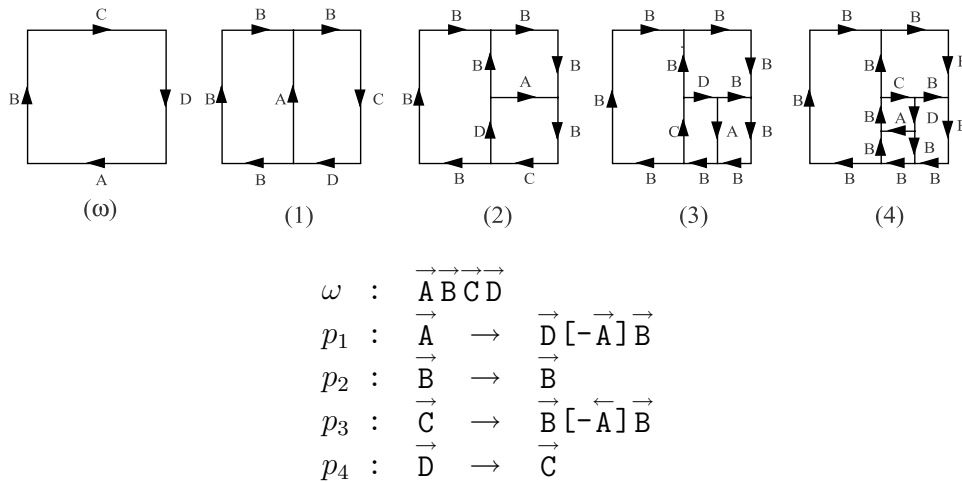


Figure 7.5: Example of a map L-system with directed edges

transforms edge  $D$  into  $C$ , so that in each derivation step there is a pair of edges  $A$  and  $C$  to which productions  $p_1$  and  $p_3$  apply. Production  $p_2$  indicates that edges  $B$  do not undergo further changes.<sup>1</sup> The resulting structure is that of a clockwise spiral.

## 7.2 Graphical interpretation of maps

Maps are topological objects without inherent geometric properties. In order to visualize them, some method for assigning geometric interpretation must be applied. In its description, the biologically-motivated terms *cell* and *wall* will be used instead of their mathematical counterparts, region and edge.

*Wall  
subdivision*

Siero, Rozenberg and Lindenmayer [131] proposed a method that, in the simplest case, is expressed by the following rules:

- walls are represented by straight lines,
- the starting map is represented by a regular polygon, bounded by the walls specified in the axiom,
- when a production subdivides a wall, all successor walls are of equal length, and
- the position of a wall resulting from the union of two matching markers is based on the position of these markers.

This *wall subdivision* method was used to draw Figures 7.2, 7.3 and 7.5. However, in a biological context it creates cells with shapes that are seldom observed in nature.

*Center of  
gravity method*

De Does and Lindenmayer [24] proposed a *center of gravity* method that produces more realistic shapes. According to this method each interior vertex of the map is placed at the center of gravity of its neighbors. Such positioning of vertices has a sound biological justification; it minimizes hypothetical forces acting along cell walls, thus bringing the entire structure to a state of minimum energy. However, if all vertices were positioned this way, the entire structure would collapse. To counteract this effect, the vertices on the map perimeter are displaced outward a fixed distance. Unfortunately, this lacks biological justification and introduces sudden shape changes after cell divisions have occurred, making it unsuitable for animation purposes.

*Dynamic  
method*

Assuming a dynamic point of view, the shape of cells and thus the shape of the entire organism results from the action of forces. The unbalanced forces due to cell divisions cause the gradual modification of cell shapes until an equilibrium is reached. At this point, new cell divisions occur, and the search for an equilibrium resumes.

---

<sup>1</sup>In further L-systems such identity productions are omitted.

The dynamic method is based on the following assumptions:

- the modeled organism forms a single cell layer,
- the layer is represented as a two-dimensional network of masses corresponding to cell vertices, connected by springs that correspond to cell walls,
- the springs are always straight and obey Hooke's law,
- each cell exerts pressure on its bounding walls directly proportional to the wall length and inversely proportional to the cell area,
- the pressure on a wall is divided evenly between the wall vertices,
- the motion of masses is damped, and
- no other forces (for example, due to friction or gravity) are considered.

The position of each vertex, and thus the shape of the layer, is computed as follows. As long as an equilibrium is not reached, unbalanced forces put masses in motion. The total force  $\vec{F}_T$  acting on a vertex  $X$  is given by the formula

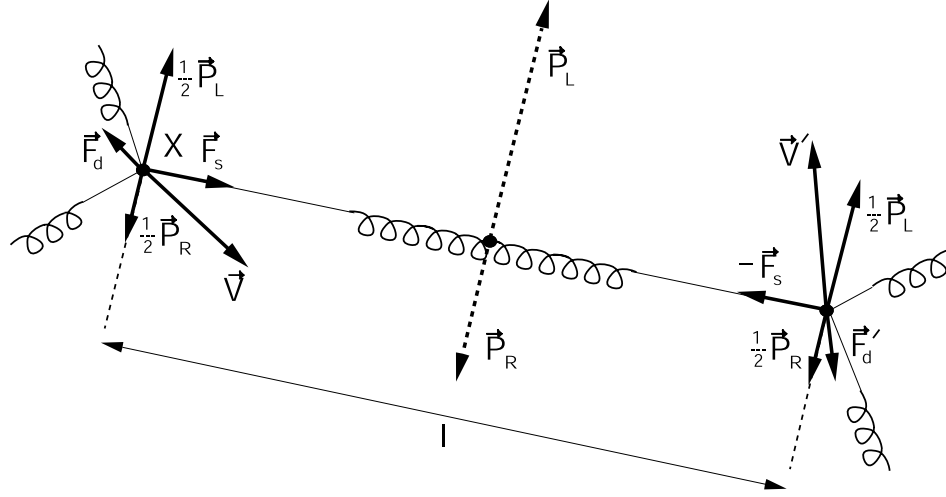
$$\vec{F}_T = \sum_{w \in W} \vec{F}_w + \vec{F}_d,$$

where  $\vec{F}_w$  are forces contributed by the set  $W$  of walls  $w$  incident to  $X$ , and  $\vec{F}_d = -b\vec{v}$  is a damping force, expressed as the product of a damping factor  $b$  and vertex velocity  $\vec{v}$ .

A wall  $w \in W$  contributes three forces acting on  $X$  (Figure 7.6). The *tension*  $\vec{F}_s$  acts along the wall, and its magnitude is determined by Hooke's law,

$$\vec{F}_s = -k(l - l_0),$$

where  $k$  is the spring constant,  $l$  is the current spring length, and  $l_0$  is its rest length. The remaining forces,  $\vec{F}_L$  and  $\vec{F}_R$ , are due to the *pressure* exerted by the cells on the left and right sides of the wall. Each force acts in a direction perpendicular to the wall and is distributed equally between the incident vertices. The magnitude of these forces equals  $p \cdot l$ , where  $p$  is the internal cell pressure and  $l$  is the wall length. The pressure is assumed to be inversely proportional to the cell area:  $p \sim A^{-1}$ . This assumption is derived from the equation describing osmotic pressure,  $p = SRT$ , as a function of the concentration of the solute  $S$  ( $n$  moles per volume  $V$ ), the ideal gas constant  $R$ , and the absolute temperature  $T$  [129]. Assuming that the cell volume  $V$  is

Figure 7.6: Forces acting on a cell vertex  $X$ 

proportional to the area  $A$  captured by the two-dimensional model under consideration ( $V = Ah$ ), pressure can be expressed as

$$p = \frac{nRT}{Ah}.$$

Thus  $p \sim A^{-1}$ , provided that the term  $nRT/h$  is constant. A convenient formula for calculating the area  $A$  is

$$A = \left| \sum_{i=1}^M (x_i - x_{i+1})(y_i + y_{i+1})/2 \right|,$$

where  $(x_i, y_i)$  are coordinates of the  $M$  vertices of the cell,  $x_{M+1} = x_1$ , and  $y_{M+1} = y_1$ .

The force  $\vec{F}_T$  acts on a mass placed at a map vertex. Newton's second law of motion applies,

$$m \frac{d^2 \vec{x}}{dt^2} = \vec{F}_T,$$

where  $\vec{x}$  is the vertex position. If the entire structure has  $N$  vertices, a system of  $2N$  differential equations is obtained,

$$\begin{aligned} m_i \frac{d\vec{v}_i}{dt} &= \vec{F}_{T_i}(\vec{x}_1, \dots, \vec{x}_N, \vec{v}_i) \\ \frac{d\vec{x}_i}{dt} &= \vec{v}_i, \end{aligned}$$

where  $i = 1, 2, \dots, N$ . The task is to find the sequence of positions  $\vec{x}_1, \dots, \vec{x}_N$  at given time intervals, assuming that the functions  $\vec{F}_{T_i}$  and the initial values of all variables  $\vec{x}_1^0, \dots, \vec{x}_N^0$  and  $\vec{v}_1^0, \dots, \vec{v}_N^0$  are known. These initial values are determined as follows.

- Coordinates of the vertices of the starting map are included in the input data for the simulation.
- Positions of existing vertices are preserved through a derivation step. New vertices partition the divided walls into segments of equal length. The initial velocities of all vertices are set to zero.

The system of differential equations with the initial values given above represents an *initial value problem*. It can be solved numerically using the *forward (explicit) Euler method* [41]. To this end, the differential equations are rewritten using finite increments  $\Delta\vec{v}_i$ ,  $\Delta\vec{x}_i$  and  $\Delta t$ ,

$$\begin{aligned}\Delta\vec{v}_i^k &= \frac{1}{m_i} \vec{F}_{T_i}(\vec{x}_1^k, \dots, \vec{x}_N^k, \vec{v}_i^k) \Delta t \\ \Delta\vec{x}_i^k &= \vec{v}_i^k \Delta t,\end{aligned}$$

where the superscripts  $k = 0, 1, 2, \dots$  indicate the progress of time,  $t = k\Delta t$ . The position and velocity of a point  $i$  after time increment  $\Delta t$  are expressed as follows:

$$\begin{aligned}\vec{v}_i^{k+1} &= \vec{v}_i^k + \Delta\vec{v}_i^k \\ \vec{x}_i^{k+1} &= \vec{x}_i^k + \Delta\vec{x}_i^k\end{aligned}$$

The iterative computation of the velocities  $\vec{v}_i^k$  and positions  $\vec{x}_i^k$  is carried out for consecutive values of index  $k$  until all increments  $\Delta\vec{v}_i$  and  $\Delta\vec{x}_i$  fall below a threshold value. This indicates that the equilibrium state has been approximated to the desired accuracy. The next derivation step is then performed. A system of equations corresponding to the resulting map is created, and the search for an equilibrium state resumes. In this way, the developmental process is simulated as periods of continuous cell expansion, delimited by instantaneous cell divisions. Continuity of cell shapes during divisions is preserved by the rule that sets the initial positions of vertices.

For example, Figure 7.7 illustrates the expansion of a structure generated by the L-system specified in Figure 7.3 in a derivation of length 4. Figure 7.7a shows the structure immediately after the insertion of division walls, Figures 7.7b and c present intermediate wall positions, and Figure 7.7d describes the final structure at equilibrium.

## 7.3 *Microsorium linguaeforme*

In this section, the described simulation method is applied to visualize the development of the fern gametophyte *Microsorium linguaeforme*. The biological data is based on observations conducted by de Boer [22]. Fern gametophytes represent the sexually reproducing life stage of fern

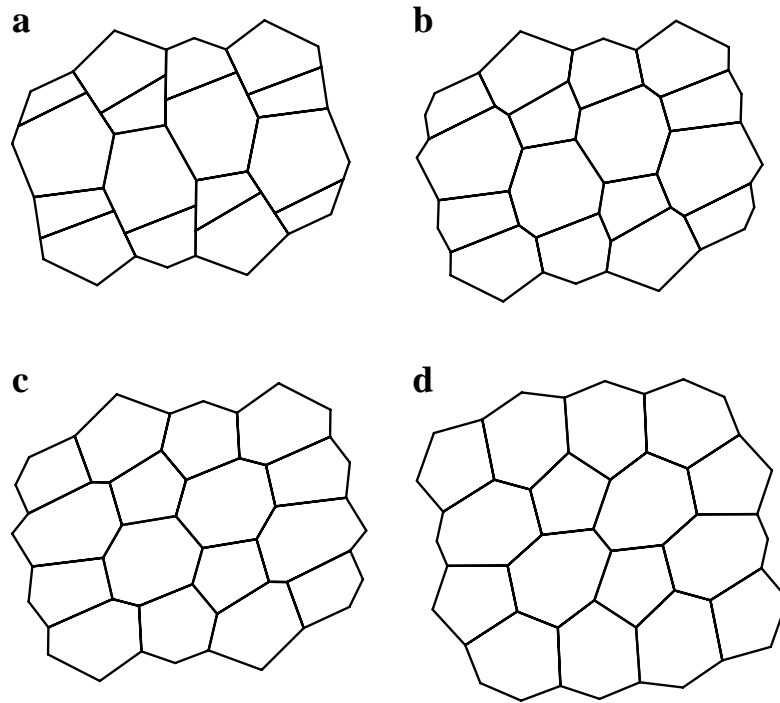


Figure 7.7: Expansion of a cellular structure: (a) after division, (b) and (c) intermediate positions, (d) equilibrium

plants. They show no differentiation into stem, leaf and root, forming a plant body called a *thallus*. The development of a thallus can be described conveniently in terms of the activity of the *apical cell* giving rise to *segments*, and the development of these segments. The modeling process captures repetitive patterns of cell divisions, so that large cellular structures can be described using a small number of productions.

#### *Apical activity*

The apical cell is the originator of the gametophyte structure. It divides repetitively, giving rise each time to a new apical cell and a primary (initial) segment cell. The segment cells subsequently develop into multicellular segments. The division wall of an apical cell is attached to the thallus border on one side and to a previously created division wall on the other side. Thus, the division walls are oriented alternately to the left and to the right, yielding two columns of segments separated by a zig-zag dividing line (Figure 7.8). The recursive nature of the apical activity can be expressed by the following formula (called a *cell division system* [22]):

$$A_L \rightarrow S_L \mid A_R \quad A_R \rightarrow A_L \mid S_R$$

This notation means that the cell on the left side of the arrow produces two daughter cells separated by a wall.

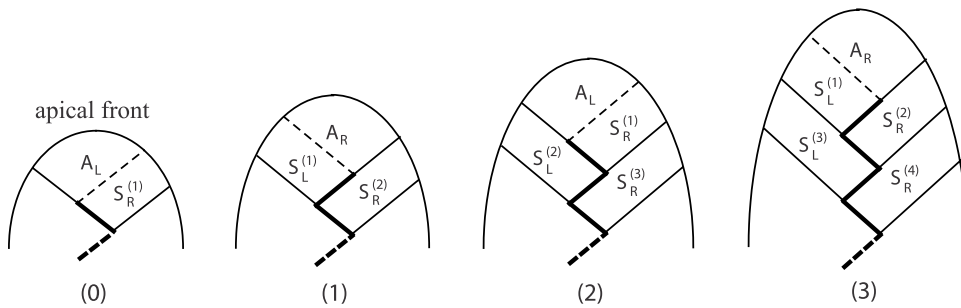


Figure 7.8: Apical production of segments. The labels  $A_R$  and  $A_L$  denote apical cells producing right segment  $S_R$  and left segment  $S_L$ , respectively. Dashed lines indicate the newly created division wall. The superscripts represent segment age. The internal structure of segments is not shown.

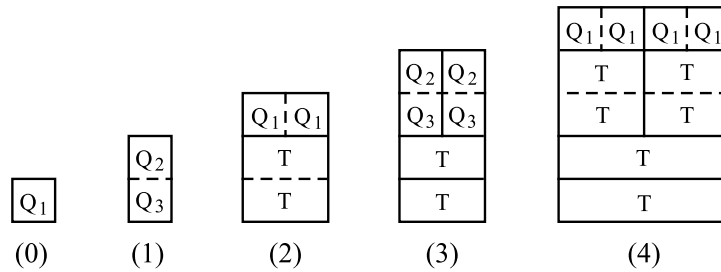


Figure 7.9: Developmental sequence of a *Microsorium* segment

In describing the structure of a segment, we distinguish between *periclinal* and *anticlinal* walls. Intuitively, periclinal walls are approximately parallel to the *apical front* of the thallus, and anticlinal walls are perpendicular to this front. A more formal definition follows.

*Division pattern of segments*

- In a primary segment, the apical front wall and one or more walls opposing it are periclinal walls. The remaining walls are anticlinal walls.
- A division wall attached to two periclinal walls is an anticlinal wall, and vice-versa.

In *Microsorium*, a wall is never attached to a periclinal wall on one side and an anticlinal wall on the other side, so the above definition comprises all possible cases.

Microscopic observations of growing *Microsorium* gametophytes reveal that most segments follow the same developmental sequence, shown diagrammatically in Figure 7.9. The primary segment cell  $Q_1$  is first divided by a periclinal wall into two cells,  $Q_2$  and  $Q_3$ . Subsequently, the

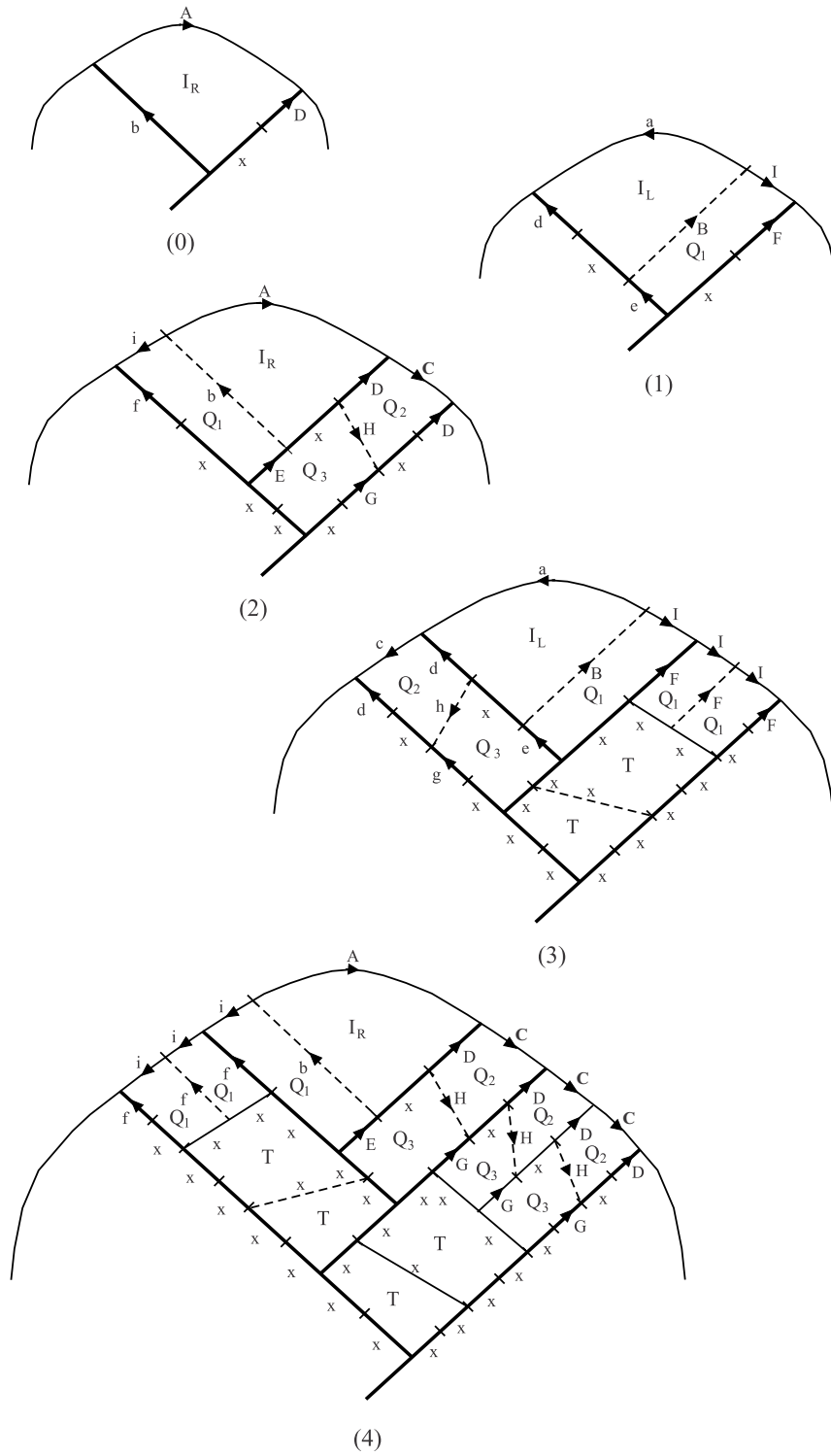
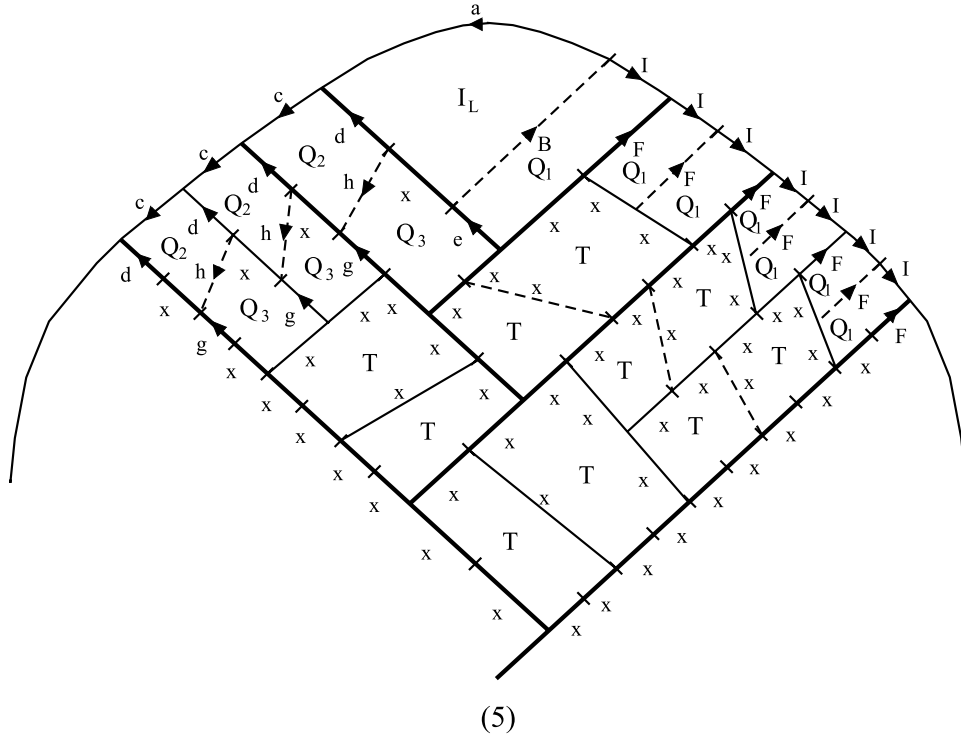


Figure 7.10: Developmental sequence of a *Microsorium* gametophyte





$$\begin{array}{ll}
 \omega : \overrightarrow{\overleftarrow{A}} \overrightarrow{\overleftarrow{D}} \overrightarrow{\overleftarrow{x}} \overrightarrow{\overleftarrow{b}} & \\
 l_1 : \overrightarrow{a} \rightarrow \overleftarrow{A} [+ \overleftarrow{b}] \overrightarrow{i} & r_1 : \overrightarrow{A} \rightarrow \overleftarrow{a} [- \overleftarrow{B}] \overrightarrow{I} \\
 l_2 : \overrightarrow{b} \rightarrow \overleftarrow{e} [- \overleftarrow{B}] \overrightarrow{x} [+ \overrightarrow{h}] \overrightarrow{d} & r_2 : \overrightarrow{B} \rightarrow \overleftarrow{E} [+ \overleftarrow{b}] \overrightarrow{x} [- \overrightarrow{H}] \overrightarrow{D} \\
 l_3 : \overrightarrow{d} \rightarrow \overleftarrow{f} & r_3 : \overrightarrow{D} \rightarrow \overleftarrow{F} \\
 l_4 : \overrightarrow{f} \rightarrow \overleftarrow{g} [- \overleftarrow{h}] \overrightarrow{x} [+ \overrightarrow{h}] \overrightarrow{d} & r_4 : \overrightarrow{F} \rightarrow \overleftarrow{G} [+ \overleftarrow{H}] \overrightarrow{x} [- \overrightarrow{H}] \overrightarrow{D} \\
 l_5 : \overrightarrow{h} \rightarrow \overleftarrow{x} [- \overleftarrow{f}] \overrightarrow{x} & r_5 : \overrightarrow{H} \rightarrow \overleftarrow{x} [+ \overleftarrow{F}] \overrightarrow{x} \\
 l_6 : \overrightarrow{i} \rightarrow \overleftarrow{c} & r_6 : \overrightarrow{I} \rightarrow \overleftarrow{C} \\
 l_7 : \overrightarrow{c} \rightarrow \overleftarrow{i} [+ \overleftarrow{f}] \overrightarrow{i} & r_7 : \overrightarrow{C} \rightarrow \overleftarrow{I} [- \overleftarrow{F}] \overrightarrow{I} \\
 l_8 : \overrightarrow{e} \rightarrow \overleftarrow{x} [+ \overleftarrow{x}] \overrightarrow{x} & r_8 : \overrightarrow{E} \rightarrow \overleftarrow{x} [- \overleftarrow{x}] \overrightarrow{x} \\
 l_9 : \overrightarrow{g} \rightarrow \overleftarrow{x} [- \overleftarrow{x}] \overrightarrow{x} [+ \overrightarrow{x}] \overrightarrow{x} & r_9 : \overrightarrow{G} \rightarrow \overleftarrow{x} [+ \overleftarrow{x}] \overrightarrow{x} [- \overrightarrow{x}] \overrightarrow{x}
 \end{array}$$

Figure 7.10 (continued): Developmental sequence of *Microsorium*

basal cell  $Q_3$  is divided by another periclinal wall into two “terminal” cells  $T$  that do not undergo further divisions. At the same time, the cell  $Q_2$  lying on the thallus border is divided by an anticlinal wall into two cells of type  $Q_1$ . Each of these cells divides in the same way as the primary cell. Consequently, the recursive nature of segment development can be captured by the following cell division system:

$$Q_1 \rightarrow \frac{Q_2}{Q_3} \qquad Q_2 \rightarrow Q_1 \mid Q_1 \qquad Q_3 \rightarrow \frac{T}{T}$$

In the above rules, a horizontal bar denotes a periclinal wall between cells, and a vertical bar denotes an anticlinal wall.

*Development of  
the thallus*

The development of the *Microsorium* thallus is a result of concurrent divisions of the apical and segment cells. A single division of the apical cell corresponds to a single step in segment development. A developmental sequence that combines the activity of the apex and the segments is shown in Figure 7.10. This figure also reveals offsets between neighboring walls. It can be assumed that periclinal division walls form S-offsets in the segments on the right side of the apex and Z-offsets in the segments on the left side.

*Map L-system*

In order to capture the development of *Microsorium* using the formalism of map L-systems, it is necessary to identify all combinations of cells that may lie on both sides of a wall. Careful examination of these combinations yields the wall labeling scheme shown in Figure 7.10. Two walls have the same label if and only if they divide in the same way.<sup>2</sup> The uppercase letters apply to right segment walls, and the corresponding lowercase letters denote symmetric walls in the left segments. A comparison of pairs of subsequent structures yields the L-system in the figure.

Apical cell division results from the application of productions  $r_1$  and  $l_2$  (creation of a right segment) or  $l_1$  and  $r_2$  (creation of a left segment). Subsequent cell divisions in right and left segments proceed symmetrically. The development of a right segment is examined in detail.

The insertion of wall segment  $B$  creates the first cell  $Q_1$  of segment  $S_R^{(1)}$  (cf. Figure 7.8). Concurrently, wall  $D$  on the opposite side of the segment is transformed into  $F$  (step 1). This transformation introduces a one-step delay before the application of production  $r_4$  which, together with  $r_2$ , splits cell  $Q_1$  into  $Q_2$  and  $Q_3$  by the first periclinal wall  $H$  (step 2). As the derivation progresses, production  $r_4$  inserts subsequent periclinal walls  $H$  between pairs of anticlinal walls  $F$  (step 4). Production

<sup>2</sup>It is conceivable to formulate an algorithm that would assign labels consistent with the above rule automatically. However, the labeling scheme given in Figure 7.10 was obtained “by hand.”

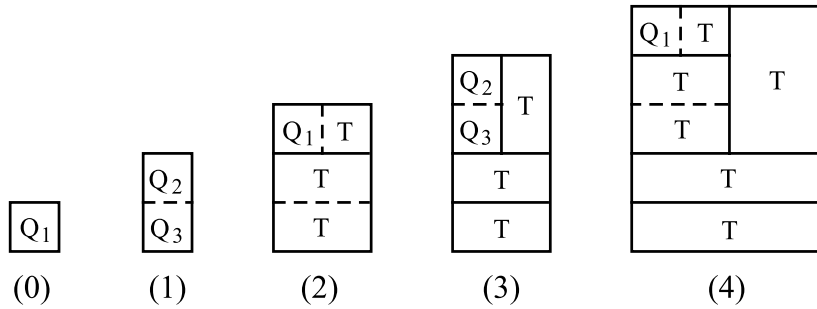


Figure 7.11: Developmental sequence of a basal *Microsorium* segment

$r_3$  introduces a delay needed to create walls  $F$ , which are inserted between periclinal walls  $H$  and apical walls  $I$  using productions  $r_5$  and  $r_7$ . Production  $r_6$  plays a role analogous to  $r_3$  — it introduces a one-step delay into the cycle which creates markers  $F$  at the apical front of the segment. Thus, periclinal walls  $H$  and anticlinal walls  $F$  are produced alternately, in subsequent derivation steps. The last two productions,  $r_8$  and  $r_9$ , create terminal walls  $x$  that do not undergo further changes. The first such wall is inserted between walls labeled  $G$  and  $E$  during derivation step 3. The subsequent walls  $x$  are inserted every second step between pairs of walls  $G$ ; only production  $r_9$  is applied in these cases.

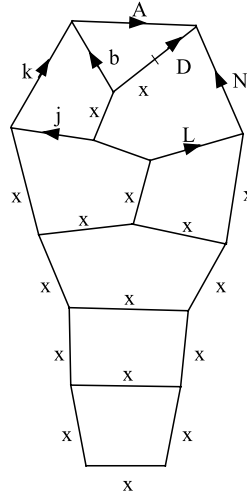
The L-system in Figure 7.10 was formulated under the assumption that all segments develop in the same way. However, in a real organism the two oldest segments, situated at the thallus base, form a modified pattern with less extensive cell divisions. The developmental sequence of a right basal segment is shown in Figure 7.11. The corresponding cell division system is given below.

*Basal segments*

$$Q_1 \rightarrow \frac{Q_2}{Q_3} \qquad Q_2 \rightarrow Q_1 | T \qquad Q_3 \rightarrow \frac{T}{T}$$

The development of a *Microsorium* gametophyte including basal segments is captured by Figure 7.12. Only productions describing the development of the right side of the thallus are given. Their predecessors are denoted by uppercase letters. The corresponding lowercase productions, which complete the L-system definition, can be obtained by switching the “case” of letters and the orientation of markers. Wall directions remain unchanged. For example, the right-side production

$$r_x : \vec{P} \rightarrow \overleftarrow{A}[-\vec{b}]C$$



$$\begin{array}{ll}
 r_1 : \vec{A} \rightarrow \overleftarrow{a} [- \overleftarrow{B}] \vec{I} & r_9 : \vec{G} \rightarrow x [+ x] x [- x] x \\
 r_2 : \vec{B} \rightarrow \vec{E} [+ \vec{b}] x [- \vec{H}] \vec{D} & r_{10} : \vec{J} \rightarrow \vec{L} \\
 r_3 : \vec{D} \rightarrow [- \vec{M}] \vec{F} & r_{11} : \vec{K} \rightarrow \vec{N} \\
 r_4 : \vec{F} \rightarrow \vec{G} [+ \overleftarrow{H}] x [- \vec{H}] \vec{D} & r_{12} : \vec{L} \rightarrow x [+ \overleftarrow{M}] x \\
 r_5 : \vec{H} \rightarrow x [+ \vec{F}] x & r_{13} : \vec{M} \rightarrow x [+ \vec{L}] x \\
 r_6 : \vec{I} \rightarrow \vec{C} & r_{14} : \vec{N} \rightarrow \vec{O} \\
 r_7 : \vec{C} \rightarrow \vec{I} [- \overleftarrow{F}] \vec{I} & r_{15} : \vec{O} \rightarrow x [+ \overleftarrow{L}] \vec{N} \\
 r_8 : \vec{E} \rightarrow x [- x] x &
 \end{array}$$

Figure 7.12: The initial map and productions for the right side of a *Microsorium linguaeforme* with basal segments

corresponds to the left-side production

$$l_x : \vec{p} \rightarrow \overleftarrow{a} [+ \vec{B}] c.$$

Additional examples can be found by comparing the left and right columns of the L-system in Figure 7.10.

Assuming the starting map specified by Figure 7.12, a simulated developmental sequence interpreted using the dynamic method to determine cell shape is given in Figure 7.13. Different colors are used to indicate the apical cell, the alternating “regular” segments, and the basal segments. A comparison of the last developmental stage with a photograph of a real gametophyte (Figure 7.14) shows good correspondence between the model and reality with respect to structure topology, the relative sizes and shapes of cells, and the overall shape of the thallus. This result is particularly interesting from a biological perspective, since it indicates that genetically controlled cell division patterns play an important role in determining the shape of a structure.

*Model  
validation*

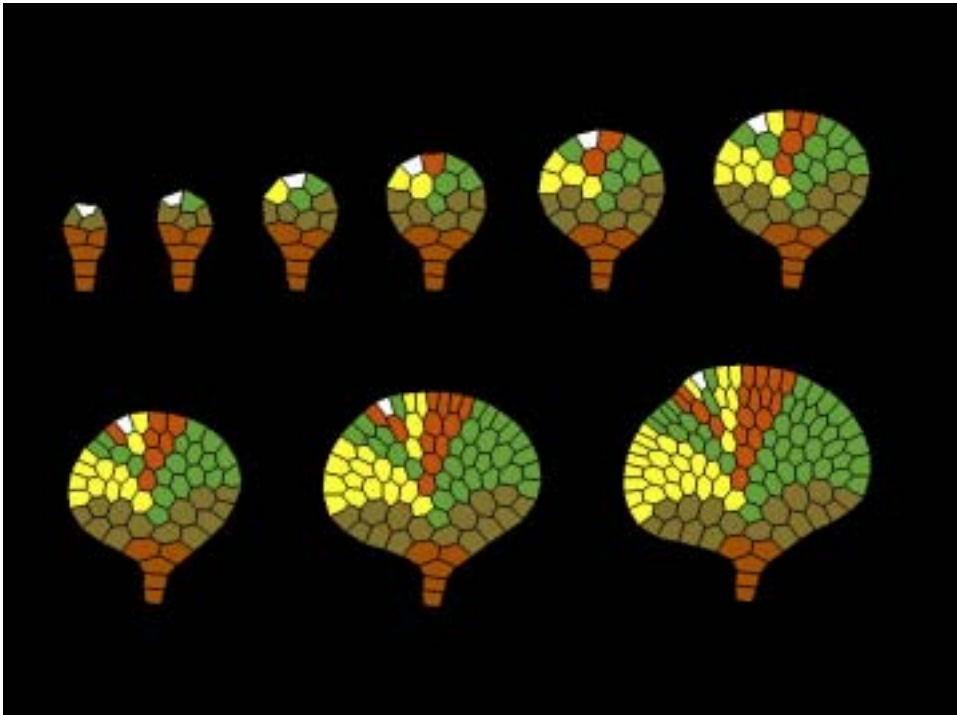


Figure 7.13: Simulated development of *Microsorium linguaeforme*

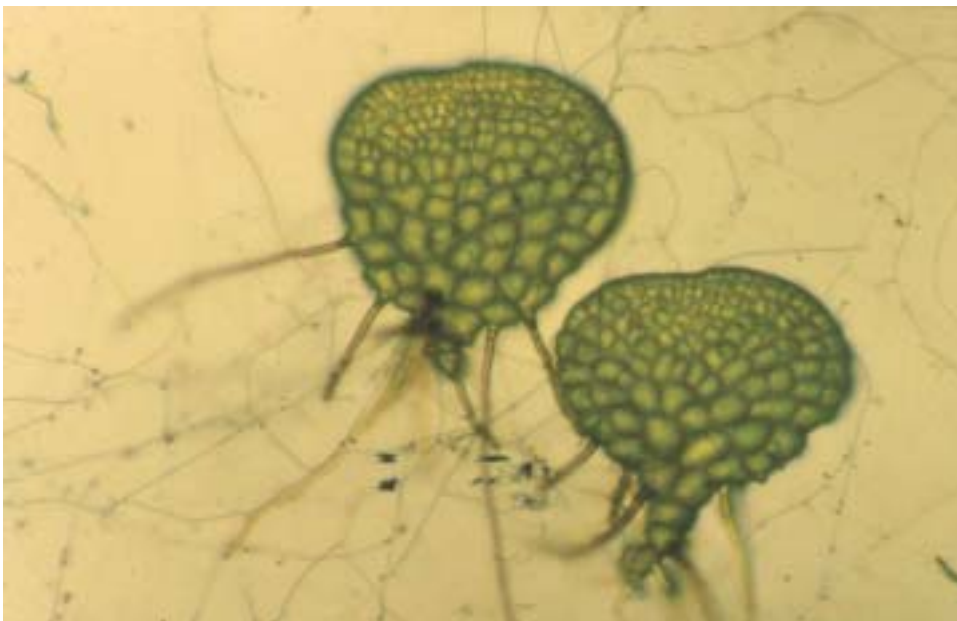


Figure 7.14: Microphotograph of *Microsorium linguaeforme* at magnification 70x

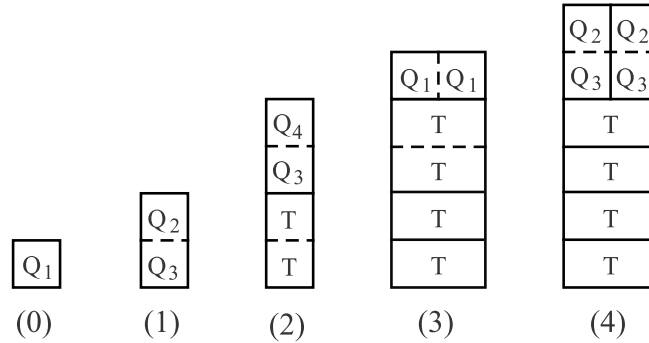


Figure 7.15: Developmental sequence of a *Dryopteris* segment

### 7.4 *Dryopteris thelypteris*

Gametophytes of other fern species follow a similar developmental pattern, with the apex producing segments alternately to the left and right. However, the cell division patterns within segments vary between species yielding different thalli shapes. For example, Figure 7.15 shows segment development in *Dryopteris thelypteris*. The corresponding cell division system is given below.

$$Q_1 \rightarrow \frac{Q_2}{Q_3} \quad Q_2 \rightarrow \frac{Q_4}{Q_3} \quad Q_3 \rightarrow \frac{T}{T} \quad Q_4 \rightarrow Q_1 | Q_1$$

A developmental cycle of length 3, starting at cell  $Q_1$ , produces two new cells  $Q_1$  separated by an anticlinal wall and a sequence of four terminal cells  $T$  separated by periclinal walls. A developmental sequence that combines the activity of the apex and the segments is shown in Figure 7.17. As in the case of the map L-system in Figure 7.12, only productions for the right side of the thallus are shown.

Map L-system

Apical cell division results from the application of productions  $r_1$  and  $l_2$  (creation of a right segment) or  $l_1$  and  $r_2$  (creation of a left segment). The subsequent cell divisions proceed in a symmetric way in right and left segments. The development of a right segment is described below.

The insertion of wall segment  $B$  creates the first cell  $Q_1$  of segment  $S_R^{(1)}$  (cf. Figure 7.8). Concurrently, wall  $D$  on the opposite side of the segment is transformed by production  $r_6$  into  $FG$  (step 1). This transformation introduces a one-step delay before the application of production  $r_7$  which, together with  $r_2$ , splits cell  $Q_1$  into  $Q_2$  and  $Q_3$  by the first periclinal wall  $x$  (step 2). Meanwhile, production  $r_3$  replaces wall  $C$  by wall  $J$  (step 1), after which  $r_4$  replaces  $J$  by  $E$  (step 2). This introduces a two-step delay before cell  $Q_3$  is subdivided periclinally into two cells  $T$  by production  $r_5$  (step 3). In the same step, productions  $r_6$  and  $r_9$  subdivide cell  $Q_2$  into cells  $Q_3$  and  $Q_4$ , separated by periclinal wall  $H$ . Wall  $O$  from step 1 is transformed into wall  $R$  by productions

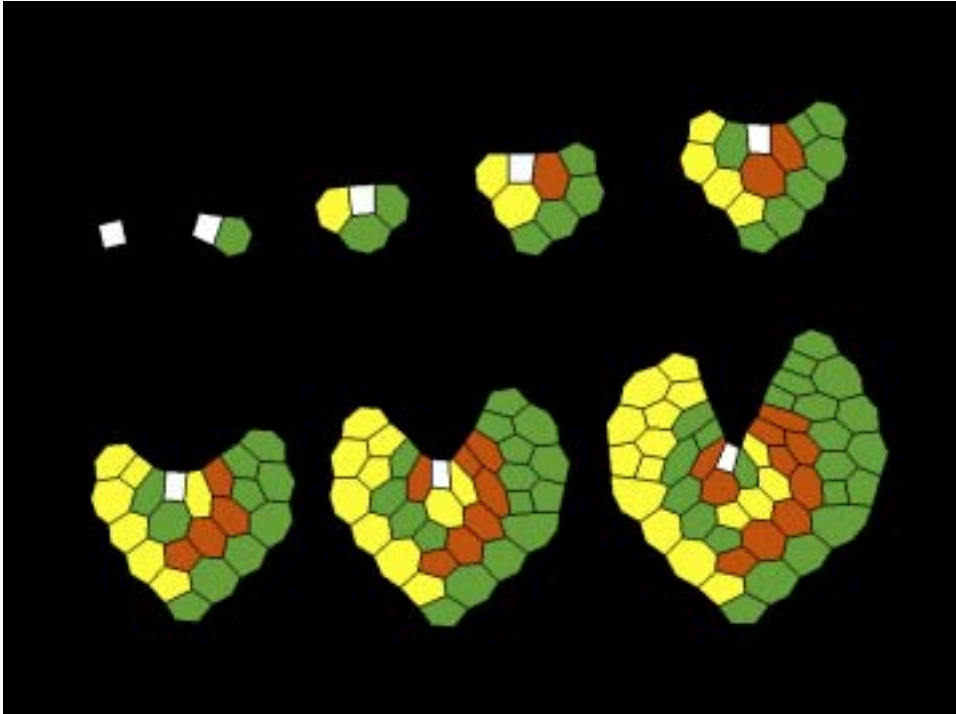


Figure 7.16: Simulated development of *Dryopteris thelypteris*

$r_{15}$  (step 2) and  $r_{16}$  (step 3). Walls  $R$  and  $H$  are replaced by  $r_{17}$  and  $r_{14}$ , resulting in the first anticlinal division of cell  $Q_4$  into two cells  $Q_1$  by wall  $I$  (step 4). At the same time, productions  $r_5$  and  $r_6$  split cell  $Q_3$  periclinally into two cells  $T$ . In the following derivation steps, each of the newly created cells  $Q_1$  undergoes a sequence of changes similar to that described above. Production  $r_8$  introduces a one-step delay before  $Q_1$  is subdivided into  $Q_2$  and  $Q_3$  using  $r_9$  and  $r_{10}$  (analogous to  $r_2$  and  $r_7$ ). Productions  $r_{11}$  and  $r_{12}$  play a role similar to  $r_5$  and  $r_6$ , while production  $r_{13}$  introduces a delay. Walls labeled  $x$  do not undergo further changes and cells  $T$  do not subdivide. A simulated developmental sequence generated by the L-system in Figure 7.17 using the dynamic method to determine cell shape is given in Figure 7.16.

A comparison of *Microsorium* and *Dryopteris* gametophytes (either real or modeled) indicates that different division patterns of segment cells have a large impact on the overall thallus shapes. In *Microsorium*, the number of *marginal cells*, situated at the apical front of a segment, is doubled every second derivation step. The segments are approximately triangular, with a wide apical front, which results in the circular thallus shape. The apical front of *Dryopteris* segments is comparatively less developed. The number of marginal cells is doubled only every third step, and the segments grow faster in length. The resulting thallus shape is concave.

*Microsorium*  
vs. *Dryopteris*

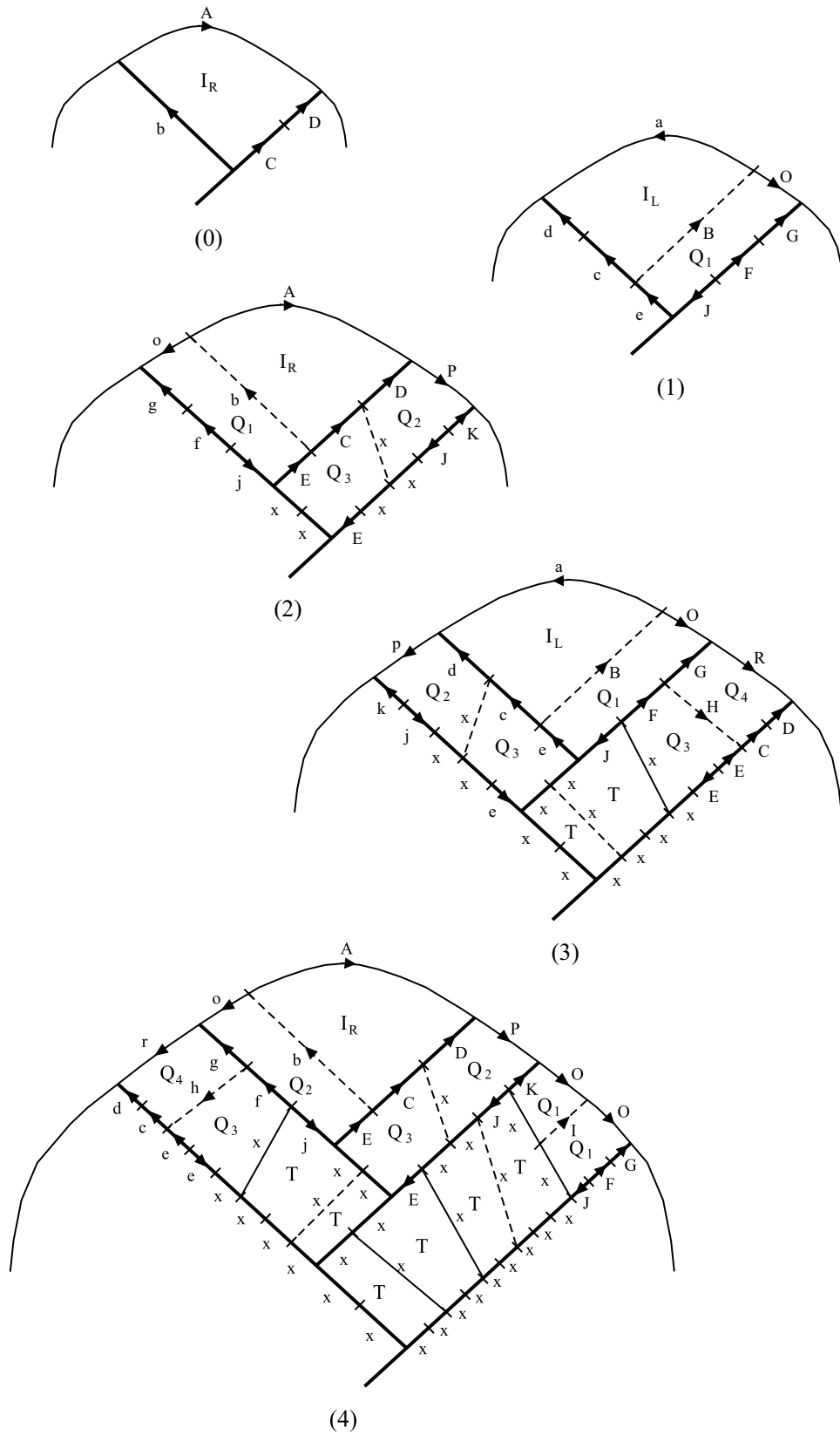
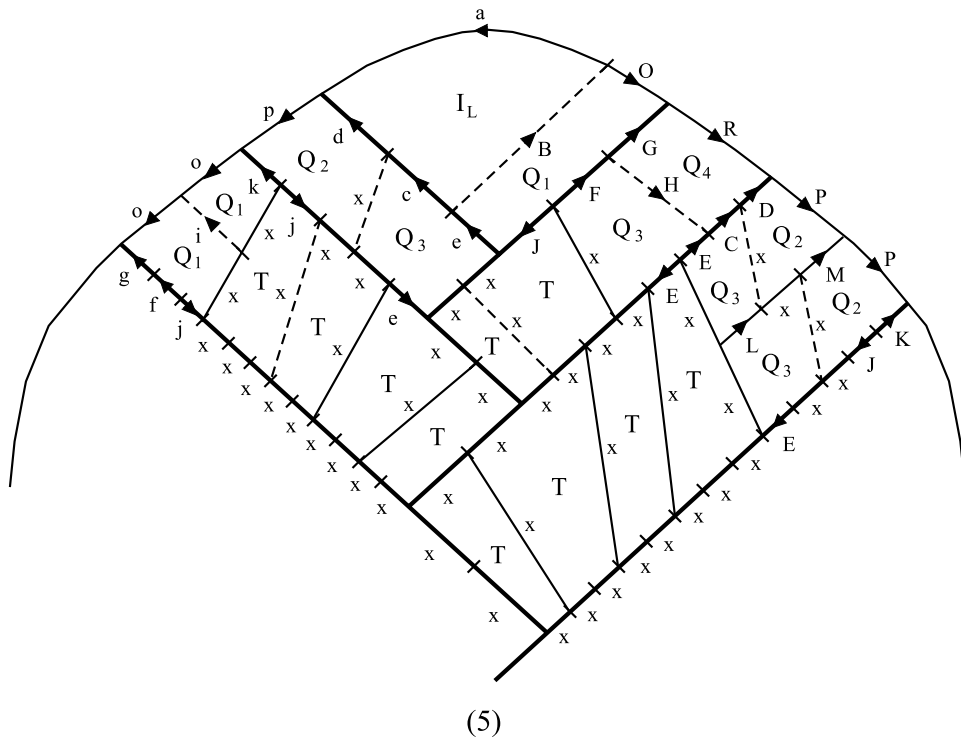


Figure 7.17: Developmental sequence of a *Dryopteris* gametophyte





$$\begin{array}{ll}
 \omega : \overleftrightarrow{ADCb} & r_{10} : \overrightarrow{I} \rightarrow \overrightarrow{L} [+x] x [-x] \overrightarrow{M} \\
 r_1 : \overrightarrow{A} \rightarrow \overleftarrow{a} [-\overrightarrow{B}] \overrightarrow{O} & r_{11} : \overrightarrow{L} \rightarrow x [+x] x [-x] x \\
 r_2 : \overrightarrow{B} \rightarrow \overrightarrow{E} [+b] \overrightarrow{C} [-x] \overrightarrow{D} & r_{12} : \overrightarrow{M} \rightarrow \overrightarrow{L} [+H] x [-H] \overrightarrow{N} \\
 r_3 : \overrightarrow{C} \rightarrow \overrightarrow{J} & r_{13} : \overrightarrow{N} \rightarrow \overrightarrow{I} \\
 r_4 : \overrightarrow{J} \rightarrow \overrightarrow{E} & r_{14} : \overrightarrow{H} \rightarrow x [+I] x \\
 r_5 : \overrightarrow{E} \rightarrow x [-x] x & r_{15} : \overrightarrow{O} \rightarrow \overrightarrow{P} \\
 r_6 : \overrightarrow{D} \rightarrow \overrightarrow{F} [-H] \overrightarrow{G} & r_{16} : \overrightarrow{P} \rightarrow \overrightarrow{Q} \\
 r_7 : \overrightarrow{F} \rightarrow x [+x] x [-x] \overleftarrow{J} & r_{17} : \overrightarrow{Q} \rightarrow \overrightarrow{O} [-I] \overrightarrow{O} \\
 r_8 : \overrightarrow{G} \rightarrow \overrightarrow{K} & \\
 r_9 : \overrightarrow{K} \rightarrow \overrightarrow{E} [+H] \overrightarrow{C} [-x] \overrightarrow{D} & 
 \end{array}$$

Figure 7.17 (continued): Developmental sequence of *Dryopteris*

In order to quantify the relationship between segment cell division pattern and thallus shape, de Boer [22] proposed an empirical measure called *periclinal ratio*. It is based on the following considerations:

- anticlinal growth takes place mainly along the margin and is exponential since all marginal cells divide; and
- periclinal growth of a segment is linear, as cells displaced away from the margin eventually stop dividing.

Since the division pattern is recursive, the average ratio of the numbers of marginal cells in neighboring segments converges to a constant  $A$ . Similarly, the difference between the numbers of cells along the periclinal boundary of two neighboring segments converges to a constant  $P$ . By computer simulation [22], it was found that if the periclinal ratio  $P/A$  is smaller than 1.25, the apical front is convex as in the case of *Microsorium linguaeforme*. In contrast, if  $P/A$  is larger than 2.0, the simulated structure develops a concave apical front, corresponding to a heart-shaped thallus as in *Dryopteris thelypteris*. These results relate local growth to global shape. Periclinal ratios from 1.25 to 2.0 were not studied in detail.

## 7.5 Modeling spherical cell layers

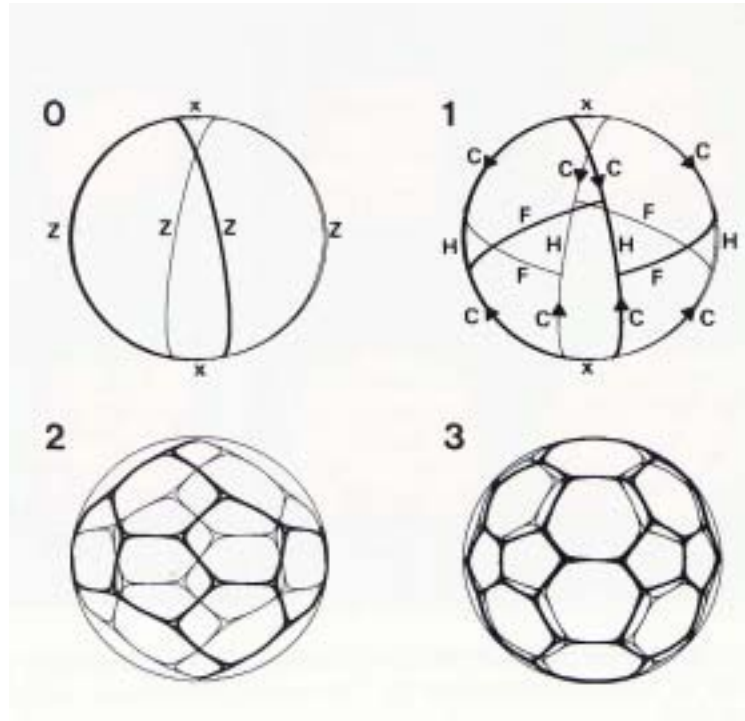
Although the scope of this book is limited to plants, it is interesting to note that the formalism of L-systems can be applied also to simulate some developmental processes in animals. For example, during the *cleavage* stage of development, an animal embryo consists of a single layer of cells that covers the surface of a spherical cavity. This structure is known as the *blastula* [6]. The cells divide synchronously in a regular pattern up to and including the 64-cell stage (6th cleavage). This development can be captured using an mBPMOL-system operating on the surface of a sphere rather than on a plane. To this end, cell walls are represented as great circle arcs connecting vertices that are constrained to the sphere surface.

The extension of the dynamic interpretation method from the plane to the surface of a sphere requires few changes. Osmotic pressure and wall tension are calculated as before. Since the resulting force may displace a vertex away from the surface of the sphere, the actual vertex position is found by projecting the displaced point back to the sphere. During the cleavage stage, cells of embryos do not expand, thus the overall size of the sphere is constant.

For example, deBoer [22] proposed the map L-system in Figure 7.18 to model the development of a snail embryo, *Patella vulgata*, according to data presented by Biggelaar [150]. The starting map and developmental sequence are shown in Figure 7.18, while Figure 7.19 presents an alternative rendering. Each cell is approximated by a sphere centered at the point obtained by raising the center of gravity of the cell

*Animal embryos*

*Patella vulgata*



$$\begin{aligned}
 p_1 : A &\rightarrow b[-a]x[+a]b \\
 p_2 : a &\rightarrow B[+A]x[-A]B \\
 p_3 : B &\rightarrow a \\
 p_4 : b &\rightarrow A \\
 p_5 : \vec{C} &\rightarrow \vec{D} [+a] \vec{E} \\
 p_6 : \vec{D} &\rightarrow \vec{C} [-A]x \\
 p_7 : \vec{E} &\rightarrow \vec{C} \\
 p_8 : F &\rightarrow \vec{E} [-a]G[+a] \vec{E} \\
 p_9 : G &\rightarrow J \\
 p_{10} : H &\rightarrow I \\
 p_{11} : I &\rightarrow B[-A]x[+A]B \\
 p_{12} : J &\rightarrow b[+a]x[-a]b \\
 p_{13} : Z &\rightarrow \vec{C} [-F]H[+F] \vec{C}
 \end{aligned}$$

Figure 7.18: Developmental sequence of *Patella vulgata* (equatorial view)

vertices to the surface of the underlying spherical cavity. The radius is the maximum distance from the center of gravity to the cell vertices. A comparison of the *Patella* model at the 16-cell stage (bottom left of Figure 7.19) with an electron microscope image (Figure 7.20) shows good correspondence between the model and reality.

## 7.6 Modeling 3D cellular structures

### *Cellworks*

The previous sections presented a method for modeling cellular layers extending in a plane or on the surface of a sphere. However, real cellular structures are three-dimensional objects. In order to capture the three-dimensional aspect of cellular layers and model more complex structures, Lindenmayer [85] proposed an extension of map L-systems called *cellwork* L-systems. The notion of a cellwork is characterized as follows.

- A cellwork is a finite set of *cells*. Each cell is surrounded by one or more *walls* (faces).
- Each wall is surrounded by a boundary consisting of a finite, circular sequence of *edges* that meet at *vertices*.
- Walls cannot intersect without forming an edge, although there can be walls without edges (in the case of cells shaped as spheres or tori).
- Every wall is part of the boundary of a cell, and the set of walls is connected.
- Each edge has one or two vertices associated with it. The edges cannot cross without forming a vertex, and there are no vertices without an associated edge.
- Every edge is a part of the boundary of a wall, and the set of edges is connected.

Note that the terms *cell* and *wall* have different meanings in the context of cellworks than in the context of maps.

### *mBPCOL-system*

The development of three-dimensional structures is captured using an extension of mBPMOL-systems called *marker Binary Propagating Cellwork OL-systems* [42]. An mBPCOL-system  $\mathcal{G}$  is defined by a finite alphabet of *edge labels*  $\Sigma$ , a finite alphabet of *wall labels*  $\Gamma$ , a *starting cellwork*  $\omega$ , and a finite set of *edge productions*  $P$ . The initial cellwork  $\omega$  is specified by a list of walls and their bounding edges. As in the case of mBPMOL-systems, edges may be directed or neutral. Each production is of the form  $A : \beta \rightarrow \alpha$ , where the edge  $A \in \Sigma$  is the *predecessor*, the string  $\beta \in \{\Gamma^+, *\}$  is a list of *applicable walls* (\* denotes all walls), and the string  $\alpha$  is the *successor*, which is composed of edge labels from  $\Sigma$ ,

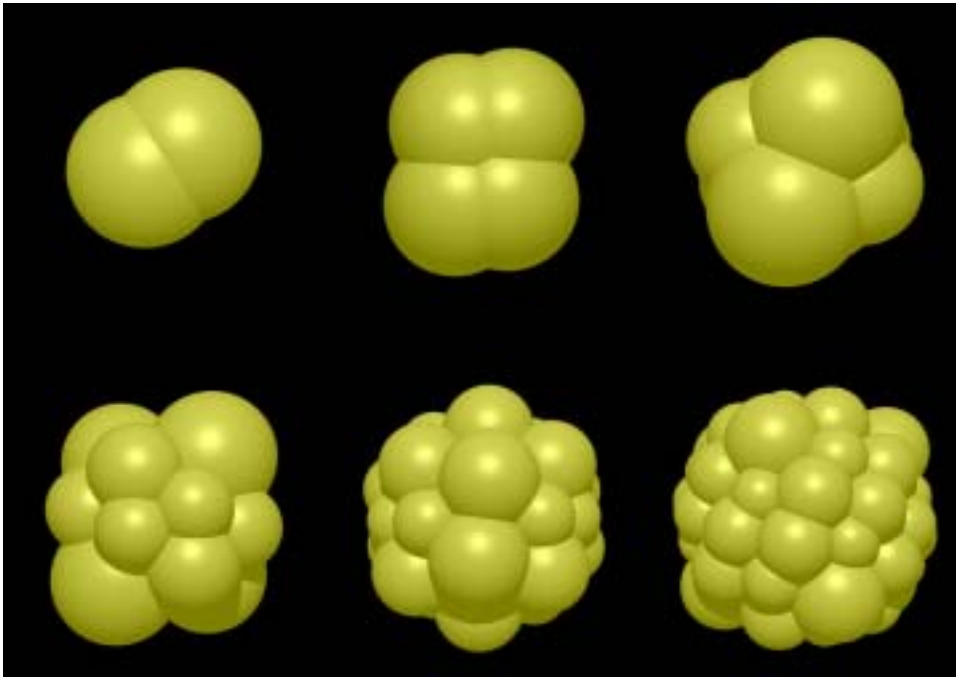


Figure 7.19: Simulated development of *Patella vulgata*

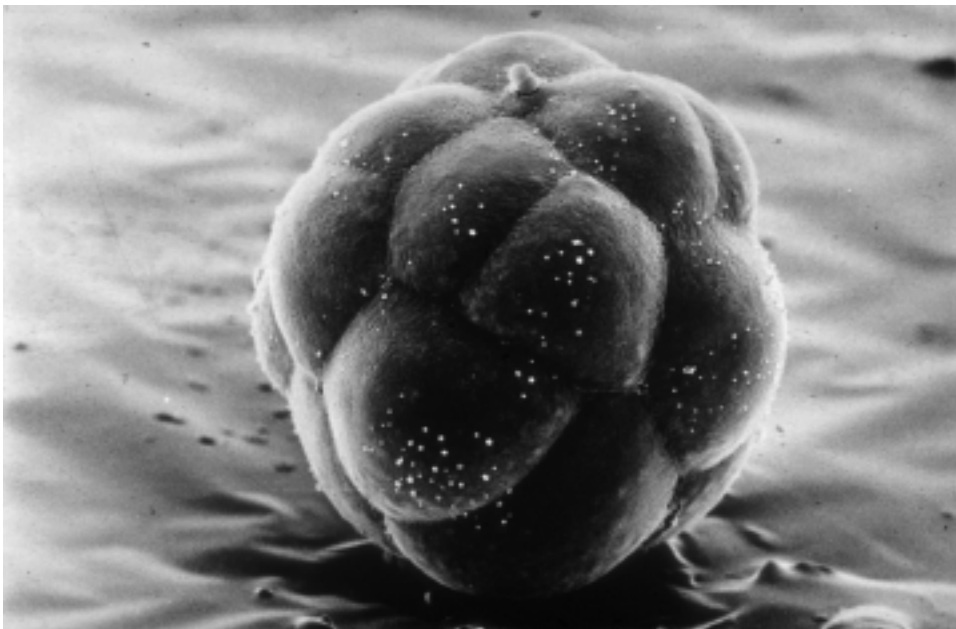


Figure 7.20: An electron microscope image of *Patella vulgata*

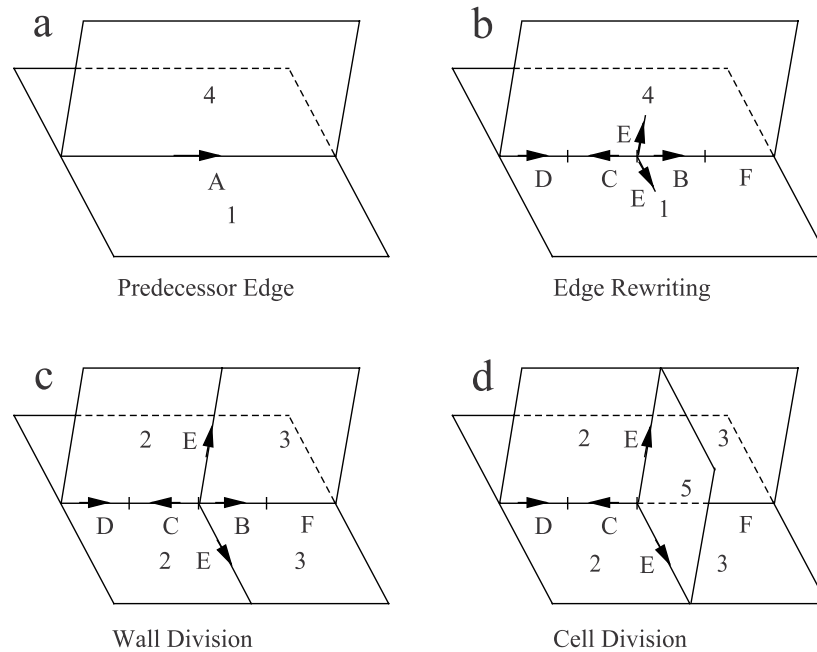


Figure 7.21: The phases of a derivation step

wall labels from  $\Gamma$  and the symbols [ and ]. The symbols outside square brackets describe the subdivision pattern for the predecessor. Pairs of matching brackets [ and ] delimit *markers* that specify possible attachment sites for new edges and walls. As in the two-dimensional case, arrows indicate the relative directions of successor edges and markers with respect to the predecessor edge. The list  $\beta$  contains all walls into which a marker should be inserted. In addition to the labels for edges and markers, a production successor specifies the labels of walls that may be created as a result of a derivation step.

*Production  
syntax*

The syntax of a production is best explained using an example. The production

$$\vec{A} : 14 \rightarrow \vec{D}\overleftarrow{C}_2[\vec{E}_5]\vec{B}_3F$$

applies to an edge  $A$  if it belongs to one or more walls labeled 1 or 4 (Figure 7.21a). The predecessor edge is subdivided into four edges  $D$ ,  $C$ ,  $B$  and  $F$ . During a derivation step, marker  $E$  is introduced into all walls of type 1 or 4 that share edge  $A$  (Figure 7.21b), and can be connected with a matching marker inserted into the same wall by another production. As a result, the wall will split into two. The daughter wall having  $C$  as one of its edges will be labeled 2, and the wall having  $B$  as an edge will be labeled 3 (Figure 7.21c). Markers  $E$  can be connected only if both productions assign labels to the daughter walls in a consistent way. Otherwise, the markers are considered non-matching and are discarded. If several walls bounding a cell split in such a way that the sequence of new edges forms a closed contour, a

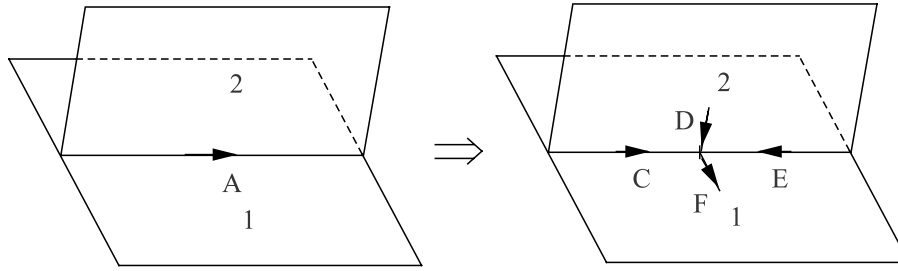


Figure 7.22: Example of consistent edge productions

new wall bound by these edges may be created. In order for this to occur, all markers involved must specify the same label for the new wall, 5 in this example (Figure 7.21d).

The limitation of the scope of a production to specific walls may create a consistency problem while rewriting edges. For instance, assume that walls 1 and 2 share edge  $A$  and the following productions are in  $P$ :

$$\begin{aligned} p_1 : \vec{A} : 1 &\rightarrow \vec{C}\overleftarrow{E} \\ p_2 : \vec{A} : 2 &\rightarrow \vec{A}\overleftarrow{B} \end{aligned}$$

Productions  $p_1$  and  $p_2$  are inconsistent since they specify two different partitions of the same edge. It is assumed that the mBPCOL-systems under consideration are free of such inconsistencies. This does not preclude the possibility of applying several productions simultaneously to the same edge. For example, a production pair,

$$\begin{aligned} p_1 : \vec{A} : 1 &\rightarrow \vec{C}_2[\vec{F}_3]\overleftarrow{E}_4 \\ p_2 : \vec{A} : 2 &\rightarrow \vec{C}_5[\vec{D}_6]\overleftarrow{E}_7, \end{aligned}$$

consistently divides edge  $A$  into segments  $C$  and  $E$ , although the markers inserted into walls 1 and 2 are different (Figure 7.22).

According to the above discussion, a *derivation step* in an mBPCOL-system consists of three phases.

*Derivation*

- Each edge in the cellwork is replaced by successor edges and markers using one or more productions in  $P$ .
- Each wall is scanned for matching markers. If a match inducing a consistent labeling of daughter cells is found, the wall is subdivided. The selection of matching markers is done by the system. Unused markers are discarded.
- Each cell is scanned for a circular sequence of new division edges. If a cycle assigning the same label to the division wall is found, it is used to bound the wall that will divide the cell into two daughter cells. If different possibilities exist, the edges are selected by the system.

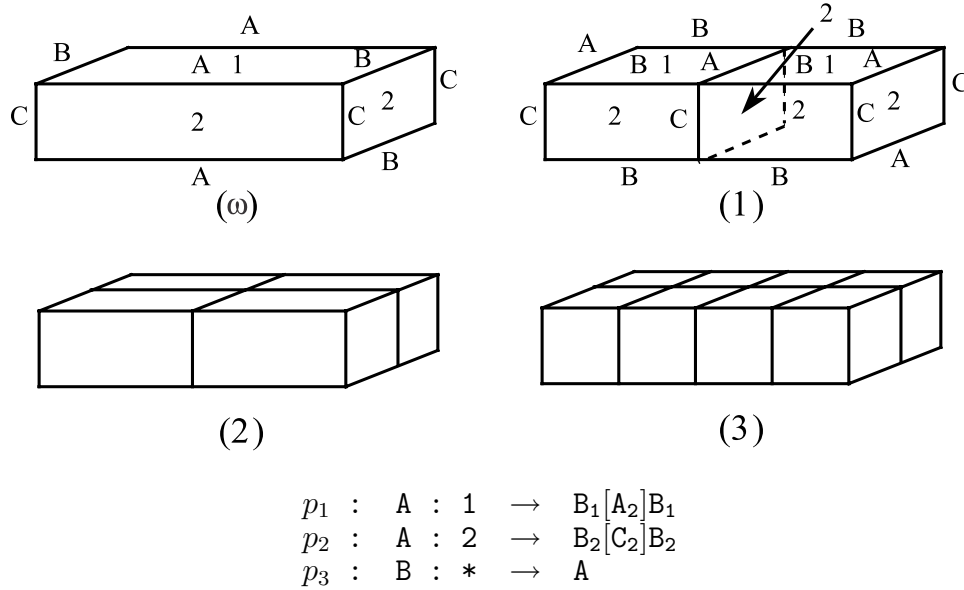


Figure 7.23: Example of a cellwork L-system

A wall may be subdivided more than once as long as new division edges do not intersect and a consistent labeling of daughter walls is possible. In contrast, a cell may be divided only once in any derivation step.

*Example*

For example, Figure 7.23 presents a three-dimensional extension of the map L-system from Figure 7.2. In the first derivation step, production  $p_1$  divides walls labeled 1, and production  $p_2$  divides walls labeled 2. The inserted edges form a cycle that divides the cell with a new wall labeled 2. In the subsequent steps this process is repeated, generating a pattern of alternating division walls. Production  $p_3$  introduces the necessary delay.

*Dynamic interpretation*

The dynamic method for interpreting map L-systems is extended to cellwork L-systems using the following assumptions:

- the structure is represented as a three-dimensional network of masses corresponding to cell vertices, connected by springs which correspond to cell edges,
- the springs are always straight and obey Hooke's law,
- for the purpose of force calculations, walls can be approximated by flat polygons,
- the cells exert pressure on their bounding walls; the pressure on a wall is directly proportional to the wall area and inversely proportional to the cell volume,



- the pressure on a wall is divided evenly between the wall vertices,
- the motion of masses is damped, and
- other forces are not considered.

The total force  $\vec{F}_T$  acting on a vertex  $X$  is given by the formula

$$\vec{F}_T = \sum_{e \in E} \vec{F}_e + \sum_{w \in W} \vec{F}_w + \vec{F}_d,$$

where  $\vec{F}_e$  are forces contributed by the set of edges  $E$  incident to  $X$ ,  $\vec{F}_w$  are forces contributed by the set of walls  $W$  incident to  $X$ , and  $\vec{F}_d = -b\vec{v}$  is a damping force. The forces  $\vec{F}_e$  act along the cell edges and represent wall *tension*. The forces  $\vec{F}_w$  are due to the *pressure* exerted by the cells on their bounding walls. The total force of pressure  $\vec{F}$  exerted by a cell on a wall  $w$  has direction normal to  $w$  and is equal to  $p \cdot A$ , where  $p$  is the internal cell pressure and  $A$  is the wall area. Calculation of the polygon area proceeds as in the two-dimensional case. The pressure  $p$  is assumed to be inversely proportional to the cell volume,  $p \sim V^{-1}$ , which corresponds to the equation describing osmotic pressure (Section 7.2). The volume  $V$  of a cell is calculated by tessellating the cell into tetrahedra. The resulting differential equations are formed and solved as in the two-dimensional case.

A division pattern that frequently occurs in epidermal cell structures is described by the L-system in Figure 7.24, based on a cyclic cellwork L-system (a slightly different formalism) proposed by Lindenmayer [85]. Productions  $p_1$ ,  $p_2$ ,  $p_6$  and  $p_7$  are responsible for cell divisions, while the remaining productions introduce delays such that the division pattern is staggered.

On the surface, the cellular structures analyzed in this chapter may appear quite unrelated to the models discussed previously. However, a closer inspection reveals many analogies. For example, consecutively created segments of a fern gametophyte exhibit a phase effect corresponding to that observed in inflorescences. Furthermore, parts of an older gametophyte situated near the apex have the same topology as the entire thallus at an earlier developmental stage, which associates the recursive structures generated by map or cellwork L-systems with self-similar patterns created using string L-systems. As observed by Oppenheimer [105], self-similarity appears to be one of the general principles organizing the world of botany. The next chapter discusses this topic in more detail.

*Epidermal cells*

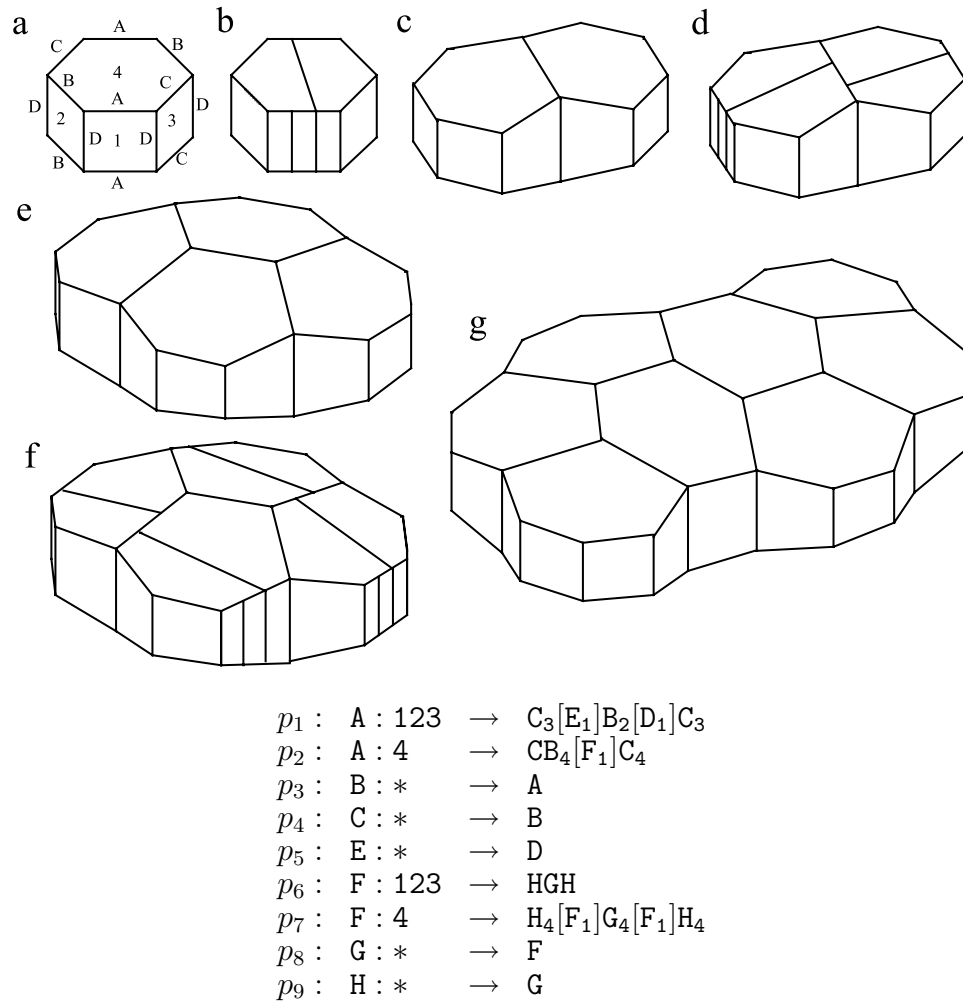


Figure 7.24: Developmental sequence of epidermal cells: (a) The starting cellwork; (b), (d) and (f) cellworks immediately after cell divisions; (c), (e) and (g) the corresponding cellworks at equilibrium

# Chapter 8

## Fractal properties of plants

What is a fractal? In his 1982 book, Mandelbrot defines it as a set with Hausdorff-Besicovitch dimension  $D_H$  strictly exceeding the topological dimension  $D_T$  [95, page 15]. In this sense, none of the figures presented in this book are fractals, since they all consist of a finite number of primitives (lines or polygons), and  $D_H = D_T$ . However, the situation changes dramatically if the term “fractal” is used in a broader sense [95, page 39]:

*Fractals vs.  
finite curves*

Strictly speaking, the triangle, the Star of David, and the finite Koch teragons are of dimension 1. However, both intuitively and from the pragmatic point of view of the simplicity and naturalness of the corrective terms required, it is reasonable to consider an advanced Koch teragon as being closer to a curve of dimension  $\log 4/\log 3$  than to a curve of dimension 1.

Thus, a finite curve can be considered an approximate rendering of an infinite fractal as long as the interesting properties of both are closely related. In the case of plant models, this distinctive feature is self-similarity.

The use of approximate figures to illustrate abstract concepts has a long tradition in geometry. After all, even the primitives of Euclidean geometry — a point and a line — cannot be *drawn* exactly. An interesting question, however, concerns the relationship between fractals and real biological structures. The latter consist of a finite number of cells, thus are not fractals in the strict sense of the word. To consider real plants as approximations of “perfect” fractal structures would be acceptable only if we assumed Plato’s view of the supremacy of ideas over their mundane realization. A viable approach is the opposite one, to consider fractals as abstract descriptions of the real structures. At first sight, this concept may seem strange. What can be gained by reducing an irregular contour of a compound leaf to an even more irregular fractal? Would it not be simpler to characterize the leaf using

*Fractals vs.  
plants*

*Complexity of  
fractals*

a smooth curve? The key to the answer lies in the meaning of the term “simple.” A smooth curve may seem intuitively simpler than a fractal, but as a matter of fact, the reverse is often true [95, page 41]. According to Kolmogorov [80], the complexity of an object can be measured by the length of the shortest algorithm that generates it. In this sense, many fractals are particularly simple objects.

*Previous  
viewpoints*

The above discussion of the relationship between fractals and plants did not emerge in a vacuum. Mandelbrot [95] gives examples of the recursive branching structures of trees and flowers, analyzes their Hausdorff-Besicovitch dimension and writes inconclusively “trees may be called fractals in part.” Smith [136] recognizes similarities between algorithms yielding Koch curves and branching plant-like structures, but does not qualify plant models as fractals. These structures are produced in a finite number of steps and consist of a finite number of line segments, while the “notion of fractal is defined only in the limit.” Oppenheimer [105] uses the term “fractal” more freely, exchanging it with self-similarity, and comments: “The geometric notion of self-similarity became a paradigm for structure in the natural world. Nowhere is this principle more evident than in the world of botany.” The approach presented in this chapter, which considers fractals as simplified abstract representations of real plant structures, seems to reconcile these previous opinions.

*Fractals in  
botany*

But why are we concerned with this problem at all? Does the notion of fractals provide any real assistance in the analysis and modeling of real botanical structures? On the conceptual level, the distinctive feature of the fractal approach to plant analysis is the emphasis on self-similarity. It offers a key to the understanding of complex-looking, compound structures, and suggests the recursive developmental mechanisms through which these structures could have been created. The reference to similarities in living structures plays a role analogous to the reference to symmetry in physics, where a strong link between conservation laws and the invariance under various symmetry operations can be observed. Weyl [159, page 145] advocates the search for symmetry as a cognitive tool:

Whenever you have to deal with a structure-endowed entity  $\Sigma$ , try to determine its group of automorphisms, the group of those element-wise transformations which leave all structural relations undisturbed. You can expect to gain a deep insight into the constitution of  $\Sigma$  in this way.

The relationship between symmetry and self-similarity is discussed in Section 8.1. Technically, the recognition of self-similar features of plant structures makes it possible to render them using algorithms developed for fractals as discussed in Section 8.2.

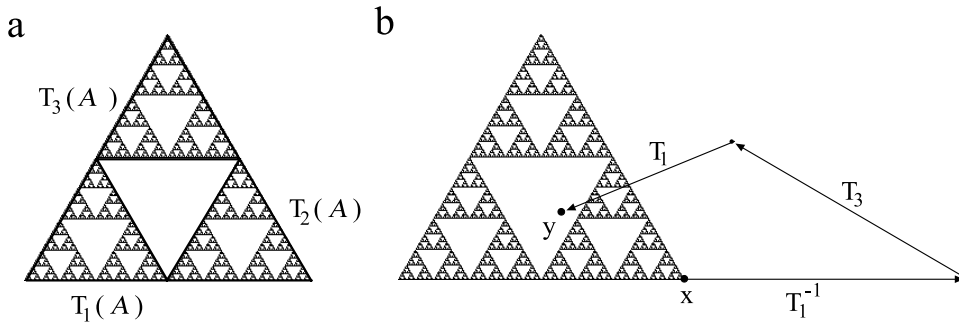


Figure 8.1: The Sierpiński gasket is closed with respect to transformations  $T_1$ ,  $T_2$  and  $T_3$  (a), but it is not closed with respect to the set including the inverse transformations (b).

## 8.1 Symmetry and self-similarity

The notion of symmetry is generally defined as the invariance of a configuration of elements under a group of automorphic transformations. Commonly considered transformations are congruences, which can be obtained by composing rotations, reflections and translations. Could we extend this list of transformations to similarities, and consider self-similarity as a special case of symmetry involving scaling operations?

On the surface, this seems possible. For example, Weyl [159, page 68] suggests: “In dealing with potentially infinite patterns like band ornaments or with infinite groups, the operation under which a pattern is invariant is not of necessity a congruence but could be a similarity.” The spiral shapes of the shells *Turritella duplicata* and *Nautilus* are given as examples. However, all similarities involved have the same fixed point. The situation changes dramatically when similarities with different fixed points are considered. For example, the Sierpiński gasket is mapped onto itself by a set of three contractions  $T_1$ ,  $T_2$  and  $T_3$  (Figure 8.1a). Each contraction takes the entire figure into one of its three main components. Thus, if  $A$  is an arbitrary point of the gasket, and  $T = T_{i_1} T_{i_2} \dots T_{i_n}$  is an arbitrary composition of transformations  $T_1$ ,  $T_2$  and  $T_3$ , the image  $T(A)$  will belong to the set  $A$ . On the other hand, if the inverses of transformations  $T_1$ ,  $T_2$  and  $T_3$  can also be included in the composition, one obtains points that do not belong to the set  $A$  nor its infinite extension (Figure 8.1b). This indicates that the set of transformations that maps  $A$  into itself forms a semigroup generated by  $T_1$ ,  $T_2$  and  $T_3$ , but does not form a group. Thus, self-similarity is a weaker property than symmetry, yet it still provides a valuable insight into the relationships between the elements of a structure.



Figure 8.2: The fern leaf from Barnsley's model [7]

## 8.2 Plant models and iterated function systems

Barnsley [7, pages 101–104] presents a model of a fern leaf (Figure 8.2), generated using an *iterated function system*, or IFS. This raises a question regarding the relationship between developmental plant models expressed using L-systems and plant-like structures captured by IFSes. This section briefly describes IFSes and introduces a method for constructing those which approximate structures generated by a certain type of parametric L-system. The restrictions of this method are analyzed, shedding light on the role of IFSes in the modeling of biological structures.

### *IFS definition*

By definition [74], a planar iterated function system is a finite set of contractive affine mappings  $\mathcal{T} = \{T_1, T_2, \dots, T_n\}$  which map the plane  $\mathcal{R} \times \mathcal{R}$  into itself. The *set defined by*  $\mathcal{T}$  is the smallest nonempty set  $\mathcal{A}$ , closed in the topological sense, such that the image  $y$  of any point  $x \in \mathcal{A}$  under any of the mappings  $T_i \in \mathcal{T}$  also belongs to  $\mathcal{A}$ . It can be shown that such a set always exists and is unique [74] (see also [118] for an elementary presentation of the proof). Thus, starting from an arbitrary point  $x \in \mathcal{A}$ , one can approximate  $\mathcal{A}$  as a set of images of  $x$  under compositions of the transformations from  $\mathcal{T}$ . On

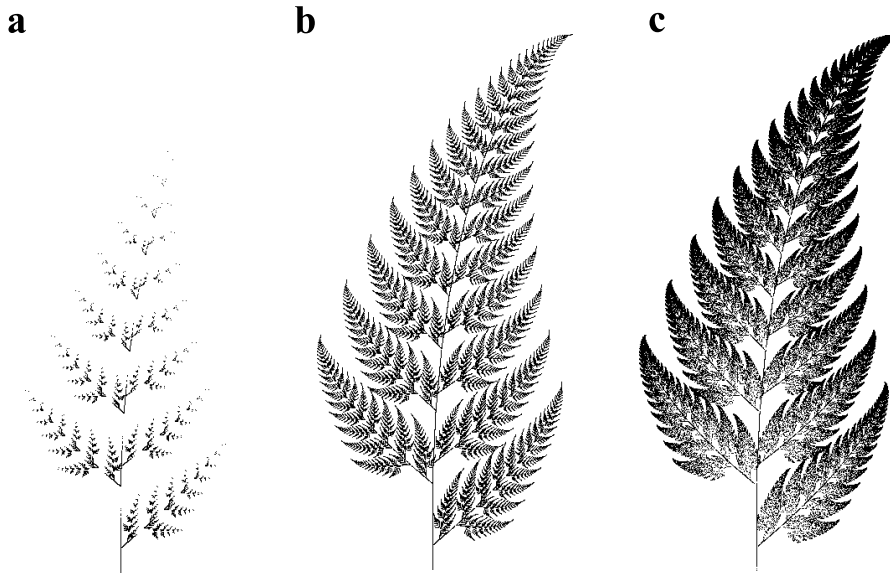


Figure 8.3: A comparison of three attracting methods for the rendering of a set defined by an IFS: (a) deterministic method using a balanced tree of depth  $n = 9$  with the total number of points  $N_1 = 349,525$ , (b) deterministic method using a non-balanced tree with  $N_2 = 198,541$  points, (c) stochastic method with  $N_3 = N_2$  points

the other hand, if the starting point  $x$  does not belong to  $\mathcal{A}$ , the consecutive images of  $x$  gradually approach  $\mathcal{A}$ , since all mappings  $T_i$  are contractions. For this reason, the set  $\mathcal{A}$  is called the *attractor* of the IFS  $\mathcal{T}$ . The methods for rendering it are based on finding the images  $T_{i_k}(T_{i_{k-1}}(\dots(T_{i_1}(x))\dots)) = xT_{i_1}\dots T_{i_{k-1}}T_{i_k}$ , and are termed *attracting methods*. According to the *deterministic approach* [123], a tree of transformations is constructed, with each node representing a point in  $\mathcal{A}$ . Various strategies, such as breadth-first or depth-first, can be devised to traverse this tree and produce different intermediate results [60]. If the transformations in  $\mathcal{T}$  do not have the same scaling factors (Lipschitz constants), the use of a balanced tree yields a non-uniform distribution of points in  $\mathcal{A}$ . This effect can be eliminated by constructing a non-balanced tree, using a proper criterion for stopping the extension of a branch [60]. An alternative approach for approximating the set  $\mathcal{A}$  is termed the *chaos game* [7] (see also [107, Chapter 5]). In this case, only one sequence of transformations is constructed, corresponding to a single path in the potentially infinite tree of transformations. The transformation applied in each derivation step is selected at random. In order to achieve a uniform distribution of points in the attractor, the probability of choosing transformation  $T_i \in \mathcal{T}$  is set according to its Lipschitz constant. Figure 8.3 illustrates the difference between the stochastic and deterministic methods of rendering the attractor. The

*Rendering  
methods*

underlying IFS consists of four transformations, given below using homogeneous coordinates [40]:

$$\begin{aligned}
 T_1 &= \begin{bmatrix} 0.00 & 0.00 & 0.00 \\ 0.00 & 0.16 & 0.00 \\ 0.00 & 0.00 & 1.00 \end{bmatrix} \\
 T_2 &= \begin{bmatrix} 0.20 & 0.23 & 0.00 \\ -0.26 & 0.22 & 0.00 \\ 0.00 & 1.60 & 1.00 \end{bmatrix} \\
 T_3 &= \begin{bmatrix} -0.15 & 0.26 & 0.00 \\ 0.28 & 0.24 & 0.00 \\ 0.00 & 0.44 & 1.00 \end{bmatrix} \\
 T_4 &= \begin{bmatrix} 0.85 & -0.04 & 0.00 \\ 0.04 & 0.85 & 0.00 \\ 0.00 & 1.60 & 1.00 \end{bmatrix}
 \end{aligned}$$

Other methods for the rendering of the set  $\mathcal{A}$ , defined by an iterated function system  $\mathcal{T}$ , include the *repelling* or *escape-time* method and the *distance* method [60, 118]. Both methods assign values to points outside of  $\mathcal{A}$ . The first method determines how fast a point is repelled from  $\mathcal{A}$  to infinity by the set of inverse transformations  $T_i^{-1}$ , where  $T_i \in \mathcal{T}$ . An example of the application of this method, with escape time values represented as a height field, is shown in Figure 8.4. The second method computes the Euclidean distance of a point from the attractor  $\mathcal{A}$ .

*IFS  
construction*

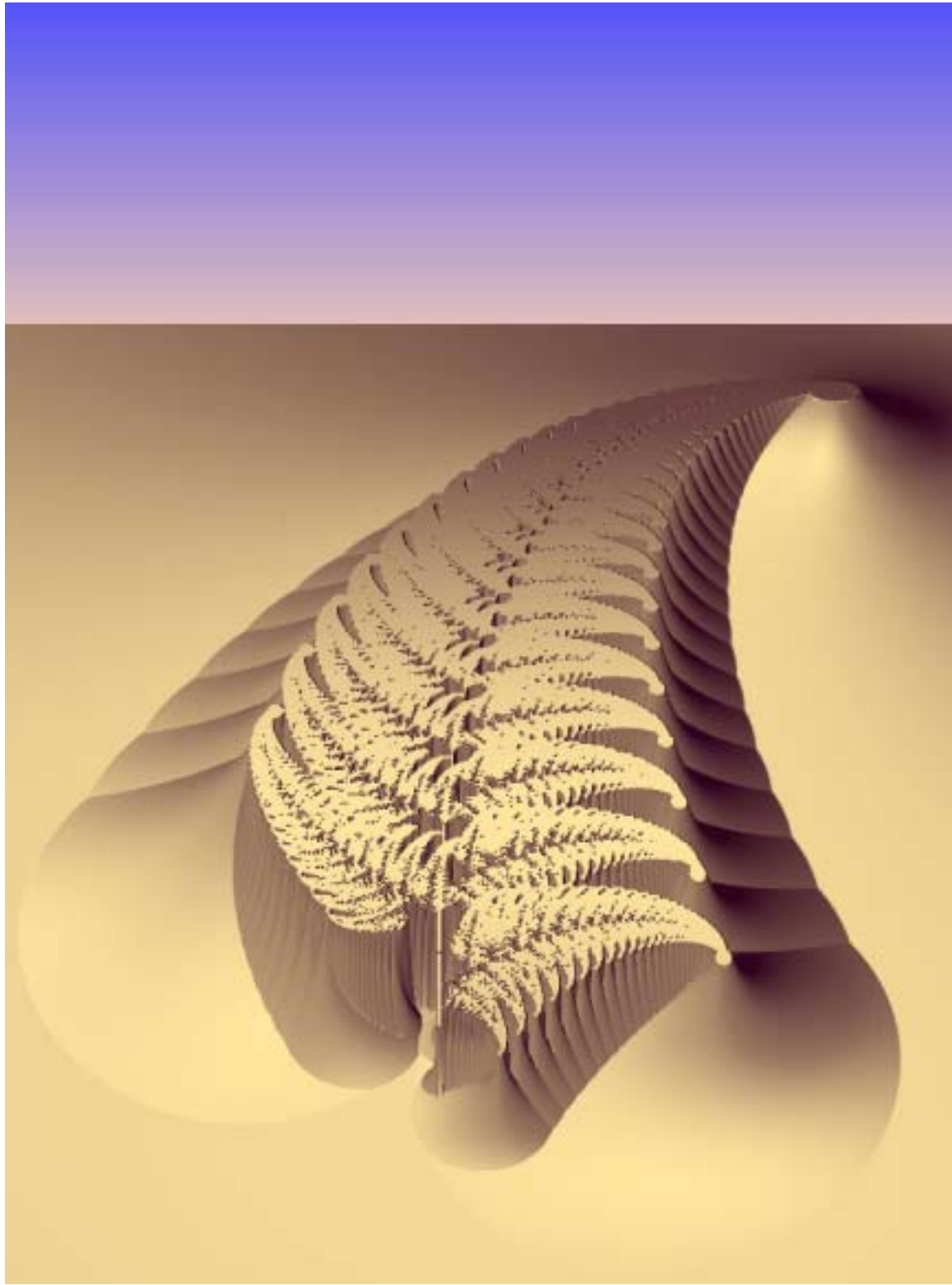
The problem of constructing an IFS that will approximate a branching structure modeled using an L-system can now be considered. This discussion focuses specifically on structures that develop in a biologically justifiable way, by subapical branching (Section 3.2). The compound leaf shown in Figure 5.11a on page 129 will be used as a working example. In this case, the apical delay  $D$  is equal to zero, and the L-system can be represented in the simplified form:

$$\begin{aligned}
 \omega &: A \\
 p_1 &: A \quad : * \rightarrow F(1)[+A][-A]F(1)A \\
 p_2 &: F(a) \quad : * \rightarrow F(a * R)
 \end{aligned} \tag{8.1}$$

---

Figure 8.4: Fern dune  $\longrightarrow$





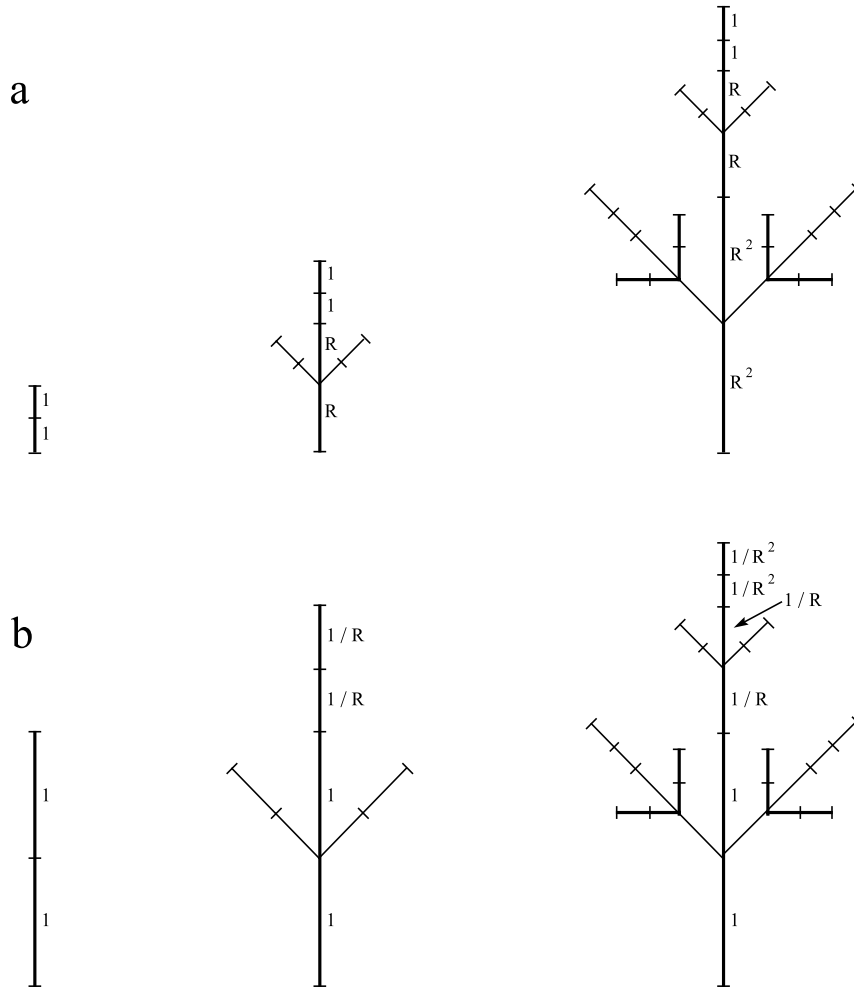


Figure 8.5: Initial sequences of structures generated by the L-systems specified in equations (8.1) and (8.2)

This L-system operates by creating segments of constant size, then increasing their length by constant factor  $R$  in each derivation step (Figure 8.5a). As discussed in Section 1.10.3, a structure with the same proportions can be obtained by successively appending segments of decreasing length (Figure 8.5b):

$$\begin{aligned} \omega &: A(1) \\ p_1 &: A(s) : * \rightarrow F(s)[+A(s/R)][-A(s/R)]F(s)A(s/R) \end{aligned} \quad (8.2)$$

Let  $A_n(s)$  denote the structure generated by module  $A(s)$  in  $n \geq 1$  derivation steps. According to production  $p_1$ , the following equality holds:

$$A_n(s) = F(s)[+A_{n-1}(s/R)][-A_{n-1}(s/R)]F(s)A_{n-1}(s/R) \quad (8.3)$$

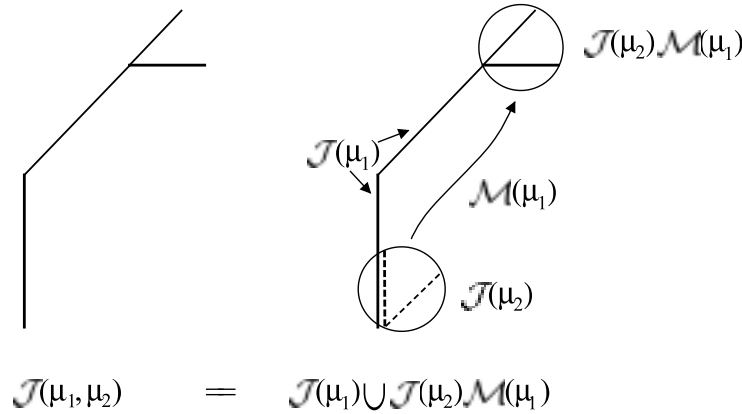


Figure 8.6: Illustration of equation (8.4), with  $\mu_1 = F(1) - (45)$  and  $\mu_2 = [-(45)F(0.5)]F(0.5)$

It is important to clearly distinguish between a parametric word  $\mu$  (a string of modules) and its turtle interpretation  $\mathcal{J}(\mu)$  (a set of points in the plane). The symbol  $\mathcal{M}(\mu)$  will be used to denote the *transformation induced by  $\mu$* . This transformation moves the turtle from its initial position and orientation to those resulting from the interpretation of word  $\mu$ . According to the definition of turtle interpretation (Chapter 1), if a word  $\mu$  is decomposed into subwords  $\mu_1$  and  $\mu_2$  such that  $\mu_2$  does not contain unbalanced right brackets, then

*Properties of turtle interpretation*

$$\mathcal{J}(\mu) = \mathcal{J}(\mu_1\mu_2) = \mathcal{J}(\mu_1) \cup \mathcal{J}(\mu_2)\mathcal{M}(\mu_1). \tag{8.4}$$

See Figure 8.6 for an illustration. By applying equation (8.4) to (8.3), we obtain

$$\begin{aligned} \mathcal{J}(A_n(s)) = & \mathcal{J}(F(s)) \cup \\ & \mathcal{J}(A_{n-1}(s/R))\mathcal{M}(F(s)+) \cup \\ & \mathcal{J}(A_{n-1}(s/R))\mathcal{M}(F(s)-) \cup \\ & \mathcal{J}(F(s))\mathcal{M}(F(s)) \cup \\ & \mathcal{J}(A_{n-1}(s/R))\mathcal{M}(F(s)F(s)), \end{aligned} \tag{8.5}$$

which is true for any  $n \geq 1$ . Now let  $\mathcal{A}(s)$  be the limit of the sequence of sets  $\mathcal{J}(A_n(s))$  from equation 8.6,

*Passage to infinity*

$$\mathcal{A}(s) = \lim_{n \rightarrow \infty} \mathcal{J}(A_n(s)).$$

At the limit we obtain:

$$\mathcal{A}(s) = \mathcal{J}(F(2s)) \cup \mathcal{A}(s/R)(T'_1 \cup T'_2 \cup T'_3), \tag{8.6}$$

where  $T'_1 = \mathcal{T}(F(s)+)$ ,  $T'_2 = \mathcal{T}(F(s)-)$ , and  $T'_3 = \mathcal{T}(F(2s))$ . Let  $S(s/R)$  be the operation of scaling by  $s/R$ , then

$$\mathcal{A}(s/R) = \mathcal{A}(s)S(s/R).$$

By noting  $T_i = T'_i S(s/R)$  for  $i = 1, 2, 3$ , equation (8.6) can be transformed to

$$\mathcal{A}(s) = \mathcal{J}(F(2s)) \cup \mathcal{A}(s)(T_1 \cup T_2 \cup T_3). \quad (8.7)$$

The solution of this equation with respect to  $\mathcal{A}(s)$  is

$$\mathcal{A}(s) = \mathcal{J}(F(2s))(T_1 \cup T_2 \cup T_3)^*, \quad (8.8)$$

where  $(T_1 \cup T_2 \cup T_3)^*$  stands for the iteration of the union of transformations  $T_1$ ,  $T_2$  and  $T_3$ . Equation (8.8) suggests the following method for constructing the set  $\mathcal{A}(s)$ :

- create segment  $\mathcal{J}(F(2s))$
- create images of  $\mathcal{J}(F(2s))$  using transformations  $T_1, T_2, T_3$  and their compositions

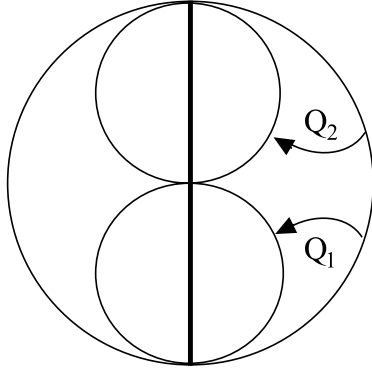
Equation (8.7) and the method of constructing the set  $\mathcal{A}(s)$  based on equation (8.8) are closely related to the definition of iterated function systems stated at the beginning of this chapter. However, instead of starting from an arbitrary point  $x \in \mathcal{A}(s)$ , the iteration begins with the set  $\mathcal{J}(F(2s))$ . Although this is simply a straight line segment, a question arises as to how its generation can be incorporated into an IFS. Two approaches can be distinguished.

### *Controlled IFS*

The first approach is related to the notions of hierarchical iterated function systems discussed by Reuter [123] and recurrent IFSes introduced recently by Barnsley [8]. The line segment  $\mathcal{J}(F(2s))$  is generated using an IFS, for example consisting of two scaling transformations  $Q_1$  and  $Q_2$  which map it onto its upper and lower half (Figure 8.7a). Subsequently, transformations  $T_1$ ,  $T_2$  and  $T_3$  are applied to create other points of the set  $\mathcal{A}(s)$ . The order of transformation application is important. Transformations  $Q_1$  and  $Q_2$  are used solely for the purpose of initial segment creation. They must not be applied after  $T_1$ ,  $T_2$  or  $T_3$ , since in this case they would affect the branching structure under consideration. The admissible sequences of transformations can be defined using a directed *control graph* (Figure 8.7b), and correspond to the infinite set of paths starting at node  $a$ .<sup>1</sup> The term *controlled iterated function system* (CIFS) denotes an IFS with restrictions on the transformation sequences imposed by a control graph. Thus, noting the angle increment associated with symbols  $+$  and  $-$  by  $\delta$ , the fractal

<sup>1</sup>Formally, the sequence of admissible transformations is the regular language accepted by the finite (Rabin-Scott) automaton represented by the graph in Figure 8.7b.

a



b

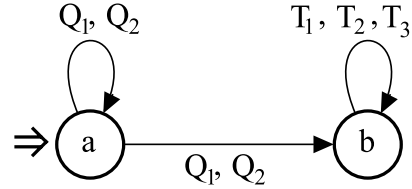


Figure 8.7: Construction of the set  $\mathcal{A}(S)$ : (a) definition of an IFS  $\{Q_1, Q_2\}$  that generates the initial line segment, (b) the control graph specifying the admissible sequences of transformation application

approximation of the leaf in Figure 5.11a is given by the CIFS with the control graph in Figure 8.7b and the transformations specified below:

*Resulting CIFS*

$$Q_1 = \begin{bmatrix} 0.5 & 0 & 0 \\ 0 & 0.5 & 0 \\ 0 & 0 & 1 \end{bmatrix} \quad Q_2 = \begin{bmatrix} 0.5 & 0 & 0 \\ 0 & 0.5 & 0 \\ 0 & s & 1 \end{bmatrix}$$

$$T_1 = \begin{bmatrix} 1/R \cos \delta & 1/R \sin \delta & 0 \\ -1/R \sin \delta & 1/R \cos \delta & 0 \\ 0 & s & 1 \end{bmatrix}$$

$$T_2 = \begin{bmatrix} 1/R \cos \delta & -1/R \sin \delta & 0 \\ 1/R \sin \delta & 1/R \cos \delta & 0 \\ 0 & s & 1 \end{bmatrix}$$

$$T_3 = \begin{bmatrix} 1/R & 0 & 0 \\ 0 & 1/R & 0 \\ 0 & 2s & 1 \end{bmatrix}$$

The second approach to the generation of the line segment  $\mathcal{J}(F(2s))$  is consistent with the method applied by Barnsley to specify the fern leaf in Figure 8.2. The idea is to map the entire branching structure  $\mathcal{A}(s)$  onto the line  $\mathcal{J}(F(2s))$ . This can be achieved using a noninvertible transformation  $Q$  which collapses all branches into a vertical line. The scaling factor along the  $y$  axis is the ratio of the desired segment length  $2s$ , and the limit height of the entire structure  $\mathcal{A}(s)$ ,

*Noninvertible transformations*

$$h = \frac{2s}{1 - 1/R}.$$

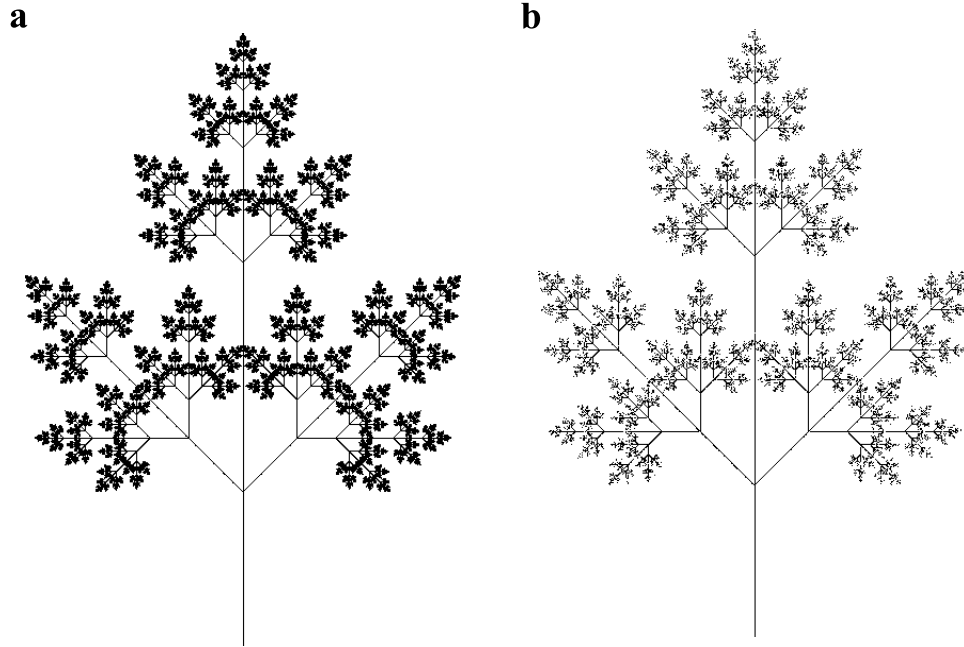


Figure 8.8: Two renderings of the compound leaf from Figure 5.11a, generated using iterated function systems

This last value is calculated as the limit of the geometric series with the first term equal to  $2s$  and the ratio equal to  $1/R$ . Thus, the compound leaf of Figure 5.11a is defined by an IFS consisting of transformation

$$Q = \begin{bmatrix} 0 & 0 & 0 \\ 0 & 1 - 1/R & 0 \\ 0 & 0 & 1 \end{bmatrix}$$

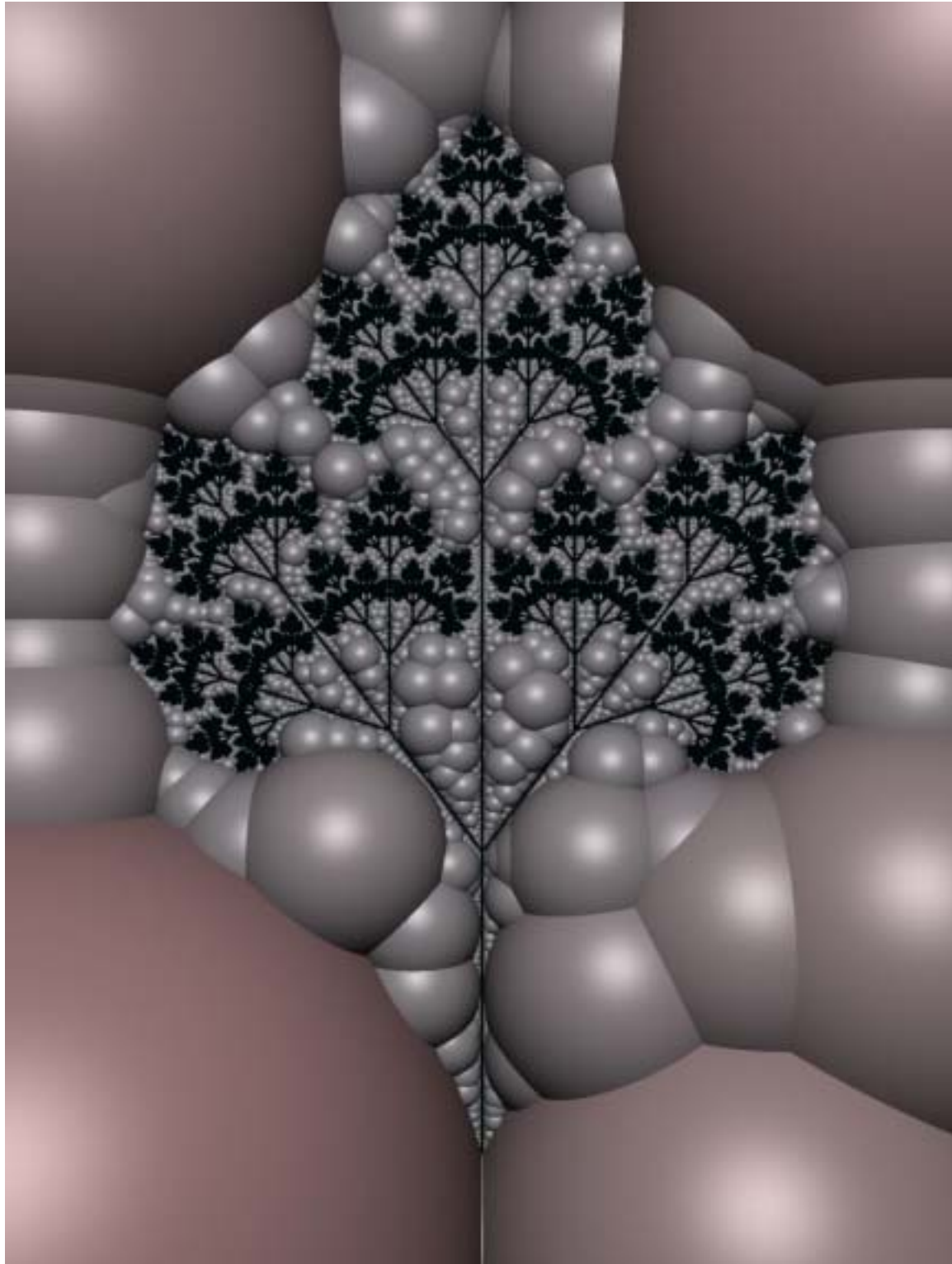
and transformations  $T_1$ ,  $T_2$  and  $T_3$  specified as in the case of the controlled IFS.

*Rendering  
examples*

Two fractal-based renderings of the set  $\mathcal{A}(s)$  are shown in Figure 8.8. Figure 8.8a was obtained using the controlled IFS and a deterministic algorithm to traverse the tree of admissible transformations. Figure 8.8b was obtained using the “ordinary” IFS and the random selection of transformations. Figure 8.9 shows another fractal-based rendering of the same structure. The spheres have radii equal to the distance from the sphere center to the leaf, within a specified  $\epsilon$ .

---

Figure 8.9: Carrot leaf  $\longrightarrow$



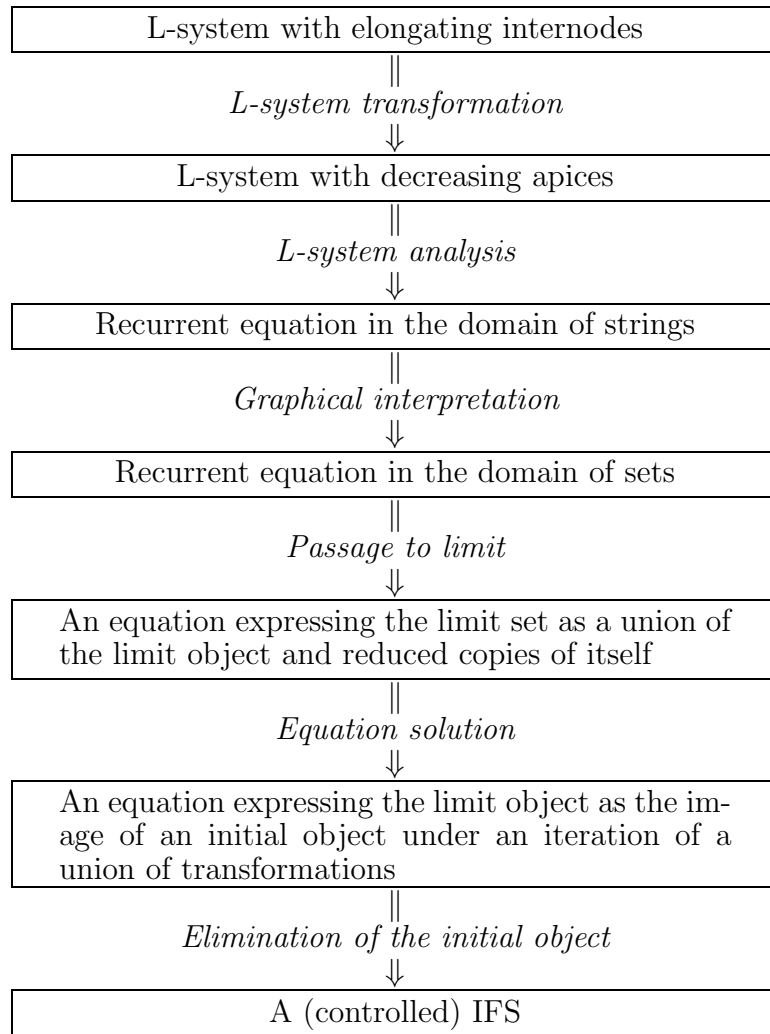


Figure 8.10: Steps in the construction of an IFS given an L-system capturing a developmental model



It is instructive to retrace the logical construction that started with an L-system, and ended with an iterated function system which can generate fractal approximations of the same object (Figure 8.10). An analysis of the operations performed in the subsequent steps of this construction reveals its limitations, and clarifies the relationship between strictly self-similar structures and real plants. The critical step is the transformation of the L-system with elongating internodes to the L-system with decreasing apices. It can be performed as indicated in the example if the plant maintains constant branching angles as well as fixed proportions between the mother and daughter segments, independent of branch order. This, in turn, can be achieved if all segments in the modeled plant elongate exponentially over time. These are strong assumptions, and may be satisfied to different degrees in real plants. Strict self-similarity is an abstraction that captures the essential properties of many plant structures and represents a useful point of reference when describing them in detail.

*Conclusions*



# Epilogue

This quiet place, reminiscent of Claude Monet's 1899 painting *Water-lilies pool — Harmony in green*, does not really exist. The scene was modeled using L-systems that captured the development of trees and water plants, and illuminated by simulated sunlight. It is difficult not to appreciate how far the theory of L-systems and the entire field of computer graphics have developed since their beginnings in the 1960's, making such images possible. Yet the results contained in this book are not conclusive and constitute only an introduction to the research on plant modeling for biological and graphics purposes. The algorithmic beauty of plants is open to further exploration.



Figure E.1: Water-lilies



# Appendix A

## Software environment for plant modeling

This book is illustrated with images of plants which exist only as mathematical models visualized by means of computer graphics. The software environment used to construct and experiment with these models includes dozens of programs and hundreds of data files. This creates the nontrivial problem of organizing all components for easy definition, saving, retrieval and modification of the models. In order to solve it, the idea of simulation was extended beyond the level of individual plants to an entire laboratory in botany [98]. Thus, a user can create and conduct experiments in a *virtual laboratory* by applying intuitive concepts and techniques from the “real” world. As an operating system defines the way a user perceives a computing environment, the virtual laboratory determines a user’s perception of the environment in which simulated experiments take place. In the future, a virtual laboratory may complement, extend, or even replace books as a means for gathering and presenting scientific information. Because of this potential, the laboratory in which the research reported in this book was produced is described here in more detail.

### A.1 A virtual laboratory in botany

A virtual laboratory, like its “real” counterpart, is a playground for experimentation. It comes with a set of *objects* pertinent to its scientific domain (in this case, plant models), *tools* which operate on these objects, a *reference book* and a *notebook*. Once the concepts and tools are understood, the user can expand the laboratory by adding new objects, creating new experiments, and recording descriptions in the notebook. An experienced user can expand the laboratory further by creating and installing new tools.

*User’s  
perspective*

*Laboratory =  
microworld +  
hypertext*

Technically, a virtual laboratory is a *microworld* which can be explored under the guidance of a *hypertext* system. The term “microworld” denotes an interactive environment for creating and conducting simulated experiments. The guidance could be provided in the form of a traditional book, but an electronic document is more suitable for integration with a microworld. In a sense, both components of the virtual laboratory are described by Nelson in *Dream Machines* [104]. The pioneering role of this book in introducing the concept of hypertext is known, but under the heading *The Mind’s Eye* the notion of a microworld is also anticipated:

Suppose that you have a computer.  
What sorts of things would you do with it?  
Things that are imaginative  
and don’t require too much else.  
I am hinting at something.  
You could have it make pictures and show you stuff  
and change what it shows depending on what you do.

*Requirements*

A virtual laboratory can be divided into two components: the application programs, data files and textual descriptions that comprise the experiments; and the system support that provides the framework on which these domain-dependent experiments are built. The following list specifies the features of this framework.

- **Consistent organization of the lab.** In the lab environment, experiments are run by applying tools (programs) to objects (data files). An object consists of files that are grouped together so that they can be retrieved easily. The format of the objects is sufficiently standardized to allow straightforward implementation of common operations such as object saving and deletion.
- **Inheritance of features.** It is often the case that several objects differ only in details. For example, two lilac inflorescences may differ only in the color of their petals. The mechanism of inheritance is employed to store such objects efficiently.
- **Version control.** Interaction with an object during experimentation may result in a temporary or permanent modification. In the latter case, the user is able to decide whether the newly created object replaces the old one or should be stored as another version of the original object.
- **Interactive manipulation of objects.** The laboratory provides a set of general-purpose tools for manipulating object parameters. For example, objects can be modified using control panels or by editing specific fields in a textual description of an experiment.

- **Flexibility in conducting experiments.** The user may apply tools to objects in a dynamic way while an experiment is being conducted. This can be contrasted to a static experiment designed when the object is initially incorporated into the system.
- **Guidance through the laboratory.** A hypertext system imposes a logical organization on the set of objects, provides a textual description of the experiments, and makes it possible to browse through the experiments in many ways. Specific experiments are invoked automatically when the corresponding text is selected, in order to facilitate demonstrations and assist a novice user.

So far, objects have been referred to in an intuitive way, relying on the analogy between a real and virtual laboratory. For example, if our interest is in the development of the gametophyte *Microsorium linguiforme*, in a real laboratory we would experiment with a specimen of the plant, while in a virtual laboratory we explore the corresponding mathematical model. However, the analogy to real objects does not extend to the level of detailed object definition. Specific design decisions are needed for software development purposes. In the current design, a laboratory object is defined as a directory containing two types of files and a subdirectory.

*Objects*

- The *data files* comprise our knowledge of a particular model.
- A *specification file* defines the data files which make up the object and the tools which apply to them.
- A directory of *extensions* lists objects which inherit some features of the current object.

The object-oriented file structure which provides the basis for lab operation can be represented by a hierarchy of directories and files (Figure A.1).

The path of subdirectories leading to an object establishes the inheritance structure for the lab. Inheritance is based on the idea of specifying new objects in reference to objects which already exist [81]. The “old” object is called a *prototype* and the new one is its *extension*. The extension contains only those files which are different from the corresponding files in the prototype. Files that remain the same are *delegated* to the prototype by establishing links. In other words, the object directory will contain those files that are unique to the object, and links to files that are inherited from its prototype (Figure A.2). This approach saves space, facilitates creation of objects similar to the prototype, and allows a single change in the prototype to propagate through all descendants.

*Inheritance of features*

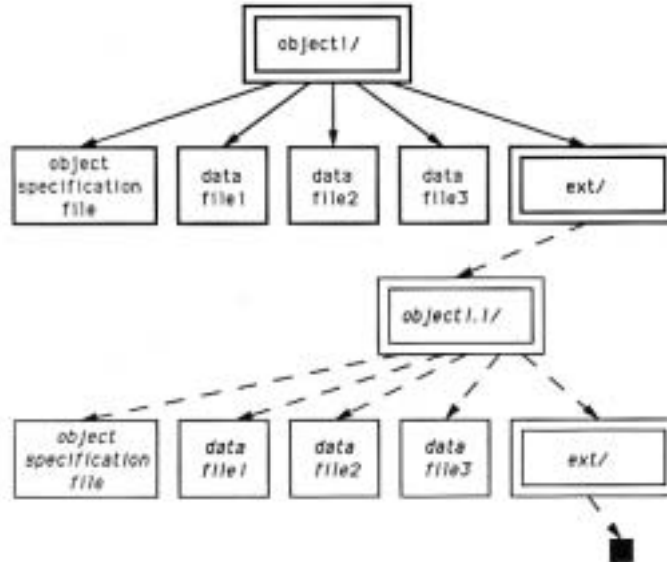


Figure A.1: The hierarchical structure of objects

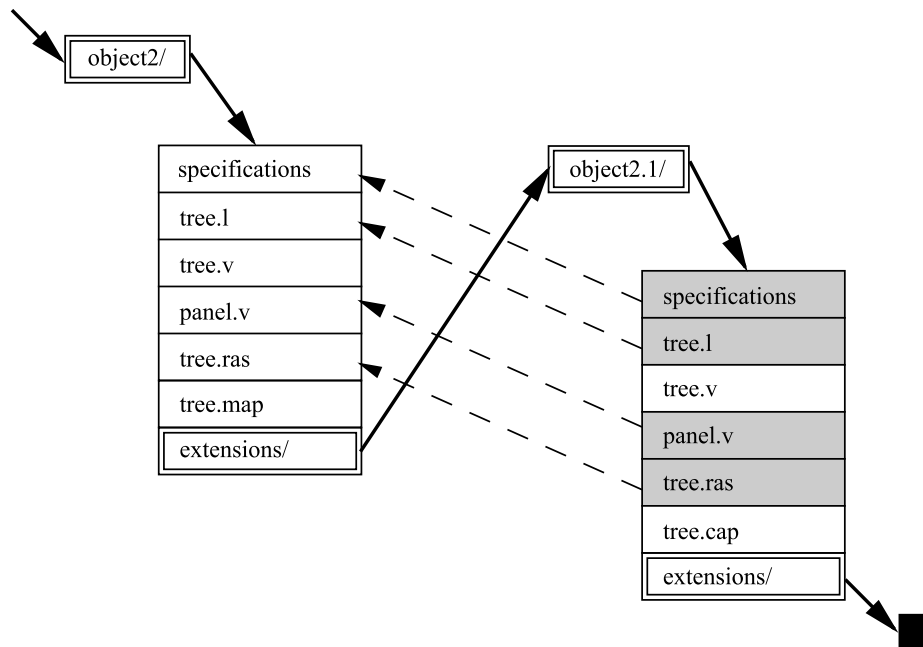


Figure A.2: A prototype and its extension. Shaded areas indicate links.



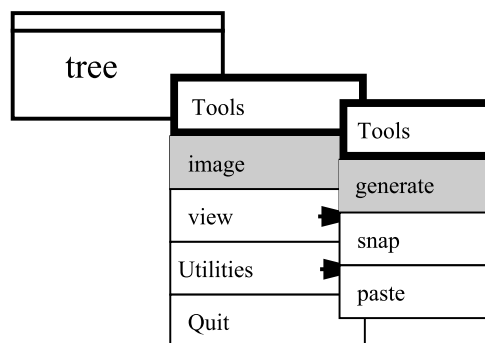


Figure A.3: An object icon with menus

To conduct an experiment, all files that make up the selected object are copied to a temporary location called the *lab table*. Consequently, manipulation of object parameters does not disturb the stored version. When the experiment is finished, the user may save the results by overwriting the original object or by creating an extension. In the latter case, the files on the lab table are compared with those in the prototype object; those files that differ from the prototype are saved, and links to the remaining files are established automatically.

The ability to manipulate the parameters in an experiment easily is an essential feature of the virtual laboratory. As a rule, all parameters involved in an experiment are supplied to the tools through the object's data files. In order to modify a parameter, the user edits the appropriate file, which is subsequently re-read by the application. Though the editing of parameters can be accomplished using a text editor, in many cases parameter modification can be performed more conveniently using *virtual control panels* [114]. The current implementation of the laboratory provides the user with a general-purpose *control manager* which creates panels according to user-supplied configuration files.

The user is able to apply a tool to an object as a whole, without detailed knowledge of the programs involved or the component files. This is achieved through the object's specification file which lists all files associated with an object and the tools that can be applied to them. This information is used to create a hierarchy of menus associated with an icon representing the object (Figure A.3). The end nodes in the hierarchy invoke tools that operate on the object. For example, selection of the item **image** followed by the item **generate** from the menus in the figure would invoke the plant modeling program *Pfg*.

A user may browse through the objects in the lab by following either the hierarchical structure of objects or hypertext links. The *browser* is used to navigate through the hierarchy, moving down through successive extensions or up through previous levels. At any time, the user may request that an object be placed on the lab table. The hypertext document associated with the lab provides an alternative method of browsing and a means of relating objects independent of the hierarchy.

*Version control**Object manipulation**Tool application**Browsing*

## A.2 List of laboratory programs

The essential programs incorporated into the virtual laboratory in botany are listed below.

- *Plant and fractal generator (Pfg)*  
P. Prusinkiewicz and J. Hanan  
Given an L-system, a set of viewing parameters and optional files specifying predefined surfaces, *Pfg* generates the modeled structure by carrying out the derivation, then interpreting the resulting string using turtle geometry. Both non-parametric and parametric L-systems are supported. The model can be visualized directly on the screen of an IRIS workstation or output to a file. The first mode of operation is used to experiment with the model interactively and present developmental sequences. The output file can be either in Postscript format, particularly suitable for printing results such as fractal curves and inflorescence diagrams on a laser printer, or in the format required by the ray-tracer *Rayshade* for realistic rendering of the modeled structures.
- *Modeling program for phyllotactic patterns (Spiral)*  
D. R. Fowler  
*Spiral* is an interactive program for modeling organs with spiral phyllotactic patterns. The user can choose between planar and cylindrical patterns, and modify parameters which define model geometry (Chapter 4). This technique is faster than “growing” organs using parametric L-systems. Once an organ has been designed, it can be expressed using an L-system and incorporated into a plant structure.
- *Interactive surface editor (Ise)*  
J. Hanan  
*Ise* makes it possible to define and modify bicubic surfaces consisting of one or several arbitrarily connected patches. The output files produced by *Ise* are compatible with *Pfg* and *Spiral*.
- *Modeling program for cellular structures (Mapl)*  
F. D. Fracchia  
*Mapl* accepts the specification of a two-dimensional cell layer captured by a map L-system and generates the resulting developmental sequence using the dynamic method of map interpretation. Options include map generation on the surface of a sphere, and the simulation of development in three dimensions according to a given cellwork L-system. As in the case of *Pfg*, the models can be visualized directly on the screen or output to a file in either Postscript or *Rayshade* format.

- *Control panel manager (Panel)*  
L. Mercer and A. Snider  
This program creates control panels containing sliders and buttons, according to a configuration file provided by the user. Upon activation of a control by the mouse, *Panel* generates a message which indicates the corresponding control value. Application programs process this information and modify the appropriate parameters. For example, a panel can be used to control parameters used by *Pfg*, *Spiral*, or *Mapl*.
- *Ray tracer (Rayshade)*  
C. Kolb, Yale University  
*Rayshade* reads a scene description from a text file, and renders it using ray tracing. Scenes can be composed of primitives such as planes, triangles, polygons, spheres, cylinders, cones and height fields, grouped together to form objects. These objects can be instantiated in other object definitions to create a hierarchical description of a scene. Transformations including translation, rotation and scaling, and a variety of procedural textures can be applied to any object. Extended light sources, simulation of depth of field, and adaptive supersampling are supported. The program uses 3D grids to partition object space for fast intersection tests.
- *Previewer for the ray tracer (Preray)*  
A. Snider  
*Preray* is a previewer for *Rayshade* used to provide a fast wire frame rendering of a scene before committing time to ray tracing. A control panel associated with *Preray* makes it possible to set viewing parameters interactively.
- *Modeling program based on Euclidean constructions (L.E.G.O.)*  
N. Fuller  
*L.E.G.O.* makes it possible to model two- and three-dimensional objects using geometric constructions. In the scope of this book, *L.E.G.O.* was used to model man-made objects such as the *Zinnia* vase and the *Water-lilies* bridge.
- *Iterated function system generator (Ifsg)*  
D. Hepting  
A fractal defined by an iterated function system is described by a finite set of contractive affine transformations with an optional finite state control mechanism. *Ifsg* accepts input from a file specifying the transformations and rendering information. The program is capable of rendering by either attracting, distance-based or escape-time methods. The output can be displayed directly on an IRIS workstation or written to a file for further processing. In the scope of this book, *Ifsg* was used to obtain results which related plant models expressed using L-systems to fractals.

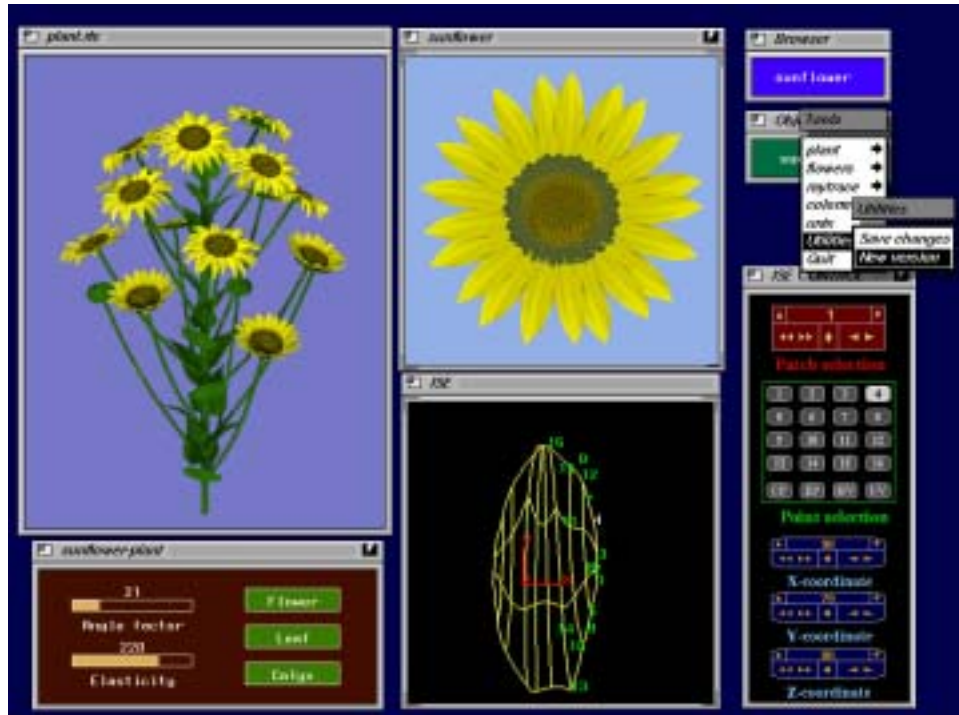


Figure A.4: A virtual laboratory screen

Figure A.4 presents a sample screen of a Silicon Graphics IRIS 4D/60 workstation running some of the above programs within the virtual laboratory framework. The icon in the top right corner represents the laboratory browser which was used to select a sunflower plant as the current object. The icon underneath and the associated menu were subsequently applied to select tools which operate on the object. The control panel in the bottom right corner of the screen is a part of the surface editor *Ise*. The manipulated petal is displayed as a wire frame in the window labeled *Ise*, and incorporated into a flower head by the modeling program *Spiral* which presents its output in the window *sunflower*. The flower heads are in turn incorporated into a complete plant model generated by *Pfg* and rendered using *Rayshade* in the window *plant.rle*. The panel below that window makes it possible to choose organs included in the model and change parameters related to the angles of the branching structure. The metaphor of a virtual laboratory provides a uniform interface to various operations on the selected plant, ranging from the modification of a petal to the rendering of the complete model.

# Appendix B

## About the figures

The following descriptions of the color images include details about the pictures not described in the main text. Unless otherwise stated, figures were created at the University of Regina.

**Figure 1.19** [page 20] *Three-dimensional Hilbert curve*  
F. D. Fracchia, P. Prusinkiewicz, N. Fuller  
(1989)

This image was rendered using ray-tracing without shadows.

**Figure 1.25** [page 26] *Three-dimensional bush*  
P. Prusinkiewicz (1986)

Simple branching structure, rendered using the firmware of a Silicon Graphics IRIS workstation. Total generating and rendering time on IRIS 4D/20: 4 seconds.

**Figure 1.28** [page 29] *Flower field*  
P. Prusinkiewicz (1986)

The field contains four rows of four plants. The scene was rendered with IRIS firmware, using depth-cueing to assign colors to petals.

**Figure 1.35** [page 45] *Developmental stages of Anabaena catenula*  
J. Hanan, P. Prusinkiewicz (1989)

**Figure 2.1** [page 52] *Organic architecture*  
Ned Greene, NYIT (1989)

An array of 300 x 300 x 300 voxel space automata was used to track a polygonal model of a house. Rendering was performed using a probabilistic radiosity method. See [54] for a full description.

**Figure 2.3** [page 54] *Acer graphics*  
Jules Bloomenthal, NYIT (1984)

A model of a maple tree. The basic branching structure was generated recursively. Limbs were modeled as generalized cylinders, obtained by moving discs of varying radii along spline curves. Real bark texture was digitized and used as a bump map. Leaf texture was obtained by digitizing a photograph of a real leaf and emphasizing the veins using a paint program. See [11] for details.

**Figure 2.4** [page 54] *Forest scene*  
Bill Reeves, Pixar (1984)

A scene from the film *The Adventures of André and Wally B*, modeled using particle systems. Shading and shadows were approximated using probabilistic techniques. Visible surfaces were determined using depth-sorting. See [119] for a full description.

**Figure 2.5** [page 55] *Oil palm tree canopy*  
CIRAD Modelisation Laboratory (1990)

A developmental model of oil palm trees, modeled using the method originated by de Reffye and described from the graphics perspective in [30].

**Figure 2.10** [page 61] *Medicine lake*  
F. K. Musgrave, C. E. Kolb, P. Prusinkiewicz,  
B. B. Mandelbrot (1988)

A scene combining a fractal terrain model, a tree generated using L-systems, and a rainbow. The rainbow model was derived from a simulation of refraction with dispersion of light through an idealized raindrop. Procedural textures were applied to the mountains, the water surface and a vertical plane modeling the sky. See [101] for further details.

**Figure 2.11** [page 62] *Surrealistic elevator*  
A. Snider, P. Prusinkiewicz, N. Fuller (1989)

The elevator was modeled using L.E.G.O. The island is a superquadratic surface. Procedural textures were applied to create stars in the sky, craters on the moon, colored layers in the rock,

waves in the lake and imperfections in the glass that covers the elevator.

**Figure 3.2** [page 69] *Crocuses*  
J. Hanan, D. R. Fowler (1990)

The petals were modeled as Bézier surfaces, with the shapes determined using Ise.

**Figure 3.4** [page 72] *Lily-of-the-valley*  
P. Prusinkiewicz, J. Hanan (1987)

**Figure 3.5** [page 74] *Development of Capsella bursa-pastoris*  
P. Prusinkiewicz, A. Lindenmayer (1987)

**Figure 3.6** [page 75] *Apple twig*  
P. Prusinkiewicz, D. R. Fowler (1990)

This twig model was developed in one spring day, looking at a real twig nearby. This time is indicative for most inflorescence models shown.

**Figure 3.11** [page 81] *A mint*  
P. Prusinkiewicz (1988)

**Figure 3.14** [page 84] *Development of Lychnis coronaria*  
P. Prusinkiewicz, J. Hanan (1987)

**Figure 3.17** [page 90] *Development of Mycelis muralis*  
P. Prusinkiewicz, A. Lindenmayer (1987)

**Figure 3.18** [page 91] *A three-dimensional rendering of the Mycelis models*  
P. Prusinkiewicz, J. Hanan (1987)

All internodes in the model are assumed to have the same length. In reality, the internodes have different lengths, and the structure is less crowded.

**Figure 3.19** [page 92] *Lilac inflorescences*  
P. Prusinkiewicz, J. Hanan, D. R. Fowler (1990)

**Figure 3.21** [page 94] *The Garden of L*  
P. Prusinkiewicz, F. D. Fracchia, J. Hanan,  
D. R. Fowler (1988)

All plants were modeled with L-systems and rendered using the IRIS firmware. Images corresponding to different viewing planes (the background lilac twigs, the apple twig and the daisies) were defocused separately using low-pass filters to simulate the depth of field, then composited with a focused image of lilac inflorescences. The sky was generated using a fractal algorithm.

**Figure 3.23** [page 96] *Wild carrot*  
P. Prusinkiewicz (1988)

**Figure 4.3** [page 102] *Close-up of a daisy capitulum*  
D. R. Fowler (1988)

The petals and florets were modeled as Bézier surfaces.

**Figure 4.4** [page 102] *Domestic sunflower head*  
D. R. Fowler, P. Prusinkiewicz (1989)

**Figure 4.5** [page 105] *Sunflower field*  
D. R. Fowler, N. Fuller, J. Hanan, A. Snider  
(1990)

This image contains approximately 400 plants, each with 15 flowers. A flower has 21 petals and 300 seeds, modeled using 600 triangles and 400 triangles respectively. Counting leaves and buds, the entire scene contains about 800,000,000 triangles. The image was ray-traced with adaptive supersampling on a grid of 1024 x 768 pixels using 45 hours of CPU time on a MIPS M-120 computer.

**Figure 4.6** [page 106] *Zinnias*  
D. R. Fowler, P. Prusinkiewicz, J. Hanan,  
N. Fuller (1990)

The vase was modeled using L.E.G.O. and rendered with a procedural texture. The scene was illuminated by one extended light source.



**Figure 4.7** [page 106] *Close-up of zinnias*  
D. R. Fowler, P. Prusinkiewicz, A. Snider  
(1990)

This scene was rendered using distributed ray-tracing to simulate the depth field.

**Figure 4.8** [page 108] *Water-lily*  
D. R. Fowler, J. Hanan (1990)

**Figure 4.9** [page 108] *Lily pond*  
D. R. Fowler, J. Hanan, P. Prusinkiewicz,  
N. Fuller (1990)

The wavelets on the water surface were obtained using bump-mapping with a procedurally defined texture.

**Figure 4.10** [page 109] *Roses*  
D. R. Fowler, J. Hanan, P. Prusinkiewicz  
(1990)

Distributed ray-tracing with one extended light source was used to simulate depth of field and create fuzzy shadows.

**Figure 4.11** [page 111] *Parastichies on a cylinder*  
D. R. Fowler (1990)

**Figure 4.15** [page 116] *Pineapples*  
D. R. Fowler, A. Snider (1990)

The image incorporates a physically-based model of a tablecloth approximated as an array of masses connected by springs and placed in a gravitational field. The scene is illuminated by three extended light sources.

**Figure 4.16** [page 117] *Spruce cones*  
D. R. Fowler, J. Hanan (1990)

**Figure 4.17** [page 117] *Carex laevigata*  
J. Hanan, P. Prusinkiewicz (1989)

The entire plant, including the leaves, was modeled using parametric L-systems.

**Figure 5.2** [page 121] *Maraldi figure*  
Ned Greene, NYIT (1984)

The shapes of leaves, calyxes and petals were defined using a paint program, by interpreting gray levels as height. Painted textures were mapped onto the surfaces of leaves and calyxes. Smooth gradation of color across the petals was obtained by assigning colors to the vertices of the polygon meshes representing flowers, then interpolating colors across polygons using Gouraud shading. The vines were rendered with bump-mapping, using a digitized image of real bark.

**Figure 5.3** [page 121] *The fern*  
P. Prusinkiewicz (1986)

**Figure 5.7** [page 125] *A rose in a vase*  
D. R. Fowler, J. Hanan, P. Prusinkiewicz  
(1990)

Petals and thorns are Bézier surfaces incorporated into a rose model expressed using L-systems. The vase was modeled as a surface of revolution.

**Figure 6.3** [page 141] *Development of Anabaena catenula*  
P. Prusinkiewicz, F. D. Fracchia (1989)

Each developmental stage is plotted in one scan line.

**Figure 7.13** [page 161] *Simulated development of Microsorium  
linguaeforme*  
F. D. Fracchia, P. Prusinkiewicz,  
M. J. M. de Boer (1989)

Cells are represented as polygons, rendered using the IRIS firmware. The development can be visualized directly on the screen of an IRIS 4D/20 workstation without resorting to single-frame animation techniques.

**Figure 7.14** [page 161] *Microphotograph of Microsorium linguaeforme*  
M. J. M. de Boer, University of Utrecht

**Figure 7.16** [page 163] *Simulated development of Dryopteris  
thelypteris*  
F. D. Fracchia, P. Prusinkiewicz,  
M. J. M. de Boer (1989)

**Figure 7.19** [page 169] *Developmental sequence of Patella vulgata*  
F. D. Fracchia, A. Lindenmayer,  
M. J. M. de Boer (1989)

Cells are represented as spheres. Intersections of spheres inside the modeled embryo are ignored, since they do not affect the ray-traced images.

**Figure 7.20** [page 169] *An electron microscope image of Patella vulgata*  
W. J. Dictus, University of Utrecht

**Figure 8.4** [page 180] *Fern dune*  
P. Prusinkiewicz, D. Hepting (1989)

The shape of the leaf has been captured using a controlled iterated function system. A continuous escape-time function defines point altitudes, resulting in a surrealistic incorporation of a leaf into the landscape.

**Figure 8.9** [page 186] *Carrot leaf*  
D. Hepting, P. Prusinkiewicz (1989)

The leaf shape has been modeled using a controlled iterated function system. The scene consists of a set of spheres, with the radius equal to the distance to the leaf. The image was rendered using ray-tracing.

**Figure E.1** [page 191] *Water-lilies*  
D. R. Fowler, J. Hanan, P. Prusinkiewicz,  
N. Fuller (1990)

A scene inspired by *Water-lilies pool - Harmony in green* by Claude Monet (1899). All trees and water-lilies were modeled using L-systems. The willow twigs bend downwards due to a strong tropism effect, simulating gravity. The bridge was modeled using L.E.G.O. The sky is a sphere with a procedural texture. The entire scene was ray-traced, then the resulting image was represented as a set of small circles, with the colors close but not equal to the average of pixel colors underneath. This last operation was aimed at creating the appearance of an impressionistic painting.

**Figure A.4** [page 200] *Virtual lab*  
L. Mercer, D. R. Fowler (1990)



# Turtle interpretation of symbols

Symbol	Interpretation	Page
$F$	Move forward and draw a line.	7, 46
$f$	Move forward without drawing a line.	7, 46
$+$	Turn left.	7, 19, 46
$-$	Turn right.	7, 19
$\wedge$	Pitch up.	19, 46
$\&$	Pitch down.	19, 46
$\backslash$	Roll left.	19, 46
$/$	Roll right.	19, 46
$ $	Turn around.	19, 46
$\$$	Rotate the turtle to vertical.	57
$[$	Start a branch.	24
$]$	Complete a branch.	24
$\{$	Start a polygon.	120, 127
$G$	Move forward and draw a line. Do not record a vertex.	122
$.$	Record a vertex in the current polygon.	122, 127
$\}$	Complete a polygon.	120, 127
$\sim$	Incorporate a predefined surface.	119
$!$	Decrement the diameter of segments.	26, 57
$'$	Increment the current color index.	26
$\%$	Cut off the remainder of the branch.	73



# Bibliography

- [1] H. Abelson and A. A. diSessa. *Turtle geometry*. M.I.T. Press, Cambridge, 1982.
- [2] M. Aono and T. L. Kunii. Botanical tree image generation. *IEEE Computer Graphics and Applications*, 4(5):10–34, 1984.
- [3] M. J. Apter. *Cybernetics and development*. Pergamon Press, Oxford, 1966. (International Series of Monographs in Pure and Applied Biology/Zoology Division Vol. 29).
- [4] W. W. Armstrong. The dynamics of tree linkages with a fixed root link and limited range of rotation. *Actes du Colloque Internationale l'Imaginaire Numérique '86*, pages 16–21, 1986.
- [5] J. W. Backus. The syntax and semantics of the proposed international algebraic language of the Zurich ACM-GAMM conference. In *Proc. Intl. Conf. on Information Processing*, pages 125–132. UNESCO, 1959.
- [6] B. I. Balinsky. *An introduction to embryology*. W. B. Saunders, Philadelphia, 1970.
- [7] M. F. Barnsley. *Fractals everywhere*. Academic Press, San Diego, 1988.
- [8] M. F. Barnsley, J. H. Elton, and D. P. Hardin. Recurrent iterated function systems. *Constructive Approximation*, 5:3–31, 1989.
- [9] B. A. Barsky. The Beta-spline: A local representation based on shape parameters and fundamental geometric measures. PhD thesis, Department of Computer Science, University of Utah, 1981.
- [10] R. Bartels, J. Beatty, and B. Barsky, editors. *An introduction to splines for use in computer graphics and geometric modeling*. Morgan Kaufman, Los Altos, California, 1987.
- [11] J. Bloomenthal. Modeling the mighty maple. Proceedings of SIGGRAPH '85 (San Francisco, California, July 22-26, 1985) in *Computer Graphics*, 19, 3 (July 1985), pages 305–311, ACM SIGGRAPH, New York, 1985.

- [12] B. G. Briggs and L. A. S. Johnson. Evolution in the Myrtaceae – evidence from inflorescence structure, Appendix I: The relevance of Troll’s system of inflorescence typology. In *Proceedings of the Linnean Society of New South Wales*, volume 102, pages 236–240, 1979.
- [13] N. Chomsky. Three models for the description of language. *IRE Trans. on Information Theory*, 2(3):113–124, 1956.
- [14] V. Claus, H. Ehrig, and G. Rozenberg, editors. *Graph grammars and their application to computer science; First International Workshop*. Lecture Notes in Computer Science 73. Springer-Verlag, Berlin, 1979.
- [15] D. Cohen. Computer simulation of biological pattern generation processes. *Nature*, 216:246–248, 1967.
- [16] E. Costes. Analyse architecturale et modelisation du litchi. PhD thesis, Université des Sciences et Techniques du Languedoc, 1988.
- [17] H. S. M. Coxeter. *Introduction to geometry*. J. Wiley & Sons, New York, 1961.
- [18] H. S. M. Coxeter. The role of intermediate convergents in Tait’s explanation for phyllotaxis. *J. Algebra*, 20:167–175, 1972.
- [19] K. Culik II and D. Wood. A mathematical investigation of propagating graph OL-systems. *Information and Control*, 43:50–82, 1979.
- [20] P. Dabadie, P. de Reffye, and P. Dinouard. Modélisation de la croissance et de l’architecture d’un bambou. In *Deuxième congrès international du bambou*, 1988.
- [21] C. Davis and D. E. Knuth. Number representations and dragon curves. *J. of Recreational Mathematics*, 3:66–81, 133–149, 1970.
- [22] M. J. M. de Boer. Analysis and computer generation of division patterns in cell layers using developmental algorithms. PhD thesis, University of Utrecht, the Netherlands, 1989.
- [23] M. J. M. de Boer and A. Lindenmayer. Map OL-systems with edge label control: Comparison of marker and cyclic systems. In H. Ehrig, M. Nagl, A. Rosenfeld, and G. Rozenberg, editors, *Graph-grammars and their application to computer science*, Lecture Notes in Computer Science 291, pages 378–392. Springer-Verlag, 1987.



- [24] M. de Does and A. Lindenmayer. Algorithms for the generation and drawing of maps representing cell clones. In H. Ehrig, M. Nagl, and G. Rozenberg, editors, *Graph-grammars and their application to computer science*, Lecture Notes in Computer Science 153, pages 39–57. Springer-Verlag, 1983.
- [25] C. G. de Koster and A. Lindenmayer. Discrete and continuous models for heterocyst differentiation in growing filaments of blue-green bacteria. In *Acta Biotheoretica*, volume 36, pages 249–273. Kluwer Academic, the Netherlands, 1987.
- [26] P. de Reffye. Modèle mathématique aléatoire et simulation de la croissance et de l’architecture du caféier robusta. Première partie, *Café-Cacao-Thé*, 25(2):83–104, 1981. Deuxième partie, *Café-Cacao-Thé*, 25(4):219–230, 1981. Troisième partie, *Café-Cacao-Thé*, 26(2):77–96, 1982. Quatrième partie, *Café-Cacao-Thé*, 27(1):3–20, 1983.
- [27] P. de Reffye. Travaux sur la caféier. CIRAD, Montpellier. Collection of earlier papers.
- [28] P. de Reffye. Modélisation et simulation de la verse de caféier, à l’aide de la théorie de la résistance des matériaux. *Café-Cacao-Thé*, XX(4):251–272, 1976.
- [29] P. de Reffye, M. Cognee, M. Jaeger, and B. Traore. Modélisation de la croissance et de l’architecture du cotonnier. Manuscript, 1988.
- [30] P. de Reffye, C. Edilin, J. Françon, M. Jaeger, and C. Puech. Plant models faithful to botanical structure and development. Proceedings of SIGGRAPH ’88 (Atlanta, Georgia, August 1-5, 1988), in *Computer Graphics* 22,4 (August 1988), pages 151–158, ACM SIGGRAPH, New York, 1988.
- [31] F. M. Dekking. Recurrent sets. *Advances in Mathematics*, 44(1):78–104, 1982.
- [32] F. M. Dekking. Recurrent sets: A fractal formalism. Report 82-32, Delft University of Technology, 1982.
- [33] H. Ehrig, M. Nagl, A. Rosenfeld, and G. Rozenberg, editors. *Graph grammars and their application to computer science; Third International Workshop*. Lecture Notes in Computer Science 291. Springer-Verlag, Berlin, 1987.
- [34] H. Ehrig, M. Nagl, and G. Rozenberg, editors. *Graph grammars and their application to computer science; Second International Workshop*. Lecture Notes in Computer Science 153. Springer-Verlag, Berlin, 1983.

- [35] P. Eichhorst and W. J. Savitch. Growth functions of stochastic Lindenmayer systems. *Information and Control*, 45:217–228, 1980.
- [36] R. O. Erickson. The geometry of phyllotaxis. In J. E. Dale and F. L. Milthrope, editors, *The growth and functioning of leaves*, pages 53–88. University Press, Cambridge, 1983.
- [37] G. Eyrolles. Synthèse d’images figuratives d’arbres par des méthodes combinatoires. PhD thesis, Université de Bordeaux I, 1986.
- [38] J. B. Fisher and H. Honda. Computer simulation of branching pattern and geometry in *Terminalia* (Combretaceae), a tropical tree. *Botanical Gazette*, 138(4):377–384, 1977.
- [39] J. B. Fisher and H. Honda. Branch geometry and effective leaf area: A study of *Terminalia*—branching pattern, Parts I and II. *American Journal of Botany*, 66:633–655, 1979.
- [40] J. D. Foley and A. Van Dam. *Fundamentals of interactive computer graphics*. Addison-Wesley, Reading, Massachusetts, 1982.
- [41] L. Fox and D. F. Mayers. *Numerical solution of ordinary differential equations*. Chapman and Hall, London, 1987.
- [42] F. D. Fracchia, P. Prusinkiewicz, and M. J. M. de Boer. Visualization of the development of multicellular structures. In *Proceedings of Graphics Interface '90*, pages 267–277, 1990.
- [43] H. Freeman. On encoding arbitrary geometric configurations. *IRE Trans. Electronic. Computers*, 10:260–268, 1961.
- [44] D. Frijters. Mechanisms of developmental integration of *Aster novae-angliae* L. and *Hieracium murorum* L. *Annals of Botany*, 42:561–575, 1978.
- [45] D. Frijters. Principles of simulation of inflorescence development. *Annals of Botany*, 42:549–560, 1978.
- [46] D. Frijters and A. Lindenmayer. A model for the growth and flowering of *Aster novae-angliae* on the basis of table (1,0)L-systems. In G. Rozenberg and A. Salomaa, editors, *L Systems*, Lecture Notes in Computer Science 15, pages 24–52. Springer-Verlag, Berlin, 1974.
- [47] D. Frijters and A. Lindenmayer. Developmental descriptions of branching patterns with paracladial relationships. In A. Lindenmayer and G. Rozenberg, editors, *Automata, languages, development*, pages 57–73. North-Holland, Amsterdam, 1976.

- [48] M. Gardner. Mathematical games: An array of problems that can be solved with elementary mathematical techniques. *Scientific American*, 216, 1967. 3:124–129 (March), 4:116–123 (April).
- [49] M. Gardner. Mathematical games: The fantastic combinations of John Conway’s new solitaire game “life”. *Scientific American*, 223(4):120–123, October 1970.
- [50] M. Gardner. Mathematical games: On cellular automata, self-reproduction, the Garden of Eden and the game “life”. *Scientific American*, 224(2):112–117, February 1971.
- [51] M. Gardner. Mathematical games – in which “monster” curves force redefinition of the word “curve”. *Scientific American*, 235(6):124–134, December 1976.
- [52] S. Ginsburg and H. G. Rice. Two families of languages related to ALGOL. *J. ACM*, 9(3):350–371, 1962.
- [53] H. Gravelius. *Flusskunde*. Goschen, Berlin, 1914.
- [54] N. Greene. Voxel space automata: Modeling with stochastic growth processes in voxel space. Proceedings of SIGGRAPH ’89 (Boston, Mass., July 31-August 4, 1989), in *Computer Graphics* 23,4 (August 1989), pages 175–184, ACM SIGGRAPH, New York, 1989.
- [55] B. E. S. Gunning. Microtubules and cytomorphogenesis in a developing organ: The root primordium of *Azolla pinnata*. In O. Kiermayer, editor, *Cytomorphogenesis in plants*, Cell Biology Monographs 8, pages 301–325. Springer-Verlag, Wien, 1981.
- [56] A. Habel and H.-J. Kreowski. On context-free graph languages generated by edge replacement. In H. Ehrig, M. Nagl, and G. Rozenberg, editors, *Graph grammars and their application to computer science; Second International Workshop*, Lecture Notes in Computer Science 153, pages 143–158. Springer-Verlag, Berlin, 1983.
- [57] A. Habel and H.-J. Kreowski. May we introduce to you: Hyperedge replacement. In H. Ehrig, M. Nagl, G. Rozenberg, and A. Posenfeld, editors, *Graph grammars and their application to computer science; Third International Workshop*, Lecture Notes in Computer Science 291, pages 15–26. Springer-Verlag, Berlin, 1987.
- [58] F. Hallé, R. A. A. Oldeman, and P. B. Tomlinson. *Tropical trees and forests: An architectural analysis*. Springer-Verlag, Berlin, 1978.

- [59] P. H. Hellendoorn and A. Lindenmayer. Phyllotaxis in *Bryophyllum tubiflorum*: Morphogenetic studies and computer simulations. *Acta Biol. Neerl*, 23(4):473–492, 1974.
- [60] D. Hepting, P. Prusinkiewicz, and D. Saupe. Rendering methods for iterated function systems. Manuscript, 1990.
- [61] G. Herman, A. Lindenmayer, and G. Rozenberg. Description of developmental languages using recurrence systems. *Mathematical Systems Theory*, 8:316–341, 1975.
- [62] G. T. Herman and G. Rozenberg. *Developmental systems and languages*. North-Holland, Amsterdam, 1975.
- [63] D. Hilbert. Ueber stetige Abbildung einer Linie auf ein Flächenstück. *Mathematische Annalen*, 38:459–460, 1891.
- [64] P. Hogeweg and B. Hesper. A model study on biomorphological description. *Pattern Recognition*, 6:165–179, 1974.
- [65] H. Honda. Description of the form of trees by the parameters of the tree-like body: Effects of the branching angle and the branch length on the shape of the tree-like body. *Journal of Theoretical Biology*, 31:331–338, 1971.
- [66] H. Honda and J. B. Fisher. Tree branch angle: Maximizing effective leaf area. *Science*, 199:888–890, 1978.
- [67] H. Honda and J. B. Fisher. Ratio of tree branch lengths: The equitable distribution of leaf clusters on branches. *Proceedings of the National Academy of Sciences USA*, 76(8):3875–3879, 1979.
- [68] H. Honda, P. B. Tomlinson, and J. B. Fisher. Computer simulation of branch interaction and regulation by unequal flow rates in botanical trees. *American Journal of Botany*, 68:569–585, 1981.
- [69] H. Honda, P. B. Tomlinson, and J. B. Fisher. Two geometrical models of branching of botanical trees. *Annals of Botany*, 49:1–11, 1982.
- [70] R. E. Horton. Eroded development of systems and their drainage basins, hydrophysical approach to quantitative morphology. *Bull. Geol. Soc. America*, 56:275–370, 1945.
- [71] R. E. Horton. Hypsometric (area-altitude) analysis of erosional topology. *Bull. Geol. Soc. America*, 63:1117–1142, 1952.
- [72] R. Hunt. *Plant growth analysis*. Studies in Biology 96. Edward Arnold, London, 1978.

- [73] R. Hunt. *Plant growth curves – the functional approach to plant growth analysis*. Edward Arnold, London, 1982.
- [74] J. E. Hutchinson. Fractals and self-similarity. *Indiana University Journal of Mathematics*, 30(5):713–747, 1981.
- [75] G. Van Iterson. *Mathematische und mikroskopisch-anatomische Studien über Blattstellungen*. Gustav Fischer, Jena, 1907.
- [76] M. Jaeger. Représentation et simulation de croissance des végétaux. PhD thesis, Université Louis Pasteur de Strasbourg, 1987.
- [77] J. M. Janssen and A. Lindenmayer. Models for the control of branch positions and flowering sequences of capitula in *Mycelis muralis* (L.) Dumont (Compositae). *New Phytologist*, 105:191–220, 1987.
- [78] R. V. Jean. Mathematical modelling in phyllotaxis: The state of the art. *Mathematical Biosciences*, 64:1–27, 1983.
- [79] H. Jürgensen and A. Lindenmayer. Modelling development by OL-systems: Inference algorithms for developmental systems with cell lineages. *Bulletin of Mathematical Biology*, 49(1):93–123, 1987.
- [80] A. N. Kolmogorov. Three approaches to the quantitative definition of information. *Int. J. Comp. Math*, 2:157–168, 1968.
- [81] H. Lieberman. Using prototypical objects to implement shared behavior in object oriented systems. In *Proceedings of the ACM Conference on Object-Oriented Programming Systems, Languages, and Applications*, pages 214–223, New York, 1986. Association for Computing Machinery.
- [82] A. Lindenmayer. Mathematical models for cellular interaction in development, Parts I and II. *Journal of Theoretical Biology*, 18:280–315, 1968.
- [83] A. Lindenmayer. Adding continuous components to L-systems. In G. Rozenberg and A. Salomaa, editors, *L Systems*, Lecture Notes in Computer Science 15, pages 53–68. Springer-Verlag, Berlin, 1974.
- [84] A. Lindenmayer. Developmental algorithms: Lineage versus interactive control mechanisms. In S. Subtelny and P. B. Green, editors, *Developmental order: Its origin and regulation*, pages 219–245. Alan R. Liss, New York, 1982.

- [85] A. Lindenmayer. Models for plant tissue development with cell division orientation regulated by preprophase bands of microtubules. *Differentiation*, 26:1–10, 1984.
- [86] A. Lindenmayer. Positional and temporal control mechanisms in inflorescence development. In P. W. Barlow and D. J. Carr, editors, *Positional controls in plant development*. University Press, Cambridge, 1984.
- [87] A. Lindenmayer. An introduction to parallel map generating systems. In H. Ehrig, M. Nagl, A. Rosenfeld, and G. Rozenberg, editors, *Graph grammars and their application to computer science; Third International Workshop*, Lecture Notes in Computer Science 291, pages 27–40. Springer-Verlag, Berlin, 1987.
- [88] A. Lindenmayer. Models for multicellular development: Characterization, inference and complexity of L-systems. In A. Keldenová and J. Kelmen, editors, *Trends, techniques and problems in theoretical computer science*, Lecture Notes in Computer Science 281, pages 138–168. Springer-Verlag, Berlin, 1987.
- [89] A. Lindenmayer and P. Prusinkiewicz. Developmental models of multicellular organisms: A computer graphics perspective. In C. Langton, editor, *Artificial Life: Proceedings of an Interdisciplinary Workshop on the Synthesis and Simulation of Living Systems held September, 1987, in Los Alamos, New Mexico*, pages 221–249. Addison-Wesley, Redwood City, 1989.
- [90] A. Lindenmayer and G. Rozenberg, editors. *Automata, languages, development*. North-Holland, Amsterdam, 1976.
- [91] A. Lindenmayer and G. Rozenberg. Parallel generation of maps: Developmental systems for cell layers. In V. Claus, H. Ehrig, and G. Rozenberg, editors, *Graph grammars and their application to computer science; First International Workshop*, Lecture Notes in Computer Science 73, pages 301–316. Springer-Verlag, Berlin, 1979.
- [92] J. Lück, A. Lindenmayer, and H. B. Lück. Models for cell tetrads and clones in meristematic cell layers. *Botanical Gazette*, 149:1127–141, 1988.
- [93] J. Lück and H. B. Lück. Generation of 3-dimensional plant bodies by double wall map and stereomap systems. In H. Ehrig, M. Nagl, and G. Rozenberg, editors, *Graph Grammars and Their Application to Computer Science; Second International Workshop*, Lecture Notes in Computer Science 153, pages 219–231. Springer-Verlag, Berlin, 1983.

- [94] N. Macdonald. *Trees and networks in biological models*. J. Wiley & Sons, New York, 1983.
- [95] B. B. Mandelbrot. *The fractal geometry of nature*. W. H. Freeman, San Francisco, 1982.
- [96] D. M. McKenna. SquaRecurves, E-tours, eddies and frenzies: Basic families of Peano curves on the square grid. In *Proceedings of the Eugene Strens Memorial Conference on Recreational Mathematics and its History*, 1989. To appear.
- [97] H. Meinhardt. *Models of biological pattern formation*. Academic Press, New York, 1982.
- [98] L. Mercer, P. Prusinkiewicz, and J. Hanan. The concept and design of a virtual laboratory. In *Proceedings of Graphics Interface '90*, pages 149–155. CIPS, 1990.
- [99] G. J. Mitchison and Michael Wilcox. Rules governing cell division in *Anabaena*. *Nature*, 239:110–111, 1972.
- [100] D. Müller-Doblies and U. Müller-Doblies. Cautious improvement of a descriptive terminology of inflorescences. *Monocot Newsletter* 4, 1987.
- [101] F. K. Musgrave, C. E. Kolb, and R. S. Mace. The synthesis and rendering of eroded fractal terrains. Proceedings of SIGGRAPH '89 (Boston, Mass., July 31-August 4, 1989), in *Computer Graphics* 23,4 (August 1989), pages 41–50, ACM SIGGRAPH, New York, 1989.
- [102] A. Nakamura, A. Lindenmayer, and K. Aizawa. Some systems for map generation. In G. Rozenberg and A. Salomaa, editors, *The Book of L*, pages 323–332. Springer-Verlag, Berlin, 1986.
- [103] P. Naur et al. Report on the algorithmic language ALGOL 60. *Communications of the ACM*, 3(5):299–314, 1960. Revised in *Comm. ACM* 6(1):1-17.
- [104] T. Nelson. *Computer lib and dream machines*. Self-published, 1980.
- [105] P. Oppenheimer. Real time design and animation of fractal plants and trees. *Computer Graphics*, 20(4):55–64, 1986.
- [106] G. Peano. Sur une courbe, qui remplit tout une aire plaine. *Math. Annln.*, 36:157–160, 1890. Translated in G. Peano, *Selected works of Giuseppe Peano*, H. C. Kennedy, editor, pages 143–149, University of Toronto Press, Toronto, 1973.

- [107] H. Peitgen and D. Saupe, editors. *The science of fractal images*. Springer-Verlag, New York, 1988.
- [108] F. P. Preparata and R. T. Yeh. *Introduction to Discrete Structures*. Addison-Wesley, Reading, Massachusetts, 1973.
- [109] P. Prusinkiewicz. Graphical applications of L-systems. In *Proceedings of Graphics Interface '86 — Vision Interface '86*, pages 247–253. CIPS, 1986.
- [110] P. Prusinkiewicz. Score generation with L-systems. In *Proceedings of the International Computer Music Conference '86*, pages 455–457, 1986.
- [111] P. Prusinkiewicz. Applications of L-systems to computer imagery. In H. Ehrig, M. Nagl, A. Rosenfeld, and G. Rozenberg, editors, *Graph grammars and their application to computer science; Third International Workshop*, pages 534–548. Springer-Verlag, Berlin, 1987. Lecture Notes in Computer Science 291.
- [112] P. Prusinkiewicz and J. Hanan. *Lindenmayer systems, fractals, and plants*, volume 79 of *Lecture Notes in Biomathematics*. Springer-Verlag, Berlin, 1989.
- [113] P. Prusinkiewicz and J. Hanan. Visualization of botanical structures and processes using parametric L-systems. In D. Thalmann, editor, *Scientific Visualization and Graphics Simulation*, pages 183–201. J. Wiley & Sons, 1990.
- [114] P. Prusinkiewicz and K. Krithivasan. Algorithmic generation of South Indian folk art patterns. In *Proceedings of the International Conference on Computer Graphics ICONCG '88*, Singapore, 1988.
- [115] P. Prusinkiewicz, K. Krithivasan, and M. G. Vijayanarayana. Application of L-systems to algorithmic generation of South Indian folk art patterns and karnatic music. In R. Narasimhan, editor, *A perspective in theoretical computer science — commemorative volume for Gift Siromoney*, pages 229–247. World Scientific, Singapore, 1989. Series in Computer Science Vol. 16.
- [116] P. Prusinkiewicz, A. Lindenmayer, and F. D. Fracchia. Synthesis of space-filling curves on the square grid. To appear in *Proceedings of FRACTAL '90*, the 1st IFIP conference on fractals, Lisbon, Portugal, June 6-8, 1990.
- [117] P. Prusinkiewicz, A. Lindenmayer, and J. Hanan. Developmental models of herbaceous plants for computer imagery purposes. Proceedings of SIGGRAPH '88 (Atlanta, Georgia, August 1-5, 1988), in *Computer Graphics* 22,4 (August 1988), pages 141–150, ACM SIGGRAPH, New York, 1988.



- [118] P. Prusinkiewicz and G. Sandness. Koch curves as attractors and repellers. *IEEE Computer Graphics and Applications*, 8(6):26–40, 1988.
- [119] W. T. Reeves and R. Blau. Approximate and probabilistic algorithms for shading and rendering structured particle systems. Proceedings of SIGGRAPH '85 (San Francisco, California, July 22-26, 1985) in *Computer Graphics*, 19, 3 (July 1985), pages 313–322, ACM SIGGRAPH, New York, 1985.
- [120] W. R. Remphrey, B. R. Neal, and T. A. Steeves. The morphology and growth of *Arctostaphylos uva-ursi* (bearberry), parts i and ii. *Canadian Journal of Botany*, 61(9):2430–2458, 1983.
- [121] W. R. Remphrey and G. R. Powell. Crown architecture of *Larix laricina* saplings: Quantitative analysis and modelling of (non-sylleptic) order 1 branching in relation to development of the main stem. *Canadian Journal of Botany*, 62(9):1904–1915, 1984.
- [122] W. R. Remphrey and G. R. Powell. Crown architecture of *Larix laricina* saplings: Sylleptic branching on the main stem. *Canadian Journal of Botany*, 63(7):1296–1302, 1985.
- [123] L. H. Reuter. Rendering and magnification of fractals using iterated function systems. PhD thesis, Georgia Institute of Technology, 1987.
- [124] J. N. Ridley. Computer simulation of contact pressure in capitula. *Journal of Theoretical Biology*, 95:1–11, 1982.
- [125] J. N. Ridley. Packing efficiency in sunflower heads. *Mathematical Biosciences*, 58:129–139, 1982.
- [126] D. F. Robinson. A notation for the growth of inflorescences. *New Phytologist*, 103:587–596, 1986.
- [127] G. Rozenberg and A. Salomaa. *The mathematical theory of L-systems*. Academic Press, New York, 1980.
- [128] A. Salomaa. *Formal languages*. Academic Press, New York, 1973.
- [129] F. W. Sears, M. W. Zemansky, and H. D. Young. *College physics*. Addison-Wesley Publ. Co., Reading, 6th edition, 1985.
- [130] M. Shebell. Modeling branching plants using attribute L-systems. Master's thesis, Worcester Polytechnic Institute, 1986.
- [131] P. L. J. Siero, G. Rozenberg, and A. Lindenmayer. Cell division patterns: Syntactical description and implementation. *Computer Graphics and Image Processing*, 18:329–346, 1982.

- [132] W. Sierpiński. Sur une courbe dont tout point est un point de ramification. *Comptes Rendus hebdomadaires des séances de l'Académie des Sciences*, 160:302–305, 1915. Reprinted in W. Sierpiński, *Oeuvres choisies*, S. Hartman et al., editors, pages 99–106, PWN – Éditions Scientifiques de Pologne, Warsaw, 1975.
- [133] G. Siromoney and R. Siromoney. Rosenfeld's cycle grammars and kolam. In H. Ehrig, M. Nagl, A. Rosenfeld, and G. Rozenberg, editors, *Graph grammars and their application to computer science; Third International Workshop*, Lecture Notes in Computer Science 291, pages 564–579. Springer-Verlag, Berlin, 1987.
- [134] G. Siromoney, R. Siromoney, and T. Robinsin. Kambi kolam and cycle grammars. In R. Narasimhan, editor, *A perspective in theoretical computer science — commemorative volume for Gift Siromoney*, Series in Computer Science Vol. 16, pages 267–300. World Scientific, Singapore, 1989.
- [135] R. Siromoney and K. G. Subramanian. Space-filling curves and infinite graphs. In H. Ehrig, M. Nagl, and G. Rozenberg, editors, *Graph grammars and their application to computer science; Second International Workshop*, Lecture Notes in Computer Science 153, pages 380–391. Springer-Verlag, Berlin, 1983.
- [136] A. R. Smith. Plants, fractals, and formal languages. Proceedings of SIGGRAPH '84 (Minneapolis, Minnesota, July 22-27, 1984) in *Computer Graphics*, 18, 3 (July 1984), pages 1–10, ACM SIGGRAPH, New York, 1984.
- [137] A. R. Smith. About the cover: Reconfigurable machines. *Computer*, 11(7):3–4, 1978.
- [138] P. S. Stevens. *Patterns in nature*. Little, Brown and Co., Boston, 1974.
- [139] R. J. Stevens, A. F. Lehar, and F. H. Perston. Manipulation and presentation of multidimensional image data using the Peano scan. *IEEE Trans. on Pattern Analysis and Machine Intelligence*, PAMI-5(5):520–526, 1983.
- [140] A. L. Szilard. Growth functions of Lindenmayer systems. Technical Report 4, Computer Science Department, University of Western Ontario, 1971.
- [141] A. L. Szilard and R. E. Quinton. An interpretation for DOL systems by computer graphics. *The Science Terrapin*, 4:8–13, 1979.

- [142] R. Thom. *Structural stability and morphogenesis. An outline of a general theory of models*. Benjamin/Cummings, Reading, Massachusetts, 1975.
- [143] d'Arcy Thompson. *On growth and form*. University Press, Cambridge, 1952.
- [144] W. Troll. *Die Infloreszenzen*, volume I. Gustav Fischer Verlag, Stuttgart, 1964.
- [145] W. Troll. *Die Infloreszenzen*, volume II. Gustav Fischer Verlag, Jena, 1969.
- [146] A. Turing. On computable numbers with an application to the Entscheidungsproblem, 1936. *Proc. Lond. Math. Soc.* (ser. 2), 42:230–265, 1936–37, and 43:544–546, 1937.
- [147] A. Turing. The chemical basis of morphogenesis. *Philosophical Trans. Roy. Soc. B*, 237(32):5–72, 1952.
- [148] W. T. Tutte. *Graph theory*. Addison-Wesley, Reading, Massachusetts, 1982.
- [149] S. Ulam. Patterns of growth of figures: Mathematical aspects. In G. Kepes, editor, *Module, Proportion, Symmetry, Rhythm*, pages 64–74. Braziller, New York, 1966.
- [150] J. A. M. van den Biggelaar. Development of dorsoventral polarity and mesentoblast determination in *Patella vulgata*. *Journal of Morphology*, 154:157–186, 1977.
- [151] A. H. Veen and A. Lindenmayer. Diffusion mechanism for phyllotaxis: Theoretical physico-chemical and computer study. *Plant Physiology*, 60:127–139, 1977.
- [152] X. G. Viennot, G. Eyrolles, N. Janey, and D. Arquès. Combinatorial analysis of ramified patterns and computer imagery of trees. Proceedings of SIGGRAPH '89 (Boston, Mass., July 31–August 4, 1989), in *Computer Graphics* 23,4 (August 1989), pages 31–40, ACM SIGGRAPH, New York, 1989.
- [153] P. M. B. Vitányi. Development, growth and time. In G. Rozenberg and A. Salomaa, editors, *The Book of L*, pages 431–444. Springer-Verlag, Berlin, 1986.
- [154] H. Vogel. A better way to construct the sunflower head. *Mathematical Biosciences*, 44:179–189, 1979.
- [155] H. von Koch. Une méthode géométrique élémentaire pour l'étude de certaines questions de la théorie des courbes planes. *Acta mathematica*, 30:145–174, 1905.

- [156] J. von Neumann. *Theory of self-reproducing automata*. University of Illinois Press, Urbana, 1966. Edited by A. W. Burks.
- [157] F. Weberling. Typology of inflorescences. *J. Linn. Soc. (Bot.)*, 59(378):215–222, 1965.
- [158] F. Weberling. *Morphologie der Blüten und der Blütenstände*. Verlag Eugen Ulmer, Stuttgart, 1981.
- [159] H. Weyl. *Symmetry*. Princeton University Press, Princeton, New Jersey, 1982.
- [160] S. Wolfram. Computer software in science and mathematics. *Scientific American*, 251(3):188–203, 1984.
- [161] S. Wolfram. Some recent results and questions about cellular automata. In J. Demongeot, E. Goles, and M. Tchuente, editors, *Dynamical systems and cellular automata*, pages 153–167. Academic Press, London, 1985.
- [162] T. Yokomori. Stochastic characterizations of EOL languages. *Information and Control*, 45:26–33, 1980.
- [163] D. A. Young. On the diffusion theory of phyllotaxis. *Journal of Theoretical Biology*, 71:421–423, 1978.
- [164] M. H. Zimmerman and C. L. Brown. *Trees — structure and function*. Springer-Verlag, Berlin, 1971.

# Index

- accumulation 67
- acrotonic structure 87
- age 135
- alphabet 4
- Anabaena catenula* 5, 136
- anastomosis 51
- angle increment 6
- apex 21
  - continuing 70
  - flowering 64
  - terminal 70
  - vegetative 64
- apical dominance 88
- apical front 155
- apple 75
- attractor 178
- axiom 4
- axis 21
  
- bicubic patch 119
- blastula 166
- blue-green bacteria 5
- branch 21
- branching
  - decussate 93
  - monopodial 55, 70
  - polypodial 70, 86
  - sympodial 50, 58, 70
  - ternary 58
- branching angles 52
- branch plane 52
  
- capitulum 96
  - daisy 102
  - sunflower 102
- Capsella bursa-pastoris* 73, 120
- Carex laevigata* 116
- catastrophe 134
- cell 150
- cell (*continued*)
  - apical 154
  - epidermal 173
  - marginal 163
  - vegetative 44
- cell division system 154
- cellular automata 51
- cellwork 168
- chaos game 178
- cleavage 166
- condition 42
- contact point 13, 119
- context 30
- continuity requirement 140
- control graph 182
- crocus 68
- curve
  - dragon 11
  - E-curve 12
  - FASS 12
  - Gosper 12
  - Hilbert 16, 21
  - Koch island 7
  - Peano 17
  - pure 16
  - Sierpiński 11
  - snowflake 1
  - space-filling 12
  - SquaRecurve 14
- cyme 82
  - closed 85
  - double 83
  - open 82
  - simple 82
  
- data base amplification 63
- da Vinci's postulate 57
- delay mechanism 66
- derivation 4, 42, 135, 147, 171

- derivation (*continued*)
  - direct 4
  - length 4
  - stochastic 28
- developmental sequence 4
- developmental switch 65
- dibotryoid 76
  - closed 79
  - open 76
- direction vector 13
- divergence angle 52, 100, 109
- Dryopteris thelypteris* 162
- edge 168
  - directed 146
  - neutral 146
- embryo 166
- encyclic number 110
- entry point 13
- entry vector 13
- Euler method 153
- exit point 13
- exit vector 13
- expression 41
- fern 120
- Fibonacci
  - angle 99
  - number 99, 102
  - series 37
- florigen 76
- flower head 96
- flowering sequence
  - acropetal 73, 78
  - basipetal 75, 78, 87
- fractal 6
- gametophyte 153
- generative helix 109
- generator 1
- golden mean 99
- grammar 2
- growth
  - exponential 36, 142
  - linear 140
  - polynomial 37, 143
  - sigmoidal 38, 39
  - square-root 38
- growth function 36, 140
- growth potential 88, 123
- heading 6
- heading vector 119
- heterocyst 44
- Hooke's law 151, 172
- IFS 177
  - controlled 182
- inference 11
- inflorescence 71
- initiator 1
- interaction 65
- internode 21
- Koch construction 1, 7
- L-system 2
  - 1L 30
  - 2L 30
  - bracketed 24
  - cellwork 168
  - complete 64
  - context-sensitive 30
  - deterministic 4
  - DOL 4
  - IL 30
  - map 146
  - mBPCOL 168
  - mBPMOL 146, 168
  - OL 4
  - parametric 41
  - partial 64
  - pseudo 18
  - scheme 64
  - stochastic 28, 66
  - string 4
  - table 66
  - timed 135
  - tree 23
- leaf
  - compound 128, 142
  - cordate 122
  - simple 123
- letter 3
  - timed 135
- letter occurrence 28

- lifetime 135
- lilac 93
- lily-of-the-valley 73, 127
- lineage 65
- Lychnis coronaria* 83
- map 145
- map interpretation
  - center of gravity 150
  - dynamic 151, 172
  - wall subdivision 150
- marker 147, 170
  - matching 147
- Microsorium linguaeforme* 153
- microworld 187
- mint 79
- module 41, 134
- Mycelis muralis* 87
- Newton's law 152
- nitrogen compound 44
- object 189
- offset 148
- order of continuity 141
- osmotic pressure 151, 173
- panicle 86
- parameter 41
- parastichy 102
  - order 110
- Pascal triangle 38
- Patella vulgata* 166
- periclinal ratio 166
- phase effect 63, 73
- phyllotaxis 99
  - cylindrical 109
  - planar 100
- pineapple 116
- plastochron 65
- predecessor 4, 42, 147
- production 1
  - edge 146, 168
  - identity 4
  - inconsistent 171
  - probabilistic 28
  - string 4
  - tree 23
- raceme 71
  - closed 75
  - compound 76, 81
  - open 71
- recursive formula 15
- region 145
- rewriting 1
  - edge 11, 46
  - node 13, 47
- root node 21
- rose 106, 126
- segment 154
  - basal 159
- signal 31, 67
  - acropetal 76, 88
  - basipetal 88
- spadix 96
- spike 95
- spruce cone 116
- statement
  - #define 44
  - #ignore 32
  - #include 44
- step size 6
- string 3
  - bracketed 24
- subapical growth 26
- subfigure 13
- successor 4, 42, 147
- terminal node 21
- thallus 154
- thyrsus 85
- tile 12
- total elapsed time 136
- tree
  - axial 21
  - rooted 21
- tribotryoid 81
- tropism vector 58
- turtle interpretation 6, 18, 26, 46, 57, 73, 119, 120, 122, 127
- umbel 95
- Umbelliferae 128
- up vector 119

virtual laboratory 187  
voxel space 51

wall 150, 168  
    anticlinal 155  
    periclinal 155  
    tension 151, 173

water-lily 106  
wild carrot 95, 131

word 3  
    parametric 41  
    timed 135

zinnia 106